Title

Developmental, Genetic, and Cognitive Correlates of Structural Brain Connectivity

Permalink

https://escholarship.org/uc/item/4v62h26t

Author

Dennis, Emily

Publication Date

2013

Peer reviewed|Thesis/dissertation

UNIVERSITY OF CALIFORNIA

Los Angeles

Developmental, Genetic, and Cognitive Correlates

of Structural Brain Connectivity

A dissertation submitted in partial satisfaction

of the requirements for the degree Doctor of Philosophy

in Neuroscience

By

Emily Larsen Dennis

2013

ABSTRACT OF THE DISSERTATION

Developmental, Genetic, and Cognitive Correlates

of Structural Brain Connectivity

by

Emily Larsen Dennis

Doctor of Philosophy in Neuroscience

University of California, Los Angeles, 2013

Professor Paul M. Thompson, Chair

Brain connectivity methods have tremendous potential to expand our understanding of the brain, especially when added to existing knowledge gained through more traditional structural and functional brain imaging methods. Instead of examining isolated brain regions performing a function or individual regions affected by a disease, a network-level approach appreciates the complex organization and interactions of the brain. Through diffusion weighted imaging, we can visualize the white matter pathways of the brain *in vivo*, thus modeling the structural highways and roads that support efficient brain function. Understanding how these measures of structural connectivity change with development is key for a fuller understanding of healthy brain development, as structure, function, and connectivity all interact. Additionally, it is necessary for determining how and when dysfunction occurs in neurodevelopmental disorders.

As many of these disorders are genetically influenced, examining how risk genes affect brain connectivity might shed light on the mechanisms by which these genes have their effect. Lastly, one of the hallmarks of development is sharpening cognitive skills, which are often significantly impaired in neurodevelopmental disorders. In order to understand both typical and atypical development, determining how connectivity supports cognition is key. Especially with new brain metrics, such as those in graph theory, the association between brain connectivity and cognition is not well known, and presents exciting research potential. Altogether, determining the development, genetic, and cognitive correlates of structural brain connectivity will integrate with existing knowledge about brain structure and function to give us a fuller understanding of the interrelated processes that occur throughout development. This will form a foundation from which we can base future investigations into how connectivity is affected in neurodevelopmental disorders.

The dissertation of Emily Larsen Dennis is approved.

Susan Y. Bookheimer

Mirella Dapretto

Adriana Galvan

Paul M. Thompson, Committee Chair

University of California, Los Angeles

2013

TABLE OF CONTENTS

LIST OF FIGURES

LIST OF TABLES

ACKNOWLEDGEMENTS

I would not be where I am without the support and patience of my family, friends, fiancé, colleagues, mentors, and professors. Thank you so much for all of your advice and your understanding.

First, thank you to my graduate mentor, Dr. Paul Thompson, whose enthusiasm and support pushed me to reach further. Working with Paul has been an extraordinary opportunity both in the resources and in the vast wealth of knowledge that have been made available to me. I would also like to thank the other members of my dissertation committee, Dr. Susan Bookheimer, Dr. Mirella Dapretto, and Dr. Adriana Galvan, whose feedback and contributions are greatly appreciated.

Thank you to Dr. Matthew Prull, my undergraduate thesis advisor who first encouraged me to pursue neuroimaging research and for connecting me with Dr. Fumiko Hoeft. Thank you to Dr. Hoeft for being my first mentor in neuroimaging, and taking me on as a summer research assistant even when that meant starting from the beginning with linux commands! Thank you to Dr. Ian Gotlib for helping me realize that research is truly what I want to do. Thank you to Dr. Moriah Thomason for being an endless source of advice and support, for being a terrific role model, for being a rock star, and for putting me in contact with Paul. Thank you to all the members of the Imaging Genetics Center, for creating the most supportive, fun, and yet highly productive environment possible! A huge thanks is owed to Dr. Neda Jahanshad. It is very telling that she is 2nd author on nearly all of my papers; she has been an incredible source of knowledge and a very patient teacher. Thank you to Madelaine Daianu, Talia Nir, Julio Villalon, Meredith

Braskie, Derrek Hibar, Omid Kohannim, Liang Zhan, Nicholus Warstadt, and all other members of Dr. Thompson's group.

Thank you to my neuroscience IDP classmates, I would have never made it through without our study groups, and I can genuinely say that I enjoyed graduate school because of our movie nights, Joshua Tree trips, and WON events. Thank you to my fiancé, Jeff Diamond. Your continuing support and encouragement keep me going. Thank you for sticking with me even when it seemed as though I was addicted to my computer.

Lastly, thank you to my family. I would never have made it here without them. Thank you to my grandparents for one of the greatest gifts of all – an education. Thank you to my parents, Susan and Harry, and brother, Owen, for your support, love, and for patiently listening when I bumble through an explanation of one of my projects.

Co-author Acknowledgements

Chapters 1 through 4 are based on the following articles, I would like to thank all of the co-authors for their contributions:

- **Dennis EL** & Thompson PM (2013a). Mapping Connectivity in the Developing Brain. *International Journal of Developmental Neuroscience*, 31(1), 525-542.

- **Dennis EL**, Jahanshad N, Toga AW, McMahon KL, de Zubicaray GI, Martin NG, Hickie IB, Wright MJ, Thompson PM. (2013b). Development of Brain Structural Connectivity between Ages 12 and 30: A 4-Tesla HARDI Study in 439 Adolescents and Adults. *NeuroImage*, 64(1), 671-684.

- **Dennis EL**, Jahanshad N, Toga AW, McMahon KL, de Zubicaray GI, Martin NG, Hickie I, Wright MJ, Thompson PM. (2013c). Development of the "Rich Club" in Brain

Networks from 438 Adolescents and Adults Aged 12 To 30. In *Proc. 10th IEEE ISBI*, San Francisco, 620-623.

- **Dennis EL**, Jahanshad N, McMahon KL, de Zubicaray GI, Martin NG, Hickie IB, Toga AW, Wright MJ, Thompson PM. (2013d). Development of Insula Connectivity Between Ages 12 and 30 Revealed by High Angular Resolution Diffusion Imaging (HARDI). *Human Brain Mapping*, In Press.

- **Dennis EL**, Jahanshad N, Rudie JD, Brown JA, Johnson K, McMahon KL, de Zubicaray GI, Montgomery G, Martin NG, Wright MJ, Bookheimer SY, Dapretto M, Toga AW, Thompson PM. (2011a). Altered Structural Brain Connectivity in Healthy Carriers of the Autism Risk Gene, *CNTNAP2. Brain Connectivity*, 1(6), 447-459.

- **Dennis EL**, Jahanshad N, Braskie MN, Warstadt NM, Hibar DP, Kohannim O, Nir T, McMahon KL, de Zubicaray GI, Montgomery G, Martin NG, Toga AW, Wright MJ, Thompson PM. (2013e). Obesity Gene *NEGR1* Affects White Matter Integrity Differently in Young and Old Adults. *NeuroImage,* **Submitted Oct 21**.

- **Dennis EL**, Jahanshad N, McMahon KL, de Zubicaray GI, Martin NG, Wright MJ, Hickie IB, Toga AW, Thompson PM. (2013f). Differences in "Rich Club" Organization Associated with Intelligence. **In Preparation.**

- **Dennis EL**, Jahanshad N, McMahon KL, de Zubicaray GI, Martin NG, Wright MJ, Hickie IB, Toga AW, Thompson PM. (2013g). Differences in Structural Connectivity Associated with Educational Attainment. **In Preparation.**

VITA

2006-2007   Summer research assistant at the Center for Interdisciplinary Brain Sciences
Research (CIBSR) with Dr. Fumiko Hoeft, Stanford University

2008   BA in Psychology at Whitman Collge

2008-2010   fMRI project coordinator/technologist at the Mood and Anxiety Disorders
Laboratory with Dr. Ian Gotlib, Stanford University

2007   Awarded Whitman Internship Grant to work at CIBSR

2008   Graduated Cum Laude, Whitman College

2010   Pacific Rim Neuroimaging Travel Fellowship recipient

2012   International Symposium on Biomedical Imaging (ISBI) Travel Award

2013   ISBI Best Student Paper Award

2013   Kappa Alpha Theta Betty B. and James B. Lambert Scholarship

2010-present   Co-author on 14 peer-reviewed publications, 9 peer-reviewed conference papers,
and 17 conference abstracts

2011-present   Invited peer-reviewer for NeuroImage, Human Brain Mapping, Journal of
Neuroscience, Medical Image Computing and Computer Assisted Intervention,
Psychiatry Research: Neuroimaging, Brain Imaging and Behavior, Research in
Autism Spectrum Disorders, Neurobiology of Aging

2012-present   Invited speaker for the International Symposium on Biomedical Imaging
(Barcelona, May 2012; San Francisco, April 2013), and the Medical Image
Computing and Computer Assisted Intervention: Mathematical Methods for Brain
Connectivity Workshop (Nagoya, September 2013)

SELECT PUBLICATIONS

1. **Dennis EL**, et al. *Anxiety Modulates Insula Recruitment in Resting-State Functional Magnetic Resonance Imaging in Youth and Adults.* Brain Connectivity. 2011b. 1(3):245-254.

2. **Dennis EL**, et al. *Altered Structural Brain Connectivity in Healthy Carriers of the Autism Risk Gene, CNTNAP2.* Brain Connectivity. 2011a. 1(6):447-459.

3. **Dennis EL**, Jahanshad N, Toga AW, McMahon KL, de Zubicaray GI, Martin NG, Wright MJ, Thompson PM. *Test-retest Reliability of Graph Theory Measures of Structural Brain Connectivity.* In Proc. 15th MICCAI, Nice. 2012. 305-312. (peer reviewed conference paper).

4. **Dennis EL**, et al. *Development of Brain Structural Connectivity between Ages 12 and 30: A 4-Tesla HARDI Study in 439 Adolescents and Adults.* NeuroImage. 2013b. 64(1):671-684.

5. Rudie J, et al. *Altered Functional and Structural Brain Network Organization in Autism.* NeuroImage: Clinical. 2013. 2:79-94.

6. **Dennis EL**, et al. *Development of the "Rich Club" in Brain Networks from 438 Adolescents and Adults Aged 12 To 30.* In Proc. 10th IEEE ISBI. 2013c. 620-623. (peer reviewed conference paper and platform talk). **ISBI 2013 Best Student Paper Award Winner.**

7. **Dennis EL**, et al. *Development of Insula Connectivity Between Ages 12 and 30 Revealed by High Angular Resolution Diffusion Imaging (HARDI).* Human Brain Mapping. 2013d. In Press, accepted March 4, 2013.

8. **Dennis EL** & Thompson PM. *Mapping Connectivity in the Developing Brain.* International Journal of Developmental Neuroscience. 2013a. 31(1):525-542.

9. **Dennis EL**, et al. Rich Club Analysis of Structural Brain Connectivity at 7 Tesla versus 3 Tesla. *MICCAI 2013 Mathematical Methods for Brain Connectivity Workshop, Nagoya.* 2013f. 10-17 (peer-reviewed conference paper).

10. Warstadt NM, et al. *Serum Cholesterol and Cholesterol Gene CETP Affects White Matter Integrity.* Neurobiol Aging. 2013. **Submitted Oct 21.**

11. **Dennis EL**, et al. *Obesity Gene NEGR1 Affects White Matter Integrity Differently in Young and Old Adults.* NeuroImage. 2013e. **Submitted Oct 21**.

12. **Dennis EL** & Thompson PM. *Functional Connectivity and Aging in Alzheimer's Disease.* Neuropsychology Review. 2013h. **Submitted Oct 23**.

CHAPTER 1

Introduction

There has been tremendous growth in the field of brain connectivity, as both the technology to assess connectivity improves, and the applications expand. Combined with existing and ever-improving knowledge about brain structure and function, research into brain connectivity is the third pillar necessary for a comprehensive understanding of the brain. Many psychiatric disorders begin to surface in adolescence, highlighting the importance of studying connectivity during this developmental stage. Traumatic brain injury during development can be especially detrimental to later cognitive function. By defining the developmental trajectory in typically developing individuals, we can determine how and when individuals with disorders or injury deviate from the typical trajectory. Further, as we know that many psychiatric disorders are genetically influenced, we can map how risk genes associated with psychiatric disorders are linked with brain connectivity in the hopes of elucidating the mechanisms of disease. For common risk genes, examining effects in healthy populations has some benefit in that the effect of the disorder itself on the brain does not need to be considered. Finally, understanding the cognitive correlates of connectivity measures is a necessary step for tying these measures, some of which can be highly mathematical, back to measures that are more tangible and more clearly associated with brain function.

The following section, 1.1 Mapping connectivity in the developing brain, gives an introduction to the work that has been done mapping structural and functional connectivity across development, both in typically developing individuals, and in individuals with neurodevelopmental disorders. In addition, this section gives an introduction the methods used in

1

this dissertation, including high angular resolution diffusion imaging (HARDI), tractography, and graph theoretical analyses. Further details of the rich club organization of the brain are discussed in section 1.4. Background and methods for Aims 2 and 3 will be covered in sections 1.2, 1.3, and 1.4. The vast majority of these analyses have been completed on data from the Queensland Twin Imaging study (QTIM), a 5-year project collecting neuroimaging, genetic, and cognitive measures on healthy twins. Most of the twins are between 20-30 years old, with additional cohorts collected at 12 years old and 16 years old. The demographics for this study are shown in **Table 1**.

	N (m/f)	Age	Zygosity (MZ/DZ/sib)
12 year old cohort	53 (26/27)	12.31 (0.18)	16/37/0
16 year old cohort	63 (35/28)	16.17 (0.36)	17/46/0
20-30 year old cohort	1051 (404/647)	22.86 (2.84)	389/556/106
Total	1167 (459/708)	21.97 (3.85)	422/639/106

Table 1. Demographic summary of the QTIM dataset. The dataset is broken into 3 main cohorts. Total number, male/female ratio, average age and standard deviation, and the number of monozygotic, dizygotic, and siblings are given for each cohort, and in total.

1.1   Mapping connectivity in the developing brain

This section is adapted from:

Dennis EL & Thompson PM (2013). Mapping Connectivity in the Developing Brain. *International Journal of Developmental Neuroscience*, 31(1), 525-542.

Review

Mapping connectivity in the developing brain

CrossMark

Emily L. Dennis *, Paul M. Thompson

Imaging Genetics Center, Laboratory of Neuro Imaging, UCLA School of Medicine, 635 Charles Young Drive South, Suite 225, Los Angeles, CA 90095-7334, USA

ABSTRACT

Recently, there has been a wealth of research into structural and functional brain connectivity, and how they change over development. While we are far from a complete understanding, these studies have yielded important insights into human brain development. There is an ever growing variety of methods for assessing connectivity, each with its own advantages. Here we review research on the development of structural and/or functional brain connectivity in both typically developing subjects and subjects with neurodevelopmental disorders. Space limitations preclude an exhaustive review of brain connectivity across all developmental disorders, so we review a representative selection of recent findings on brain connectivity in autism, Fragile X, 22q11.2 deletion syndrome, Williams syndrome, Turner syndrome, and ADHD. Major strides have been made in understanding the developmental trajectory of the human connectome, offering insight into characteristic features of brain development and biological processes involved in developmental brain disorders. We also discuss some common themes, including hemispheric specialization – or asymmetry – and sex differences. We conclude by discussing some promising future directions in connectomics, including the merger of imaging and genetics, and a deeper investigation of the relationships between structural and functional connectivity.

© 2013 ISDN. Published by Elsevier Ltd. All rights reserved.

Contents

* Corresponding author. Tel.: +1 323 442 7246.
  E-mail address: eldennis@ucla.edu (E.L. Dennis).

1. Introduction

After birth, the brain undergoes remarkable changes as it adapts and learns in a new environment. Over a century of neuroanatomical research has revealed how the brain changes structurally and functionally throughout development; the last thirty years have also seen the widespread use of brain imaging to probe functional activation and coherence, as well as other dynamic brain changes (reviewed by Casey et al., 2000). In addition to understanding these changes, it is equally important to understand how the underlying structural and functional connectivity of the mature adult brain are set up and refined in childhood and adolescence. With novel variants of MRI – such as diffusion imaging and resting state functional MRI – we now have the technology to image neural pathways reliably, and to assess relationships between the activity of different brain regions, opening up new avenues for research.

Diffusion weighted imaging (DWI) is a method that allows us to visualize the diffusion of water along axons and thus visualize axonal pathways. Originally based on the observation that the MRI signal is reduced when water is diffusing (Stejskal and Tanner, 1965), increasingly elaborate scanning methods were developed to assess the primary directions in which water is diffusing, at each location in the living brain. By modeling the directional diffusion of water as an ellipsoidal shape, or "tensor", at each voxel in the brain, diffusion tensor imaging (or DTI) may be used to follow the major fiber bundles of the white matter, and map smooth tracts running from one brain region to another. More recently, high angular resolution diffusion imaging (HARDI) has been developed, offering some advantages over DTI, as it can better map tracts in regions with crossing fibers (Jahanshad et al., 2011). Fractional anisotropy (FA), the degree to which water tends to diffuse in one concentrated direction (along the axon), is one of the most common measures used to assess axon integrity. Apparent diffusion coefficient (ADC) or mean diffusivity (MD) measures the overall magnitude of diffusion, regardless of the directions; low values for mean diffusivity indicate greater organization. As a general rule of thumb – which has many exceptions – higher FA and lower MD tend to reflect more highly developed, more strongly myelinated tracts, with a higher axonal conduction speed. Many comparisons of diseased versus normal subjects find lower FA and higher MD in disease—this is also a general trend in the studies below, but is not universally the case.

The improved ability to disentangle fibers that mix and cross results from collecting more diffusion-weighted images at more angles, in conjunction with mathematical models that can resolve more than one dominant fiber direction in any given voxel (Cetingul et al., 2012a, 2012b). HARDI – essentially a more advanced form of diffusion imaging than DTI – differs from DTI in collecting diffusion data in more directions. It models the overall diffusion profile at each point in the brain using orientation distribution functions (ODFs) instead of tensors. ODFs estimate the probability of diffusion in each direction at each voxel, instead of assigning a single dominant diffusion direction to a given voxel (Tournier et al., 2004). For these reasons, HARDI is better at resolving crossing fibers (such as the corpus callosum and the long association fibers), a major issue for DTI (Tuch et al., 2002). These can then be separated and individually analyzed, giving a more accurate view of the brain's anatomical connections (Zhan et al., 2009a; Jin et al., 2012). As more directional scans are collected, longer scan times are needed, and

this has provoked major efforts to speed up diffusion imaging (Zhan et al., 2011).

Resting-state fMRI (rsfMRI) is a branch of research based on the idea that distant brain regions can be functionally coupled, whether or not they are structurally connected. Rs-fMRI data can be collected either in the presence or absence of a task. This coupling can be measured through the blood oxygenation level dependent (BOLD) time-courses of these distant regions. The phenomenon of synchronized low-frequency fluctuations (~0.01–0.1 Hz) in the BOLD signal of known functional networks was first found by Biswal et al. (1995), and led to the discovery of a number of temporally coherent networks (Damoiseaux et al., 2006; Fox et al., 2005) that have been replicated across individuals (Beckmann et al., 2005) and have high test-retest reliability, even in children (Thomason et al., 2011). There are three main methods to assess functional connectivity that we will consider here: seed-based, ICA (i.e., independent components analysis), and graph theory. In the seed-based approach, the researcher extracts the time course of a seed (region of interest) and then correlates that time course with the time courses of the rest of the voxels in the brain, to search for matches (Fox and Raichle, 2007). Brain regions with a high degree of positive correlation with the seed – i.e., those with a very similar time course – are thought to be functionally coupled. ICA (independent components analysis) is model-free, meaning that the researcher does not select a seed or ROI. Rather, the four-dimensional resting-state data can be decomposed into time courses and associated spatial maps, describing the temporal and spatial characteristics of the components making up the data (Beckmann et al., 2005). The same intrinsic connectivity networks (ICNs) can be seen with both seed-based and ICA approaches, and each method offers some advantages and disadvantages. Many possible roles have been attributed to ICNs, including memory functions, organization and coordination of neuronal activity, and priming the brain for coordinated activity (Fox and Raichle, 2007; Seeley et al., 2007). ICNs are altered in a wide range of psychiatric and developmental disorders, further motivating the need to establish how they develop in healthy individuals (Greicius, 2008), as well as metrics of normal brain function based on resting state data.

More pragmatically, there is also a major effort to understand how quickly information on brain connectivity can be collected, with techniques available today. When young children are assessed, scan times should be as short as possible without sacrificing important information, to avoid placing undue burden on the participants (Jahanshad et al., 2010; Zhan et al., 2008, 2009b, 2012a). Ongoing work is also determining how the chosen scanning protocols affect the maps of brain connectivity that are recovered (Zhan et al., 2012b). Clearly, the ability to pool and compare data collected worldwide on brain connectivity – including changes across development – depends on understanding how connectivity measures might depend on the scanners, protocols and methods used to extract maps of the brain's connections.

In this review, we will cover developmental changes in functional and structural connectivity in healthy, typically developing individuals (Table 1), along with a few illustrative examples of how connectivity may be disrupted in developmental disorders (Table 2). There is a much wider body of research covering how functional and structural connectivity are affected in individuals with neurological or psychiatric disorders, but those are beyond the scope of this review (Greicius, 2008; Lim and Helpern, 2002; Sexton et al., 2009; Seyffert and Silva, 2005; Uddin et al., 2010; please also

Table 1
Studies of age effects on structural and functional connectivity in typically developing subjects covered in this review.

Authors	Ages studied	Func(tional) or Struct(ural)	Analyses
Morriss et al. (1999)	30 subjects, 1 day–17 y	Struct	DTI
Mukherjee et al. (2001)	153 subjects, 1 day–11 y	Struct	DTI
Zhai et al. (2003)	20 neonates, 8 adults (mean age 28 y)	Struct	DTI
Gilmore et al. (2004)	20 neonates	Struct	DTI
Ben Bashat et al. (2005)	36 subjects, 4 mo–23 y	Struct	DTI, DWI
Barnea-Goraly et al. (2005)	30 subjects, 6–19 y	Struct	DTI
Schneider et al. (2004)	52 subjects, 1 day–16 y	Struct	DTI (high angular resolution)
McLaughlin et al. (2007)	10 subjects, 7–12 y; 36 sub 13–18 y, 25 sub 25–40 y, 11 sub 60–80 y	Struct	DTI
Hasan et al. (2009a,b)	36 subjects, 6–19 y; 63 subjects, 20–59 y	Struct	DTI, tractography
Giorgio et al. (2008)	42 subjects, 13–21; 20 subjects, 23–42 y	Struct	DTI (high angular resolution)
Gao et al. (2009a)	60 subjects, 3 weeks–2 y	Struct	DTI
Kochunov et al. (2010)	831 subjects, 11–90 y	Struct	DTI
Asato et al. (2010)	114 subjects, 8–28 y	Struct	DTI
Chiang et al. (2011)	705 subjects, 12–29 y	Struct	DTI
Supekar et al. (2010)	In total: 23 sub 7–9 y, 22 sub 19–22 y, for DTI: 18 sub 7–9 y, 15 sub 19–22 y	Struct and Func	DTI, tractography, ICA
Taki et al. (2012)	246 subjects 5–19 y	Struct	DTI
Jahanshad et al. (2012)	615 subjects 20–30 y	Struct	DTI
Gong et al. (2009)	95 subjects 19–85 y	Struct	graph theory
Hagmann et al. (2010)	30 subjects 18 mo–18 y	Struct	graph theory
Fan et al. (2011)	28 subjects 1 mo–2 y (longitudinal)	Struct	graph theory
Dennis et al. (2013)	439 subjects 12–30 y	Struct	graph theory
Redcay et al. (2007)	13 subjects 30–50 mo	Func	seed-based
Lin et al. (2008)	38 sub 2–4 w (26 1 y, 21 2y	Func	seed-based
Fair et al. (2008)	66 sub 7–9 y, 53 10–15 y, 91 19–31 y	Func	seed-based
Kelly et al. (2009)	14 sub 8–13, 12 13–17, 14 19–24	Func	seed-based
Dosenbach et al. (2010)	61 sub 7–11 y, 61 24–30 y	Func	seed-based
Fransson et al. (2007)	12 premature 24–27 w GA	Func	ICA
Liu et al. (2008)	11 sub 11–14 mo	Func	ICA
Thomason et al. (2008)	16 sub 9–12 y	Func	ICA
Gao et al. (2009b)	20 neonates, 24 1 y, 27 2 y, 15 adults (mean age 30)	Func	ICA, graph theory
Stevens et al. (2009)	100 sub 12–30 y	Func	ICA, Granger causality
Thomason et al. (2011)	65 sub 9–15 y (longitudinal)	Func	seed-based/ICA
Fair et al. (2007)	49 sub 7–9 y, 43 10–15 y, 47 21–31 y	Func	graph theory
Supekar et al. (2009)	23 sub 7–9 y, 22 19–22 y	Func	graph theory
Fair et al. (2009)	66 sub 7–9 y, 53 10–15 y, 91 19–31 y	Func	graph theory

Y indicates years, mo indicates months when referring to age of subjects. GA: gestational age, func: functional, struct: structural.

see our previous review: Thomason and Thompson, 2011). Here we consider a few developmental disorders that have been linked to alterations in structural and/or functional connectivity: autism, fragile X syndrome, 22q11.2 DS (deletion syndrome), Williams syndrome, ADHD (attention deficit hyperactivity disorder), and Turner syndrome. A few other recent reviews focus on the development of functional connectivity (Power et al., 2010; Uddin et al., 2010) or structural connectivity (Cascio et al., 2007; Schmithorst and Yuan, 2010) either in typically developing or atypically developing individuals (Uddin et al., 2010; Walter et al., 2009). Here we consider how structural and functional connectivity develop in typically developing subjects and subjects with developmental disorders. Measures of structural and functional connectivity are related, and the patterns of coherent activity depend on the anatomical scaffolding where they take place. Establishing the developmental trajectory of these measures in typically developing individuals is critical to a thorough understanding of disorders that may affect them.

2. Structural brain development in healthy subjects

2.1. Developmental studies using structural MRI in typically developing individuals

Before we launch into our review of brain connectivity, first we give a brief background on brain structural development to put the subsequent sections in context. Changes in brain structure after birth are well established, from both *post mortem* and *in vivo* neuroimaging studies: the cerebrum increases in size into early adulthood (Giedd et al., 1999; Sowell et al., 2002; Gilmore et al., 2007; Knickmeyer et al., 2008), gray matter (GM) volume rises in infancy and then later decreases at different rates across the brain (Fig. 1; Giedd et al., 1999; Sowell et al., 1999, 2003a,b; Gogtay et al., 2004; Gilmore et al., 2007), and white matter (WM) volume increases well beyond adolescence into middle age (Giedd et al., 1999; Sowell et al., 2002; Gilmore et al., 2007; Knickmeyer et al., 2008). Rates of growth for different brain regions have even been mapped in neonates and infants, based on anatomical MRI (Gilmore et al., 2007; Knickmeyer et al., 2008). Building on early work by Gogtay et al. (2004), Shaw et al. (2008) found that cortical thickness follows different trajectories depending on the brain region. Intriguingly, the complexity of the growth trajectory of the brain region (linear vs. quadratic vs. cubic) seemed to correspond to the complexity of the laminar architecture. As a general principle, many of the last cortical areas to mature – those with the most protracted period of development – are typically those that are phylogenetically most recent and responsible for higher order cognitive processes, such as the frontal and prefrontal cortices (Gogtay et al., 2004). A great deal of work in developmental neuroscience has focused on studying the relatively late maturation and remodeling of the frontal lobe gray matter, which shows detectable changes on MRI well into late adolescence, long after the maturation of primary sensorimotor and visual cortices. It has been argued that the natural process of gray matter reduction in adolescence is abnormally intensified or derailed in some forms of psychosis, including schizophrenia. "Time-lapse maps" of abnormal cortical development show a dynamically spreading wave of adolescent gray matter loss in schizophrenia (Thompson et al.,
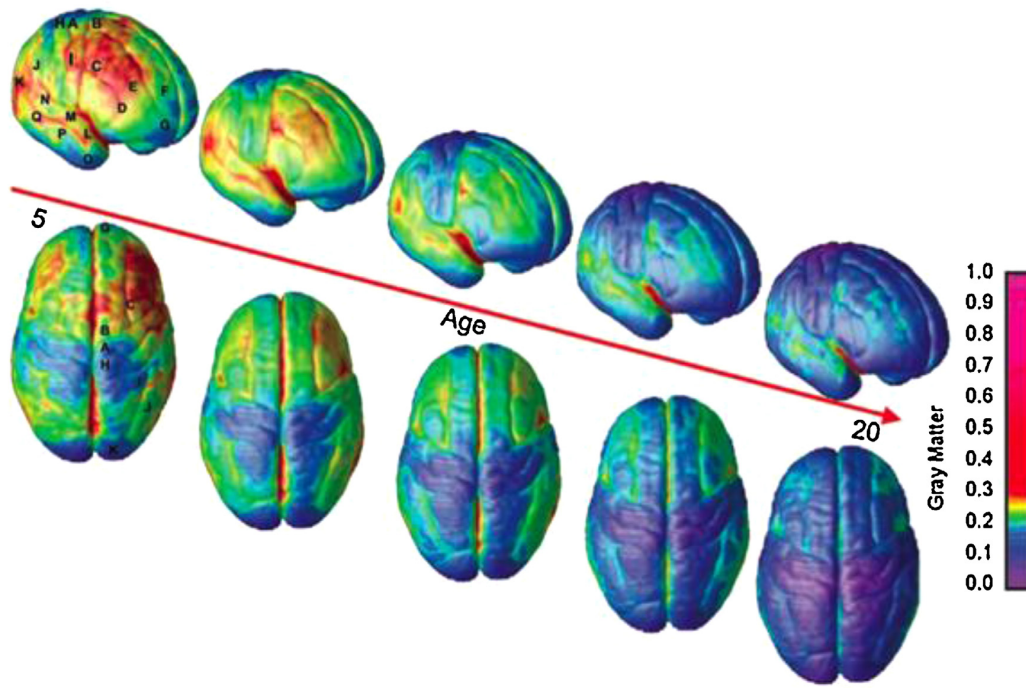
Fig. 1. Decreases in regional gray matter volume, in normal children, between age 5 and age 20. As a general principle of development, cortical regions that are concerned with more low-level, primary functions – such as vision and sensation – mature more quickly than the regions subserving higher order cognition. Here the loss of gray matter volume is thought to be due to greater myelination of the cortex, rather than solely due to synaptic and dendritic pruning. Vascular and glial changes many also play a role. Reprinted with permission from Gogtay et al. (2004).

2001; Vidal et al., 2006), which may even be partially opposed by some antipsychotics (Thompson et al., 2009). As the cellular basis of these cortical changes has remained enigmatic and hotly debated, there is renewed interest in whether new methods to probe brain connectivity will reveal more about normal changes in the frontal circuitry—whether connections are eliminated or "pruned", and to what extent aberrant myelination is implicated.

Zielinski et al. (2010) examined the structural covariance of regions known to be "seeds" for functional connectivity networks and found different trajectories for different networks. Some continuously grew in extent, while others peaked in adolescence and were then pruned. On a much smaller scale, Huttenlocher found that the number and density of synapses peaks within the first few years after birth, then steadily declines over the lifespan (Huttenlocher, 1990). The age at which synaptic number and density peaks differs for different brain regions (Huttenlocher and Dabholkar, 1997).

2.2. Developmental studies using diffusion weighted imaging in typically developing individuals

Changes in structural brain connectivity (i.e., anatomical connections) have been mapped using diffusion tensor imaging (DTI), and more recently with high angular resolution diffusion imaging (HARDI). Both HARDI and DTI allow us to non-invasively visualize axonal pathways *in vivo* by modeling the diffusion of water along axons. From the set of diffusion tensors at each point in the brain, we can determine vectors along which the diffusion is greatest and line them up to create smooth tracts (Fig. 2). A vast range of methods are available to perform fiber tracking—also known as tractography; the methods vary in terms of whether any manual interaction is needed, and whether they extract a specific tract in the brain

(such as the arcuate fasciculus, which is involved in language) or whether they extract all the fibers in the brain at once. Whole-brain tractography can extract all the fibers in the brain at once. The vast number of resulting curves can be clustered or grouped into bundles that an anatomist would recognize, prior to further analysis or cross-subject comparison. The integrity and geometry of the tracts can also be measured.

Morriss et al. (1999) scanned 30 subjects between 1 day old and 17 years old with DTI, and found a decrease in ADC across a number of WM areas with age. In cellular terms, the growth of myelin sheaths tends to restrict water diffusion, and the overall amount of diffusion (the ADC) tends to fall as the brain develops. In a retrospective analysis, Mukherjee et al. (2001) examined DTI data from 153 subjects between 1 day old and 11 years old and found increases in apparent anisotropy (AA; a measure similar to FA) in the corpus callosum (CC), basal ganglia and thalamus. Again, this is in line with a general pattern where higher FA values reflect more directionally constrained diffusion, which increases as children grow older, largely because of myelin sheaths hindering water diffusion across axons. Zhai et al. (2003) examined healthy adults and neonates with DTI and found higher ADC and lower FA in the CC, internal capsule (IC), and WM of the frontal and occipital cortex of neonates compared to adults, as expected. In another study of neonates, Gilmore et al. (2004) saw an increase in FA in the splenium of the CC with age. Gao et al. (2009a) scanned 60 subjects between 3 weeks and 2 years old and found that FA increased between 3 weeks and 1 year while axial and radial diffusivity decreased. Between 1 and 2 years old, however, only radial diffusivity showed a significant age effect, which makes sense as the primary barrier to diffusion, myelin, is hindering diffusion orthogonal to the axon. These were averaged over ROIs (regions of interest) across the CC, internal capsule, corticospinal tract, optic radiations, frontal peripheral and posterior peripheral WM.

7
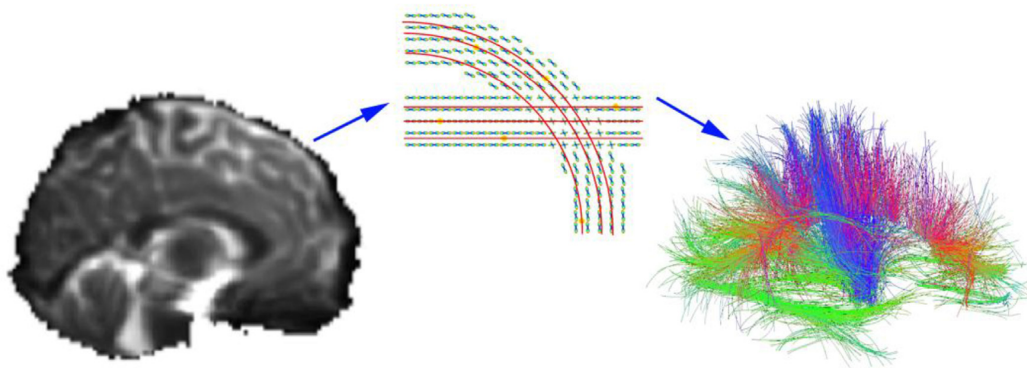
Fig. 2. Diffusion tensor imaging and tractography. In whole brain tractography, a set of diffusion weighted images (left) are collected to show how rapidly water is diffusing in a range of different directions. By sampling a large number of directions, a diffusion function (little crosses in the middle panel) can be reconstructed—the peaks in this function tend to point along axons and major tracts. Tract tracing algorithms can sew together the paths of maximal diffusion into curves and fiber bundles. The right panel shows the set of recovered fibers—red, green, and blue colors show the directions of the fibers. These can be grouped into meaningful anatomical bundles and their integrity and connectivity can be assessed. Adapted with permission from Aganj et al. (2011).

Covering a wider age range, Ben Bashat et al. (2005) scanned 36 subjects between 4 months and 23 years old with DTI and also found FA increasing in the CC, IC, and subcortical WM, leveling off in early adulthood. Similarly, Taki et al. (2012) examined the developmental trajectories of FA in 30 WM ROIs in 246 subjects aged 6–18 and found that FA increased with age across all ROIs. Covering the same age range, Barnea-Goraly et al. (2005) examined age-related

Table 2
Studies of age effects on structural and functional connectivity in subjects with developmental disorders covered in this review.

Authors	Disorder	Func or Struct	Analyses
Barnea-Goraly et al. (2004)	Autism	Struct	DTI
Ben Bashat et al. (2007)	Autism	Struct	DTI (high b value)
Barnea-Goraly et al. (2010)	Autism	Struct	DTI
Shukla et al. (2010)	Autism	Struct	DTI
Barnea-Goraly et al. (2003)	Fragile X	Struct	DTI
Haas et al. (2009)	Fragile X	Struct	DTI, tractography
Simon et al. (2005)	22q DS	Struct	DTI
Simon et al. (2008)	22q DS	Struct	DTI
Sundram et al. (2010)	22q DS	Struct	DTI
Villalon et al. (2013)	22q DS	Struct	DTI, tractography
Hoeft et al. (2007)	Williams	Struct	DTI, tractography
Arlinghaus et al. (2011)	Williams	Struct	DTI
Haas et al. (2011)	Williams	Struct	DTI, tractography
Jabbi et al. (2012)	Williams	Struct	DTI, tractography
Molko (2004)	Turner	Struct	DTI
Holzapfel (2006)	Turner	Struct	DTI
Yamagata et al. (2012)	Turner	Struct	DTI, tractography
Ashtari et al. (2005)	ADHD	Struct	DTI
Hamilton et al. (2008)	ADHD	Struct	DTI
Pavuluri et al. (2009)	ADHD	Struct	DTI
Silk et al. (2009)	ADHD	Struct	DTI, tractography
Li et al. (2011)	ADHD	Struct	DTI
Cherkassky et al. (2006)	Autism	Func	seed-based
Just et al. (2007)	Autism	Func	seed-based
Kennedy and Courchesne (2008)	Autism	Func	seed-based
Monk et al. (2009)	Autism	Func	seed-based
Noonan et al. (2009)	Autism	Func	seed-based
Weng et al. (2010)	Autism	Func	seed-based
Rudie et al. (2012b)	Autism	Func	seed-based
Debbané et al. (2012)	22q DS	Func	ICA
Kesler (2007)	Turner	Func	unknown
Bray et al. (2011)	Turner	Func	seed-based
Bray et al. (2012)	Turner	Func	seed-based
Cao et al. (2006)	ADHD	Func	Voxel-wise seed-based
Tian et al. (2006)	ADHD	Func	seed-based
Castellanos et al. (2008)	ADHD	Func	seed-based
Wang et al. (2009)	ADHD	Func	Graph theory

Func: functional, struct: structural.

effects on FA on a voxel-by-voxel basis in 34 subjects between 6 and 19 years old. FA increased with age in prefrontal regions as well as a number of subcortical regions. This is the general trend across adolescence (review by Schmithorst and Yuan, 2010). Two studies examining the corpus callosum across almost the entire lifespan found that both CC volume and FA increased from childhood into adulthood, then declined in the elderly (McLaughlin et al., 2007; Hasan et al., 2009a). Just like the rest of the brain, different regions of the CC follow different developmental trajectories (Thompson et al., 1999, 2000). Using a protocol with higher angular resolution, Schneider et al. (2004) examined WM regions of interest, including several across the corpus callosum, and found an exponential increase in FA between birth and age 12, leveling off around age 2. In contrast, they found that the FA of deep WM areas continued to increase throughout the age range of their participants, suggesting continuing maturation in these areas. Also using higher angular resolution, Giorgio et al. (2008) compared 42 adolescents to 20 young adults and found age-related increases in FA in the body of the corpus callosum and the right superior *corona radiata*.

In one of the largest DTI studies to date, Kochunov et al. (2010) examined the trajectory of FA across subjects aged 11–90, finding that FA, when averaged across nine major WM tracts, peaked around 32 years of age. The 'age at peak' for the FA of the nine tracts they studied varied widely, from 23 years for the sagittal stratum, which connects subcortical, temporal, and occipital regions, to 39 for the cingulum, connecting the cingulate gyrus and the entorhinal cortex. The only tract showing no significant age trends was the cortico-spinal tract (Kochunov et al., 2010); this fundamental tract for sensation and primary motor function develops so early that it is fully mature before the age range studied. In a similarly large study, Chiang et al. (2011) found that FA increased by as much as 10% between adolescence and adulthood. They also examined how the heritability of FA changes with age (i.e., how much of the observed variation in a population is due to genetic factors). Roughly twice as much of the variance in FA was explained by genetic factors in adolescents as was explained by genetic factors in adults (Chiang et al., 2011). Environmental factors (such as education and diet) also play an important role in shaping tract development as we age (Jahanshad et al., 2013a).

Asato et al. (2010) also examined this period of development, scanning 114 subjects between 8 and 28 years with DTI. Instead of FA, however, they looked at radial diffusivity (RD), a measure of the degree of restriction due to membranes, which is thought to be more closely related to demyelination than other DTI measures (Asato et al., 2010). The last tracts to reach maturity were those
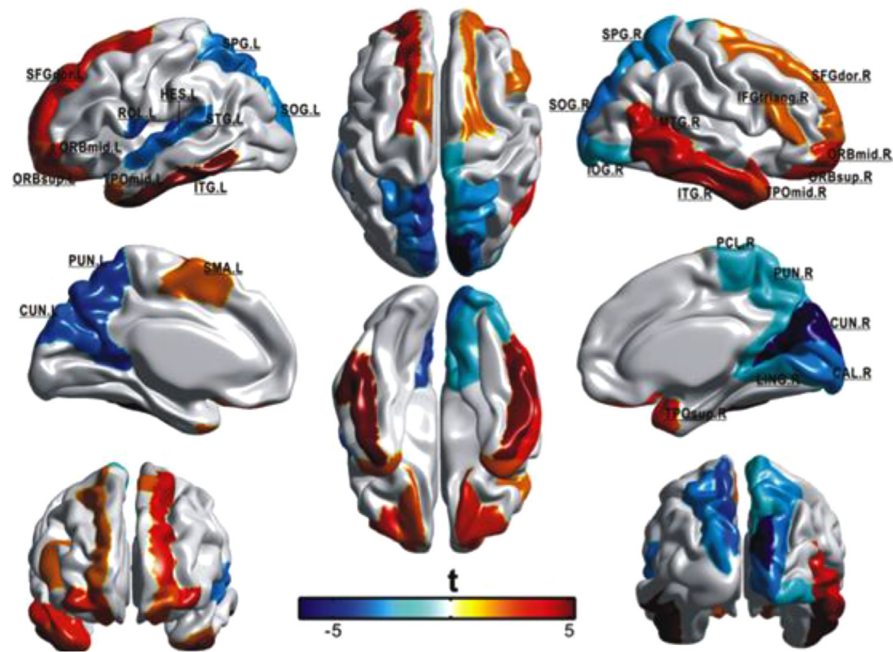
Fig. 4. Regions that show age-related effects in regional efficiency in 95 subjects 19–85 years old. Red indicates increases in efficiency with age, blue indicates decreases in efficiency with age. Reprinted with permission from Gong et al. (2009). See Gong et al. (2009) supplemental material for abbreviations of cortical regions.

where the most active connections are maintained, while others die off, leading to a more clearly defined network with hubs and clusters.

Another network measure, *Gamma*, is MCC normalized to what its value would be in artificially created random networks, with the same numbers of nodes and connections. *Global efficiency* is the inverse of CPL—networks with a lower CPL are more efficient. Another popular concept – "*small-worldness*" – represents the balance between network differentiation and integration. *Modularity* is the degree to which a system may be subdivided into smaller networks. *Degree* is the number of nodes to which a given node is connected; *strength* is the degree in a weighted (instead of binarized) network. *Regional efficiency* is efficiency calculated on nodal neighborhoods. Graph theory can be applied to structural or functional networks (Rubinov and Sporns, 2010).

There are still relatively few studies examining how graph theory metrics of structural brain connectivity change with development. Gong et al. (2009) examined the standard network measures calculated from connectivity probability matrices generated from diffusion images in 95 subjects between ages 19 and 85. Overall connectivity and local efficiency decreased with age, and there was a shift in regional efficiency from some brain regions to others (Fig. 4). Hagmann et al. (2010) studied changes in connection density matrices from the diffusion images of 30 subjects aged 18 months to 18 years old. They examined these matrices with two parcellations with different numbers of nodes, and found increases in node strength and global efficiency as well as decreases in clustering coefficient. Fan et al. (2011) studied these measures longitudinally in very young subjects, between 1 month and 2 years old. They found increases in network efficiency and modularity with age.

Our group has investigated these questions as well, generating fiber density matrices from HARDI data in 439 subjects aged 12–30 (Dennis et al., 2013). Path length, mean clustering coefficient, gamma (normalized clustering), small-worldness, and modularity all decreased with age, suggesting that this period of development is marked by an increase in network integration. Interestingly, the left and right intrahemispheric networks, when analyzed separately, showed opposing age trends, with a number of parameters increasing with age in the left hemisphere while they decreased in the right. If this is corroborated in future studies, it could point to different developmental processes occurring in each hemisphere, perhaps due to the known structural asymmetry of the brain. We also found age effects in the fiber density matrices, with more connections decreasing in fiber density than increasing. In these analyses, for a connection between two regions of interest, the fiber density is defined as the proportion of the total number of recovered fibers in the brain that pass between those two regions. However, these increases and decreases were not distributed evenly around the brain, consistent with prior research pointing to different developmental trajectories for various brain regions (Fig. 5).

3. Functional brain development in healthy subjects

In functional connectivity analyses, the activity of several different brain regions is assessed, and the relationship between them is studied and modeled. This may be done in several different ways, depending on whether the researcher is interested in the correlations in the time courses of activation between a given pair (or all pairs) of brain regions. The statistical coherence of activity measured from different parts of the brain can also be studied, including more complex measures such as mutual information. The coordination of distant regions during rest is thought to be involved in coordinating and organizing neuronal activity (Fox and Raichle, 2007).

3.1. Developmental studies using seed-based or ICA rsfMRI approaches in typically developing individuals

Studies of functional connectivity using resting-state functional MRI have also yielded substantial data on typical brain changes during development. Supekar et al. (2010) examined developmental changes in the structural and functional connectivity of the nodes of the "*default mode network*" (DMN). The DMN is a generally thought

9
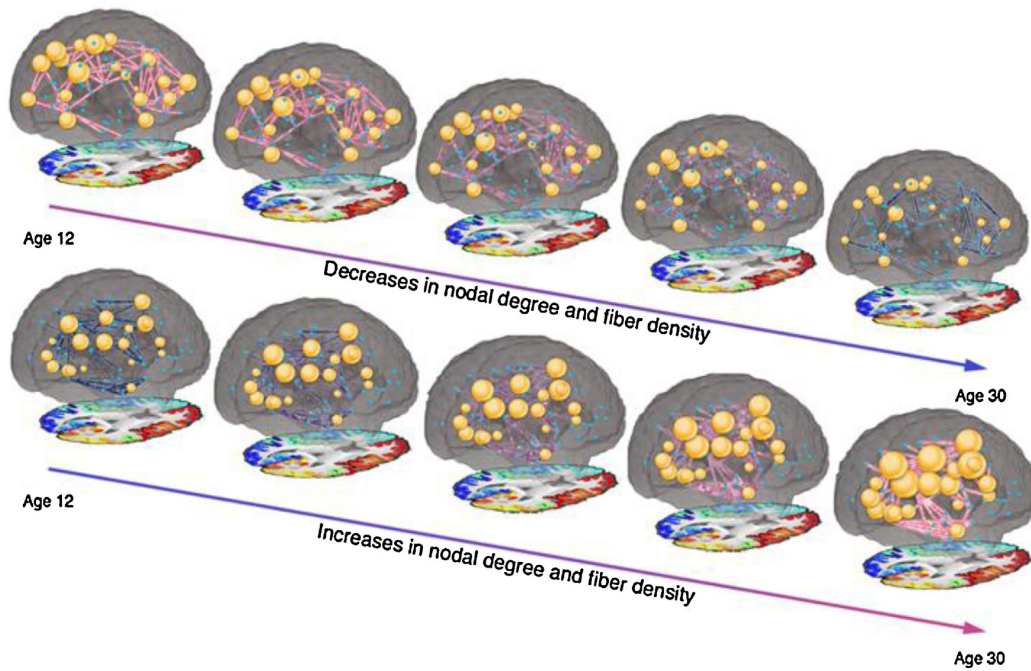
Fig. 5. Age-related increases and decreases in nodal degree and edge fiber density in 439 subjects aged 12–30. This study is based on HARDI, a form of diffusion imaging that can be used to recover anatomical connections. Colors correspond to the fiber density, with red indicating greater values and blue indicating smaller values. The diameter of nodes corresponds to their degree. Reprinted with permission from Dennis et al. (2013).

to include the posterior cingulate cortex (PCC), medial prefrontal cortex (mPFC), inferior parietal lobules, lateral temporal cortices, and hippocampal formation (Buckner et al., 2008; Raichle et al., 2001). These regions tend to be more active during rest than during a task, hence the name 'default mode', or 'task negative' network (Fox et al., 2005). Supekar et al. (2010) also found that the fiber density and FA of the connection between the PCC and the mPFC was greater in young adults than in children (Fig. 6).

Using the seed-based approach, Redcay et al. (2007) examined functional connectivity in 13 subjects between 30 and 50 months old with seeds from tasks completed in the same scan session. They detected functional connectivity between the auditory system and the prefrontal cortex (PFC) but not between the visual system and PFC. Looking at a similar age group, Lin et al. (2008) examined the visual and sensorimotor networks of 38 subjects. Both the strength of the connectivity, and the percentage of the brain volume participating in the networks, increased with age. In a study of 12 premature infants between 24 and 27 weeks gestational age, Fransson et al. (2007) used ICA and were able to identify networks in the visual, auditory, motor and somatosensory, and prefrontal cortices, as well as one including areas of the parietal cortex and cerebellum. Networks were largely characterized by short-range connections, and they did not detect a DMN. Liu et al. (2008) also used ICA to examine connectivity in very young subjects (11 sub 11–14 months) while asleep, and found a midline parietal network and a sensorimotor network (that separated into two lateralized networks in most subjects), suggesting greater intrahemispheric than interhemispheric connectivity. Similarly, Gao et al. (2009a,b) scanned 71 subjects ranging from neonates to 2 years old and used ICA to detect the DMN. They found a primitive DMN in neonates that grew through age 2 to include some of the same regions found in the adult DMN. They also identified some additional regions not typically seen in the adult DMN. The PCC and MPFC were the two adult

DMN regions that were present throughout all three developing groups as well.

Examining later stages of development, Fair et al. (2008) scanned 210 subjects between 7 and 31 years old and compared connectivity within the DMN. Children had sparser connections
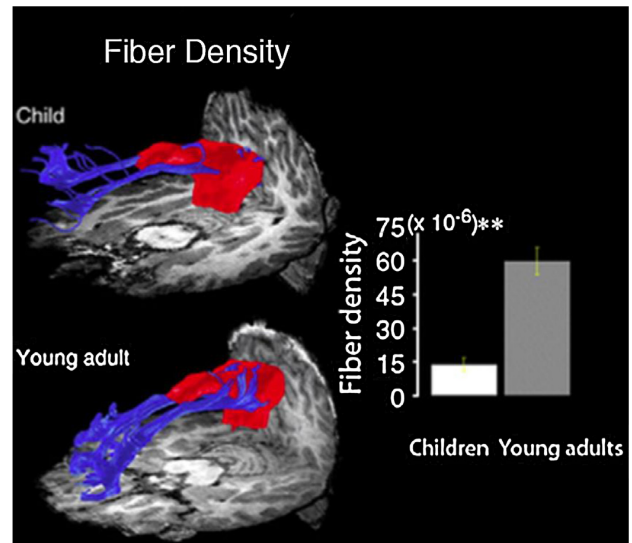
Fig. 6. Maturation of the connection between the PCC (posterior cingulate cortex) and mPFC (medial prefrontal cortex), two main hubs of the DMN (default mode network) between 18 7–9 year olds and 15 19–22 year olds. DTI tractography depicting developmental effects in fibers between PCC and mPFC. Bar graph showing significant difference in fiber density ($p \ll 0.0001$, indicated by **). Reprinted with permission from Supekar et al. (2010).
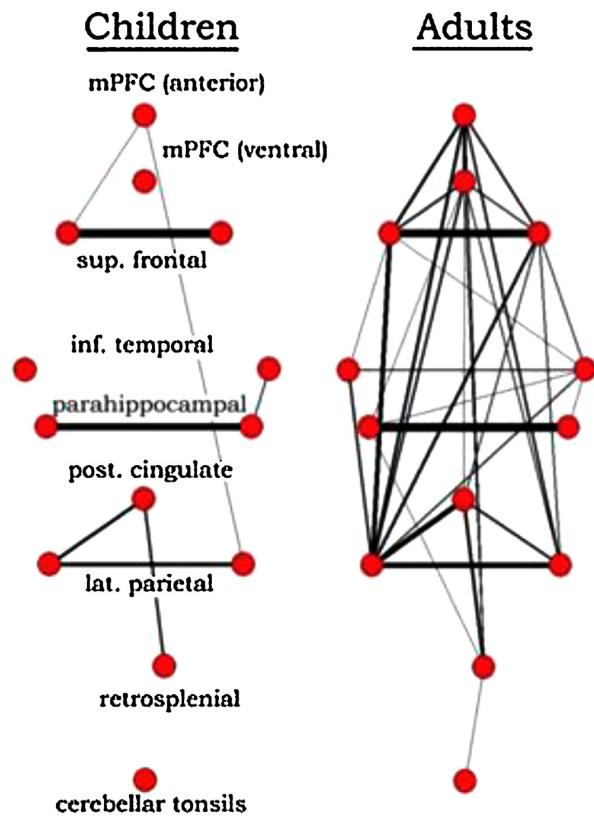
Children   Adults

Fig. 7. Differences in the connectivity of the DMN between children (7–9 y) and adults (21–31 y). Graph visualization of DMN regions in children and adults generated by correlating the time series' of 13 regions, including hubs of the DMN. In children (7–9 years old), DMN regions are sparsely connected, while they appear highly integrated in adults (21–31 years old). Reprinted with permission from Fair et al. (2008).

between DMN seeds than did adults (Fig. 7). Kelly et al. (2009) looked at ICNs generated by using 5 seeds for 40 subjects in the cingulate cortex and found that children had more diffuse patterns of connectivity in voxels proximal to the seed, while over adolescence and into adulthood there were more focal patterns of local connectivity. Adults also had a greater number of long-range connections than did children. This was most apparent in networks that included areas responsible for conflict monitoring, emotion regulation, and mentalizing. Providing strong support for using rsfMRI measures as biomarkers, Dosenbach et al. (2010) were able to classify individuals as either children (7–11 y) or adults (24–30 y) with 91% accuracy using multivariate pattern analysis and an SVM (support vector machine) algorithm. They scanned 238 subjects and generated time courses for 160 ROIs for use in their algorithm. Impressively, they were able to replicate these results with a different data set.

Using ICA, Thomason et al. (2008) studied the DMN in 16 subjects aged 9–12 years to verify that the regions of the DMN in children are indeed those that deactivate during cognitive tasks. They also found evidence of greater integration between the DMN and sensory regions in children. Stevens et al. (2009) scanned 100 subjects between 12 and 30 years and examined the relationships between networks using ICA and 'Granger causality'—a statistical hypothesis test for deciding when one time-series is useful for forecasting another. Where there were age effects, they were decreases in connection strength between networks with age, reflecting a trend towards differentiated networks. Specifically, they found

decreases in the influence that some networks had on the DMN. Supekar et al. (2010) used ICA to investigate age-related effects on the DMN in 45 subjects in two age cohorts. The DMN in children had weaker connectivity and included a smaller portion of the mPFC. This resulted in lower functional connectivity between the mPFC and the PCC, a central node of the DMN. Using seeds motivated by ICA analysis, Thomason et al. (2011) detailed the ICNs of 65 children/adolescents between 9 and 15 years old (Fig. 8). 21 of the 65 subjects were scanned a second or third time, allowing for longitudinal analyses. They found that the within-session Kendall's *W* concordance ranged between 0.71 and 0.78 across the whole brain, while between sessions it was 0.60–0.65, supporting the notion that rsfMRI can be reliably assessed in children.

3.2. Developmental studies using functional graph theory analyses in typically developing individuals

Graph theory may also be applied to study functional connectivity, using any measure of functional coupling between nodes that can be expressed in a connectivity matrix–correlation, coherence, or mutual information (Bullmore and Sporns, 2009). So far, developmental studies of functional connectivity with graph theory are few. Fair et al. (2007) examined 210 subjects in three different age cohorts between 7 and 31 years old and extracted the time courses for 39 ROIs. In graph analyses of the connectivity matrices, adults had both greater integration within networks and greater segregation between networks than did children. Both of these processes are important for establishing mature networks that can support specific functions, while also efficiently participating in the brain network as a whole. In a larger sample including the same subjects, Fair et al. (2009) found that the pattern of functional connectivity matures from being more anatomically based to being more functionally based. Initially, functional networks are organized by lobe, but across development connections within the lobe weaken as networks segregate. Concurrently, in childhood, networks such as the DMN are initially segregated, and they consist of many spatially distributed regions. Across development, however, functional networks such as the DMN become more cohesive (Fig. 9). In a similar age group, Supekar et al. (2009) also examined ICNs and whole brain connectivity using graph theory in 45 subjects in two age groups (7–9 years and 19–22 years). Results did depend on the frequency range examined, so the authors chose to focus on one. Children had lower levels of hierarchical organization than adults, as well as stronger subcortical–cortical connectivity and weaker cortico-cortical connectivity. Additionally, the authors saw a shift from stronger short-range connections in children to stronger long-range connections in adults, consistent with many other studies on this topic.

4. Structural and functional connectivity in atypical brain development

4.1. Autism

Autism is a prevalent neurodevelopmental disorder marked by deficits in communication and social interaction, and by repetitive behavior. It has some genetic basis, but the large and increasing number of genes linked to autism indicates a rather complicated mechanism (Szatmari et al., 2007). Diffusion imaging studies show widespread disruption of white matter tracts, especially between regions implicated in social behavior (Barnea-Goraly et al., 2004, 2010; Shukla et al., 2010). Ben Bashat et al. (2007) found evidence to support abnormally *accelerated* maturation of white matter in children with autism, consistent with earlier morphometric work that showed accelerated brain growth in infancy, for at least one subgroup of children with autism.
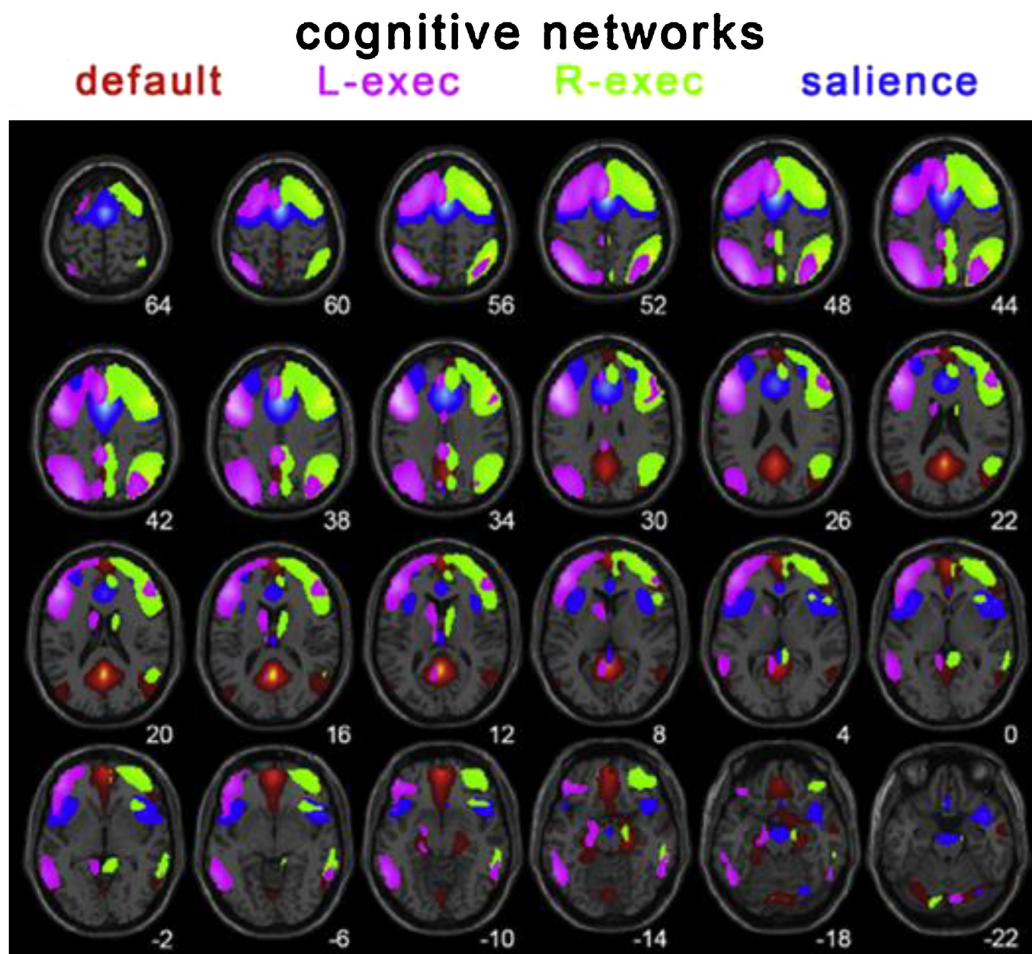
Fig. 8. Spatial renderings of components corresponding to the default (red), left executive (pink), right executive (green) and salience networks (blue) generated from group ICA analysis of 65 children aged 9–15 years. Reprinted with permission from Thomason et al. (2011).

A number of studies have examined ICNs (intrinsic connectivity networks) in individuals with autism. They have largely found evidence for reduced network integration in autism, especially in areas important for social cognition (Cherkassky et al., 2006; Just et al., 2007; Kennedy and Courchesne, 2008; Weng et al., 2010), but some found results in the opposite direction (Monk et al., 2009; Noonan et al., 2009). Additionally, some have reported reduced segregation between networks, suggesting that both within- and between-network dynamics may be affected (Rudie et al., 2012b).

4.2. Fragile-X

A related syndrome, fragile X, accounts for around 5% of autism cases, making it the most common known single-gene cause of autism (Budimirovic and Kaufmann, 2011). Haas et al. (2009) found an increased density in the fibers of the left ventral fronto-striatal pathway in young boys with fragile X. Barnea-Goraly et al. (2003) scanned girls with fragile X and found that they had lower FA in fronto-striatal pathways – usually a sign of poorer myelination – relative to healthy controls. To date, we know of no studies examining the development of functional connectivity in individuals with fragile X.

4.3. 22q11.2 deletion syndrome

22q11.2 deletion syndrome (22q DS) is a developmental syndrome resulting from a deletion of genetic material on chromosome 22, and is associated with cognitive deficits, differences in appearance, and other physiological changes. DTI studies in people with 22q DS report a number of abnormalities, including reduced interhemispheric FA, increased FA in frontal and parietal regions, and reduced FA in some anterior–posterior projecting tracts (Simon et al., 2005, 2008; Sundram et al., 2010; Villalon et al., 2013).

Only one group so far has investigated resting state connectivity in 22q DS. Debbané et al. (2012) used ICA to compare the ICNs of individuals with 22q DS, finding both increased and decreased connectivity in individuals with 22q DS, depending on the brain regions assessed. Individuals with 22q DS had decreased connectivity in the visual network. They had greater connectivity in the sensorimotor network and visuospatial processing network. Additionally, they had altered connectivity in the default mode network, with decreased connectivity between a number of midline frontal regions and the precuneus, and increased connectivity between more lateral frontal regions and the inferior parietal lobule.

12
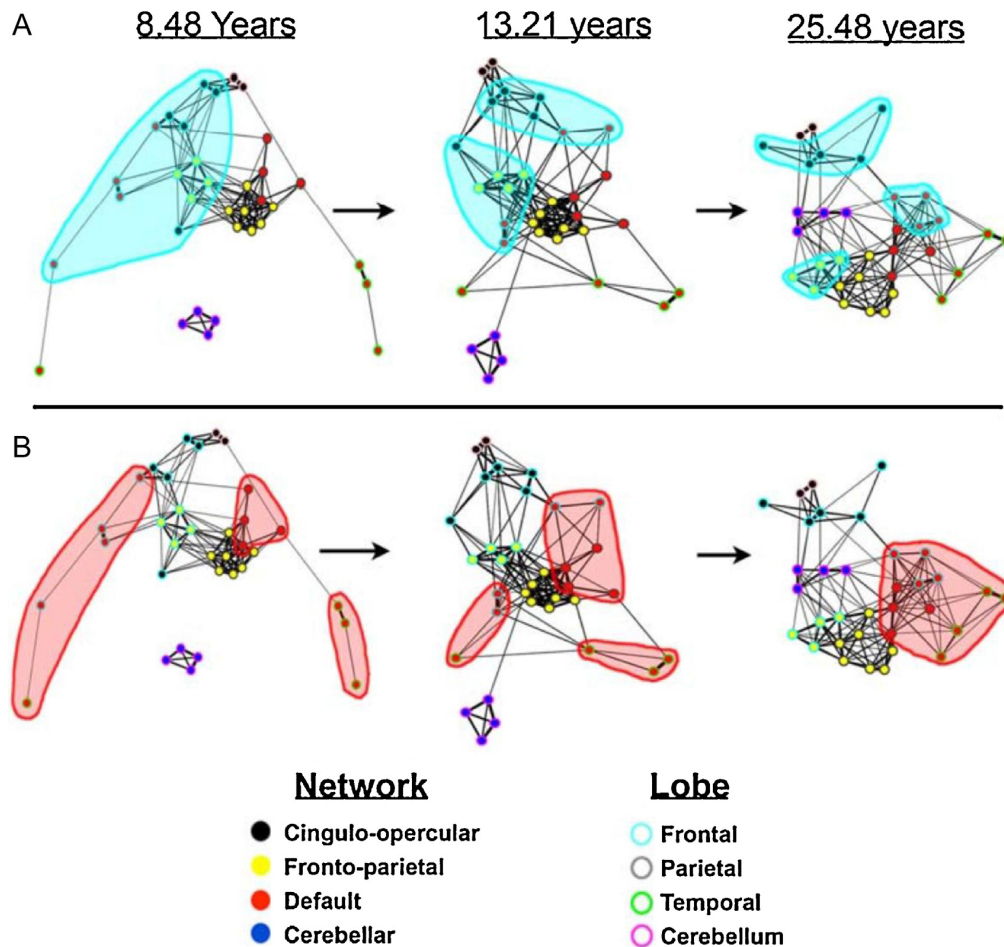
Fig. 9. Maturation from "local" organization to "distributed" organization, as measured by functional graph theoretical measures. Frontal regions are highlighted in blue in A; notice they are closely connected in children and less so in adults. The DMN, a collection of anatomically distributed regions, is highlighted in red in B. Notice they are segregated in children and highly integrated in adults. Reprinted with permission from Fair et al. (2009).

4.4. Williams syndrome

Williams syndrome is another neurodevelopmental disorder caused by a deletion, this time on chromosome 7q11.23. Hallmarks of Williams syndrome (WS) include hypersociability and decreased social inhibition. Structural connectivity studies of WS have found increased FA in the right superior longitudinal fasciculus, an increase that was associated with visuospatial deficits (Hoeft et al., 2007). Similarly, Jabbi et al. (2012) linked decreases in uncinate integrity to the severity of the WS personality profile. Researchers have also found increased fiber volume, density, and FA in the fusiform gyrus, an area important for facial processing and thus social interaction (Haas et al., 2011). Still others have found scattered increases and decreases in FA across tracts connecting regions implicated in the syndrome (Arlinghaus et al., 2011). This very complex picture is in line with morphometric work on WS, which tends to show a pattern of relative excesses and deficits in cortical gray matter thickness, and even differences in the gyral complexity of the cortical surface (Thompson et al., 2005). Earlier studies with MRI found imbalances in the distribution of white matter in the WS brain (Chiang et al., 2007), making tract tracing studies of particular interest in these regions. In cases where the fissuration pattern of the cortex is very different from that

seen in typically developing children, one must be somewhat cautious in applying the standard cortical parcellation schemes derived from normal subjects, to define the network nodes in connectivity studies. Clearly, tractography and connectivity analysis will shed considerable light on the unusual sulcal, gyral and corpus callosum abnormalities that have long been known to be characteristic of WS (Eckert et al., 2006; Gaser et al., 2006; Luders et al., 2007). As yet, we do not know of any studies examining the development of functional connectivity in individuals with Williams syndrome.

4.5. Turner syndrome

Turner syndrome results from partial or complete absence of one X chromosome in females, and is associated with a number of physical and physiological abnormalities. Molko (2004) was the first to examine white matter integrity with DTI in girls with Turner syndrome (TS), finding disruptions in anterior–posterior running temporal tracts. Holzapfel (2006) found lower FA in the bilateral internal capsule as well as in the left parieto-occipital region, extending along the superior longitudinal fasciculus. Yamagata et al. (2012) found widespread reductions in FA in girls with TS in a number of tracts connecting regions implicated in the cognitive deficits characteristic of TS. Turner syndrome (TS) is marked

by widespread deficits in white matter pathways, especially in anterior–posterior tracts, so it is not surprising that functional connectivity is altered as well. Kesler (2007) report unpublished data in which they found negative correlations between the time series of frontal and parietal regions in girls with TS, while controls had positive correlations between those regions' time series. Bray et al. (2011) found decreased functional connectivity to a seed in the right intraparietal sulcus (rIPS), an area shown to differ structurally in TS, in girls with TS during a working memory task. Later, Bray et al. (2012) found alterations in the functional connectivity of the posterior parietal cortex of girls with TS.

4.6. Attention deficit/hyperactivity disorder

As one of the most prevalent developmental disorders (Froehlich et al., 2007), ADHD (attention-deficit/hyperactivity disorder) is also one of the most commonly studied. ADHD is disproportionately diagnosed in boys (Anderson et al., 1987). It is a heterogeneous disorder, with a strong familial factor (Biederman, 2005). As such, we will only summarize a sample of the work on altered connectivity in ADHD. Some studies report lower FA in children with ADHD (Ashtari et al., 2005; Hamilton et al., 2008; Pavuluri et al., 2009), which is typically interpreted as evidence of disruption of the motor and attentional circuits. Others find higher FA in children with ADHD (Li et al., 2011; Silk et al., 2009), perhaps due to decreased neuronal branching. Additionally, Li et al. (2011) were able to correlate FA in the right frontal region with scores on the Stroop test, a test of inhibition and interference control. A line of interesting work will be to relate these patterns of aberrant connectivity to the last decade of work on structural brain abnormalities in ADHD, including, for example, the reported anomalies in callosal thickness (Luders et al., 2008) and cortical gray matter thickness (Sowell et al., 2003a,b).

A number of studies have examined functional connectivity in ADHD (attention-deficit/hyperactivity disorder), with some conflicting results. Part of this may lie in the heterogeneity of ADHD (Wåhlstedt et al., 2009). Cao et al. (2006) found increased temporal synchrony between a number of visual regions and the parahippocampal gyrus, while they found decreased synchrony between a number of frontal regions, the caudate, and precuneus. Examining the DMN, Castellanos et al. (2008) found decreased connectivity between the anterior cingulate (ACC) and the precuneus/posterior cingulate. Tian et al. (2006) also studied the connectivity of the ACC and found increased connectivity with the thalamus, cerebellum, insula, and pons. Taking a graph theoretical approach, Wang et al. (2009) found increased local efficiency and decreased global efficiency in children with ADHD, suggesting a disruption in the balance of small-world characteristics. There were also differences in nodal efficiency in prefrontal, temporal, and occipital regions implicated in previous studies.

5. Common themes

A number of themes have been common in investigations of structural and functional connectivity networks. Brain asymmetry has interested researchers for years (Hellige, 1993; Toga and Thompson, 2003), and sex differences in the brain are a controversial topic that has generated much research that is occasionally conflicting, partly due to the nonlinear scaling of brain structures as brain size increases (Gur et al., 1999; Kimura, 2000; Sowell et al., 2006; Brun et al., 2009; Luders et al., 2013). Even sex differences in the degree of brain asymmetry have been investigated in some depth (McGlone, 1978, 1980; Shaywitz et al., 1995; Toga and Thompson, 2003). Examining how these each change over development is an important part of understanding development and the factors that give rise to asymmetry or sex differences in the

brain. Because asymmetry and sex differences in the brain are broad enough topics to be a review or book in themselves (Dimond and Beaumont, 1974; Hellige, 1993; Kimura, 2000), here we will limit our review to the asymmetry and sex difference findings in studies we have already discussed here.

5.1. Asymmetry

Giedd et al. (1996) detailed the developmental changes in regional tissue volumes across different lobes, noted a right greater than left asymmetry in the temporal lobe, amygdala, and hippocampus. They did not see any changes in this asymmetry with age, however. In their study of 20 neonates, Gilmore et al. (2004) found a significant asymmetry in the lateral ventricles with the left being greater than the right; this asymmetry involves the left occipital horn projecting further back in the brain than its counterpart on the right, and it is almost universally found in studies of brain morphometry, regardless of the age and diagnosis of the subjects. In a more in-depth study, Gilmore et al. (2007) assessed 74 infants between 38 and 48 weeks gestational age. The left hemisphere was larger in volume than the right, which is opposite to typical findings in older children and adults (even the literature on this overall asymmetry in hemispheric volume is somewhat mixed, see Toga and Thompson, 1997). This left-greater-than-right asymmetry was detected in the GM, WM, subcortical GM, and lateral ventricles. Examining diffusion-weighted images in 108 subjects aged 7–68, Hasan et al. (2009b) found a leftward asymmetry in the FA of the uncinate fasciculus. They found this to be due to a leftward asymmetry in the axial diffusivity and a lack of asymmetry in the radial diffusivity. Jahanshad et al. (2010) even found that asymmetry in the FA of major WM tracts had a genetic basis. Our group found an unexpected asymmetry in the developmental trends for graph theoretical measures of structural connectivity, with measures increasing with age in the left hemisphere and decreasing in the right hemisphere (Dennis et al., 2013). Ongoing studies are revealing complex differences in the wiring patterns of each brain hemisphere, some of them in language-related regions, in line with the well-known morphometric asymmetries of the *planum temporale* and perisylvian cortices (Daianu et al., 2012).

5.2. Sex differences

Sex differences in the brain are a controversial topic, and research in this area can be conflicting, but there are sex differences in vulnerability to various neuropsychiatric disorders or recovery from brain injury (Turkheimer and Farace, 1992). As such, investigating sex differences in the brain will hopefully shed light on key health issues and their determinants. Giedd et al. (1996) found greater overall cerebral volumes in males, even when controlling for height and weight. In a later study, Giedd et al. (1999) similarly found greater overall GM volumes in males, as well as sex differences in the age at which cortical GM volume peaked. Sowell et al. (2002) found a few structures for which females had greater relative volume, including the temporal cortex, thalamus, caudate, and basomesial diencephalic structures. Finding differences even in neonates, Gilmore et al. (2004) recorded larger lateral ventricular volume in females than males. Later, Gilmore et al. (2007) found significantly greater intracranial volume (ICV) in males than females, even controlling for body weight.

Turning to structural connectivity, Gong et al. (2009) found a number of graph theoretical measures of structural brain connectivity that showed sex differences. Regional efficiency differed between sexes across many nodes, with some showing greater efficiency in females and some in males. Men had greater efficiency in a few frontal nodes while females had greater efficiency in a number

of temporal, parietal, and occipital nodes. Dennis et al. (2013) found sex differences in a number of global and nodal measures in graph theoretical measures of structural brain connectivity. We found greater clustering in females, who may have more segregated networks. We also found differences in the regional efficiency and degree (number of connections) in a few nodes. As the brain's components do not scale proportionately to the overall size of the brain, some care is needed when interpreting sex differences.

In functional connectivity, Schmithorst and Holland (2007) found a sex difference in correlations between intelligence and functional connectivity, with males and females showing intelligence scores correlated with functional connectivity of different regions. They also found an age by sex interaction in this effect. Kilpatrick et al. (2006) found that the functional connectivity of the amygdala demonstrated a sex effect, with males showing more expansive connectivity of the right amygdala and females showing more expansive connectivity of the left amygdala. Examining functional connectivity using graph theoretical methods, Wang et al. (2008) found a sex effect on nodal efficiency. Females had greater nodal efficiency in frontal and temporal regions, but males had greater efficiency in limbic and paralimbic regions. A review by Gong et al. (2011) provides greater detail on sex differences found across these various neuroimaging methods.

6. Future directions

Connectivity is a popular research topic now and has been for a few years. This growing popularity has led to major advances in the methods we use to assess connectivity. No doubt these improvements will continue as we search the human connectome in more depth and in new ways (see Toga and Thompson, 2013; Engel et al., 2013, for up to date reviews). Another topic that we expect to attract more attention is the relationship between structural and functional connectivity. Some studies are beginning to examine changes in function–structure relationships during development, and there are still many intriguing questions on how the two interact.

6.1. Imaging genetics

Imaging genetics (reviewed in Glahn et al., 2007; Thompson et al., 2010) is another topic that is gaining momentum and has already amassed a sizeable body of research. With the advent of better genomic methods and cooperative groups that can collect larger datasets, genetic analysis of variations in brain images can be pursued to discover specific genetic variants that affect brain integrity and connectivity (Jahanshad et al., 2013b). Several autism risk genes, for example, may be associated with consistent differences in brain "wiring", in both anatomical and functional connectivity analyses (Dennis et al., 2011; Rudie et al., 2012a). Also, new methods have recently been developed to screen connectivity maps and genomic data at the same time, to discover new genes that affect brain organization and disease risk (see Jahanshad et al., 2013c; Thompson et al., 2013).

One of the main issues with imaging genetics is sample size. Well over a million commonly-carried variants in the genome – including, for example, single nucleotide polymorphisms, or SNPs – can be assessed using widely available technology for performing genome-wide scans. For many years, vast studies have searched for SNPs that are over-represented in patients with certain types of disease. These genome-wide association scans (GWAS) need notoriously large samples because the effect of any one SNP is usually small (Jahanshad et al., 2013d).

The high risk of false positives when scouring the genome makes it necessary to amass huge samples to confirm any promising results, or to use complex methods to reduce the dimension of the search space (Silver et al., 2012; Hibar et al., 2013a,b). In the past few years, very large imaging genetics consortia have been formed with sample sizes numbering tens of thousands of subjects—enough subjects to pick up the effects of single letter changes in the genome on features derived from brain images. In these consortium efforts, multiple sites pool their data to increase the chances of finding significant associations between genetic variants and brain measures. One of the largest imaging genetics networks is the ENIGMA Consortium (Enhancing Neuroimaging Genetics through Meta-Analysis). This is an effort between 125 institutions across 12 countries, analyzing over 26,000 scans at the time of writing. This dataset has already been used to discover genes that affect brain structure, for example in the hippocampus (Stein et al., 2011), and jointly analyzing DTI data from thousands of subjects (Kochunov et al., 2012; Jahanshad et al., 2013b). The advantage of these efforts for studies of brain connectivity is that many connectivity measures are still poorly understood, so even the most general statements about changes in network efficiency must be confirmed and tested across developmental samples worldwide. This is particularly important in genetics, as a huge number of candidate genes have been asserted to affect brain maturation but findings are not always consistent.

Many studies have related specific genetic variants to individual differences in white matter integrity, as measured by FA (Braskie et al., 2011; Kohannim et al., 2012; McIntosh et al., 2008; Winterer et al., 2008). With greater subject numbers, consortia such as ENIGMA are beginning to offer the sample sizes needed to discover specific genes influencing brain connectivity. Studies in both healthy subjects (Buckholtz et al., 2007, 2008; Pezawas et al., 2005; Thomason et al., 2009) and those with neurodevelopmental or neuropsychiatric disorders (Meyer-Lindenberg et al., 2007; Scott-Van Zeeland et al., 2010) have found associations between specific genetic variants and changes in functional connectivity; clearly, large samples are needed to allow meta-analysis and corroboration of these subtle effects.

6.2. Functional and structural connectivity

Some researchers have begun to investigate the link between functional and structural connectivity, but only one study that the authors are aware of has examined the joint effects age has on structural and functional connectivity. In addition to the age effects seen in functional and structural connectivity separately that are discussed above, Supekar et al. (2010) also found an age difference in the relationship between functional and structural connectivity. When examining the connection between the PCC and mPFC, Supekar et al. (2010) found a significantly positive partial correlation between the functional time courses and fiber densities between the ROIs. There was no significant relationship between partial correlation strength and fiber density in the PCC-mPFC connection in children. Structural and functional connectivity are closely related, but one does not imply the other—regions that are structurally connected are also functionally correlated, but two regions that are functionally connected are not necessarily directly structurally linked (Greicius et al., 2008; Bullmore and Sporns, 2009; Honey et al., 2009). Very little work has been done on the question of how alterations of the structural network are correlated with alterations in the functional networks (Rudie et al., 2013). As functional connectivity may arise between areas with no direct structural connection, further investigation is necessary into how these complementary systems interact.

6.3. Other methods

In this review, space limitations meant that we did not cover the literature addressing development using MEG (magnetoencephalography) or EEG (electroencephalography). A number of

studies have examined developmental changes in MEG or EEG signals (Meyer-Lindenberg, 1996; Polonnikov et al., 2003; Eswaran et al., 2004). These data can also be used to examine brain connectivity. By examining the coherence between MEG or EEG signals across the brain, connectivity can be assessed (Bullmore and Sporns, 2009). One study has even linked EEG-based networks to intelligence (Langer et al., 2012). As several studies have reported developmental effects on MEG and EEG signals, and the link between EEG network measures and cognition, examining the developmental trajectory of MEG- and EEG-based networks would be of great interest.

7. Conclusions

Dramatic changes occur in the structural and functional connectivity of the brain, as it matures into adulthood. Structural and functional connectivity both support healthy brain function—a disruption in either can lead to a neurodevelopmental or neuropsychiatric disorder. Characterizing the developmental trajectory of these measures in healthy subjects serves an important function in understanding disease and in understanding the fundamental processes by which the brain matures. Here we have detailed a number of studies that examined the developmental trajectory of various measures of structural or functional connectivity in typically developing subjects. We also discussed a few examples of research into how structural and functional connectivity can be affected in developmental disorders. We also discussed a few of the themes commonly considered in connectivity, from developmental point of view—the structure–function relationship, asymmetry, and sex differences, and some future directions for the field.

Acknowledgments

References

Aganj, I., Lenglet, C., Jahanshad, N., Yacoub, E., Harel, N., Thompson, P.M., Sapiro, G., 2011. A Hough transform global probabilistic approach to multiple-subject diffusion MRI tractography. Medical Image Analysis 15 (4), 414–425.

Anderson, J.C., Williams, S., McGee, R., Silva, P.A., 1987. DSM-III disorders in preadolescent children. Prevalence in a large sample from the general population. Archives of General Psychiatry 44 (1), 69–76.

Arlinghaus, L.R., Thornton-Wells, T.A., Dykens, E.M., Anderson, A.W., 2011. Alterations in diffusion properties of white matter in Williams syndrome. Magnetic Resonance Imaging 29 (9), 1165–1174.

Asato, M.R., Terwilliger, R., Woo, J., Luna, B., 2010. White matter development in adolescence: a DTI study. Cerebral Cortex 20 (9), 2122–2131.

Ashtari, M., Kumra, S., Bhaskar, S.L., Clarke, T., Thaden, E., Cervellione, K.L., Rhinewine, J., Kane, J.M., Adesman, A., Milanaik, R., Maytal, J., Diamond, A., Szeszko, P., Ardekani, B.A., 2005. Attention-deficit/hyperactivity disorder: A preliminary diffusion tensor imaging study. Biological Psychiatry 57 (5), 448–455.

Barnea-Goraly, N., Eliez, S., Hedeus, M., Menon, V., White, C.D., Moseley, M., Reiss, A.L., 2003. White matter tract alterations in fragile X syndrome: Preliminary evidence from diffusion tensor imaging. American Journal of Medical Genetics Part B: Neuropsychiatric Genetics 118B (1), 81–88.

Barnea-Goraly, N., Kwon, H., Menon, V., Eliez, S., Lotspeich, L., Reiss, A.L., 2004. White matter structure in autism: preliminary evidence from diffusion tensor imaging. Biological Psychiatry 55 (3), 323–326.

Barnea-Goraly, N., Lotspeich, L., Reiss, A., 2010. Similar white matter aberrations in children with autism and their unaffected siblings: a diffusion tensor imaging study using tract-based spatial statistics. Archives of General Psychiatry 67 (10), 1052–1060.

Barnea-Goraly, N., Menon, V., Eckert, M., Tamm, L., Bammer, R., Karchemskiy, A., Dant, C.C., Reiss, A.L., 2005. White matter development during childhood and adolescence: a cross-sectional diffusion tensor imaging study. Cerebral Cortex 15, 1848–1854.

Beckmann, C.F., DeLuca, M., Devlin, J.T., Smith, S.M., 2005. Investigations into resting-state connectivity using independent component analysis. Philosophical Transactions of the Royal Society 360, 1001–1013.

Ben Bashat, D., Ben Sira, L., Graif, M., Pianka, P., Hendler, T., Cohen, Y., Assaf, Y., 2005. Normal white matter development from infancy to adulthood: comparing diffusion tensor and high b value diffusion weighted MR images. Journal of Magnetic Resonance Imaging 21 (5), 503–511.

Ben Bashat, D., Kronfeld-Duenias, V., Zachor, D.A., Ekstein, P.M., Hendler, T., Tarrasch, R., Even, A., Levy, Y., Ben Sira, L., 2007. Accelerated maturation of white matter in young children with autism: A high b value DWI study. NeuroImage 37, 40–47.

Biederman, J., 2005. Attention-deficit/hyperactivity disorder a selective overview. Biological Psychiatry 57, 1215–1220.

Biswal, B., Yetkin, F.Z., Haughton, V.M., Hyde, J.S., 1995. Functional connectivity in the motor cortex of resting human brain using echo-planar MRI. Magnetic Resonance in Medicine 34, 537–541.

Braskie, M., Jahanshad, N., Stein, J., Barysheva, M., McMahon, K., de Zubicaray, G.I., Martin, N.G., Wright, M.J., Ringman, J.M., Toga, A.W., Thompson, P.M., 2011. Common Alzheimer's Disease risk variant within the CLU gene affects white matter microstructure in young adults. Journal of Neuroscience 31, 6764–6770.

Bray, S., Dunkin, B., Hong, D.S., Reiss, A.L., 2011. Reduced functional connectivity during working memory in Turner syndrome. Cerebral Cortex 21 (11), 2471–2481.

Bray, S., Hoeft, F., Hong, D.S., Reiss, A.L., 2012. Aberrant functional network recruitment of posterior parietal cortex in Turner syndrome. Human Brain Mapping, 19 June 2012 [Epub ahead of print].

Brun, C.C., Luders, E., Lepore, N., Chou, Y.Y., Madsen, S.K., Toga, A.W., Thompson, P.M., 2009. Sex differences in brain structure in auditory and cingulate regions. NeuroReport 20 (10), 930–935.

Budimirovic, D.B., Kaufmann, W.E., 2011. What can we learn about autism from studying Fragile X syndrome? Developmental Neuroscience 33 (5), 379–394.

Buckholtz, J.W., Callicott, J.H., Kolachana, B., Hariri, A.R., Golberg, T.E., Gendersen, M., Egan, M.F., Mattay, V.S., Weinberger, D.R., Meyer-Lindenberg, A., 2008. Genetic variation in MAOA modulates ventromedial prefrontal circuitry mediating individual differences in human personality. Molecular Psychiatry 13, 313–324.

Buckholtz, J.W., Meyer-Lindenberg, A., Honea, R.A., Straub, R.E., Pezawas, L., Egan, M.F., Vakkalanka, R., Kolachana, B., Verchinski, B.A., Sust, S., Mattay, V.S., Weinberger, D.R., Callicott, J.H., 2007. Allelic variation in RGS4 impacts functional and structural connectivity in the human brain. Journal of Neuroscience 27 (7), 1584–1593.

Buckner, R.L., Andrews-Hanna, J.R., Schacter, D.L., 2008. The brain's default network: anatomy, function, and relevance to disease. Annals of the New York Academy of Sciences 1124 (1), 1–38.

Bullmore, E., Sporns, O., 2009. Complex brain networks: graph theoretical analysis of structural and functional systems. Nature Reviews Neuroscience 10 (3), 186–198.

Cao, Q., Zang, Y., Sun, L., Sui, M., Long, X., Zou, Q., Wang, Y., 2006. Abnormal neural activity in children with attention deficit hyperactivity disorder: a resting-state functional magnetic resonance imaging study. NeuroReport 17 (10), 1033–1036.

Cascio, C.J., Gerig, G., Piven, J., 2007. Diffusion Tensor Imaging: Application to the Study of the Developing Brain. Journal of the American Academy of Child & Adolescent Psychiatry 46 (2), 213–223.

Casey, B., Giedd, J.N., Thomas, K.M., 2000. Structural and functional brain development and its relation to cognitive development. Biological Psychiatry 54, 241–257.

Castellanos, F.X., Margulies, D.S., Kelly, C., Uddin, L.Q., Ghaffari, M., Kirsch, A., Shaw, D., Shehzad, Z., Di Martino, A., Biswal, B., Sonuga-Barke, E.J.S., Rotrosen, J., Adler, L.A., Milham, M.P., 2008. Cingulate-precuneus interactions: a new locus of dysfunction in adult attention-deficit/hyperactivity disorder. Biological Psychiatry 63 (3), 332–337.

Cetingul, H.E., Afsari, B., Wright, M., Thompson, P.M., Vidal, R., 2012a. A Riemannian framework for processing orientation distribution functions on the joint orientation and shape space. In: ISBI 2012, Barcelona, Spain, May 2–5 2012.

Cetingul, H.E., Sapiro, G., Nadar, M., Thompson, Paul M., Lenglet, C., 2012b. Simultaneous ODF estimation and robust probabilistic tractography from HARDI. MICCAI CDMRI, accepted.

Cherkassky, V.L., Kana, R.K., Keller, T.A., Just, M.A., 2006. Functional connectivity in a baseline resting-state network in autism. NeuroReport 17, 1687–1690.

Chiang, M.-C., McMahon, K.L., de Zubicaray, G.I., Martin, N.G., Hickie, I., Toga, A.W., Wright, M.J., Thompson, P.M., 2011. Genetics of white matter development: A DTI study of 705 twins and their siblings aged 12 to 29. NeuroImage 54 (3), 2308–2317.

Chiang, M.C., Reiss, A.L., Lee, A.D., Bellugi, U., Galaburda, A.M., Korenberg, J., Mills, D.L., Toga, A.W., Thompson, P.M., 2007. 3D pattern of brain abnormalities in Williams syndrome visualized using tensor-based morphometry. NeuroImage, Apr 20 [Epub ahead of print].

Daianu, M., Jahanshad, N., Dennis, E.L., Toga, A.W., McMahon, K.L., de Zubicaray, G.I., Wright, M.J., Hickie, I., Thompson, P.M., 2012. Left versus right hemisphere differences in brain connectivity: 4-tesla HARDI tractography in 567 twins. In: ISBI 2012, Barcelona, Spain, May 2–5, 2012.

Damoiseaux, J.S., Rombouts, S.A.R.B., Barkhof, F., Scheltens, P., Stam, C.J., Smith, S.M., Beckmann, C.F., 2006. Consistent resting-state networks across healthy subjects. PNAS 103 (37), 13848–13853.

Debbané, M., Lazouret, M., Lagioia, A., Schneider, M., Van de Ville, D., Eliez, S., 2012. Resting-state networks in adolescents with 22q11.2 deletion syndrome: Associations with prodromal symptoms and executive functions. Schizophrenia Research 139, 33–39.

Dennis, E.L., Jahanshad, N., McMahon, K.L., de Zubicaray, G.I., Martin, N.G., Hickie, I.B., Toga, A.W., Wright, M.J., Thompson, P.M., 2013. Development of brain structural connectivity between ages 12 and 30: A 4-Tesla diffusion imaging study in 439 adolescents and adults. NeuroImage 64, 671–684.

Dennis, E.L., Jahanshad, N., Rudie, J.D., Brown, J.A., Johnson, K., McMahon, K.L., de Zubicaray, G.I., Montgomery, G., Martin, N.G., Wright, M.J., Bookheimer, S.Y., Dapretto, M., Toga, A.W., Thompson, P.M., 2011. Altered structural brain connectivity in healthy carriers of the autism risk gene, CNTNAP2. Brain Connectivity 1 (6), 447–459.

Dimond, S.J., Beaumont, J., 1974. Hemisphere Function in the Human Brain. John Wiley & Sons, Oxford, England.

Dosenbach, N.U.F., Nardos, B., Cohen, A.L., Fair, D.A., Power, J.D., Church, J.A., Nelson, S.M., Wig, G.S., Vogel, A.C., Lessov-Schlaggar, C.N., Barnes, K.A., Dubis, J.W., Feczko, E., Coalson, R.S., Pruett, J.R., Barch, D.M., Petersen, S.E., Schlaggar, B.L., 2010. Prediction of Individual Brain Maturity Using fMRI. Science 329 (5997), 1358–1361.

Eckert, M.A., Galaburda, A.M., Karchemskiy, A., Liang, A., Thompson, P.M., Dutton, R.A., Lee, A.D., Bellugi, U., Korenberg, J.R., Mills, D.L., Rose, F., Reiss, A.L., 2006. Anomalous Sylvian fissure morphology in Williams Syndrome. NeuroImage (July) (published online).

Engel, J.P., Thompson, P.M., Stern, J.M., Staba, R.J., Bragin, A., Mody, I., 2013. Connectomics and epilepsy. Current Opinion in Neurology 26 (2), 186–194.

Eswaran, H., Lowery, C.L., Wilson, J.D., Murphy, P., Preissl, H., 2004. Functional development of the visual system in human fetus using magnetoencephalography. Experimental Neurology 190, 52–58.

Fair, D.A., Cohen, A.L., Dosenbach, N.U.F., Church, J.A., Miezin, F.M., Barch, D.M., Raichle, M.E., Petersen, S.E., Schlaggar, B.L., 2008. The maturing architecture of the brain's default network. Proceedings of the National Academy of Sciences 105 (10), 4028–4032.

Fair, D.A., Cohen, A.L., Power, J.D., Dosenbach, N.U.F., Church, J.A., Miezin, F.M., Schlaggar, B.L., Petersen, S.E., 2009. Functional brain networks develop from a local to distributed organization. PLoS Computational Biology 5 (5), e1000381.

Fair, D.A., Dosenbach, N.U.F., Church, J.A., Cohen, A.L., Brahmbhatt, S., Miezin, F.M., Barch, D.M., Raichle, M.E., Petersen, S.E., Schlaggar, B.L., 2007. Development of distinct control networks through segregation and integration. PNAS 104 (33), 13507–13512.

Fan, Y., Shi, F., Smith, J.K., Lin, W., Gilmore, J.H., Shen, D., 2011. Brain anatomical networks in early human brain development. NeuroImage 54 (3), 1862–1871.

Fox, M.D., Raichle, M.E., 2007. Spontaneous fluctuations in brain activity observed with functional magnetic resonance imaging. Nature Reviews Neuroscience 8 (9), 700–711.

Fox, M.D., Snyder, A.Z., Vincent, J.L., Corbetta, M., Essen, D.C.V., Raichle, M.E., 2005. The human brain is intrinsically organized into dynamic, anticorrelated functional networks. PNAS 102 (27), 9673–9678.

Fransson, P., Skiöld, B., Horsch, S., Nordell, A., Blennow, M., Lagercrantz, H., Aden, U., 2007. Resting-state networks in the infant brain. PNAS 104 (39), 15531–15536.

Froehlich, T.E., Lanphear, B.P., Epstein, J.N., Barbaresi, W.J., Katusic, S.K., Kahn, M.R.S., 2007. Prevalence, recognition, and treatment of attention-deficit/hyperactivity disorder in a national sample of US children. Archives of Pediatrics & Adolescent Medicine 161 (9), 857–864.

Gaser, C., Luders, E., Thompson, P.M., Lee, A.D., Dutton, R.A., Geaga, J.A., Hayashi, K.M., Bellugi, U., Galaburda, A.M., Korenberg, J.R., Mills, D.L., Toga, A.W., Reiss, A.L., 2006. Increased local gyrification mapped in Williams Syndrome. NeuroImage 33 (1), 46–54 (Epub 2006 August 9).

Gao, W., Lin, W., Chen, Y., Gerig, G., Smith, J.K., Jewells, V., Gilmore, J.H., 2009a. Temporal and spatial development of axonal maturation and myelination of white matter in the developing brain. AJNR 30 (2), 290–296.

Gao, W., Zhu, H., Giovanello, K.S., Smith, J.K., Shen, D., Gilmore, J.H., Lin, W., 2009b. Evidence on the emergence of the brain's default network from 2-week-old to 2-year-old healthy pediatric subjects. PNAS 106 (16), 6790–6795.

Giedd, J.N., Blumenthal, J., Jeffries, N.O., Castellanos, F.X., Liu, H., Zijdenbos, A., Paus, T., Evans, A.C., Rapoport, J.L., 1999. Brain development during childhood and adolescence: a longitudinal MRI study. Nature Neuroscience 2 (10), 861–863.

Giedd, J.N., Vaituzis, A.C., Hamburger, S.D., Lange, N., Rajapakse, J.C., Kaysen, D., Vauss, Y.C., Rapoport, J.L., 1996. Quantitative MRI of the temporal lobe, amygdala, and hippocampus in normal human development: ages 4–18 years. Journal of Comparative Neurology 355, 223–230.

Gilmore, J.H., Lin, W., Prastawa, M.W., Looney, C.B., Vetsa, Y.S.K., Knickmeyer, R.C., Evans, D.D., Smith, J.K., Hamer, R.M., Lieberman, J.A., Gerig, G., 2007. Regional gray matter growth, sexual dimorphism, and cerebral asymmetry in the neonatal brain. Journal of Neuroscience 27 (6), 1255–1260.

Gilmore, J.H., Zhai, G., Wilber, K., Smith, J.K., Lin, W., Gerig, G., 2004. 3 Tesla magnetic resonance imaging of the brain in newborns. Psychiatry Research 132 (1), 81–85.

Giorgio, A., Watkins, K.E., Douaud, G., James, A.C., James, S., De Stefano, N., Matthews, P.M., Smith, S.M., Johansen-Berg, H., 2008. Changes in white matter microstructure during adolescence. NeuroImage 39, 52–61.

Glahn, D.C., Paus, T., Thompson, P.M., 2007. Imaging genomics: mapping the influence of genetics on brain structure and function. Human Brain Mapping 17 (Special Issue on Genomic Imaging, published online, April 2007).

Gogtay, N., Giedd, J.N., Lusk, L., Hayashi, K.M., Greenstein, D., Vaituzis, A.C., Nugent III, T.F., Herman, D.H., Clasen, L.S., Toga, A.W., Rapoport, J.L., Thompson, P.M., 2004. Dynamic mapping of human cortical development during childhood through early adulthood. PNAS 101 (21), 8174–8179.

Gong, G., He, Y., Evans, A.C., 2011. Brain connectivity: Gender makes a difference. The Neuroscientist 17 (5), 575–591.

Gong, G., Rosa-Neto, P., Carbonell, F., Chen, Z.J., He, Y., Evans, A.C., 2009. Age- and gender-related differences in the cortical anatomical network. Journal of Neuroscience 29 (50), 15684–15693.

Greicius, M., 2008. Resting-state functional connectivity in neuropsychiatric disorders. Current Opinion in Neurology 21, 424–430.

Greicius, M.D., Supekar, K., Menon, V., Dougherty, R.F., 2008. Resting-state functional connectivity reflects structural connectivity in the default mode network. Cerebral Cortex 19 (1), 72–78.

Gur, R.C., Turetsky, B.I., Matsui, M., Yan, M., Bilker, W., Hughett, P., Gur, R.E., 1999. Sex differences in brain gray and white matter in healthy young adults: correlations with cognitive performance. Journal of Neuroscience 19 (10), 4065–4072.

Haas, B.W., Barnea-Goraly, N., Lightbody, A.A., Patnaik, S.S., Hoeft, F., Hazlett, H., Piven, J., Reiss, A.L., 2009. Early white-matter abnormalities of the ventral frontostriatal pathway in fragile X syndrome. Developmental Medicine and Child Neurology 51 (8), 593–599.

Haas, B.W., Hoeft, F., Barnea-Goraly, N., Golarai, G., Bellugi, U., Reiss, A.L., 2011. Preliminary evidence of abnormal white matter related to the fusiform gyrus in Williams syndrome: a diffusion tensor imaging tractography study. Genes, Brain and Behavior 11 (1), 62–68.

Hagmann, P., Sporns, O., Madan, N., Cammoun, L., Pienaar, R., Wedeen, V.J., Meuli, R., Thiran, J.-P., Grant, P.E., 2010. White matter maturation reshapes structural connectivity in the late developing human brain. PNAS 107 (44), 19067–19072.

Hamilton, L.S., Levitt, J.G., O'Neill, J., Alger, J.R., Luders, E., Phillips, O.R., Caplan, R., Toga, A.W., McCracken, J., Narr, K., 2008. Reduced white matter integrity in attention-deficit hyperactivity disorder. NeuroReport 19 (17), 1705–1708.

Hasan, K.M., Iftikhar, A., Kamali, A., Kramer, L.A., Ashtari, M., Cirino, P.T., Papanicolaou, A.C., Fletcher, J.M., Ewing-Cobbs, L., 2009a. Development and aging of the healthy human brain uncinate fasciculus across the lifespan using diffusion tensor tractography. Brain Research 1276, 67–76.

Hasan, K.M., Kamali, A., Iftikhar, A., Kramer, L.A., Papanicolaou, A.C., Fletcher, J.M., Ewing-Cobbs, L., 2009b. Diffusion tensor tractography quantification of the human corpus callosum fiber pathways across the lifespan. Brain Research 1249, 91–100.

Hellige, J.B., 1993. Hemispheric Asymmetry: What's Right And What's Left. Harvard University Press, Cambridge, MA.

Hibar, D., Medland, S.E., Stein, J.L., Kim, S., Shen, L., Saykin, A.J., de Zubicaray, G.I., McMahon, K.L., Montgomery, G.W., Martin, N.G., Wright, M.J., Djurovic, S., Agartz, I., Andreassen, O.A., Thompson, P.M., 2013a. Genetic clustering on the hippocampal surface for genome-wide association studies. In: MICCAI 2013, Nagoya, Japan, September 22–26, 2013 (8-page paper; peer-reviewed), accepted.

Hibar, D., Stein, J.L., Jahanshad, N., Toga, A.W., McMahon, K.L., de Zubicaray, G.I., Montgomery, G.W., Martin, N.G., Wright, M.J., Weiner, M.W., Thompson, P.M., 2013b. Exhaustive search of the SNP-SNP interactome identifies replicated epistatic effects on brain volume. In: MICCAI 2013, Nagoya, Japan, September 22–26, 2013 (8-page paper; peer-reviewed), accepted.

Hoeft, F., Barnea-Goraly, N., Haas, B.W., Golarai, G., Ng, D., Mills, D., Korenberg, J., Bellugi, U., Galaburda, A., Reiss, A.L., 2007. More is not always better: increased fractional anisotropy of superior longitudinal fasciculus associated with poor visuospatial abilities in Williams syndrome. Journal of Neuroscience 27 (44), 11960–11965.

Holzapfel, M., 2006. Selective alterations of white matter associated with visuospatial and sensorimotor dysfunction in Turner Syndrome. Journal of Neuroscience 26 (26), 7007–7013.

Honey, C., Sporns, O., Cammoun, L., Gigandet, X., Thiran, J., Meuli, R., Hagmann, P., 2009. Predicting human resting-state functional connectivity from structural connectivity. PNAS 106 (6), 2035–2040.

Huttenlocher, P., 1990. Morphometric study of human cerebral cortex development. Neuropsychologia 28 (6), 517–527.

Huttenlocher, P.R., Dabholkar, A.S., 1997. Regional differences in synaptogenesis in human cerebral cortex. The Journal of Comparative Neurology 387, 167–178.

Jabbi, M., Kippenhan, J.S., Kohn, P., Marenco, S., Mervis, C.B., Morris, C.A., Meyer-Lindenberg, A., Berman, K.F., 2012. The Williams syndrome chromosome 7q11.23 hemideletion confers hypersocial, anxious personality coupled with altered insula structure and function. PNAS, e860–e866.

Jahanshad, N., Aganj, I., Lenglet, C., Jin, Y., Joshi, A., Barysheva, M., McMahon, K.L., de Zubicaray, G.I., Martin, N.G., Wright, M.J., Toga, A.W., Sapiro, G., Thompson, P.M., 2011. High angular resolution diffusion imaging (HARDI) tractography in 234 young adults reveals greater frontal lobe connectivity in women. ISBI 2011.

Jahanshad, N., Kochunov, P., Glahn, D., Blangero, J., Nichols, T.E., McMahon, K.L., de Zubicaray, G.I., Martin, N.G., Wright, M.J., Nir, T., Jack Jr., C.R., Weiner, M.W., The ADNI, Toga, A.W., Thompson, P.M., 2013d. Power estimates for voxel-based genetic association studies using diffusion imaging. In: Workshop on Mathematical Methods for Brain Connectivity (MMBC), Medical Image Computing and Computer Assisted Intervention (MICCAI), Nagoya, Japan, September 22, 2013 (8-page paper; peer-reviewed), accepted.

Jahanshad, N., Kochunov, P., Sprooten, E., Mandl, R.C., Nichols, T.E., Booth, T., Blangero, J., de Zubicaray, G.I., Hong, E.L., Landman, B.A., Martin, N.G., McMahon, K.L., Medland, S.E., Mitchell, B.D., Peterson, C.P., Starr, J.M., Sussmann, J.E., Toga, A.W., Wardlaw, J.M., Wright, M.J., Hulshoff Pol, H.E., Bastin, M.E., McIntosh, A.M., Deary, I.J., Thompson, P.M., Glahn, D.C., 2013b. Multi-site genetic analysis

17

of diffusion images and voxelwise heritability analysis: a pilot project of the ENIGMA–DTI Working Group. NeuroImage, in press.

Jahanshad, N., Kohannim, O., Hibar, D.P., Stein, J.L., McMahon, K.L., de Zubicaray, G.I., Medland, S.E., Montgomery, G., Whitfield, J.B., Martin, N.G., Wright, M.J., Toga, A.W., Thompson, P.M., 2012. Brain structure in healthy adults is related to serum transferrin and the H63D polymorphism in the HFE gene. PNAS 109 (14), e851–e859.

Jahanshad, N., Rajagopalan, P., Thompson, P., 2013a. Invited review: Neuroimaging, nutrition, and iron-related genes. Cellular Molecular and Life Science Reviews (CMLS Reviews) 4 (February), in press.

Jahanshad, N., Toga, A.W., McMahon, K.L., de Zubicaray, G.I., Martin, N.G., Wright, M.J., Thompson, P.M., 2013c. Connectome-wide genome-wide search discovers SPON1 gene variant influencing dementia severity. PNAS (February).

Jahanshad, N., Zhan, L., Bernstein, M.A., Borowski, B., Jack, C.R., Toga, A.W., 2010. Thompson PM diffusion tensor imaging in seven minutes: determining trade-offs between spatial and directional resolution. In: ISBI 2010, Rotterdam, The Netherlands, 14–17 April 2010 (4 pages, peer-reviewed paper).

Jin, Y., Shi, Y., Zhan, L., Li, J., de Zubicaray, G.I., McMahon, K.L., Martin, N.G., Wright, M.J., Thompson, P.M., 2012. Automatic population HARDI white matter tract clustering by label fusion of multiple tract atlases. In: MICCAI MBIA Workshop 2012, (accepted).

Just, M.A., Cherkassky, V.L., Keller, T.A., Kana, R.K., Minshew, N.J., 2007. Functional and anatomical cortical underconnectivity in autism: evidence from an fMRI study of an executive function task and corpus callosum morphometry. Cerebral Cortex 17 (4), 951–961.

Kelly, A.M.C., Di Martino, A., Uddin, L.Q., Shehzad, Z., Gee, D.G., Reiss, P.T., Margulies, D.S., Castellanos, F.X., Milham, M.P., 2009. Development of anterior cingulate functional connectivity from late childhood to early adulthood. Cerebral Cortex 19 (3), 640–657.

Kennedy, D.P., Courchesne, E., 2008. The intrinsic functional organization of the brain is altered in autism. NeuroImage 39, 1877–1885.

Kesler, S.R., 2007. Turner Syndrome. Child and Adolescent Psychiatric Clinics of North America 16 (3), 709–722.

Kilpatrick, L.A., Zald, D.H., Pardo, J.V., Cahill, L.F., 2006. Sex-related differences in amygdala functional connectivity during resting conditions. NeuroImage 30, 452–461.

Kimura, D., 2000. Sex and Cognition. MIT Press, Cambridge, MA.

Knickmeyer, R.C., Gouttard, S., Kang, C., Evans, D., Wilber, K., Smith, J.K., Hamer, Robert M., Lin, W., Gerig, G., Gilmore, J.H., 2008. A structural MRI study of human brain development from birth to 2 years. The Journal of Neuroscience 28 (47), 12176–12182.

Kochunov, P., Jahanshad, N., Sprooten, E., Thompson, P., McIntosh, A., Deary, I., Bastin, M., Toga, A., McMahon, K., de Zubicaray, G., Martin, N., Wright, M., Montgomery, G., Medland, S., Carless, M., Curran, J., Hong, E., Duggirala, R., Olvera, R., Dyer, T., Blangero, J., Glahn, D., 2012. Genome-wide association of full brain white matter integrity—from the ENIGMA DTI working group. In: Presented at the 18th Annual Meeting of the Organization for Human Brain Mapping, Beijing, China, June 10–14, 2012.

Kochunov, P., Williamson, D.E., Lancaster, J., Fox, P., Cornell, J., Blangero, J., Glahn, D.C., 2010. Fractional anisotropy of water diffusion in cerebral white matter across the lifespan. Neurobiology of Aging, 1–12.

Kohannim, O., Jahanshad, N., Braskie, M.N., Stein, J.L., Chiang, M.-C., Reese, A.H., Hibar, D.P., Toga, A.W., McMahon, K.L., de Zubicaray, G.I., Medland, S.E., Montgomery, G., Martin, N.G., Wright, M.J., Thompson, P.M., 2012. Predicting white matter integrity from multiple common genetic variants. Neuropsychopharmacology 37 (9), 2012–2019.

Langer, N., Pedroni, A., Gianotti, L.R.R., Hänggi, J., Knoch, D., Jäncke, L., 2012. Functional brain network efficiency predicts intelligence. Human Brain Mapping 33 (6), 1393–1406.

Li, Q., Sun, J., Guo, L., Zang, Y., Feng, Z., Huang, X., Yang, H., Lv, Y., Huang, M., Gong, Q., 2011. Increased fractional anisotropy in white matter of the right frontal region in children with attention-deficit/hyperactivity disorder: a diffusion tensor imaging study. Activitas Nervosa Superior Rediviva 52 (3), 193–199.

Lim, K.O., Helpern, J.A., 2002. Neuropsychiatric applications of DTI—a review. NMR in Biomedicine 15 (7–8), 587–593.

Lin, W., Zhu, Q., Gao, W., Chen, Y., Toh, C.-H., Styner, M., Gerig, G., Smith, J.K., Biswal, B., Gilmore, J.H., 2008. Functional connectivity MR imaging reveals cortical functional connectivity in the developing brain. AJNR 29 (10), 1883–1889.

Liu, W.-C., Flax, J.F., Guise, K.G., Sukul, V., Benasich, A.A., 2008. Functional connectivity of the sensorimotor area in naturally sleeping infants. Brain Research 1223, 42–49.

Luders, E., Di Paola, M., Tomaiuolo, F., Thompson, P.M., Toga, A.W., Vicari, S., Petrides, M., Caltagirone, C., 2007. Callosal morphology in Williams syndrome—a new evaluation of shape and thickness. Neuroreport 18 (February (3)), 203–207.

Luders, E., Narr, K.L., Hamilton, L.S., Phillips, O.R., Thompson, P.M., Valle, J.S., Del'Homme, M., Strickland, T., Toga, A.W., McCracken, J.T., Levitt, J.G., 2008. Decreased callosal thickness in Attention Deficit/Hyperactivity Disorder (ADHD). Biological Psychiatry (Epub ahead of print, 2008 October 6). PMID: 18842255 NIHMSID 133661.

McGlone, J., 1978. Sex differences in brain asymmetry. Cortex 14 (1), 122–128.

McGlone, J., 1980. Sex differences in human brain asymmetry: a critical survey. Behavioral and Brain Sciences 3, 215–227.

McIntosh, A.M., Moorhead, T.W.J., Job, D., Lymer, G.K.S., Muñoz Maniega, S., McKirdy, J., Sussman, J.E.D., Baig, B.J., Bastin, M.E., Porteous, D., Evans, K.L., Johnstone, E.C., Lawrie, S.M., Hall, J., 2008. The effects of a neuregulin 1 variant on white matter density and integrity. Molecular Psychiatry 13, 1054–1059.

McLaughlin, N.C.R., Paul, R.H., Grieve, S.M., Williams, L.M., Laidlaw, D., DiCarlo, M., Clark, C.R., Whelihan, W., Cohen, R.A., Whitford, T.J., Gordon, E., 2007. Diffusion tensor imaging of the corpus callosum: a cross-sectional study across the lifespan. International Journal of Developmental Neuroscience 25 (4), 215–221.

Meyer-Lindenberg, A., 1996. The evolution of complexity in human brain development: An EEG study. Electroencephalography and Clinical Neurophysiology 99 (5), 405–411.

Meyer-Lindenberg, A., Straub, R.E., Lipska, B.K., Verchinski, B.A., Golberg, T., Callicott, J.H., Egan, M.F., Huffaker, S.S., Mattay, V.S., Kolachana, B., Kleinman, J.E., Weinberger, D.R., 2007. Journal of Clinical Investigation 117 (3), 672–682.

Molko, N., 2004. Brain anatomy in Turner syndrome: evidence for impaired social and spatial-numerical networks. Cerebral Cortex 14 (8), 840–850.

Monk, C.S., Peltier, S.J., Wiggins, J.L., Weng, S.-J., Carrasco, M., Risi, S., Lord, C., 2009. Abnormalities of intrinsic functional connectivity in autism spectrum disorders. NeuroImage 47 (2), 764–772.

Morriss, M.C., Zimmerman, R.A., Bilaniuk, L.T., Hunter, J.V., 1999. Changes in brain water diffusion during childhood. Neuroradiology 41, 929–934.

Mukherjee, P., Miller, J.H., Shimony, J.S., Conturo, T.E., Lee, B.C., Almli, C.R., McKinstry, R.C., 2001. Normal brain maturation during childhood: developmental trends characterized with diffusion-tensor MR imaging. Radiology 221 (2), 349–358.

Noonan, S.K., Haist, F., Müller, R.-A., 2009. Aberrant functional connectivity in autism: Evidence from low-frequency BOLD signal fluctuations. Brain Research 1262 (C), 48–63.

Pavuluri, M.N., Yang, S., Kamineni, K., Passarotti, A.M., Srinivasan, G., Harral, E.M., Sweeney, J.A., Zhou, X.J., 2009. Diffusion tensor imaging study of white matter fiber tracts in pediatric bipolar disorder and attention-deficit/hyperactivity disorder. BPS 65 (7), 586–593.

Pezawas, L., Meyer-Lindenberg, A., Drabant, E.M., Verchinski, B.A., Munoz, K.E., Kolachana, B.S., Egan, M.F., Mattay, V.S., Hariri, A.R., Weinberger, D.R., 2005. 5-HTTLPR polymorphism impacts human cingulate-amygdala interactions: a genetic susceptibility mechanism for depression. Nature Neuroscience 8, 828–834.

Polonnikov, R.I., Wasserman, E.L., Kartashev, N.K., 2003. Regular developmental changes in EEG multifractal characteristics. International Journal of Neuroscience 113 (11), 1615–1639.

Power, J.D., Fair, D.A., Schlaggar, B.L., Petersen, S.E., 2010. The development of human functional brain networks. Neuron 67, 735–748.

Raichle, M.E., MacLeod, A.M., Snyder, A.Z., Powers, W.J., Gusnard, D.A., Shulman, G.L., 2001. A default mode of brain function. PNAS 98 (2), 676–682.

Redcay, E., Kennedy, D.P., Courchesne, E., 2007. fMRI during natural sleep as a method to study brain function during early childhood. NeuroImage 38 (4), 696–707.

Rubinov, M., Sporns, O., 2010. Complex network measures of brain connectivity: uses and interpretations. NeuroImage 52 (3), 1059–1069.

Rudie, J., Brown, J., Beck-Pancer, D., Hernandez, L., Dennis, E., Thompson, P., Bookheimer, S., Dapretto, M., 2013. Altered functional and structural brain network organization in autism. NeuroImage: Clinical 2, 79–94.

Rudie, J.D., Hernandez, L.M., Brown, J.A., Colich, N.L., Beck-Pancer, D., Gorrindo, P., Thompson, P.M., Geschwind, D.H., Bookheimer, S.Y., Levitt, P., Dapretto, M., 2012a. Autism-associated promoter variant in MET impacts structural and functional brain networks. Neuron 75 (5), 904–915.

Rudie, J.D., Shehzad, Z., Hernandez, L.M., Colich, N.L., Bookheimer, S.Y., Iacoboni, M., Dapretto, M., 2012b. Reduced functional integration and segregation of distributed neural systems underlying social and emotional information processing in autism spectrum disorders. Cerebral Cortex 22 (5), 1025–1037.

Schmithorst, V.J., Holland, S.K., 2007. Sex differences in the development of neuroanatomical functional connectivity underlying intelligence found using Bayesian connectivity analysis. NeuroImage 35 (1), 406–419.

Schmithorst, V.J., Yuan, W., 2010. White matter development during adolescence as shown by diffusion MRI. Brain and Cognition 72 (1), 16–25.

Schneider, J.F.L., Il-Yasov, K.A., Hennig, J., Martin, E., 2004. Fast quantitative diffusion-tensor imaging of cerebral white matter from the neonatal period to adolescence. Neuroradiology 46, 258–266.

Scott-Van Zeeland, A., Abrahams, B., Alvarez-Retuerto, A., Sonnenblick, L., Rudie, J., Ghahremani, D., Mumford, J.A., Poldrack, R.A., Dapretto, M., Geschwind, D.H., Bookheimer, S.Y., 2010. Altered functional connectivity in frontal lobe circuits is associated with variation in the autism risk gene CNTNAP2. Science Translational Medicine 2, 1–6.

Seeley, W.W., Menon, V., Schatzberg, A.F., Keller, J., Glover, G.H., Kenna, H., Reiss, A.L., Greicius, M.D., 2007. Dissociable intrinsic connectivity networks for salience processing and executive control. Journal of Neuroscience 27 (9), 2349–2356.

Sexton, C.E., Mackay, C.E., Ebmeier, K.P., 2009. A systematic review of diffusion tensor imaging studies in affective disorders. Biological Psychiatry 66 (9), 814–823.

Seyffert, M., Silva, R., 2005. FMRI in pediatric neurodevelopmental disorders. Current Pediatric Reviews 1, 17–24.

Shaw, P., Kabani, N.J., Lerch, J.P., Eckstrand, K., Lenroot, R., Gogtay, N., Greenstein, D., Clasen, L., Evans, A., Rapoport, J.L., Giedd, J.N., Wise, S.P., 2008. Neurodevelopmental trajectories of the human cerebral cortex. Journal of Neuroscience 28 (14), 3586–3594.

Shaywitz, B.A., Shaywitz, S.E., Pugh, K.R., Constable, R.T., Skudlarski, P., Fulbright, R.K., Bronen, R.A., Fletcher, J.M., Shankweiler, D.P., Katz, L., Gore, J.C., 1995. Sex differences in the functional organization of the brain for language. Nature 373, 607–609.

Shukla, D.K., Keehn, B., Müller, R.-A., 2010. Tract-specific analyses of diffusion tensor imaging show widespread white matter compromise in autism spectrum disorder. Journal of Child Psychology and Psychiatry 52 (3), 286–295.

18

Silk, T.J., Vance, A., Rinehart, N., Bradshaw, J.L., Cunnington, R., 2009. White-matter abnormalities in attention deficit hyperactivity disorder: A diffusion tensor imaging study. Human Brain Mapping 30 (9), 2757–2765.

Silver, M., Janousova, E., Hua, X., Thompson, P.M., Montana, G., The Alzheimer's Disease Neuroimaging Initiative, 2012. Identification of gene pathways implicated in Alzheimer's disease using longitudinal imaging phenotypes with sparse regression. NeuroImage 63 (3), 1681–1694.

Simon, T.J., Ding, L., Bish, J.P., McDonald-McGinn, D.M., Zackai, E.H., Gee, J., 2005. Volumetric, connective, and morphologic changes in the brains of children with chromosome 22q11.2 deletion syndrome: an integrative study. NeuroImage 25 (1), 169–180.

Simon, T.J., Wu, Z., Avants, B., Zhang, H., Gee, J.C., Stebbins, G.T., 2008. Atypical cortical connectivity and visuospatial cognitive impairments are related in children with chromosome 22q11.2 deletion syndrome. Behavioral and Brain Functions 4 (25).

Sowell, E.R., Peterson, B.S., Thompson, P.M., Kan, E., Yoshii, J., Toga, A.W., 2006. Sex differences in cortical thickness mapped in 176 healthy individuals between 7 and 87 years. Cerebral Cortex 17 (7), 1550–1560.

Sowell, E.R., Peterson, B.S., Thompson, P.M., Welcome, S.E., Henkenius, A.L., Toga, A.W., 2003a. Mapping cortical change across the human life span. Nature Neuroscience 6 (3), 309–315.

Sowell, E.R., Thompson, P.M., Holmes, C.J., Batth, R., Jernigan, T.L., Toga, A.W., 1999. Localizing age-related changes in brain structure between childhood and adolescence using statistical parametric mapping. NeuroImage 9, 587–597.

Sowell, E.R., Thompson, P.M., Welcome, S.E., Henkenius, A.L., Toga, A.W., Peterson, B.S., 2003b. Cortical abnormalities in children and adolescents with attention-deficit hyperactivity disorder. The Lancet 22: 362 (9397), 1699–1707.

Sowell, E.R., Trauner, D.A., Gamst, A., Jernigan, T.L., 2002. Development of cortical and subcortical brain structures in childhood and adolescence: a structural MRI study. Developmental Medicine and Child Neurology 44, 4–16.

Sporns, O., Chialvo, D.R., Kaiser, M., Hilgetag, C.C., 2004. Organization, development and function of complex brain networks. Trends in Cognitive Sciences 8 (9), 418–425.

Stein, J.L., Medland, S.E., Vasquez, A.A., et al., 2011. Identification of common variants associated with hippocampal and intracranial volumes. Nature Genetics 44 (5), 552–561.

Stejskal, E.O., Tanner, J.E., 1965. Spin diffusion measurements: Spin-echoes in the presence of a time-dependent field gradient. Journal of Chemical Physics 42, 288–292.

Stevens, M.C., Pearlson, G.D., Calhoun, V.D., 2009. Changes in the interaction of resting-state neural networks from adolescence to adulthood. Human Brain Mapping 30 (8), 2356–2366.

Sundram, F., Campbell, L.E., Azuma, R., Daly, E., Bloemen, O.J.N., Barker, G.J., Chitnis, X., Jones, D.K., van Amelsvoort, T., Murphy, K.C., Murphy, D.G.M., 2010. White matter microstructure in 22q11 deletion syndrome: a pilot diffusion tensor imaging and voxel-based morphometry study of children and adolescents. Journal of Neurodevelopmental Disorders 2 (2), 77–92.

Supekar, K., Musen, M., Menon, V., 2009. Development of large-scale functional brain networks in children. PLOS Biology 7 (7), 1–15.

Supekar, K., Uddin, L.Q., Prater, K., Amin, H., Greicius, M.D., Menon, V., 2010. Development of functional and structural connectivity within the default mode network in young children. NeuroImage 52 (1), 290–301.

Szatmari, P., Paterson, A., Zwaigenbaum, L., et al., 2007. Mapping autism risk loci using genetic linkage and chromosomal rearrangements. Nature Genetics 39, 319–328.

Taki, Y., Thyreau, B., Hashizume, H., Sassa, Y., Takeuchi, H., Wu, K., Kotozaki, Y., Nouchi, R., Asano, K., Fukuda, H., Kawashima, R., 2012. Linear and curvilinear correlations of brain white matter volume, fractional anisotropy, and mean diffusivity with age using voxel-based and region-of-interest analyses in 246 healthy children. Human Brain Mapping, 22 March 2012 [Epub ahead of print].

Tian, L., Jiang, T., Wang, Y., Zang, Y., He, Y., Liang, M., Sui, M., Cao, Q., Hu, S., Peng, M., Zhuo, Y., 2006. Altered resting-state functional connectivity patterns of anterior cingulate cortex in adolescents with attention deficit hyperactivity disorder. Neuroscience Letters 400 (1–2), 39–43.

Thomason, M.E., Chang, C.E., Glover, G.H., Gabrieli, J.D.E., Greicius, M.D., Gotlib, I.H., 2008. Default-mode function and task-induced deactivation have overlapping brain substrates in children. NeuroImage 41 (4), 1493–1503.

Thomason, M.E., Dennis, E.L., Joshi, A.A., Joshi, S.H., Dinov, I.D., Chang, C., Henry, M.L., Johnson, R.F., Thompson, P.M., Toga, A.W., Glover, G.H., Van Horn, J.D., Gotlib, I.H., 2011. Resting-state fMRI can reliably map neural networks in children. NeuroImage 55 (1), 165–175.

Thomason, M.E., Thompson, P.M., 2011. Diffusion imaging, white matter and psychopathology. Annual Review of Clinical Psychology 7 (April), 63–85.

Thomason, M.E., Yoo, D.J., Glover, G.H., Gotlib, I.H., 2009. BDNF genotype modulates resting functional connectivity in children. Frontiers in Human Neuroscience 3 (55), 1–10.

Thompson, P.M., Bartzokis, G., Hayashi, K.M., Klunder, A.D., Lu, P.H., Edwards, N., Hong, M.S., Yu, M., Geaga, J.A., Toga, A.W., Charles, C., Perkins, D.O., McEvoy, J., Hamer, R.M., Tohen, M., Tollefson, G.D., Lieberman, J.A., for the HGDH Study Group, 2009. Time-lapse mapping reveals different disease trajectories in schizophrenia depending on antipsychotic treatment. Cerebral Cortex 19, 1107–1123, PMID: 18842668.

Thompson, P.M., Giedd, J.N., Woods, R.P., MacDonald, D., Evans, A., Toga, A., 2000. Growth patterns in the developing brain detected by using continuum mechanical tensor maps. Nature 404, 1–4.

Thompson, P.M., Ge, T., Glahn, D.C., Jahanshad, N., Nichols, T.E., 2013. Genetics of the connectome, invited review paper for the special issue on the connectome. NeuroImage, in press.

Thompson, P.M., Jahanshad, N., 2012. Ironing out neurodegeneration: Is iron intake important during the teenage years? Expert Review of Neurotherapeutics (June).

Thompson, P.M., Lee, A.D., Dutton, R.A., Geaga, J.A., Hayashi, K.M., Eckert, M.A., Bellugi, U., Galaburda, A.M., Korenberg, J.R., Mills, D.L., Toga, A.W., Reiss, A.L., 2005. Abnormal cortical complexity and thickness profiles mapped in Williams Syndrome. Journal of Neuroscience 25 (April (18)), 4146–4158.

Thompson, P.M., Martin, N.G., Wright, M.J., 2010. Invited review: Imaging genomics. Current Opinion in Neurology 23 (August (4)), 368–373.

Thompson, P.M., Narr, K.L., Blanton, R.E., Toga, A.W., 1999. Mapping structural alterations of the corpus callosum during brain development and degeneration. In: Iacoboni, M., Zaidel, E. (Eds.), The Corpus Callosum. Klüwer, Boston, MA.

Thompson, P.M., Vidal, C.N., Giedd, J.N., Gochman, P., Blumenthal, J., Nicolson, R., Toga, A.W., Rapoport, J.L., 2001. Mapping adolescent brain change reveals dynamic wave of accelerated gray matter loss in very early-onset schizophrenia. Proceedings of the National Academy of Sciences of the United States of America 98 (September (20)), 11650–11655.

Toga, A.W., Thompson, P.M., 1997. 1997 Measuring, Mapping, and Modeling Brain Structure and Function SPIE Medical Imaging Symposium, Newport Beach, CA USA. SPIE Lecture Notes 3033 (February).

Toga, A.W., Thompson, P.M., 2003. Mapping brain asymmetry. Nature Neuroscience 4, 37–48.

Toga, A.W., Thompson, P.M., 2013. Connectomics sheds new light on Alzheimer's disease. Biological Psychiatry 73 (5), 390–392.

Tournier, J.-D., Calamante, F., Gadian, D.G., Connelly, A., 2004. Direct estimation of the fiber orientation density function from diffusion-weighted MRI data using spherical deconvolution. NeuroImage 23 (3), 1176–1185.

Tuch, D.S., Reese, T.G., Wiegell, M.R., Makris, N., Belliveau, J.W., Wedeen, V.J., 2002. High angular resolution diffusion imaging reveals intravoxel white matter fiber heterogeneity. Magnetic Resonance in Medicne 48, 577–582.

Turkheimer, E., Farace, E., 1992. A reanalysis of gender differences in IQ scores following unilateral brain lesions. Psychological Assessment 4 (4), 498–501.

Uddin, L.Q., Supekar, K., Menon, V., 2010. Typical and atypical development of functional human brain networks: insights from resting-state FMRI. Frontiers in Systems Neuroscience 4, 21.

Vidal, C.N., Hayashi, K.M., Geaga, J.A., Sui, Y., McLemore, L.E., Alaghband, Y., Giedd, J.N., Gochman, P., Blumenthal, J., Gogtay, N., Nicolson, R., Toga, A.W., Rapoport, J.L., Thompson, P.M., 2006. Dynamically spreading frontal and cingulate deficits mapped in adolescents with schizophrenia. Archives of General Psychiatry 63 (January (1)), 25–34.

Villalon, J., Jahanshad, N., Beaton, E., Toga, A.W., Thompson, P.M., Simon, T.J., 2013. White matter microstructural abnormalities in children with chromosome 22q11.2 deletion syndrome Fragile X or Turner syndrome as evidenced by diffusion tensor imaging. NeuroImage, in press.

Wåhlstedt, C., Thorell, L.B., Bohlin, G., 2009. Heterogeneity in ADHD: Neuropsychological pathways, comorbidity, and symptom domains. Journal of Abnormal Child Psychology 37 (4), 551–564.

Walter, E., Mazaika, P.K., Reiss, A.L., 2009. Insights into brain development from neurogenetic syndromes: evidence from Fragile X syndrome, Williams syndrome, Turner syndrome and Velocardiofacial syndrome. Neuroscience 164, 257–271.

Wang, L., Zhu, C., He, Y., Zang, Y., Cao, Q., Zhang, H., Zhong, Q., Wang, Y., 2009. Altered small-world brain functional networks in children with attention-deficit/hyperactivity disorder. Human Brain Mapping 30 (2), 638–649.

Wang, L., Zhu, C., He, Y., Zhong, Q., Zang, Y., 2008. Gender effect on functional networks in resting brain. Medical Imaging and Informatics 4987, 160–168.

Weng, S.-J., Wiggins, J.L., Peltier, S.J., Carrasco, M., Risi, S., Lord, C., Monk, C.S., 2010. Alterations of resting state functional connectivity in the default network in adolescents with autism spectrum disorders. Brain Research 1313, 202–214.

Winterer, G., Konrad, A., Vucurevic, G., Musso, F., Stoeter, P., Dahmen, N., 2008. Association of the 5′ end neuregulin-1 (NRG1) gene variation with subcortical medial frontal microstructure in humans. NeuroImage 40, 712–718.

Yamagata, B., Barnea-Goraly, N., Marzelli, M.J., Park, Y., Hong, D.S., Mimura, M., Reiss, A.L., 2012. White matter aberrations in prepubertal estrogen-naive girls with monosomic Turner Syndrome. Cerebral Cortex 22 (12), 2761–2768.

Zhai, G., Lin, W., Wilber, K.P., Gerig, G., Gilmore, J.H., 2003. Comparisons of regional white matter diffusion in healthy neonates and adults performed with a 3.0-T head-only MR Imaging Unit. Radiology 229 (3), 673–681.

Zhan, L., Chiang, M.C., Barysheva, M., Toga, A.W., McMahon, K.L., de Zubicaray, G.I., Meredith, M., Wright, M.J., Thompson, P.M., 2008. How many gradients are sufficient in High-Angular Resolution Diffusion Imaging (HARDI)? Workshop on Diffusion Tensor Imaging, In: Medical Image Computing and Computer Assisted Intervention (MICCAI), New York, 10 September 2008.

Zhan, L., Franc, D., Patel, V., Jahanshad, N., Jin, Yan, Mueller, B.A., Bernstein, M.A., Borowski, B.J., Jack Jr., C.R., Toga, A.W., Lim, K.O., Thompson, P.M., 2012a. How do spatial and angular resolution affect brain connectivity maps from diffusion MRI? In: Proceedings of 9th IEEE ISBI, Barcelona (to appear).

Zhan, L., Leow, A.D., Aganj, I., Lenglet, C., Sapiro, G., Yacoub, E., Harel, N., Toga, A.W., Thompson, P.M., 2011. Differential information content in staggered multiple shell HARDI measured by the tensor distribution function. ISBI.

Zhan, L., Leow, A.D., Barysheva, M., Feng, A., Toga, A.W., Sapiro, G., Harel, N., Lim, K.O., Lenglet, C., McMohan, K.L., de Zubicaray, G.I., Wright, M.J., Thompson, P.M., 2009a. Investigating the uncertainty in multi-fiber estimation in High Angular Resolution Diffusion Imaging. In: Pohl, Kilian, Joshi, Sarang, Wells, Sandy

(Eds.), Workshop on Probabilistic Modeling in Medical Image Analysis (PMMIA), Medical Image Computing and Computer Assisted Intervention (MICCAI). London, September 20, 2009.

Zhan, L., Leow, A.D., Jahanshad, N., Chiang, M.C., Barysheva, M., Lee, A.D., Toga, A.W., McMahon, K.L., de Zubicaray, G.I., Wright, M.J., Thompson, P.M., 2009b. How does angular resolution affect diffusion imaging measures? NeuroImage 49 (2), 1357–1371.

Zhan, L., Jahanshad, N., Ennis, D.B., Bernstein, M.A., Borowski, B.J., Jack Jr., C.R., Toga, A.W., Leow, A.D., Thompson, P.M., 2012b. Angular versus spatial resolution trade-offs for diffusion imaging under time constraints. Human Brain Mapping (April) [Epub ahead of print].

Zielinski, B.A., Gennatas, E.D., Zhou, J., Seeley, W.W., 2010. Network-level structural covariance in the developing brain. Proceedings of the National Academy of Sciences 107 (42), 18191–18196.

1.2   Genetic underpinnings of structural connectivity

Many aspects of brain structure are under moderately strong genetic control, including total brain volume [Posthuma et al., 2000], cortical thickness [Schmitt et al., 2008; Thompson et al., 2001], and DTI-derived measures of white matter integrity [Chiang et al., 2009, 2011; Pfefferbaum et al., 2001]. While genome-wide approaches can perform unbiased searches, which are especially useful in uncovering associations when no prior hypotheses exist [Thompson et al., 2010], these approaches require very large numbers of subjects (tens of thousands). Candidate gene approaches, such as testing SNPs (single nucleotide polymorphisms) of interest, can be appropriate when a prior hypothesis exists, and are more practical with smaller subject numbers. Using this approach, Braskie et al. (2011) found that healthy young adults who carry the risk allele of an Alzheimer's risk gene (*CLU*-C) had lower white matter integrity. Jahanshad et al. (2012) found associations between white matter integrity and a gene key in iron regulation (*HFE*). In the first study to link graph theoretical measures of structural connectivity to genetics, Brown et al. (2011) found that healthy *APOE*-4 carriers had accelerated decline of measures of interconnectivity with age. As will be discussed in Chapter 3, we have also examined genetic associations with both graph theoretical measures of connectivity and HARDI-based measures of white matter integrity. Results such as these can reveal information about the mechanisms by which these disease risk genes confer vulnerability.

For the vast majority of the studies presented, we have used a large dataset of twins scanned in Australia. In addition to examining associations between SNPs and brain measures, with this dataset we can also examine the heritability of brain measures. By examining the similarity between dizygotic twins vs. monozygotic twins, we can get an estimate of the

proportions of variance in the brain measures that are due to genetics, shared environment, and unique environment (or the unexplained remainder). This is based on the assumption that monozygotic twins share 100% of their genetics, while dizygotic twins share 50% of their genetics, but both share environments with their twins. Thus, if a brain measure is significantly more correlated between monozygotic twins than between dizygotic twins, it has a significant genetic component. Our lab has used this method to determine the heritability of brain asymmetry [Jahanshad et al., 2010] and the influence of transferrin (iron transporter) on brain structure [Jahanshad et al., 2012]. We have used this modeling to determine the heritability of graph theoretical measures of structural connectivity [Dennis et al., SFN 2011].

1.3   Cognitive correlates of structural connectivity

There have been a number of investigations into the cognitive correlates of diffusion weighted imaging measures, finding that it is associated with reading ability [Deutsch et al., 2005], working memory [Takeuchi et al., 2010], and IQ [Schmithorst et al., 2005]. Studies of cognitive correlates of graph theoretical measures of structural connectivity, however, are far fewer. In fact, at this time I only am aware of one published study linking IQ and graph theoretical measures of structural connectivity [Li et al., 2009]. As will be discussed in Chapter 4, we have examined the association between IQ and one set of parameters from graph theory, describing the "rich club" organization of the brain.

Cognitive development is a dynamic process that requires development of the underlying brain structure, activity in a coordinated manner, and enough input from the environment to stimulate development and learning. There are many studies showing that some of the latest

regions to develop structurally are those responsible for higher-level cognitive function [Gogtay et al., 2004]. In additional to showing immature recruitment of brain regions typically used by adults for cognitive tasks, studies have shown children also use different brain regions altogether in fMRI studies [Bunge et al., 2002; Durston et al., 2002; Monk et al., 2003]. Lastly, the developmental environment, and how much stimuli-rich the surroundings are, can also play a significant role in the development of a child's cognitive abilities [Burchinal et al., 1996; Rijlaarsdam et al., 2013].

Structural graph theoretical measures of connectivity are highly mathematical, and perhaps a little more removed from the biology than other measures of connectivity. Given that there is a lack of research examining the link between cognition and these measures, it would seem prudent to examine in order to determine their utility in this domain. Linking these mathematical measures back to cognitive measures, which are more obviously related to neurological function, will give them a firmer biological grounding.

1.4   Graph theory and the rich club

Graph theory is a branch of mathematics concerned with the description and analysis of graphs. It has recently been applied to brain networks to describe network topology. Graph theory represents the brain as a set of nodes (brain regions) and edges (the connections between them). A number of standard parameters such as path length and modularity, to name a few, are used to describe network topology [Sporns et al., 2004]. *Characteristic path length* measures the average path length in a network. It does not refer to the physical length of the tracts, but the number of edges, or individual 'jumps', between nodes in the network. *Modularity* is the degree

23

to which a system may be subdivided into smaller networks. Graph theory can quantify both local and global features in brain connectivity patterns.

Van den Heuvel and Sporns (2011) first discussed the existence of "rich-club" organization in the human connectome, building on previous network analysis of a "rich-club" phenomenon [Colizza et al., 2006]. The rich club coefficient assesses the presence and interconnectedness of a "rich club" of nodes within a network – nodes that are highly central and densely interconnected with each other and participate as hub nodes in multiple sub-networks. It is given by the following:

$$\phi(k) = \frac{2\,E_{>k}}{N_{>k}(N_{>k} - 1)}$$

Where k is the degree of the nodes, $E_{>k}$ is the number of links between nodes with degree k or greater, and $N_{>k}$ is the total number of possible connections if those nodes of degree k were to be fully connected. They also introduced $\phi_{norm}(k)$, which is $\phi(k)$ divided by the rich club coefficient calculated in a series of random networks ($\phi_{random}(k)$) of the same size with a similar distribution of edges. A $\phi_{norm}(k)$ value greater than 1 indicates the presence of rich-club organization in the network. In additional to investigating the density of connections between rich club nodes, which nodes are included in the rich club can be informative as well. These highly central, highly interconnected nodes are crucial for efficient network function [Van den Heuvel & Sporns, 2011], so differences in which nodes are included in the rich club can point to substantial structural differences between groups or remodeling with age.

1.5   Organization of the dissertation

All of the studies in this dissertation are unified by the use of structural connectivity measures as the neuroimaging phenotype. Each of the aims attempts to address an area of research where significant gaps in knowledge exist regarding structural connectivity. The aims are additionally linked by hopefully serving future research efforts into neurodevelopmental disorders, which I intend to pursue following completion of my doctoral degree. In Chapter 2 we discuss efforts to determine the developmental trajectory of graph theoretical measures of structural connectivity, including basic measures such as characteristic path length and clustering, as well as more complex measures such as rich club organization. In addition, we discuss work to define how the connectivity of the insula changes between adolescence and early adulthood, which a critical region for many psychiatric disorders. In Chapter 3 we detail studies of the genetic associations of measures of connectivity, starting with a study finding altered graph theoretical measures of connectivity in healthy individuals carrying the risk allele of an autism risk gene (*CNTNAP2*). We also detail results linking an obesity risk gene (*NEGR1*) to changes in white matter integrity, in an age-dependent fashion. In Chapter 4 we examine work investigating the cognitive correlates of structural connectivity, beginning with a study finding associations between IQ and both rich club organization and voxel-wise FA. Additionally, we detail work linking educational attainment to differences in fiber density and nodal graph theoretical measures of structural connectivity. In Chapter 5 we offer a summary of these works. In Chapter 6 we detail our plans for future work and ongoing studies.

CHAPTER 2

Developmental trajectory of structural brain connectivity

2.1 Development of brain structural connectivity between ages 12 and 30

This section is adapted from:

Dennis EL, Jahanshad N, Toga AW, McMahon KL, de Zubicaray GI, Martin NG, Hickie IB, Wright MJ, Thompson PM. (2013). Development of Brain Structural Connectivity between Ages 12 and 30: A 4-Tesla HARDI Study in 439 Adolescents and Adults. *NeuroImage*, 64(1), 671-684.

Development of brain structural connectivity between ages 12 and 30: A 4-Tesla diffusion imaging study in 439 adolescents and adults

Emily L. Dennis [a], Neda Jahanshad [a], Katie L. McMahon [b], Greig I. de Zubicaray [c], Nicholas G. Martin [d], Ian B. Hickie [e], Arthur W. Toga [a], Margaret J. Wright [c,d], Paul M. Thompson [a,*]

[a] Imaging Genetics Center, Laboratory of Neuro Imaging, UCLA School of Medicine, Los Angeles, CA, USA
[b] Center for Advanced Imaging, University of Queensland, Brisbane, Australia
[c] School of Psychology, University of Queensland, Brisbane, Australia
[d] Queensland Institute of Medical Research, Brisbane, Australia
[e] Brain and Mind Research Institute, University of Sydney, Australia

ARTICLE INFO

ABSTRACT

Understanding how the brain matures in healthy individuals is critical for evaluating deviations from normal development in psychiatric and neurodevelopmental disorders. The brain's anatomical networks are profoundly re-modeled between childhood and adulthood, and diffusion tractography offers unprecedented power to reconstruct these networks and neural pathways *in vivo*. Here we tracked changes in structural connectivity and network efficiency in 439 right-handed individuals aged 12 to 30 (211 female/126 male adults, mean age = 23.6, SD = 2.19; 31 female/24 male 12 year olds, mean age = 12.3, SD = 0.18; and 25 female/22 male 16 year olds, mean age = 16.2, SD = 0.37). All participants were scanned with high angular resolution diffusion imaging (HARDI) at 4 T. After we performed whole brain tractography, 70 cortical gyral-based regions of interest were extracted from each participant's co-registered anatomical scans. The proportion of fiber connections between all pairs of cortical regions, or nodes, was found to create symmetric fiber density matrices, reflecting the structural brain network. From those 70×70 matrices we computed graph theory metrics characterizing structural connectivity. Several key global and nodal metrics changed across development, showing increased network integration, with some connections pruned and others strengthened. The increases and decreases in fiber density, however, were not distributed proportionally across the brain. The frontal cortex had a disproportionate number of decreases in fiber density while the temporal cortex had a disproportionate number of increases in fiber density. This large-scale analysis of the developing structural connectome offers a foundation to develop statistical criteria for aberrant brain connectivity as the human brain matures.

Introduction

The human brain changes profoundly, both functionally and structurally, between childhood and adulthood (Dosenbach et al., 2010; Gogtay et al., 2004; Lenroot et al., 2007; Shaw et al., 2008; Sowell et al., 2003). Following the massive growth in the number of synapses after birth, anatomical studies show a decline in synaptic density, as short-range connections are pruned in favor of long-range ones (Huttenlocher, 1979, 1990). Studies of structural connectivity using diffusion imaging show that the fractional anisotropy of water along white matter tracts – an index of myelination and axonal coherence – increases in childhood, plateaus in adulthood, and declines in old age (Kochunov et al., 2010). Studies of functional connectivity have

employed resting-state fMRI data to estimate the "developmental ages" or relative maturity of participants, finding that chronological age accounts for over half of the variance in functional brain connectivity in developmental samples (Dosenbach et al., 2010). Defining the developmental trajectory for various measures of brain structure and function is critical for understanding the general principles of neural network development. Determining the normal developmental trajectory will also help to identify deviations in structural circuitry implicated in neuropsychiatric disorders such as autism or schizophrenia (Scott-Van Zeeland et al., 2010).

Graph theory is a branch of mathematics developed to describe and analyze networks, offering a variety of metrics that have become popular for characterizing networks in the brain. By modeling the brain as a collection of nodes (hubs) and edges (connections between them), graph theory quantifies network topology through a number of standard parameters (Sporns et al., 2004). One of these is path length, a measure of the distance, in edges, between one brain region (node) and another (Rubinov and Sporns, 2010). Global efficiency is

the inverse of path length — networks with shorter average path lengths are generally more efficient in transferring information. These metrics are genetically influenced (Dennis et al., 2011) and their properties are known to depend on specific genetic variants in normal adults and cognitively impaired adults (Brown et al., 2011; Dennis et al., 2012a).

To date, a few studies have begun to assess how graph theory metrics of structural connectivity change during development. Gong et al. (2009) examined anatomical connectivity in 95 subjects aged 19–85. Hagmann et al. (2010) tracked white matter maturation in 30 subjects between 18 months and 18 years of age. We were particularly interested in the developmental period from early adolescence to early adulthood, when the brain fully matures. The pioneering study by Hagmann and colleagues was limited by small sample size (30 subjects), so we set out to chart the developmental trajectory of network metrics in a much larger cross-sectional sample (439 subjects).

To map structural brain connectivity between childhood and adulthood, we scanned 439 subjects between ages 12 and 30, with high-field (4-Tesla) high angular resolution diffusion imaging (HARDI). We computed standard graph theory metrics from 70×70 connectivity matrices of fiber density. These connection matrices were probed for linear and non-linear relationships with age. We hypothesized that we would find evidence of decreased path length with age, reflecting a developmental process of pruning short-range connections and strengthening long-range connections (Casey et al., 2000; Hagmann et al., 2010; Thomason et al., 2011).

Material and methods

Participants

Participants were recruited as part of a 5-year research project examining healthy Australian twins with structural MRI and diffusion weighted imaging, with a projected sample size of approximately 1150 at completion (de Zubicaray et al., 2008). Our analysis included 439 right-handed subjects (adult sample: 211 females/126 males, mean age = 23.6, SD = 2.19; 12 year old sample: 31 females/24 males, mean age = 12.3, SD = 0.18; 16 year old sample: 25 females/22 males, mean age = 16.2, SD = 0.37). This population included 146 monozygotic (MZ) twins, 259 dizygotic (DZ) twins, and 34 non-twin siblings, from 275 families. 337 were adults, 55 were adolescents, and 47 were children, as shown in Table 1. Since our current focus is on the description of network growth trajectories, the present analyses make no use of twin relatedness to estimate genetic and environmental components.

The population was racially homogeneous: 100% of subjects were Caucasian. Subjects were screened to exclude those with a history of significant head injury, neurological or psychiatric illness, substance abuse or dependence, or had a first-degree relative with a psychiatric disorder. All participants were right-handed, as assessed by 12 items on the Annett's Handedness Questionnaire (Annett, 1970). The adult cohort and the 16 year old cohort both completed the Multi-dimensional Aptitude Battery II (MAB-II) IQ test (Jackson, 1998). Most participants who completed the MAB-II did so at age 16 (92%); the others completed the MAB-II at a later session, some at the scan session (4% were between 17 and 20 years, 3% were between 20 and 23 years,

1% was between 25 and 29 years). The 12-year-old cohort did not complete the MAB IQ scale. Study participants gave informed consent; institutional ethics committees at the Queensland Institute of Medical Research, the University of Queensland, the Wesley Hospital, and at UCLA approved the study. The adult subjects in this sample partially overlap with a sample examined in prior studies (Braskie et al., 2011; Braskie et al., 2012), which revealed single-gene effects on measures of brain integrity and connectivity, but did not assess children.

Scan acquisition

Whole-brain anatomical and high angular resolution diffusion images (HARDI) were collected with a 4 T Bruker Medspec MRI scanner. T1-weighted anatomical images were acquired with an inversion recovery rapid gradient echo sequence. Acquisition parameters were: TI/TR/TE = 700/1500/3.35 ms; flip angle = 8°; slice thickness = 0.9 mm, with a 256×256 acquisition matrix. HARDI was also acquired using single-shot echo planar imaging with a twice-refocused spin echo sequence to reduce eddy-current induced distortions. Imaging parameters were: 23 cm FOV, TR/TE 6090/91.7 ms, with a 128×128 acquisition matrix. Each 3D volume consisted of 55 2-mm thick axial slices with no gap and 1.79×1.79 mm^2 in-plane resolution. 105 images were acquired per subject: 11 with no diffusion sensitization (i.e., T2-weighted b_0 images) and 94 diffusion-weighted (DW) images ($b = 1159$ s/mm^2) with gradient directions evenly distributed on a hemisphere in the q-space. Some subjects' HARDI scans were acquired with a 77-gradient protocol ($b = 1177$ s/mm^2), as the 105-gradient protocol was too long for some adolescents to sit through. We have previously undertaken several detailed studies (Zhan et al., 2009a, 2012a,b) to determine how angular and spatial resolution affects brain connectivity maps, and the results and stability at high numbers of diffusion gradients are reported in those papers. The number of gradients affects the accuracy of reconstruction of the diffusion profile, but by the time 50–60 gradients are reached, the primary measures of diffusion, including the principal eigenvector, have converged (Zhan et al., 2008, 2009a,b). The connectivity matrix has been found to depend more on the voxel size than the number of gradients, and the voxel size was kept the same in the adolescents. Scan time for the 105-gradient HARDI scan was 14.2 min. Scan time for the 77-gradient HARDI scan was 10.8 min.

Cortical extraction and HARDI tractography

Connectivity analysis was performed exactly as in Jahanshad et al. (2011). Briefly, non-brain regions were automatically removed from each T1-weighted MRI scan using ROBEX (JE Iglesias, TMI 2011), and from a T2-weighted image from the DWI set, using the FSL tool "BET" (FMRIB Software Library, http://fsl.fmrib.ox.ac.uk/fsl/). Intracranial volume estimates were obtained from the full brain mask, and included cerebral, cerebellar, and brain stem regions. All T1-weighted images were linearly aligned using FSL (with 9 DOF) to a common space (Holmes et al., 1998) with 1 mm isotropic voxels and a $220 \times 220 \times 220$ voxel matrix. Raw diffusion-weighted images were corrected for eddy current distortions using the FSL tool, "eddy_correct". For each subject, the 11 eddy-corrected images with no diffusion sensitization were averaged, linearly aligned and resampled to a downsampled version of their corresponding T1 image ($110 \times 110 \times 110$, $2 \times 2 \times 2$ mm). Averaged b_0 maps were elastically registered to the structural scan using a mutual information cost function (Leow et al., 2005) to compensate for EPI-induced susceptibility artifacts.

35 cortical labels per hemisphere, as listed in the Desikan–Killiany atlas (Desikan et al., 2006), were automatically extracted from all aligned T1-weighted structural MRI scans using FreeSurfer (http://surfer.nmr.mgh.harvard.edu/). As a linear registration is performed by the software, the resulting T1-weighted images and cortical models were aligned to the original T1-weighted input image space and down-sampled using nearest neighbor interpolation (to avoid

Table 1
Demographics of study sample. IQ was not collected for the 12-year-old cohort. yo=years old.

Group	N	Mean age (SD)	M/F	FIQ	PIQ	VIQ
Adults	337	23.6 (2.19)	126/211	112	115	115
Kids	102	14.4 (1.95)	49/53	112	119	117
12 yo	55	12.3 (0.18)	24/31	NA	NA	NA
16 yo	47	16.2 (0.37)	25/22	112	119	117

intermixing of labels) to the space of the DWIs. To ensure tracts would intersect cortical labeled boundaries, labels were dilated with an isotropic box kernel of width 5 voxels.

The transformation matrix from the linear alignment of the mean b_0 image to the T1-weighted volume was applied to each of the 94 gradient directions to properly re-orient the orientation distribution functions (ODFs). At each HARDI voxel, ODFs were computed using the normalized and dimensionless ODF estimator, derived for q-ball imaging (QBI) in Aganj et al. (2010). We performed HARDI tractography on the linearly aligned sets of DWI volumes using these ODFs. Tractography was performed using the Hough transform method as described in Aganj et al. (2011).

Elastic deformations obtained from the EPI distortion correction, mapping the average b_0 image to the T1-weighted image, were then applied to the tracts' 3D coordinates for accurate alignment of the anatomy. Each subject's dataset contained 5,000–10,000 useable fibers (3D curves). Fibers were filtered to eliminate those that may have arbitrarily been drawn on the brain-boundary due to noise and high FA. All duplicate fibers were removed.

For each subject, a full 70×70 connectivity matrix was created. Each element described the proportion of the total number of fibers connecting each of the labels; diagonal elements of the matrix describe the total number of fibers passing through a certain cortical region of interest. These values were calculated as a proportion – they were normalized to the total number of fibers traced for each person in the study – so that results were not skewed by raw fiber count.

Graph theory analyses

On the 70×70 matrices generated above, we used the Brain Connectivity Toolbox (Rubinov and Sporns, 2010; https://sites.google.com/a/brain-connectivity-toolbox.net/bct/Home) to compute seven standard measures of global brain connectivity — characteristic path length (CPL), mean clustering coefficient (MCC), global efficiency (EGLOB), small-worldness (SW), and modularity (MOD), as well as normalized path length (lambda) and normalized clustering coefficient (gamma). CPL measures the average path length in a network, where the path length is defined as the minimum number of edges that must be traversed to get from one node to another (note this depends on the number of nodes traversed, and does not depend on the physical length of axons or how they are organized spatially in the brain). MCC is a measure of how many neighbors of a given node are also connected to each other, in proportion to the maximum number of connections in the network. EGLOB is inversely related to CPL: networks with a small average CPL are generally more efficient than those with large average CPL. SW represents the balance between network differentiation and network integration, calculated as a ratio of local clustering and characteristic path length of a node relative to the same ratio in a randomized network. We created 15 simulated random networks. The ratio of clustering in our network to the average clustering in a simulated random network – with the same number of nodes and connections – is gamma, while the ratio of characteristic path length in our network to the average path length in a simulated random network is lambda. MOD is the degree to which a system may be subdivided into smaller networks (Bullmore and Bassett, 2010). We also calculated 4 standard nodal measures of connectivity — regional efficiency (EREG), "betweenness centrality" (BC), degree, and clustering coefficient (CC). EREG is the global efficiency computed for each node and is related to the clustering coefficient (Latora and Marchiori, 2001). BC is the fraction of all of the shortest paths in a network that contain a given node with higher numbers indicating participation in a large number of shortest paths (Kintali, 2008). Degree is the number of links (edges) connected to a node (Sporns, 2002). Equations to calculate these measures may be found in Rubinov and Sporns (2010).

One possible step in graph theory analyses is selecting a sparsity, which is related to thresholding the network (removing nodes and edges based on their weightings). The sparsity is the fraction of connections retained from the full network: setting a sparsity level of 0.2 means that only the top 20% of connections are retained for calculations. Selecting a single sparsity level may arbitrarily affect the network measures, so we computed measures at multiple sparsities, and integrated the measures across that range to generate more stable scores. As noted in Dennis et al. (2012b), the sparsity (threshold) determines which nodes remain in a network and is typically defined with the goal of eliminating noisy or unreliable connections. To minimize any effects of arbitrary thresholding, we calculated our network measures over a range of thresholds (Achard and Bullmore, 2007; Bassett et al., 2008; He et al., 2008; Khundrakpam et al., 2012) and integrated over that range. We have shown that this can improve their robustness and test–retest reliability (Dennis et al., 2012c). We selected the range 0.2–0.3 to calculate and integrate these measures, as that range is biologically plausible (Sporns, 2011) and more stable (Dennis et al., 2012a). We calculated these measures for the whole brain over a range of sparsities (0.2–0.3, in 0.01 increments), and calculated the area under the curve of those 11 data points to generate an integrated score for each measure. We also computed network measures for the left and right hemispheres independently.

Age regression

Age-related effects on graph theory metrics of structural brain connectivity were estimated using a general linear model including mixed effects, as well as a simpler linear mixed effects model, as follows:

$$\text{Graph theory metrics} \sim A + \beta_{\text{age}}\text{Age} + \beta_{\text{sex}}\text{Sex} + \beta_{\text{ICV}}\text{ICV}$$
$$+ \beta_{\text{age}^2}\text{Age}^2 + \alpha + \varepsilon \tag{1}$$

$$\text{Graph theory metrics} \sim A + \beta_{\text{age}}\text{Age} + \beta_{\text{sex}}\text{Sex} + \beta_{\text{ICV}}\text{ICV} + \alpha + \varepsilon. \tag{2}$$

Here, "graph theory metrics" could be any of CPL, MCC, EGLOB, SW, MOD, lambda, or gamma. A is the constant graph theory metric term, the βs are the covariate regression coefficients, and α is a coefficient that accounts for random effects. Random effects were used to account for familial relatedness. Both *age* and *age²* were included as variables to model both linear and non-linear age effects. We modeled these variables (*age*, sex, ICV, *age²*) as fixed effects. We initially included an interaction term, *age∗sex*, as well, but it was not kept in the model as it did not fit. ICV denotes intracranial volume, in mm³. We additionally tested the raw 70×70 fiber density matrices on an element-by-element basis to test for any effects of *age* and *age²*, using the same models as above.

Results

Whole brain analyses

The model that included *age* and *age²* together, with sex and ICV as additional covariates (as shown in Eq. (1)), revealed significant linear trends of decreasing CPL, lambda (normalized path length), gamma (normalized clustering coefficient), SW, and MOD with age. Most of these also had a significant *age²* term in the *opposite* direction, indicating an age effect that leveled off. This slowing down of the age effect would be expected, in early adulthood. Scatterplots of these results, and those for the left and right hemispheres treated separately, are shown in Fig. 1. Studies of sex differences in graph theoretical measures of structural brain connectivity are few (Gong et al., 2011; Yan et al., 2011). From these few studies we expected females to have higher global efficiency and higher regional efficiency in temporal nodes. We also expected males to have higher regional efficiency in frontal
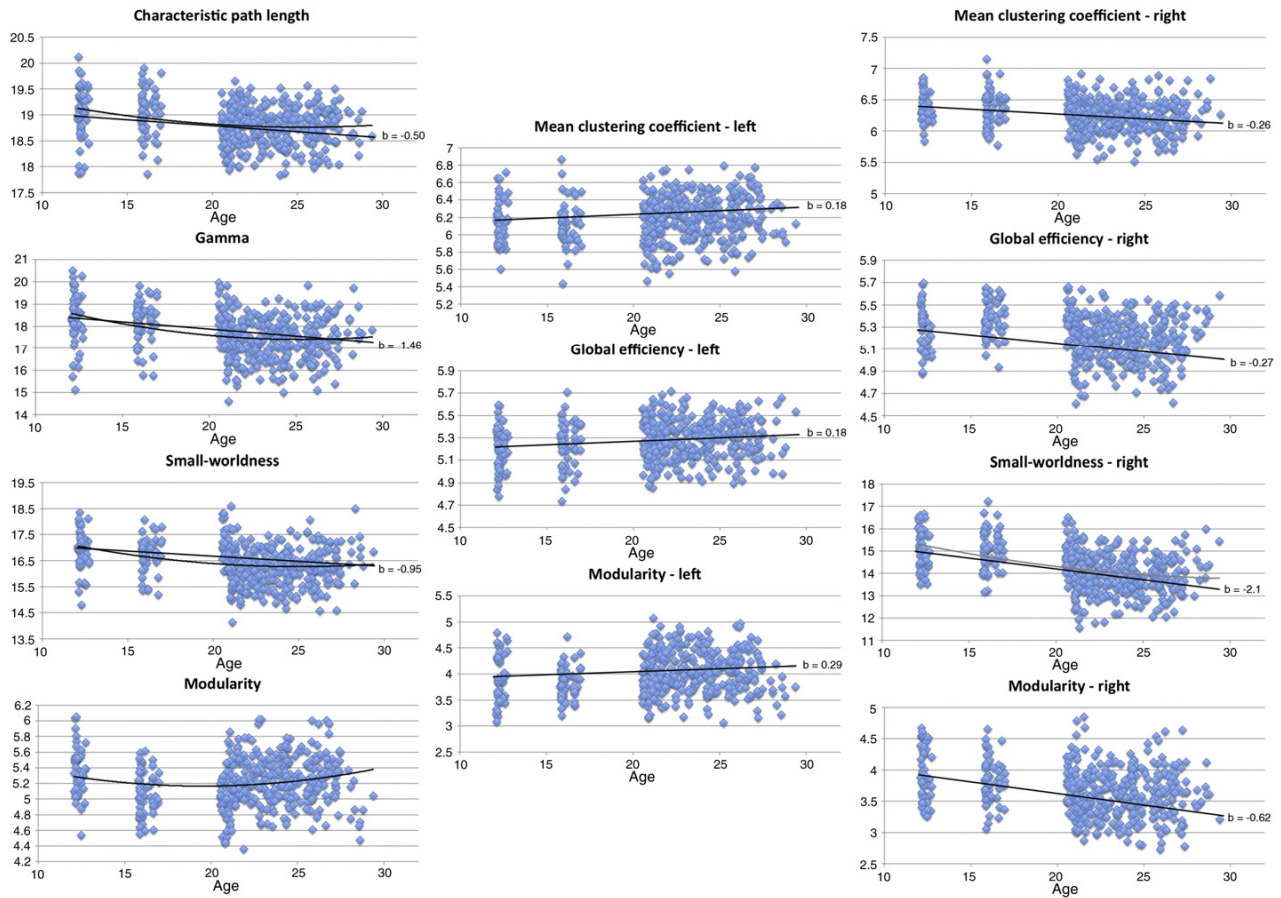
Fig. 1. Scatterplots showing significant associations between global graph theory connectivity scores and *age* in whole brain, left, and right hemispheres. Linear trendlines added with slopes and *b* values (regression coefficients) corresponding to results from Tables 2–4. Slopes taken from *b* values from Eq. (2) results, no linear trendline is included for modularity (whole brain), as that analysis was not significant.

Table 2
Effects of *age* and *age²*, both modeled together (Eq. (1)) and just *age* (Eq. (2)) on global connectivity metrics for the whole brain. FDR corrected within model, with left and right hemisphere analyses FDR corrected separately from whole brain analyses.

Age and *Age²* combined (Eq. (1))

	Age	Age²
Characteristic path length/lambda	−0.11 (0.0043)/−0.038 (0.0073)	0.050 (0.022)/0.024 (0.033)
Mean clustering coefficient/gamma	ns/−0.38 (0.00018)	ns/0.18 (0.0018)
Global efficiency	ns	ns
Small-worldness	−0.26 (0.00053)	0.13 (0.0034)
Modularity	−0.077 (0.013)	0.044 (0.013)

	Sex
Small-worldness	0.018 (0.011)
Gamma	0.022 (0.020)

Age (Eq. (2))

	Age
Characteristic path length/lambda	−0.023 (1.0×10^{-6})/−0.011 (1.9×10^{-6})
Mean clustering coefficient/gamma	ns/−0.066 (8.0×10^{-8})
Global efficiency	ns
Small-worldness	−0.043 (3.1×10^{-6})
Modularity	ns

	Sex
Small-worldness	0.014 (0.034)

nodes. We found significant sex effects for SW and gamma. For both, females tended to have greater values than males. The model described by Eq. (2), modeling *age*, sex, and ICV yielded significant age effects for CPL, gamma, and SW, with all of them decreasing with age, as hypothesized. The beta coefficients and corresponding *p*-values for these whole brain analyses are shown in Table 2. We also found a borderline

Table 3
Effects of *age* and *age²*, both modeled together (Eq. (1)) and just *age* (Eq. (2)) on global connectivity metrics for the left hemisphere. FDR corrected as described for Table 2 (*q*<0.05).

Age and *Age²* combined (Eq. (1))

	Age	Age²
Characteristic path length/lambda	ns/ns	ns/ns
Mean clustering coefficient/gamma	ns/ns	ns/ns
Global efficiency	ns	ns
Small-worldness	ns	ns
Modularity	ns	ns

Age (Eq. (2))

	Age
Characteristic path length/lambda	ns/−0.0054 (0.021)
Mean clustering coefficient/gamma	**0.0082 (0.0036)**/−0.024 (0.027)
Global efficiency	**0.0082 (3.6×10^{-5})**
Small-worldness	ns
Modularity	**0.013 (0.0043)**

Bolded entries are those passing FDR.

31

Table 4

Effects of *age* and *age²*, both modeled together (Eq. (1)) and just *age* (Eq. (2)) on global connectivity metrics for the right hemisphere. FDR corrected as described for Table 2 ($q < 0.05$).

Age and Age² combined (Eq. (1))		
	Age	Age²
Characteristic path length/lambda	ns/ns	ns/ns
Mean clustering coefficient/gamma	−0.054 (0.033)/−0.28 (0.0041)	ns/ns
Global efficiency	ns	ns
Small-worldness	−0.27 (0.0022)	0.10 (0.041)
Modularity	−0.086 (0.025)	ns
	Sex	
Global efficiency	0.0050 (0.0079)	

Age (Eq. (2))	
	Age
Characteristic path length/lambda	ns/ns
Mean clustering coefficient/gamma	**−0.012 (5.7×10^{-5})/−0.095 (4.2×10^{-5})**
Global efficiency	**−0.012 (1.9×10^{-7})**
Small-worldness	**−0.095 (3.7×10^{-16})**
Modularity	**−0.028 (1.4×10^{-9})**
	Sex
Global efficiency	**0.0050 (0.01)**

Bolded entries are those passing FDR.

significant sex effect (it did not survive multiple comparison correction for the number of whole brain global measures tested within this model, FDR correction) for SW for this model. Results were all corrected for multiple comparisons using the false discovery rate

method (FDR; Benjamini and Hochberg, 1995). Linear best-fit lines are charted in Fig. 1, with their regression coefficients, or estimated slopes. These linear trend lines and *b* values come from the regression model including sex and ICV as covariates, not simply age and the BCT measure of interest. The regression coefficients (*b* values) for *age* and *age²* are often of opposite sign, meaning that as we adjust for one co-variate, the other tends to fit in the opposite direction. This indicates a plateau in adulthood, in line with intuition and empirical data on developmental trajectories for other anatomical measures (Thompson et al., 2005).

Left hemisphere analyses

When restricted to the intra-hemispheric connections within the left hemisphere (meaning those that began *and* terminated at left hemisphere nodes), the simpler linear model with only *age* described by Eq. (2) yielded significant results for MCC, EGLOB, and MOD, as well as borderline significant results for lambda and gamma. FDR correction for multiple comparisons was applied across the left and right hemisphere analyses together, within model ($q = 0.05$). The beta coefficients and corresponding *p*-values for the whole-brain analyses are presented in Table 3 and Fig. 1. There were no significant sex effects for the left hemisphere analyses.

Right hemisphere analyses

The model with *age* and *age²* together (Eq. (1)), when restricted to only intra-hemispheric connections within the right hemisphere, yielded borderline significant results for MCC, gamma, SW, and MOD ($p < 0.05$) but not FDR correction. The simpler model with only *age* described by Eq. (2) yielded significant results for MCC, gamma, EGLOB,

Table 5

Effects of *age* and *age²* together on nodal graph theory metrics, as modeled by Eq. (1). 'ns' corresponds to non-significant effect. FDR corrected within model across all nodal metrics tested ($q < 0.05$). Bolded entries survive FDR across all metrics and all nodes within model. Non-bolded entries survive FDR within metric but did not survive FDR across all metrics tested.

	Betweenness centrality	Clustering	Degree	Regional efficiency
Age				
L cuneus	ns	ns	**10 (0.0035)**	ns
L entorhinal	ns	ns	**13 (0.00024)**	ns
L inferior parietal	**−72 (4.6×10^{-6})**	**0.24 (0.00052)**	**−12 (1.2×10^{-6})**	**−0.10 (4.5×10^{-6})**
L lat occipital	**−54 (3.7×10^{-5})**	**0.25 (0.0021)**	−7.2 (0.0059)	ns
L parahippocampal	ns	**−0.50 (9.6×10^{-5})**	**14 (0.00043)**	**0.16 (0.00020)**
L paracentral	**−130 (0.0011)**	ns	ns	ns
L postcentral	−24 (0.0069)	ns	−9.1 (0.0025)	−0.072 (0.0088)
L post cingulate	220 (0.00044)	**−0.22 (3.4×10^{-6})**	**19 (6.4×10^{-6})**	**0.14 (6.9×10^{-6})**
L precentral	**−120 (0.00088)**	ns	−9.5 (0.0099)	−0.082 (0.0051)
L rostral ant cingulate	ns	ns	10 (0.0096)	ns
L rostral mid frontal	**−95 (0.0012)**	**0.26 (0.0020)**	**−10 (0.0017)**	**−0.091 (0.0040)**
L sup frontal	ns	ns	11(0.0085)	0.086 (0.0055)
L supra-marginal	ns	ns	−5.9 (0.010)	ns
L frontal pole	ns	ns	**−8.2 (0.0020)**	−0.34 (0.0053)
R caudal ant cingulate	−44 (0.0086)	**0.21(0.0029)**	**−11(0.0026)**	−0.091(0.0075)
R isthmus of the cingulate	−100 (0.011)	ns	ns	ns
R parahippocampal	ns	ns	ns	0.12 (0.0056)
R paracentral	-54 (0.0049)	ns	ns	ns
R postcentral	ns	**−0.34 (5.1×10^{-6})**	**12 (0.00065)**	**0.10 (0.0014)**
R precuneus	**−190 (0.0026)**	ns	ns	ns
R rostral ant cingulate	−63 (0.0052)	ns	−7.7 (0.005.4)	ns
R rostral mid frontal	ns	ns	−7.2 (0.0021)	ns
R sup temporal	**−50 (0.0012)**	ns	**−9.5 (2.1×10^{-6})**	**−0.091 (2.9×10^{-5})**
R supra-marginal	ns	ns	ns	0.077 (0.0066)
Age²				
L entorhinal	ns	ns	−6.3 (0.0010)	ns
L inferior parietal	**32 (0.00033)**	ns	**5.0 (0.00020)**	**0.050 (0.00023)**
L parahippocampal	ns	**0.22 (0.0021)**	ns	ns
L post cingulate	ns	**0.95 (0.00047)**	**−8.2 (0.00088)**	**−0.054 (0.0011)**
R postcentral	ns	**0.17 (6.9×10^{-5})**	ns	ns
R sup temporal	ns	ns	**5.0 (2.5×10^{-5})**	**0.045 (0.00019)**

Table 6

Effects of *age* alone on nodal graph theory metrics, as modeled by Eq. (2). All 70 connections were tested but only those significant in one of the analyses are included in the table in the interest of space. 'ns' corresponds to non-significant effect. FDR corrected ($q<0.05$). All entries included survive FDR within model across all four metrics tested and all nodes tested.

	Betweenness centrality	Clustering	Degree	Regional efficiency
Age				
L caudal ant cingulate	ns	-0.032 (7.4×10^{-05})	2.7 (0.0054)	0.022 (0.0031)
L caudal mid frontal	ns	-0.022 (0.024)	-1.4 (0.025)	ns
L cuneus	ns	-0.037 (0.0029)	2.6 (7.5×10^{-09})	0.027 (8.7×10^{-09})
L entorhinal	ns	0.10 (0.0039)	1.5 (0.00025)	0.050 (0.00012)
L fusiform	16 (0.0022)	-0.037 (0.00036)	1.6 (6.8×10^{-05})	0.019 (1.8×10^{-07})
L inferior parietal	-17 (2.0×10^{-16})	0.059 (9.3×10^{-13})	-2.9 (3.0×10^{-20})	-0.023 (1.5×10^{-14})
L isthmus of the cingulate	35 (0.00033)	-0.028 (9.7×10^{-07})	3.6 (3.0×10^{-12})	0.027 (2.6×10^{-12})
L lat occipital	-14 (5.4×10^{-17})	0.072 (3.1×10^{-12})	-2.2 (1.6×10^{-11})	-0.020 (6.5×10^{-09})
L lat orbitofrontal	ns	0.042 (0.00050)	-1.6 (0.011)	ns
L lingual	ns	-0.031 (0.00080)	1.6 (5.0×10^{-06})	0.014 (6.5×10^{-06})
L mid temporal	-4.4 (0.00023)	0.031 (0.0020)	-1.4 (0.00016)	-0.013 (0.0013)
L parahippocampal	8.2 (0.0038)	-0.11 (2.4×10^{-12})	4.2 (5.7×10^{-17})	0.044 (2.5×10^{-16})
L paracentral	-27 (3.2×10^{-08})	ns	ns	ns
L pars opercularis	ns	ns	-0.95 (0.0017)	ns
L pars orbitalis	-0.50 (0.021)	ns	-0.82 (0.00041)	-0.0086 (0.025)
L pars triangularis	ns	ns	-0.91 (0.0065)	ns
L peri-calcarine	11 (0.0030)	-0.045 (3.1×10^{-06})	2.1 (3.8×10^{-06})	0.018 (5.34×10^{-06})
L postcentral	-7.7 (7.8×10^{-12})	0.063 (4.3×10^{-11})	-3.1 (1.3×10^{-14})	-0.025 (8.0×10^{-13})
L post cingulate	59 (3.1×10^{-14})	-0.059 (1.7×10^{-20})	5.4 (6.5×10^{-21})	0.040 (6.2×10^{-22})
L precentral	-23 (3.6×10^{-07})	0.023 (0.011)	-2.0 (7.2×10^{-06})	-0.014 (4.9×10^{-05})
L precuneus	-23 (0.0056)	ns	1.1 (0.0020)	0.0086 (0.0017)
L rostral ant cingulate	54 (2.8×10^{-14})	-0.063 (3.8×10^{-14})	3.3 (1.6×10^{-11})	0.028 (1.2×10^{-10})
L rostral mid frontal	-26 (2.7×10^{-12})	0.063 (4.0×10^{-10})	-4.0 (2.2×10^{-19})	-0.034 (1.6×10^{-17})
L sup frontal	42 (8.2×10^{-06})	-0.028 (7.1×10^{-07})	3.0 (4.7×10^{-09})	0.024 (5.3×10^{-10})
L sup parietal	-28 (1.2×10^{-13})	0.034 (1.7×10^{-07})	-1.9 (2.9×10^{-08})	-0.016 (3.4×10^{-08})
L supra-marginal	-7.7 (9.8×10^{-06})	ns	-1.5 (7.8×10^{-08})	-0.0082 (0.00057)
L frontal pole	ns	ns	-2.5 (9.9×10^{-14})	-0.054 (0.00014)
L transverse temporal	ns	-0.072 (6.9×10^{-12})	1.6 (2.4×10^{-06})	0.020 (3.7×10^{-05})
L insula	ns	-0.015 (0.0018)	0.68 (0.015)	0.0082 (0.00093)
R caudal ant cingulate	-12 (2.2×10^{-08})	0.033 (9.8×10^{-05})	-2.1 (6.3×10^{-07})	-0.014 (0.00025)
R caudal mid frontal	-6.8 (0.00081)	ns	ns	ns
R entorhinal	ns	0.14 (6.5×10^{-05})	ns	ns
R isthmus of the cingulate	-15 (0.0012)	ns	ns	ns
R lat occipital	-20 (1.4×10^{-09})	0.039 (9.8×10^{-05})	-1.1 (0.00020)	-0.010 (0.00095)
R lingual	15 (0.011)	-0.034 (0.00014)	1.0 (0.0060)	0.011 (0.0026)
R med orbitofrontal	ns	ns	-1.8 (0.0020)	-0.014 (0.0085)
R mid temporal	11 (3.1×10^{-09})	-0.054 (1.4×10^{-07})	1.8 (1.0×10^{-08})	0.018 (4.7×10^{-08})
R paracentral	-7.7 (0.00048)	0.038 (0.00014)	-1.3 (0.0025)	-0.0086 (0.021)
R pars opercularis	3.9 (4.5×10^{-08})	-0.042 (1.2×10^{-05})	1.6 (3.2×10^{-06})	0.020 (2.5×10^{-07})
R postcentral	8.2 (4.9×10^{-05})	-0.045 (1.6×10^{-07})	2.6 (2.2×10^{-09})	0.022 (6.3×10^{-08})
R post cingulate	-12 (0.00065)	0.015 (0.022)	ns	ns
R precentral	-18 (0.00024)	ns	ns	ns
R precuneus	-38 (1.1×10^{-06})	0.022 (3.9×10^{-05})	-1.1 (0.0017)	-0.0077 (0.0070)
R rostral ant cingulate	-6.3 (0.014)	ns	-1.4 (9.2×10^{-06})	-0.010 (0.0014)
R rostral mid frontal	-20 (2.2×10^{-06})	0.032 (5.2×10^{-06})	-1.8 (3.8×10^{-11})	-0.013 (4.4×10^{-07})
R sup temporal	-6.3 (0.0010)	0.026 (0.0090)	-1.2 (6.2×10^{-07})	-0.011 (1.9×10^{-05})
R supra-marginal	15 (1.2×10^{-10})	-0.041 (2.0×10^{-09})	2.3 (5.5×10^{-09})	0.027 (5.6×10^{-14})
R transverse temporal	ns	ns	1.1 (0.00060)	0.012 (0.0021)

SW, and MOD. The beta coefficients and corresponding *p*-values for whole brain analyses are shown in Table 4 and Fig. 1. Results are FDR corrected across left and right hemisphere analyses within model for multiple comparisons ($q=0.05$). There were sex effects for SW in the right hemisphere, but they only survived FDR for the model described by Eq. (2).

Nodal analyses

Analyses of nodal measures of connectivity (regional efficiency — EREG, degree, clustering coefficient — CC, and betweenness centrality — BC) yielded a number of significant results for the model described by Eq. (1), which are shown in Table 5. When *age* was assessed alone

Table 7

Distribution of significant age-related effects on 4 nodal measures tested, with increases and decreases separated.

	Betweenness centrality		Clustering coefficient		Degree		Regional efficiency		Number of nodes belonging to each lobe
	Incr.	Decr.	Incr.	Decr.	Incr.	Decr.	Incr.	Decr.	
Frontal	4	10	6	6	5	13	5	9	26
Temporal	3	2	4	5	7	2	7	2	20
Parietal	3	8	5	3	4	5	4	5	14
Occipital	2	2	2	4	4	2	4	2	8

1 R Postcentral
6 L Post cingulate
7 L Sup Frontal
8 L Rostral Ant Cingulate
9 L Entorhinal
10 L Parahippocampal
11 L Cuneus

2 R Sup Temporal
3 R Caudal Mid Frontal
4 R Caudal Ant Cingulate
5 R Rostral Ant Cingulate
12 L Inf Parietal
13 L Frontal Pole
14 L Rostral Mid Frontal
15 L Precental
16 L Postcentral
17 L Supramarginal
18 L Lat Occipital
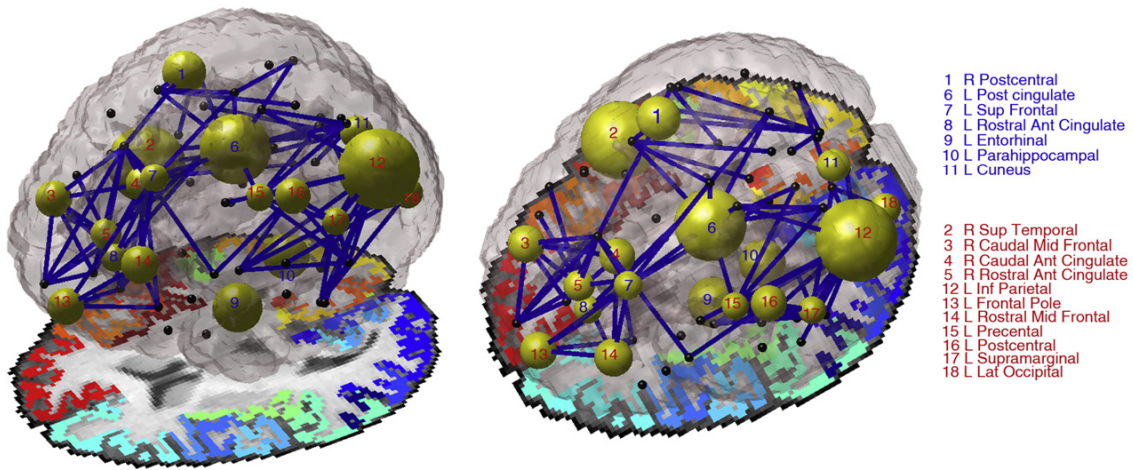
Fig. 2. Image depicting developmental effects, comparing children (12 and 16 year olds) to adults (20–30 year olds). The diameter of each node is inversely proportional to the p-value for the degree analyses — large diameter means node was significantly different in degree between children and adults. Non-significant nodes are colored black. Nodes numbered in blue increase in degree with age, while those numbered with red decrease in degree with age. Blue connections are those that changed with age, corresponding to significant boxes in Fig. 4. For this image we looked only at connections present in at least 95% of subjects. Author NJ is the creator of this image.

(Eq. (2)), age showed effects on several nodal measures (Table 6). Results are FDR corrected for multiple comparisons within model across all nodes and across all four metrics tested ($q = 0.05$). Details of how the significant changes break down by lobe can be found in Table 7. Fig. 2 summarizes the developmental results, showing the differences in paths between groups and the differences in degree

at certain nodes. Additionally, Supplementary Video 1 and Supplementary Video 2 online and Fig. 3 display the increases and decreases, respectively, in degree and fiber density across ages 12–30. While we lack scan data for some parts of the age range, we used the regression coefficients from our analysis to estimate network metrics at each year.
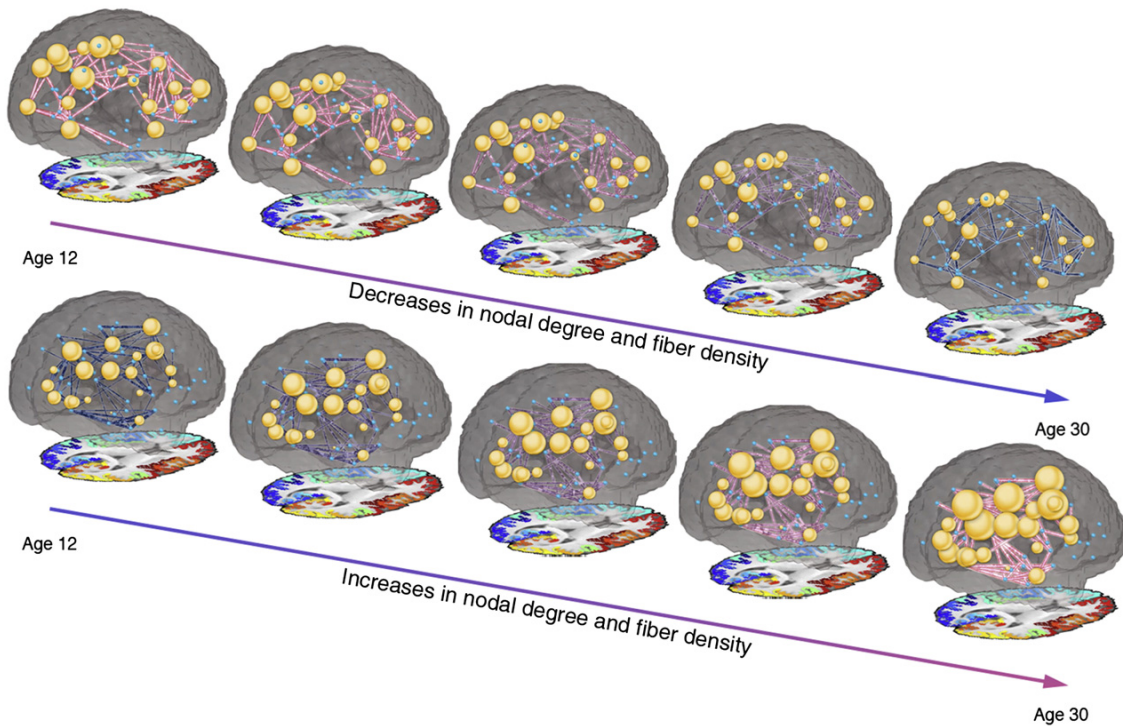
Fig. 3. Still images from Supplementary Video 1 and Supplementary Video 2 displaying the increases and decreases in degree and fiber density between age 12 and age 30. While we lack scan data for some parts of this age range, we used the regression coefficients from our analysis to estimate network metrics at each year. For this image, node size is proportional to the degree (number of connections), and connection thickness is proportional to relative fiber density. The connection color is simulated to make the connections easier to see. The rate of increase or decrease for each node and connection was the regression coefficients from our age analyses for those nodes and connections. Small blue dots indicate nodes for which there was no significant age-related increase or decrease in degree. Only connections that had a significant age-related increase or decrease in fiber density are included in this image, other connections exist but are not drawn in for clarity. In this image are both weighted (fiber density) and binary (degree) measures. These images are created from the results when analyses were restricted to only connections existing in at least 95% of subjects.

34

70×70 fiber density matrices

As we found significant results at the hierarchical levels, we also examined the original 70×70 fiber density matrices, from which these metrics were calculated, for age effects to focus on specific connections. When modeled together (Eq. (1)), we found 112 connections with a significant association with *age* and 50 connections with a significant association with *age²*, out of 1280 connections tested. We ran our analyses in two different ways — the first analysis examined connections existing in at least 95% of subjects, designed to reveal connections that exist in all age groups but change in fiber density. The second kind of analysis examined connections existing in at least 5% of subjects, designed to reveal connections that are gained or lost with age. Out of 2485 possible connections (70×70, symmetrical), we tested only those where at least 5% of subjects had a connection,
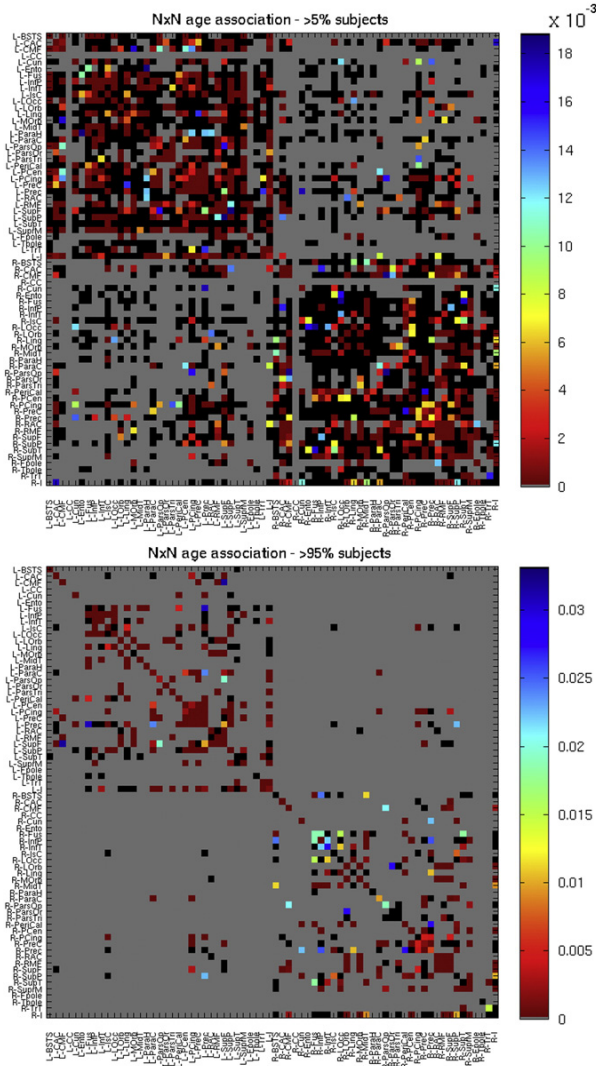
Fig. 4. *P* map of *age* effects, when modeled alone (Eq. (2)), with 70×70 fiber density matrix from which graph theory metrics were calculated. Colors correspond to strength of *p* value as indicated by color bar. Gray boxes were not tested as those connections were not present. For the top *p* map connections that were present in at least 5% of subjects were tested, for the bottom *p* map, connections that were present in at least 95% of subjects were tested. Black boxes were tested but not significant. FDR corrected (*q*<0.05). See Table 9 for region key.

Table 8
List of 10 most significant age-related increases and 10 most significant age-related decreases in proportional fiber density when *age* is examined alone. When only one region is listed, an age-related increase or decrease in the proportion of fibers going through that node was found.

Connection	b-Val
Top 10 increases in fiber density	
L supramarginal×L inferior parietal	−0.000358
R caudal middle frontal	−0.000347
L lateral orbitofrontal×L rostral mid frontal	−0.000255
L med orbitofrontal×L rostral mid frontal	−0.000314
L postcentral×L insula	−0.000276
L insula×L supramarginal	−0.000429
L inferior parietal	−0.00108
L supramarginal×L posterior cingulate	−0.000296
L sup frontal×L rostral mid frontal	−0.000483
R sup frontal×R rostral ant cingulate	−0.000309
Top 10 decreases in fiber density	
L posterior cingulate	0.00337
L paracentral×L posterior cingulate	0.00143
L posterior cingulate×L precuneus	0.000967
L posterior cingulate×L sup frontal	0.000999
R postcentral×R insula	0.000593
L isthmus of the cingulate	0.00277
R postcentral	0.000956
L sup frontal×R prefrontal	0.000168
L isthmus of the cingulate×L precuneus	0.00176
L caudal ant cingulate×L sup frontal	0.00101

resulting in 1280 connections tested. When effects of *age* were modeled alone (Eq. (2)), we found 483 connections with a significant association with age, as shown in Fig. 4. Results are FDR-corrected across all tested connections (*q*=0.05). When *age* was modeled alone, and analyses were restricted to only connections present in at least 95% of subjects, there were 309 connections tested, 213 of which survived FDR, also shown in Fig. 4. Table 8 shows the top 10 increases and top 10 decreases — *i.e.* those with the most significant age association (based on lowest *p*-value) when age was modeled alone and analyses were restricted to connections present in at least 95% of subjects. The left hemisphere is over-represented in these most significant results, perhaps due to the greater effect sizes in the left hemisphere than in the right. There were more connections that decreased in proportional fiber density than increased. The overall number of connections did not change with age; changes were seen in the proportional fiber density of specific connections. Fiber decreases were disproportionally seen in the frontal cortex, while the temporal cortex had disproportionally more fiber density increases.

These analyses were all performed on matrices than had been normalized by the number of fibers tracked, meaning that the results depict changes in proportional fiber density rather than absolute fiber density. However, when analyses were run on the absolute fiber density data, the results were generally unchanged. Compared to the 213 connections found to have a significant age effect on the proportional fiber density data, the absolute fiber density age analysis revealed 220 significant connections. 203 of the 220 significant connections from the absolute fiber density analysis were the same ones that showed significance in the proportional fiber density analysis. 17 new connections were found in the absolute analysis and 10 connections that had been significant in the proportional fiber density analysis were no longer significant in the absolute fiber density analysis. Importantly, however, all significant results were in the same direction, so decreases in proportional fiber density are in fact true decreases in absolute fiber density, and do not simply imply that some connections are increasing to a lesser degree than the average. Fig. 5 shows the developmental trajectory for 70×70 connections and degree, with an average network shown for each group. Supplementary Video 1 and Supplementary Video 2 online, and Fig. 3 display these changes as well.
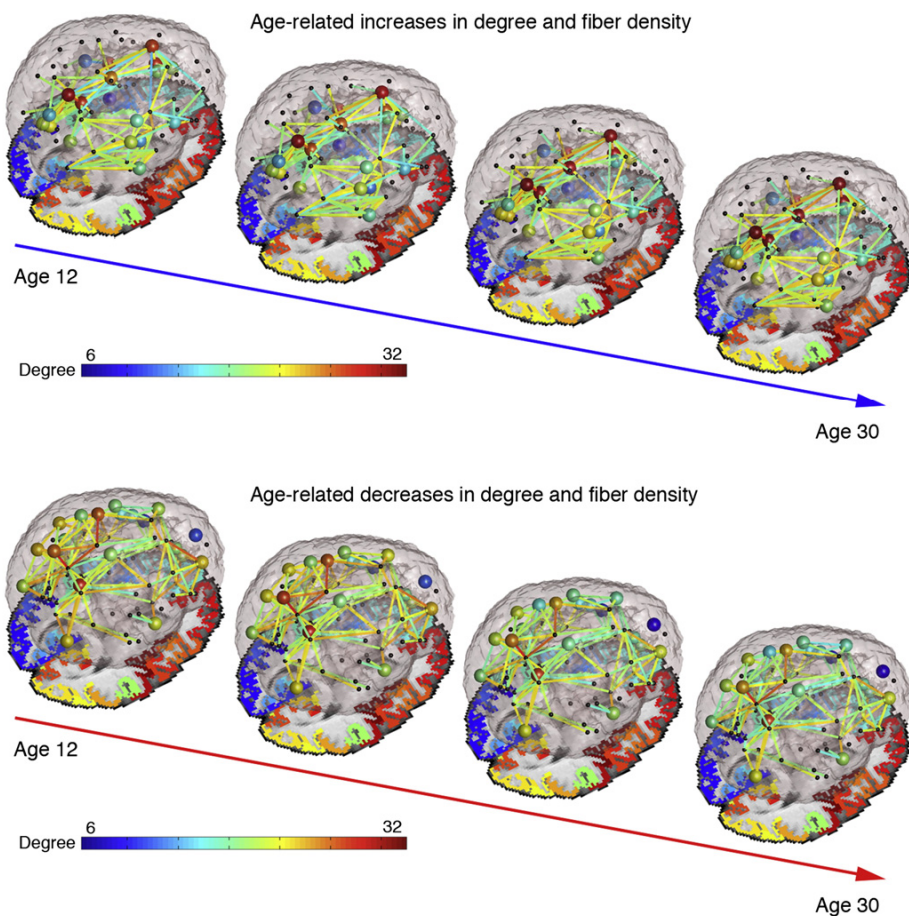
Fig. 5. Image depicting developmental trajectory, with averaged networks shown for four groups (12 year olds, 16 year olds, 20–24 year olds, 24–30 year olds). The color of each connection is proportional to the average fiber density within group with red signifying the thickest connections and blue the thinnest connections; the color of the node is proportional to the average degree of that node within group. For this image we looked only at connections present in at least 95% of subjects. Author NJ is the creator of this image.

Cross-hemisphere connections

Of the 213 connections that survived FDR correction above, 9 were interhemispheric connections. We decided to further examine cross-hemisphere connections by restricting our 70×70 matrices to just assess interhemispheric connections. Of the 20 connections tested, 7 connections showed an age effect — those between the left isthmus of the cingulate and the right posterior cingulate, the left posterior cingulate and right paracentral gyrus, the left and right posterior cingulate, the left posterior cingulate and right precuneus, the left posterior cingulate and right superior frontal gyrus, the left precuneus and the right posterior cingulate, and the left superior frontal gyrus and right precuneus. All of these increased in fiber density with age (Fig. 6).

Sex differences

In addition to the sex differences found above, there were also a few differences in nodal measures of EREG and degree. While few, these results do fit with previous ones from Gong et al. (2009). These are shown in Table 10 and Fig. 7. Results are FDR corrected ($q = 0.05$) with respect to the total number of nodes and measures tested.

Discussion

The current study sought to characterize the developmental trajectory of graph theory metrics of structural connectivity from early adolescence to early adulthood. Although our study was cross-sectional, its sample size was much larger than most prior studies of the developing structural connectome, offering greater power to detect age effects. The brain continues to mature into the twenties (Gogtay et al., 2004) and myelination and network remodeling continue throughout life (Bartzokis, 2004). Between ages 12 and 30, we found a number of linear and nonlinear age effects across the whole brain, for left and right hemispheres, and for specific nodes. These age effects were also seen in the connectivity matrices that served as the basis to compute the graph theory metrics, with significant age effects on fiber density. We also found significant sex differences in a few nodal measures.

For the whole-brain graph theory measures, we found significant effects of decreasing path length, clustering, small-worldness, and modularity with age, and all of these plateaued in early adulthood. Changes in "small-worldness" reflect a network property that itself depends on changes in either normalized clustering coefficient (gamma), normalized path length (lambda), or the ratio between those two. In our results it appears that it was the ratio between these two that changed, as gamma decreased at a faster rate than did lambda. These results are mostly in line with those of Hagmann et al. (2010), who

Fig. 6. *P* maps of *age* effects, when modeled alone (Eq. (2)), with 35×35 interhemispheric fiber density matrix. Colors correspond to strength of *p* value as indicated by color bar. Blue highlighting on regions indicate significance. Gray boxes were not tested as those connections were not present. Black boxes were tested but not significant. FDR corrected (*q*<0.05). See Table 9 for region key.

are strengthened (Casey et al., 2000; Hagmann et al., 2010; Thomason et al., 2011), we might expect the anatomical network as a whole to have a shorter path length, and this is indeed what we found. The fiber density of connections where an age effect was detectable decreased in many connections, disproportionately in the frontal cortex, while it increased in some connections, disproportionately in the temporal and parietal cortices (Fig. 5).

In the left hemisphere analyses, we found linear effects of increasing clustering, global efficiency and modularity with age. In the right hemisphere, we found opposite trends of linear decreases in clustering, global efficiency, small-worldness, and modularity with age. It is curious that the left hemisphere shows trends opposite to the right, and to the network as a whole; this may point to different developmental processes occurring within each hemisphere (Paus et al., 1999; Scheibel et al., 1985; Shaw et al., 2009; Sowell et al., 2003). It appears that these results are driven by asymmetries in the adults for global efficiency and modularity, as both were higher in the left hemisphere than the right for adults, but roughly the same for the 12 year olds. Trends for the clustering coefficient may also be due to anatomical asymmetries for both age groups. Recent work from our laboratory studied asymmetry of these measures in the same sample, finding greater small-worldness in the right hemisphere (Daianu et al., 2012a). Our results are contrary to those of Iturria-Medina et al. (2011), who found greater global efficiency in the right hemisphere, but these were from a relatively small sample of 11 subjects, and our sample is over 40 times larger. One possible explanation is the consistent finding of right/left asymmetry in overall cerebral hemispheric volume, with the right hemisphere being larger on average (Bilder et al., 1994; Giedd et al., 1996). The asymmetry of the many structural and functional features of the brain has long been noted (Dimond and Beaumont, 1974; Hellige, 1993; Toga and Thompson, 2003), with researchers finding asymmetry in FA (Büchel et al., 2004) and regional volumes (Good et al., 2001), as well as finding that the level of asymmetry in fiber integrity was heritable (Jahanshad et al., 2010).

For the nodal analyses, we found many linear and non-linear age effects, for all four of the nodal metrics tested. For betweenness

also reported decreased clustering and small-worldness in a much smaller sample of 30 subjects. The global results of decreasing path length, clustering, and modularity suggest that structural network integration increases during the teenage years. All subjects, regardless of age, showed a small-world topology in their brain networks. Adolescence is marked by parallel decreases in gray matter density, due in part to synaptic pruning (Gogtay et al., 2004), and increases in intracortical myelination through young adulthood (Giedd et al., 1999). As some short-range connections are pruned and other long-range ones

Fig. 7. Bar graphs of nodes showing significant sex effects for degree (integrated over range of sparsities). FDR corrected (*q*<0.05).

centrality, there were more decreases with age than increases, perhaps demonstrating network refinement as fibers are pruned from some connections. Betweenness centrality shows how "central" a node is to the network, based on how many of the shortest paths go through that node. The clustering coefficient increased in about the same number of nodes as it decreased with age — this network measure refers to how many of a node's neighbors are also connected to each other. For both betweenness centrality and the clustering coefficient, we could not discern any obvious pattern in the nodal locations of the increases or decreases. The nodal degree reflects the number of nodes a given node is connected to, and we found roughly equal representations of statistically significant increases in degree and decreases in degree with age. However, in the frontal cortex, many more nodes *decreased* in degree than increased. Conversely, of the nodes in the temporal cortex showing an age effect, more increased in degree than decreased. Similarly, we found roughly equal increases and decreases in regional efficiency with age, but there were more frontal nodes that decreased in efficiency than increased, and more temporal nodes that increased in efficiency than decreased. This may be a manifestation of the more protracted developmental trajectory of the frontal lobe compared to other lobes (Gogtay et al., 2004), or it may point to different processes occurring in different regions of the brain. A few of these nodes also had significant age^2 terms that fit in the opposite direction, suggesting that these age effects plateaued in early adulthood. Gong et al. (2009) also reported more increases in regional efficiency in the temporal cortex with age, but they were examining a different age range (19–85). Regional efficiency is a

Table 9
Region key.

Abbreviation	Region	Abbreviation	Region
L-BSTS	L Banks of the Superior Temporal Sulcus	R-BSTS	R Banks of the Superior Temporal Sulcus
L-CAC	L Caudal Anterior Cingulate	R-CAC	R Caudal Anterior Cingulate
L-CMF	L Caudal Middle Frontal	R-CMF	R Caudal Middle Frontal
L-CC	L Corpus Callosum	R-CC	R Corpus Callosum
L-Cun	L Cuneus	R-Cun	R Cuneus
L-Ento	L Entorhinal	R-Ento	R Entorhinal
L-Fus	L Fusiform	R-Fus	R Fusiform
L-InfP	L inferior Parietal	R-InfP	R Inferior Parietal
L-InfT	L inferior Temporal	R-InfT	R Inferior Temporal
L-IsC	L Isthmus of the Cingulate	R-IsC	R Isthmus of the Cingulate
L-LOcc	L Lateral Occipital	R-LOcc	R Lateral Occipital
L-LOrb	L Lateral Orbitofrontal	R-LOrb	R Lateral Orbitofrontal
L-Ling	L Lingual	R-Ling	R Lingual
L-MOrb	L Medial Orbitofrontal	R-MOrb	R Medial Orbitofrontal
L-MidT	L Middle Temporal	R-MidT	R Middle Temporal
L-ParaH	L Parahippocampal	R-ParaH	R Parahippocampal
L-ParaC	L Paracentral	R-ParaC	R Paracentral
L-ParsOp	L Pars opercularis	R-ParsOp	R Pars opercularis
L-ParsOr	L Pars orbitalis	R-ParsOr	R Pars orbitalis
L-ParsTri	L Pars triangularis	R-ParsTri	R Pars triangularis
L-PeriCal	L Peri-calcarine	R-PeriCal	R Peri-calcarine
L-PCen	L Postcentral	R-PCen	R Postcentral
L-PCing	L Posterior Cingulate	R-PCing	R Posterior Cingulate
L-PreC	L Precentral	R-PreC	R Precentral
L-Prec	L Precuneus	R-Prec	R Precuneus
L-RAC	L Rostral Anterior Cingulate	R-RAC	R Rostral Anterior Cingulate
L-RMF	L Rostral Middle Frontal	R-RMF	R Rostral Middle Frontal
L-SupF	L Superior Frontal	R-SupF	R Superior Frontal
L-SupP	L Superior Parietal	R-SupP	R Superior Parietal
L-SupT	L Superior Temporal	R-SupT	R Superior Temporal
L-SuprM	L Supra-marginal	R-SuprM	R Supra-marginal
L-Fpole	L Frontal Pole	R-Fpole	R Frontal Pole
L-Tpole	L Temporal Pole	R-Tpole	R Temporal Pole
L-TrT	L Transverse Temporal	R-TrT	R Transverse Temporal
L-I	L Insula	R-I	R Insula

Table 10
Sex differences in nodal measures of connectivity. Males were coded as '1' and females as '2', thus a positive b value indicates greater nodal scores in females. FDR corrected ($q<0.05$).

	Degree	Regional efficiency
L precuneus	ns	−0.0082 (0.00057)
L temporal pole	1.3 (0.00038)	ns
R pars orbitalis	−0.91 (0.00049)	−0.019 (8.5×10^{-5})

nodal measure related to global efficiency, computed on node neighborhoods.

Tests of age effects on the 70×70 connectivity matrices revealed that fiber density decreased in more connections than it increased, but these decreases were distributed disproportionately around the brain. Follow-up analyses on the absolute fiber density data confirm that a decrease in proportional fiber density truly reflects a decrease in absolute fiber density, rather than just a more modest increase than average. Connections to and from the frontal cortex disproportionately decreased with age, relative to the changes detected in other brain regions (Figs. 3 and 5, Supplementary Video 2). This was partially due to lower overall variance in the frontal cortex relative to both the temporal or parietal cortices, and also due to the greater effect sizes detected in the frontal cortex (and parietal cortex) than in the temporal cortex. Conversely, those connections leading to and from regions in the temporal cortex showed disproportionately more fiber density increases with age (Figs. 3 and 5, Supplementary Video 1). Of all the significant age-related changes in fiber density, 57% were decreases and 43% were increases. Within the significant changes in connections that terminate in the frontal cortex, however, 70% were decreases and 30% were increases. Of the significant changes in the temporal cortex, 43% were decreases and 57% were increases. In the occipital cortex, 55% were decreases and 45% were increases. In the parietal cortex, 52% were decreases and 48% were increases. This mirrors the distribution of our nodal results assessing regional efficiency: the nodal degree is likely a driving factor behind these nodal results.

Prior work has revealed different developmental trajectories for the volumes of different cortical gray matter regions as well as lobar volumes that include white matter as well (Gogtay et al., 2004; Sowell et al., 2003). Giedd et al. (1999) found that the temporal cortex tended to achieve its peak for both gray and white matter volume at a later age than other lobar brain regions. Sowell et al. (2003) found that gray matter density (GMD) in the superior frontal sulcus steadily declined from age 7 on, but it increased in the superior temporal sulcus until age 30, after which it steadily declined. They found this same inverted U-shaped trajectory for a number of temporal regions, but the frontal regions all showed a steady decline in GMD from age 7 on. These findings were supported by similar results from a previous study (Sowell et al., 2002a). Several processes are active throughout development, and if they occur at different rates across the cortex, they could lead to these different trajectories and patterns of differences. Huttenlocher (1979, 1990) found different rates of synaptic pruning across the cortex. Additionally, continuing myelination (Bartzokis, 2004; Bartzokis et al., 2010), and the addition of new neurons (reviewed by Gould, 2007) may contribute to the changes we report here.

Studies of callosal development during adolescence show developmental increases in volume or cross-sectional area for the splenium and isthmus (Chung et al., 2001; Thompson et al., 1999; Thompson et al., 2000), suggesting an increase with age in the level of myelination and/or axon count for interhemispheric connections traveling through those regions. The splenium and isthmus connect the temporal, parietal, and occipital cortices with their counterparts on the opposite hemisphere, as well as with some other cortical regions (Hofer and Frahm,

2006; Witelson, 1989). All of our 7 interhemispheric connections with detectable age effects had a terminus in the parietal lobe or posterior cingulate. This is perhaps most likely to be due to increased myelination (Bartzokis et al., 2010).

We found a few sex differences in global and nodal connectivity as well. Females had greater small-worldness and gamma (which are related measures) in whole brain parameters. Gamma (normalized clustering coefficient) is a measure of network segregation as it measures how many of a node's neighbors are interconnected. This result suggests that females have more clustered, highly segregated networks than males do. Females also had greater degree in the left temporal pole, while males had greater degree in the right *pars orbitalis* and greater efficiency in the left precuneus and right *pars orbitalis*. While there are both consistent and conflicting results when it comes to sex differences in the brain (Kimura, 2000), a number of previous studies have noted proportionally larger temporal lobes in females than in males (Harasty et al., 1997; Sowell et al., 2002b; Luders et al., 2009) with thicker cortices (Sowell et al., 2007), possibly contributing to this effect on degree and efficiency. Gong et al. (2009), found greater global and local efficiency in females, which we did not, but they did find greater regional efficiency in females in temporal nodes and greater regional efficiency in males in frontal nodes, which overlaps with our results. Yan et al. (2011), found similar results, also revealing a sex by brain size interaction, where smaller brains showed higher local efficiency in women but not on men. Studies of sex differences in brain structural networks are important for possibly explaining the differences in susceptibility to disease or outcome after brain injury (Turkheimer and Farace, 1992). Future work should investigate whether these differences have any consequences for sex differences in cognition or vulnerability to disease, or if they are simply due to allometry (non-proportional scaling of brain structures relative to body size; Brun et al., 2009).

One limitation of the current study is the uneven sampling of the different age ranges, due to the availability of cohorts assessed at 12 and 16 but not in between. Nonparametric regression models may therefore be more appropriate for deriving *p*-values for the fitted regression coefficients. Obviously, the specific parcellation scheme chosen will affect graph theory metrics. Zalesky et al. (2010) found that graph theory metrics were sensitive to parcellation resolution (*i.e.*, the number of nodes), but Hagmann et al. (2010) found very similar developmental trajectories at two different parcellation resolutions. Other future parcellation schemes may be more sensitive to developmental effects, but the Desikan–Killiany atlas has been shown by our laboratory to yield connectivity measures that are genetically influenced (Jahanshad et al., 2011; Jahanshad et al., 2012); it was one of the atlases used by Hagmann et al. (2010).

Conclusions

In summary, we found that structural brain networks decrease in path length, clustering, small-worldness, and modularity with age, although this effect may differ by hemisphere. We found significant sex differences in nodal measures of connectivity, but it remains to be seen whether these differences are related to any sex differences in cognitive function or in resilience to disease. Graph theory metrics have been associated with disease and cognitive function (Brown et al., 2011; Daianu et al., 2012b; Langer et al., 2012; Li et al., 2009), so investigating this difference further may shed light on sex differences in aspects of cognition or disease vulnerability. Defining the expected developmental trajectory of structural connectivity measures in healthy individuals is critical for gauging the effect of neuropsychiatric disorders, and ultimately of interventional factors, on development.

Supplementary data to this article can be found online at http://dx.doi.org/10.1016/j.neuroimage.2012.09.004.

References

Achard, S., Bullmore, E., 2007. Efficiency and cost of economical brain functional networks. PLoS Comput. Biol. 3, e17.
Aganj, I., Lenglet, C., Sapiro, G., 2010. Reconstruction of the orientation distribution function in single-and multiple-shell q-ball imaging within constant solid angle. Magn. Reson. Med. 64 (2), 554–566.
Aganj, I., Lenglet, C., Jahanshad, N., Yacoub, E., Harel, N., Thompson, P.M., Sapiro, G., 2011. A Hough transform global probabilistic approach to multiple-subject diffusion MRI tractography. Med. Image Anal. 15 (4), 414–425.
Annett, M., 1970. A classification of hand preference by association analysis. Br. J. Psychol. 61 (3), 303–321.
Bartzokis, G., 2004. Quadratic trajectories of brain myelin content: unifying construct for neuropsychiatric disorders. Neurobiol. Aging 25, 49–62.
Bartzokis, G., Lu, P.H., Tingus, K., Mendez, M.F., Richard, A., Peters, D.G., Oluwadara, B., Barrall, K.A., Finn, J.P., Villablanca, P., Thompson, P.M., Mintz, J., 2010. Lifespan trajectory of myelin integrity and maximum motor speed. Neurobiol. Aging 31 (9), 1554–1562.
Bassett, D.S., Bullmore, E., Verchinski, B.A., Mattay, V.S., Weinberger, D.R., Meyer-Lindenberg, A., 2008. Hierarchical organization of human cortical networks in health and schizophrenia. J. Neurosci. 28 (37), 9239–9248.
Benjamini, Y., Hochberg, Y., 1995. Controlling the false discovery rate: a practical and powerful approach to multiple testing. J. R. Stat. Soc. Ser. B 57 (1), 289–300.
Bilder, R.M., Wu, H., Bogerts, B., Degreef, G., Ashtari, M., Alvir, J.M., Snyder, P.J., Lieberman, J.A., 1994. Absence of regional hemisphere volume asymmetries in first episode schizophrenia. Am. J. Psychiatry 151, 1437–1447.
Braskie, M., Jahanshad, N., Stein, J., Barysheva, M., McMahon, K., de Zubicaray, G.I., Martin, N.G., Wright, M.J., Ringman, J.M., Toga, A.W., Thompson, P.M., 2011. Common Alzheimer's Disease Risk Variant Within the CLU Gene Affects White Matter Microstructure in Young Adults. J. Neurosci. 31, 6764–6770.
Braskie, M., Jahanshad, N., Stein, J., Barysheva, M., Johnson, K., McMahon, K., de Zubicaray, Martin, N.G., Wright, M.J., Ringman, J.M., Toga, A.W., Thompson, P.M., 2012. Relationship of a Variant in the NTRK1 Gene to White Matter Microstructure in Young Adults. J. Neurosci. 32, 5964–5972.
Brown, J.A., Terashima, K.H., Burggren, A.C., Ercoli, L.M., Miller, K.J., Small, G.W., Bookheimer, S.Y., 2011. Brain network local interconnectivity loss in aging APOE-4 allele carriers. Proc. Natl. Acad. Sci. 108 (51), 20760–20765.
Brun, C., Lepore, N., Luders, E., Chou, Y., 2009. Sex differences in brain structure in auditory and cingulate regions. Neuroreport 20 (10), 930–935.
Büchel, C., Raedler, T., Sommer, M., Sach, M., Weiller, C., Koch, M.A., 2004. White matter asymmetry in the human brain: a diffusion tensor MRI study. Cereb. Cortex 14 (9), 945–951.
Bullmore, E.T., Bassett, D.S., 2010. Brain graphs: graphical models of the human brain connectome. Reviews in Advance, pp. 1–37.
Casey, B.J., Giedd, J.N., Thomas, K.M., 2000. Structural and functional brain development and its relation to cognitive development. Biol. Psychiatry 54, 241–257.
Chung, M.K., Worsley, K.J., Paus, T., Cherif, C., Collins, D.L., Giedd, J.N., Rapoport, J.L., Evans, A.C., 2001. A unified statistical approach to deformation-based morphometry. NeuroImage 14, 595–606.
Daianu, M., Jahanshad, N., Dennis, E., Toga, A.W., de Zubicaray, G., Martin, N.G., Wright, M.J., Hickie, I., Thompson, P.M., 2012a. Left versus right hemisphere differences in brain connectivity: 4-Tesla HARDI tractography in 569 twins. Proc. 9th IEEE ISBI. IEEE, Piscataway, NJ, Barcelona, pp. 526–529.
Daianu, M., Jahanshad, N., Nir, T., Dennis, E., Toga, A.W., Jack Jr., C.R., Weiner, M.W., Thompson, P.M., the Alzheimer's Disease Neuroimaging Initiative, 2012b. Analyzing the Structural k-core of Brain Connectivity Networks in Normal Aging and Alzheimer's Disease. Workshop on Novel Imaging Biomarkers for Alzheimer's Disease and Related Disorders. 15th Medical Image Computing and Computer Assisted Intervention (MICCAI). Nice, (to appear) 2012.
de Zubicaray, G.I., Chiang, M.-C., McMahon, K.L., Shattuck, D.V., Toga, A.W., Martin, N.G., Wright, M.J., Thompson, P.M., 2008. Meeting the challenges of neuroimaging genetics. Brain Imaging Behav. 2, 258–263.
Dennis, E.L., Jahanshad, N., Toga, A., Brown, J., Rudie, J., Bookheimer, S., Dapretto, M., Johnson, K., McMahon, K., de Zubicaray, G., Martin, N., Wright, M., Thompson, P., 2011. Heritability of structural brain connectivity network measures in 188 twins. Proc. 41st Annual Meeting of the Society for Neuroscience. Washington, D.C., 12 to 16 November 2011.

Dennis, E.L., Jahanshad, N., Rudie, J.D., Brown, J.A., Johnson, K., McMahon, K.L., de Zubicaray, G.I., Montgomery, G., Martin, N.G., Wright, M.J., Bookheimer, S.Y., Dapretto, M., Toga, A.W., Thompson, P.M., 2012a. Altered structural brain connectivity in healthy carriers of the autism risk gene, CNTNAP2. Brain Connectivity 1 (6), 447–459.

Dennis, E.L., Jahanshad, N., Toga, A., Johnson, K., McMahon, K., de Zubicaray, G., Martin, N., Hickie, I.B., Wright, M., Thompson, P., 2012b. changes in anatomical brain connectivity between ages 12 and 30: a HARDI study of 467 adolescents and adults. Proc. 9th IEEE ISBI, pp. 904–907. IEEE, Piscataway, NJ, Barcelona.

Dennis, E.L., Jahanshad, N., Toga, A.W., McMahon, K.L., de Zubicaray, G.I., Martin, N.G., Wright, M.J., Thompson, P.M., 2012c. Test–retest reliability of graph theory measures of structural brain connectivity. Proc. 15th MICCAI. Nice, (to appear) 2012.

Desikan, R., Ségonne, F., Fischl, B., Quinn, B., 2006. An automated labeling system for subdividing the human cerebral cortex on MRI scans into gyral based regions of interest. NeuroImage 31, 968–980.

Dimond, Beaumont, 1974. Hemisphere Function in the Human Brain. John Wiley & Sons, Oxford, England.

Dosenbach, N.U.F., Nardos, B., Cohen, A.L., Fair, D.A., Power, J.D., Church, J.A., Nelson, S.M., Wig, G.S., Vogel, A.C., Lessov-Schlaggar, C.N., Barnes, K.A., Dubis, J.W., Feczko, E., Coalson, R.S., Pruett, J.R., Barch, D.M., Petersen, S.E., Schlaggar, B.L., 2010. Prediction of individual brain maturity using fMRI. Science 329 (5997), 1358–1361.

Giedd, J.N., Snell, J.W., Lange, N., Rajapakse, J.C., Casey, B.J., Kozuch, P.L., Vaituzis, A.C., Vauss, Y.C., Hamburger, S.D., Kaysen, D., Rapoport, J.L., 1996. Quantitative magnetic resonance imaging of human brain development: ages 4–18. Cereb. Cortex 6 (4), 551–559.

Giedd, J.N., Blumenthal, J., Jeffries, N.O., Castellanos, F.X., Liu, H., Zijdenbos, A., Paus, T., Evans, A.C., Rapoport, J.L., 1999. Brain development during childhood and adolescence: a longitudinal MRI study. Nat. Neurosci. 2 (10), 861–863.

Gogtay, N., Giedd, J.N., Lusk, L., Hayashi, K.M., Greenstein, D., Vaituzis, A.C., Nugent III, T.F., Herman, D.H., Clasen, L.S., Toga, A.W., Rapoport, J.L., Thompson, P.M., 2004. Dynamic mapping of human cortical development during childhood through early adulthood. Proc. Natl. Acad. Sci. 101 (21), 8174–8179.

Gong, G., Rosa-Neto, P., Carbonell, F., Chen, Z.J., He, Y., Evans, A.C., 2009. Age- and gender-related differences in the cortical anatomical network. J. Neurosci. 29 (50), 15684–15693.

Gong, G., He, Y., Evans, A.C., 2011. Brain connectivity: gender makes a difference. Neuroscientist 17 (5), 575–591.

Good, C.D., Johnsrude, I.S., Ashburner, J., Henson, R.N.A., Friston, K.J., Frackowiak, R.S.J., 2001. A voxel-based morphometric study of ageing in 465 normal adult human brains. NeuroImage 14, 21–36.

Gould, E., 2007. How widespread is adult neurogenesis in mammals? Nat. Rev. Neurosci. 8, 481–488.

Hagmann, P., Sporns, O., Madan, N., Cammoun, L., Pienaar, R., Wedeen, V.J., Meuli, R., Thiran, J.-P., Grant, P.E., 2010. White matter maturation reshapes structural connectivity in the late developing human brain. Proc. Natl. Acad. Sci. 107 (44), 19067–19072.

Harasty, J., Double, K., Halliday, G., Kril, J., 1997. Language-associated cortical regions are proportionally larger in the female brain. Arch. Neurol. 54 (2), 171–176.

He, Y., Chen, Z., Evans, A., 2008. Structural insights into aberrant topological patterns of large-scale cortical networks in Alzheimer's disease. J. Neurosci. 28, 4756–4766.

Hellige, J.B., 1993. Hemispheric Asymmetry: What's Right and What's Left. Harvard University Press, Cambridge, MA.

Hofer, S., Frahm, J., 2006. Topography of the human corpus callosum revisited — comprehensive fiber tractography using diffusion tensor magnetic resonance imaging. NeuroImage 32 (3), 989–994.

Holmes, C., Hoge, R., Collins, L., 1998. Enhancement of MR images using registration for signal averaging. J. Comput. Assist. Tomogr. 22 (2), 324–333.

Huttenlocher, P., 1979. Synaptic density in the human frontal cortex — developmental changes and effects of aging. Brain Res. 163 (2), 195–205.

Huttenlocher, P., 1990. Morphometric study of human cerebral cortex development. Neuropsychologia 28 (6), 517–527.

Iturria-Medina, Y., Fernández, A.P., Morris, D.M., Canales-Rodríguez, E.J., Haroon, H.A., Pentón, L.G., Augath, M., García, L.G., Logothetis, N., Parker, G.J.M., Melie-García, L., 2011. Brain hemispheric structural efficiency and interconnectivity rightward asymmetry in human and nonhuman primates. Cereb. Cortex 21, 56–67.

Jackson, D.N., 1998. Multidimensional Aptitude Battery II. Sigma Assessment Systems, Port Huron, MI.

Jahanshad, N., Lee, A., Barysheva, M., McMahon, K.L., de Zubicaray, G.I., Martin, N.G., Wright, M.J., Toga, A.W., Thompson, P.M., 2010. Genetic influences on brain asymmetry: a DTI study of 374 twins and siblings. NeuroImage 52, 455–469.

Jahanshad, N., Aganj, I., Lenglet, C., Joshi, A., Jin, Y., Barysheva, M., McMahon, K.L., de Zubicaray, G.I., Martin, N.G., Wright, M.J., Toga, A.W., Sapiro, G., Thompson, P.M., 2011. Sex differences in the human connectome: 4-Tesla high angular resolution diffusion imaging (HARDI) tractography in 234 young adult twins. Proc. 8th IEEE ISBI. IEEE, Piscataway, NJ, Chicago, pp. 939–943.

Jahanshad, N., Hibar, D.P., Ryles, A., McMahon, K.L., de Zubicaray, G.I., Martin, N.G., Wright, M.J., Toga, A.W., Thompson, P.M., 2012. Discovery of genes that affect human brain connectivity: a genome-wide analysis of the connectome. Proc. 9th IEEE ISBI. IEEE, Piscataway, NJ, Barcelona.

Khundrakpam, B.S., Reid, A., Brauer, J., Carbonell, F., Lewis, J., Ameis, S., Karama, S., Lee, J., Chen, Z., Das, S., Evans, A.C., & Brain Development Cooperative Group, 2012. Developmental changes in organization of structural brain networks. Cereb. Cortex. Jul 10. [Epub ahead of print].

Kimura, D., 2000. Sex and Cognition. MIT Press, Cambridge, MA.

Kintali, S., 2008. Betweenness centrality: algorithms and lower bounds. (arXiv, 0809.1906v0802) .

Kochunov, P., Williamson, D.E., Lancaster, J., Fox, P., Cornell, J., Blangero, J., Glahn, D.C., 2010. Fractional anisotropy of water diffusion in cerebral white matter across the lifespan. Neurobiol. Aging 1–12.

Langer, N., Pedroni, A., Gianotti, L.R., Hänggi, J., Knoch, D., Jäncke, L., 2012. Functional brain network efficiency predicts intelligence. Hum. Brain Mapp. 33 (6), 1393–1406.

Latora, V., Marchiori, M., 2001. Efficient behavior of small-world networks. Phys. Rev. Lett. 87 (19), 1–4.

Lenroot, R.K., Gogtay, N., Greenstein, D.K., Molloy, E., Wallace, G.L., Clasen, L.S., Blumenthal, J.D., Lerch, J., Zijdenbos, A.P., Evans, A.C., Thompson, P.M., Giedd, J.N., 2007. Sexual dimorphism of brain developmental trajectories during childhood and adolescence. NeuroImage 36 (4), 1065–1073.

Leow, A., Huang, S., Geng, A., Becker, J., Davis, S., Toga, A., Thompson, P., 2005. Inverse consistent mapping in 3D deformable image registration: its construction and statistical properties. Process. Med. Imaging 3565, 23–57.

Li, Y., Liu, Y., Li, J., Qin, W., Li, K., Yu, C., 2009. Brain anatomical network and intelligence. PLoS Comput. Biol. 5 (5), 1–17.

Luders, E., Gaser, C., Narr, K., Toga, A.W., 2009. Why sex matters: brain size independent differences in gray matter distributions between men and women. J. Neurosci. 29 (45), 14265–14270.

Paus, T., Zijdenbos, A., Worsley, K., Collins, D.L., Blumenthal, J., Giedd, J.N., Rapoport, J.L., Evans, A.C., 1999. Structural maturation of neural pathways in children and adolescents: in vivo study. Science 283 (5409), 1908–1911.

Rubinov, M., Sporns, O., 2010. Complex network measures of brain connectivity: uses and interpretations. NeuroImage 52, 1059–1069.

Scheibel, A.B., Paul, L.A., Fried, I., Forsythe, A.B., Tomiyasu, U., Wechsler, A., Kao, A., Slotnick, J., 1985. Dendritic organization of the anterior speech area. Exp. Neurol. 87 (1), 109–117.

Scott-Van Zeeland, A., Abrahams, B., Alvarez-Retuerto, A., Sonnenblick, L., Rudie, J., Ghahremani, D., Mumford, J.A., Poldrack, R.A., Dapretto, M., Geschwind, D.H., Bookheimer, S.Y., 2010. Altered Functional Connectivity in Frontal Lobe Circuits Is Associated with Variation in the Autism Risk Gene CNTNAP2. Sci. Trans. Med. 2, 1–6.

Shaw, P., Kabani, N.J., Lerch, J.P., Eckstrand, K., Lenroot, R., Gogtay, N., Greenstein, D., Clasen, L., Evans, A., Rapoport, J.L., Giedd, J.N., Wise, S.P., 2008. Neurodevelopmental trajectories of the human cerebral cortex. J. Neurosci. 28 (14), 3586–3594.

Shaw, P., Lalonde, F., Lepage, C., Rabin, C., Eckstrand, K., Sharp, W., Greenstein, D., Evans, A., Giedd, J.N., Rapoport, J., 2009. Development of cortical asymmetry in typically developing children and its disruption in attention-deficit/hyperactivity disorder. Arch. Gen. Psychiatry 66 (8), 888–896.

Sowell, E.R., Thompson, P.M., Rex, D., Kornsand, D., Tessner, K.D., Jernigan, T.L., Toga, A.W., 2002a. Mapping sulcal pattern asymmetry and local cortical surface gray matter distribution in vivo: maturation in perisylvian cortices. Cereb. Cortex 12, 17–26.

Sowell, E.R., Trauner, D.A., Gamst, A., Jernigan, T.L., 2002b. Development of cortical and subcortical brain structures in childhood and adolescence: a structural MRI study. Dev. Med. Child Neurol. 44, 4–16.

Sowell, E.R., Peterson, B.S., Thompson, P.M., Welcome, S.E., Henkenius, A.L., Toga, A.W., 2003. Mapping cortical change across the human life span. Nat. Neurosci. 6 (3), 309–315.

Sowell, E., Peterson, B., Kan, E., Woods, R., Yoshii, J., Bansal, R., Xu, D., Zhu, H., Thompson, P.M., Toga, A.W., 2007. Sex differences in cortical thickness mapped in 176 healthy individuals between 7 and 87 years of age. Cereb. Cortex 17, 1550–1560.

Sporns, O., 2002. Graph theory methods for the analysis of neural connectivity patterns. In: Kötter, R. (Ed.), Neuroscience Databases. A Practical Guide. Klüwer, Boston, MA, pp. 171–186.

Sporns, O., 2011. Networks of the Brain. The MIT Press, Cambridge, MA.

Sporns, O., Chialvo, D.R., Kaiser, M., Hilgetag, C.C., 2004. Organization, development and function of complex brain networks. Trends Cogn. Sci. 8 (9), 418–425.

Thomason, M.E., Dennis, E.L., Joshi, A.A., Joshi, S.H., Dinov, I.D., Chang, C., Henry, M.L., Johnson, R.F., Thompson, P.M., Toga, A.W., Glover, G.H., Van Horn, J.D., Gotlib, I.H., 2011. Resting-state fMRI can reliably map neural networks in children. Neuroimage 55 (1), 165–175.

Thompson, P.M., Narr, K.L., Blanton, R.E., Toga, A.W., 1999. Mapping structural alterations of the corpus callosum during brain development and degeneration. In: Iacoboni, M., Zaidel, E. (Eds.), The Corpus Callosum. Klüwer, Boston, MA.

Thompson, P.M., Giedd, J.N., Woods, R.P., MacDonald, D., Evans, A.C., Toga, A.W., 2000. Growth patterns in the developing brain detected by using continuum mechanical tensor maps. Nature 404, 190–193.

Thompson, P.M., Sowell, E.R., Gogtay, N., Giedd, J.N., Vidal, C.N., Hayashi, K.M., Leow, A., Nicolson, R., Rapoport, J.L., Toga, A.W., 2005. Structural MRI and brain development. Int. Rev. Neurobiol. 67PB, 285–323.

Toga, A.W., Thompson, P.M., 2003. Mapping brain asymmetry. Nat. Neurosci. 4, 37–48.

Turkheimer, E., Farace, E., 1992. A reanalysis of gender differences in IQ scores following unilateral brain lesions. Psychol. Assess. 4 (4), 498–501.

Witelson, S., 1989. Hand and sex differences in the isthmus and genu of the human corpus callosum: a postmortem morphological study. Brain 112, 799–835.

Yan, C., Gong, G., Wang, J., Wang, D., Liu, D., Zhu, C., Chen, Z.J., Evans, A., Zang, Y., He, Y., 2011. Sex- and brain size-related small-world structural cortical networks in young adults: a DTI tractography study. Cereb. Cortex 21 (2), 449–458.

Zalesky, A., Fornito, A., Harding, I.H., Cocchi, L., Yücel, M., Pantelis, C., Bullmore, E., 2010. Whole-brain anatomical networks: Does the choice of nodes matter? Neuroimage 50 (3), 970–983.

Zhan, L., Chiang, M.C., Barysheva, M., Toga, A.W., McMahon, K.L., de Zubicaray, G.I., Meredith, M., Wright, M.J., Thompson, P.M., 2008. How many gradients are sufficient in high-angular resolution diffusion imaging (HARDI)? Workshop on Diffusion Tensor Imaging, 11th Medical Image Computing and Computer Assisted Intervention (MICCAI), New York, September 10 (2008), pp. 216–224.

Zhan, L., Leow, A.D., Chiang, M.C., Barysheva, M., Lee, A.D., Toga, A.W., McMahon, K.L., de Zubicaray, G.I., Wright, M.J., Thompson, P.M., 2009a. How does angular resolution affect diffusion imaging measures? NeuroImage 2009 Oct 9. [Epub ahead of print].

Zhan, L., Leow, A.D., Zhu, S., Chiang, M.C., Barysheva, M., Toga, A.W., McMahon, K.L., de Zubicaray, G.I., Wright, M.J., Thompson, P.M., 2009b. Analyzing (2009c). Multi-fiber reconstruction in high angular resolution diffusion imaging using the tensor distribution function. Proc. 6th IEEE ISBI. IEEE, Piscataway, NJ, Boston, pp. 1402–1405.

Zhan, L., Franc, D., Patel, V., Jahanshad, N., Jin, Yan, Mueller, B.A., Bernstein, M.A., Borowski, B.J., Jack Jr., C.R., Toga, A.W., Lim, K.O., Thompson, P.M., 2012a. How do spatial and angular resolution affect brain connectivity maps from diffusion MRI? Proc. 9th IEEE ISBI. IEEE, Piscataway, NJ, Barcelona.

Zhan, L., Jahanshad, N., Ennis, D.B., Bernstein, M.A., Borowski, B.J., Jack Jr., C.R., Toga, A.W., Leow, A.D., Thompson, P.M., 2012b. Angular versus spatial resolution trade-offs for diffusion imaging under time constraints. Hum. Brain Mapp. April 25. [Epub ahead of print].

2.2 Development of the "rich club" in brain connectivity networks from 438 adolescents and adults aged 12 to 30

This section is adapted from:

Dennis EL, Jahanshad N, Toga AW, McMahon KL, de Zubicaray GI, Martin NG, Hickie I, Wright MJ, Thompson PM. (2013). Development of the "Rich Club" in Brain Networks from 438 Adolescents and Adults Aged 12 To 30. In Proc. *10th IEEE ISBI*, San Francisco, 620-623. (peer reviewed conference paper and platform talk). **ISBI 2013 Best Student Paper Award Winner.**

DEVELOPMENT OF THE "RICH CLUB" IN BRAIN CONNECTIVITY NETWORKS FROM 438 ADOLESCENTS & ADULTS AGED 12 TO 30

Emily L. Dennis[1], Neda Jahanshad[1], Arthur W. Toga[1], Katie L. McMahon[2],
Greig I. de Zubicaray[3], Ian Hickie[4], Margaret J. Wright[3,5], Paul M. Thompson[1]

[1] Imaging Genetics Center, Laboratory of Neuro Imaging, UCLA School of Medicine, Los Angeles, CA, USA
[2] Center for Advanced Imaging, Univ. of Queensland, Brisbane, Australia
[3] School of Psychology, University of Queensland, Brisbane, Australia
[4] Brain and Mind Research Institute, University of Sydney, Australia
[5] Queensland Institute of Medical Research, Brisbane, Australia

ABSTRACT

The 'rich club' coefficient describes a phenomenon where a network's hubs (high-degree nodes) are on average more intensely interconnected than lower-degree nodes. Networks with rich clubs often have an efficient, higher-order organization, but we do not yet know how the rich club emerges in the living brain, or how it changes as our brain networks develop. Here we chart the developmental trajectory of the rich club in anatomical brain networks from 438 subjects aged 12-30. Cortical networks were constructed from 68x68 connectivity matrices of fiber density, using whole-brain tractography in 4-Tesla 105-gradient high angular resolution diffusion images (HARDI). The adult and younger cohorts had rich clubs that included different nodes; the rich club effect intensified with age. Rich-club organization is a sign of a network's efficiency and robustness. These concepts and findings may be advantageous for studying brain maturation and abnormal brain development.

Index Terms – rich club coefficient, high angular resolution diffusion imaging (HARDI), tractography, network analyses, development, structural connectivity

1. INTRODUCTION

First reported for brain networks by Van den Heuval and Sporns in 2011 [1] and described in 2006 by Colizza et al. [2] for other complex networks, the 'rich club' coefficient is a metric that can inform us about the fundamental organization of the brain's networks, structural or functional. A *rich club* exists in a network, if there is a core of nodes with a high degree (k) – that is, *rich* in connections – that are more densely interconnected among themselves than lower-degree nodes in the network. In other words, the high-degree nodes form a *club*. The rich club *coefficient* $\Phi(k)$ is a ratio of the number of connections among nodes of degree k or higher versus the total possible number of connections if those nodes were fully connected. It is defined as:

$$\Phi(k) = \frac{2\,E_{>k}}{N_{>k}(N_{>k}-1)} \qquad \text{(Eq. 1)}$$

As higher-degree nodes have a higher probability of being interconnected with each other simply by chance, $\Phi(k)$ is typically normalized relative to Φ calculated on a set of simulated random networks with the same degree distribution, and the same edge distribution, as a function of the nodal degree k. If $\Phi_{norm}>1$ (i.e., $\Phi(k)>\Phi_{rand}$, for some k), then there is evidence of rich club organization (formal statistical testing of the rich club effect uses a null model based on randomized networks as a reference distribution).

Across development, the brain changes tremendously as we mature into adults. Ideally, networks adapt and become highly efficient. Short-range connections are pruned in favor of long-range ones [3], myelination continues [4], and the connectome continually changes. Through *in vivo* diffusion imaging and tractography, we can visualize and analyze fiber pathways. Graph theory has been applied to networks of anatomical fibers to model the brain as a set of nodes and edges and analyze the network topology and dynamics [5]. We previously showed how some graph theory metrics change over development [6]; here we set out to detect developmental changes in the rich club.

2. METHODS

2.1. Subjects and Image Acquisition

Participants were recruited as part of a 5-year research project scanning healthy young adult Australian twins with structural brain MRI and DTI [7]. We analyzed scans from 438 right-handed subjects (adult cohort: 210 female/126 male, average age=23.6 years, SD=2.2, 16-year-old cohort: 30 female/25 male, average age=16.2 years, SD=0.37, 12-year-old cohort: 23 female/24 male, average age=12.3 years, SD=0.18). This population included 145 monozygotic (MZ) twins, 260 dizygotic (DZ) twins, and 33 non-twin siblings, from 275 families. 336 were adults, 55 were adolescents, and 47 were children. Whole-brain anatomical and high angular resolution diffusion images (HARDI) were collected with a 4T Bruker Medspec MRI scanner. T1-weighted anatomical images were acquired with an inversion recovery rapid gradient echo sequence, with parameters: TI/TR/TE = 700/1500/3.35ms; flip angle = 8 degrees; slice thickness = 0.9mm, and a 256x256 acquisition

matrix. HARDI was also acquired using single-shot echo planar imaging with a twice-refocused spin echo sequence to reduce eddy-current induced distortions. Imaging parameters were: 23cm FOV, TR/TE 6090/91.7ms, with a 128x128 acquisition matrix. Each 3D volume consisted of 55 2-mm thick axial slices with no gap and 1.79x1.79 mm^2 in-plane resolution. 105 images were acquired per subject: 11 with no diffusion sensitization (i.e., T2-weighted b_0 images) and 94 diffusion-weighted (DW) images (b = 1159 s/mm^2) with gradient directions evenly distributed on a hemisphere in the q-space. Some subjects' HARDI scans were acquired with a 77-gradient protocol (b = 1177 s/mm^2), as the 105-gradient protocol was too long for some adolescents to sit through. For a fuller explanation of how the connectivity maps, and orientation density functions, are stable when such relatively high numbers of gradients are collected, please see [6]. Scan time was 14.2 min for the 105-gradient HARDI scan, and 10.8 min for the 77-gradient HARDI scan.

2.2. Cortical Extraction and HARDI Tractography

Connectivity analysis was performed as in [8]. Briefly, non-brain regions were automatically removed from each T1-weighted MRI scan, and from a T2-weighted image from the DWI set, using the FSL tool "BET" (FMRIB Software Library, http://fsl.fmrib.ox.ac.uk/fsl). A neuroanatomical expert manually edited the T1-weighted scans to refine the brain extraction. All T1-weighted images were linearly aligned using FSL (with 9 DOF) to a common space with 1mm isotropic voxels and a 220×220×220 voxel matrix. For each subject, the 11 eddy-corrected images (using FSL tool "eddy_correct") with no diffusion sensitization were averaged, linearly aligned and resampled to a downsampled version of their corresponding T1 image (110×110×110, 2×2×2mm). Averaged b_0 maps were elastically registered to the structural scan using a mutual information cost function to compensate for EPI-induced susceptibility artifacts. 34 cortical labels per hemisphere, as listed in the Desikan-Killiany atlas [9], were automatically extracted from all aligned T1-weighted structural MRI scans using FreeSurfer (http://surfer.nmr.mgh.harvard.edu/). T1-weighted images and cortical models were aligned to the original T1 input image space and down-sampled to the space of the DWIs, using nearest neighbor interpolation (to avoid intermixing of labels). To ensure tracts would intersect cortical labeled boundaries, labels were dilated with an isotropic box kernel of size 5×5×5 voxels.

The matrix transforming the mean b_0 image to the T1-weighted volume was applied to each of the 94 gradient directions to properly re-orient the orientation distribution functions (ODFs). At each HARDI voxel, ODFs were computed using the normalized and dimensionless ODF estimator derived for q-ball imaging (QBI) [10]. We performed HARDI tractography on the linearly aligned sets of DWI volumes using these ODFs, using the Hough transform method [11]. Elastic deformations obtained from

the EPI distortion correction, mapping the average b_0 image to the T1-weighted image, were then applied to the tracts' 3D coordinates to accurately align the anatomy. Each subject's dataset contained 5000-10000 useable fibers (3D curves). For each subject, a full 68×68 connectivity matrix was created. Each element described the proportion of the total number of fibers connecting each of the labels; diagonal elements describe the total number of fibers passing through a certain cortical region of interest. Values were calculated as a proportion - normalized to the total number of fibers traced for each individual participant, to avoid skewing results by the raw fiber count.

2.3. Rich Club Analyses

On the 68x68 matrices generated above, we used the Brain Connectivity Toolbox (12, https://sites.google.com/site/bctnet/) to compute the rich club coefficient (Φ). The fiber count matrices were first binarized for each subject. We normalized our rich club coefficient based on coefficients calculated from 50 random networks to generate a normalized rich club coefficient (Φ_{norm}). Below we use the same symbols as the original paper on this topic [1].

2.4. Age Regression

Age effects on rich club coefficient were estimated using the general linear mixed effects model, as well as two simpler linear mixed effects models, as follows:

Rich club coefficient $\sim A + \beta_{age}$Age $+$ (Eq. 2)
β_{sex}Sex $+ \beta_{TBV}$TBV $+ \beta_{age\text{-}squared}Age^2 + \alpha$

Rich club coefficient $\sim A + \beta_{age}$Age $+$ (Eq. 3)
β_{sex}Sex $+ \beta_{TBV}$TBV $+ \alpha$

Here, "rich club coefficient" could be either the normalized or non-normalized version; both were assessed. A is a constant for each regression model, the βs are the covariate regression coefficients, and α is a coefficient that accounts for random effects. Random effects were used to account for family relatedness. We modeled the other variables (age, sex, TBV, age^2) as fixed effects. TBV denotes total brain volume.

2.5. Null Model of Change

To test whether changes in node degree distribution that determined rich club membership could be attributed to sampling, we split the adults into 2 random groups and examined differences between them. We did this 20 times to generate a distribution of the change due to sampling. Degree was quite stable for each node, and the average change in which nodes were in the rich club was 1.05 nodes, SD 0.67.

3. RESULTS

We found a significant linear age effect on Φ across the k-range 13-22; adults had a higher Φ across that whole range (**Eq. 3**). All groups had rich club organization (meaning
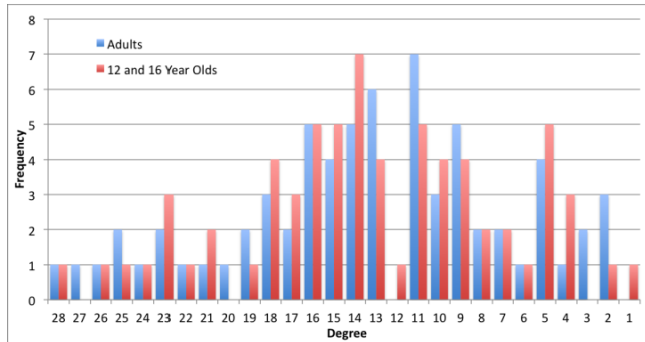
Figure 1. Histogram of degree distribution for adults (blue) and young cohort (red, 12 and 16 year olds combined).

Φ_{norm} was significantly >1) until *k*-level 26. **Figure 1** shows the degree distribution for the adults and the young cohort. This histogram was made by generating a mean matrix for the 2 groups, thresholding them to only include connections found in at least 75% of the subjects, and then finding the degree of that average group network. The ranges of Φ and Φ_{norm} for all 3 cohorts are shown in **Figure 2**, along with a zoomed-in view of the significant differences across *k*-range 13-22. There were no significant non-linear age effects (**Eq. 2**). These plots were made by taking the mean of Φ and Φ_{norm} within each group.
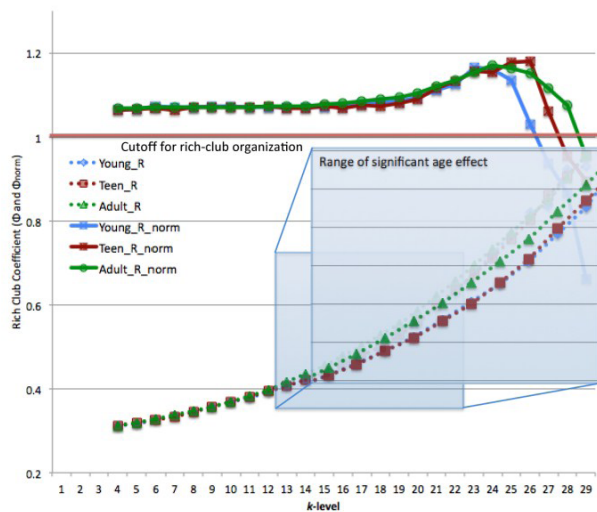
Figure 2. Range of Φ and Φ_{norm} for all three groups, 12 year olds (young) in blue, 16 year olds (teen) in red, 20-30 year olds (adult) in green. Zoomed in blue box highlights the range of Φ showing significant age effects.

Perhaps more interesting than the quantitative analysis of the rich club coefficients is differences in which nodes constitute the rich club. When examining the nodes that were included in the rich club, we found a difference between the adult cohort and the younger cohort (12 and 16 year olds; to simplify testing we combined the two younger
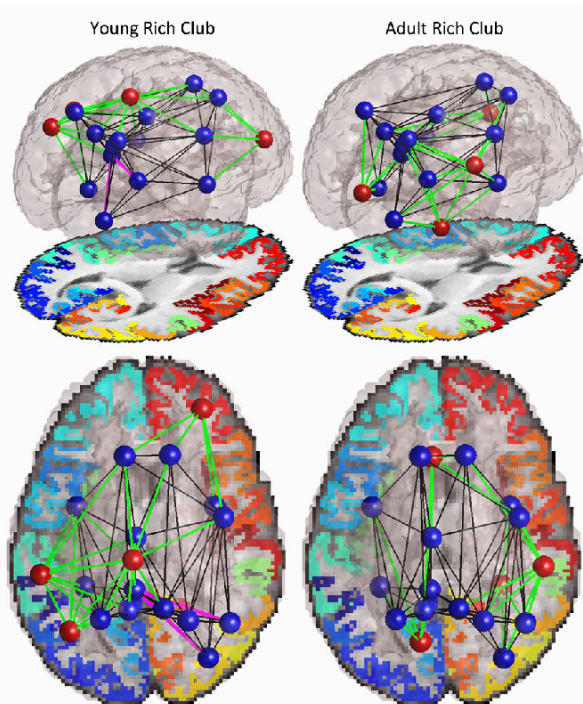
Figure 3. Rich club networks in young (12 and 16 year old) and adult (20-30 year old) cohorts. Blue nodes were present in the rich clubs of both groups; red nodes were unique to one of the groups. Black edges were present in both groups, green edges were unique to one of the groups as they involved unique nodes, magenta edges were unique to one of the groups among nodes common to both groups. Edges are thresholded to only show those present in >75% of subjects in either group.

groups) (**Figure 3**). We examined these differences at *k* = 17, because at this degree threshold both groups had rich club organization and both groups had the same number of nodes included in the trimmed network, making comparison more appropriate. At this level there were 18 nodes in the rich club. Of these, 14 were in common between the adult and younger cohorts, and 4 were unique to each group. Both groups' rich clubs included the bilateral insula, bilateral superior frontal gyrus, bilateral precuneus, bilateral superior parietal gyrus, left fusiform gyrus, left isthmus of the cingulate, left posterior cingulate gyrus, right inferior parietal gyrus, right lateral occipital gyrus, and right precentral gyrus. The adult-unique rich club nodes were the left caudal anterior cingulate gyrus, left lingual gyrus, right fusiform gyrus, and right supramarginal gyrus. The young-unique rich club nodes were the left inferior parietal gyrus, right rostral middle frontal gyrus, left paracentral gyrus, and left supramarginal gyrus.

As for the connections within the rich club, there were many differences, most stemming from differences in the nodes included in each group's rich clubs. Among the connections of the nodes common to both groups' rich

clubs, there were a few differences as well. The young cohort had connections between the left isthmus of the cingulate and the right inferior parietal gyrus, and the left isthmus and the right lateral occipital gyrus, which the adults did not have. This connection did not completely vanish, but it was not present in enough adults (>75%) to warrant inclusion in this analysis.

4. DISCUSSION

We found a linear increase in the non-normalized rich club coefficient between ages 12 and 30 in 438 subjects. The rich club coefficient represents the density of connections between rich club nodes. As our subjects aged, their rich club nodes became more closely integrated as the core of the connectome. This fits with prior reports of increased integration as brain networks develop [6]. We previously found shorter path length as subjects age; path length is the average distance, in edges, between all pairs of nodes in a network. A more densely connected rich club - the core of the connectome through which many network paths pass - would most likely lead to a shorter path length overall.

Among the nodes making up the rich club, we saw some differences between young and adult groups. With only 4 unique nodes to look at in each group, it is difficult to find a pattern, but it is interesting that they are changing, more than could be due to sampling ($p<0.05$). As rich club nodes, these nodes are central and highly important as hub nodes. For rich club membership to change in adolescence suggests that there are still significant maturational processes at work with non-trivial effects on the connectome as a whole.

The nodes that we found to make up the rich club overlap with the previous description [1], although here we considered only cortical nodes while Van den Heuval and Sporns also included subcortical nodes, and their sample was much smaller (N=21). The rich club nodes had members from both hemispheres across the frontal, parietal, temporal and occipital lobes, and many were included bilaterally. The rich club nodes overlapped largely with previously identified structural hub nodes [13]. Some nodes in our rich clubs had not been previously identified as hub nodes, such as the insula and the fusiform gyrus. This could be a result of our looking at binarized matrices, rather than matrices with the full weight. It may be that we were better able to recover fibers reaching those nodes with our 105-gradient HARDI scans and Hough-based tractography.

One recognized limitation of this study is the uneven sampling of different age groups; subjects aged 12 or 16 were available for scanning, but not in between. Nonparametric regression models may therefore be advantageous to derive empirical p-values for the fitted regression coefficients, but are unlikely to materially affect the conclusions as the age effects here are relatively strong.

5. CONCLUSION

This is the first study to our knowledge to investigate the developmental trajectory of the rich club across adolescence into early adulthood. The rich club coefficient increased with age, implying increasing integration of the rich club nodes as the brain develops. We also saw some changes in which nodes make up the rich club, evidence of significant re-modeling of the structural connectome through adolescence. Establishing the developmental trajectory of these brain connectivity metrics in healthy individuals is a first step towards determining how and when children with neurodevelopmental disorders may deviate from this trajectory.

6. REFERENCES

[1] Van den Heuval & Sporns, Rich-club organization of the human connectome. **J Neuroscience**, 31(44):15775-15786, 2011.
[2] Colizza et al. Detecting rich-club ordering in complex networks. **Nat Phys**, 2:110-115, 2006.
[3] Huttenlocher, Synaptic density in the human frontal cortex – developmental changes and effects of aging. **Brain Res**, 163(2):195-205, 1979.
[4] Bartzokis et al., Lifespan trajectory of myelin integrity and maximum motor speed. **Neurobiol Aging**, 31(9):1554-1562, 2010.
[5] Sporns et al., Organization, development and function of complex brain networks. **Trends in Cogn Sci**, 8:418-425, 2004.
[6] Dennis et al., Development of structural connectivity between ages 12 and 30: A 4-Tesla diffusion imaging study in 439 adolescents and adults. **NeuroImage**, In Press, 2012.
[7] de Zubicaray et al., Meeting the challenges of neuroimaging genetics. **Brain Imaging and Behavior**, 2:258-263, 2008.
[8] Jahanshad et al., High angular resolution diffusion imaging (HARDI) tractography in 234 young adults reveals greater frontal lobe connectivity in women. **ISBI**, 2011. 1-5.
[9] Desikan et al., An automated labeling system for subdividing the human cerebral cortex on MRI scans into gyral based regions of interest. **NeuroImage**, 31:968-980, 2006.
[10] Aganj et al., Reconstruction of the orientation distribution function in single- and multiple-shell q-ball imaging within constant solid angle. **Mag Res Med**, 64:554-566, 2010.
[11] Aganj et al., A Hough transform global probabilistic approach to multiple-subject diffusion MRI tractography. **Med Image Analysis**, 15:414-425, 2011.
[12] Rubinov & Sporns, Complex brain networks: graph theoretical analysis of structural and functional systems. **Nature Reviews Neuroscience**. 10:186-198, 2009.
[13] Hagmann et al., Mapping the structural core of the human cerebral cortex. **PLoS Biology**. 6(7):1479-1493.

2.3   Development of insula connectivity between ages 12 and 30 revealed by high angular resolution diffusion imaging

This section is adapted from:

Dennis EL, Jahanshad N, McMahon KL, de Zubicaray GI, Martin NG, Hickie IB, Toga AW, Wright MJ, Thompson PM. (2013). Development of Insula Connectivity Between Ages 12 and 30 Revealed by High Angular Resolution Diffusion Imaging (HARDI). *Human Brain Mapping*, In Press.

Development of Insula Connectivity Between Ages 12 and 30 Revealed by High Angular Resolution Diffusion Imaging

Emily L. Dennis,[1] Neda Jahanshad,[1] Katie L. McMahon,[2]
Greig I. de Zubicaray,[3] Nicholas G. Martin,[4] Ian B. Hickie,[5]
Arthur W. Toga,[1] Margaret J. Wright,[3,4] and Paul M. Thompson[1]*

[1]Imaging Genetics Center, Laboratory of Neuro Imaging, UCLA School of Medicine, Los Angeles, California
[2]Center for Advanced Imaging, University of Queensland, Brisbane, Australia
[3]School of Psychology, University of Queensland, Brisbane, Australia
[4]Queensland Institute of Medical Research, Brisbane, Australia
[5]Brain and Mind Research Institute, University of Sydney, Australia

◆ ══════════════════════════════════════ ◆

Abstract: The insula, hidden deep within the Sylvian fissures, has proven difficult to study from a connectivity perspective. Most of our current information on the anatomical connectivity of the insula comes from studies of nonhuman primates and post mortem human dissections. To date, only two neuroimaging studies have successfully examined the connectivity of the insula. Here we examine how the connectivity of the insula develops between ages 12 and 30, in 307 young adolescent and adult subjects scanned with 4-Tesla high angular resolution diffusion imaging (HARDI). The density of fiber connections between the insula and the frontal and parietal cortex decreased with age, but the connection density between the insula and the temporal cortex generally increased with age. This trajectory is in line with well-known patterns of cortical development in these regions. In addition, males and females showed different developmental trajectories for the connection between the left insula and the left precentral gyrus. The insula plays many different roles, some of them affected in neuropsychiatric disorders; this information on the insula's connectivity may help efforts to elucidate mechanisms of brain disorders in which it is implicated. *Hum Brain Mapp 00:000–000, 2013.* © 2013 Wiley-Periodicals, Inc.

Key words: insula; development; tractography; HARDI; structural connectivity

◆ ══════════════════════════════════════ ◆

INTRODUCTION

The insula, located deep in the lateral sulcus of the Sylvian fissure and spanning Brodmann areas 13 through 16 [Augustine, 1996], is a relatively old structure evolutionarily [Mega et al., 1997] and develops earlier than the frontal cortex [Benes, 1994]. The structure of the insula differentiates early [Benes, 1994; Chi et al., 1977] and its fibers are some of the earliest to form [Huang et al., 2006], but its structure has a protracted development, like many other cortical areas [Hasan et al., 2009; Herting et al., 2012; Kalani et al., 2009; Muftuler et al., 2011; Paus et al., 1999]. Our current understanding of the structural connectivity of the insula comes primarily from studies of non-human primates and *post mortem* human studies. Only two studies have detailed the structural connectivity of the insula in humans *in vivo* [Cerliani et al., 2011; Cloutman et al., 2012].

In humans, the insula is perhaps best known for its role in emotional processing and anxiety [Etkin and Wager, 2007; Stein et al., 2007]. It is a heterogeneous structure with many other functions, including interoception, monitoring external sensory processes, and autonomic regulation [Augustine, 1996; Craig, 2008]. This diverse range of functions derives from the many sub-regions of the insula, distinguished from each other by cytoarchitectonics and connectivity with other brain regions [Kurth et al., 2010; Mesulam and Mufson, 1982; Wager and Barrett, 2004]. By analyzing prior anatomical studies, Wager and Barrett [2004] divided the insula into an anterior ventral region involved in emotion, a dorsal anterior region involved in motivation and goal directed behavior, a posterior region involved in pain perception, and a mid-insula region for which they did not assign a specific role. Kurth et al. [2010] conducted a meta-analysis of functional neuroimaging data and developed a similar parcellation: a dorsal anterior aspect involved in cognitive tasks, an anterior ventral aspect involved in social-emotional tasks, a mid-insula aspect involved in smell and taste, and a mid-posterior insular aspect involved in sensorimotor tasks.

Research using functional connectivity suggests that the insula is involved in modulating resting-state functional network dynamics [Hamilton et al., 2011; Sridharan et al., 2008]. Sridharan et al. proposed that the insula was responsible for switching between the default mode and executive control networks. The default mode network, or 'task-negative' network, is a collection of brain regions that are more active during rest than during a task. It has been assigned many roles, ranging from monitoring the external environment to supporting mind wandering [Buckner et al., 2008; Fransson, 2005; Gusnard and Raichle, 2001]. The executive control networks, or 'task-positive' network, includes a number of prefrontal and parietal regions and is thought to support executive functions such as memory and goal-directed behavior [Seeley et al., 2007]. A recent paper by Cauda et al. [2011] details the functional connectivity of the insular cortex. By dividing the insula into 10 'seeds' – loci where they assessed functional coherence with activation in other brain regions – they parsed out separate networks for the ventral-anterior and the dorsal-posterior insula. The ventral-anterior insula was functionally linked to the middle and inferior temporal cortex and to the anterior cingulate cortex, while the dorsal-posterior insula was linked to the premotor, sensorimotor, supplementary motor and middle-posterior cingulate cortex.

There have not been many *in vivo* investigations of structural connectivity in humans that report results for the insula [Cerliani et al., 2011; Cloutman et al., 2012; Uddin et al., 2010; van den Heuvel et al., 2009]. Tract tracing in nonhuman primates shows that the insula is extensively connected to the surrounding cortex, basal ganglia, amygdala, limbic areas, and thalami [Augustine, 1996]. In the frontal lobe, the frontal operculum, orbital, orbitofrontal, and prefrontal cortices all have reciprocal connections with the insula. The premotor cortex, inferior frontal gyrus, and ventral granular frontal cortex all receive efferents from the insula but do not send afferents to the insula. In the parietal lobe, the anterior inferior parietal cortex, parietal operculum, somatosensory cortex, and retroinsular cortex all have reciprocal connections with the insula. In the temporal lobe, the temporal pole and superior temporal sulcus have reciprocal connections with the insula. The insula receives fibers from the auditory cortices and temporal operculum and sends to the supratemporal plane and temporopolar cortex. In the cingulate cortex, Brodmann areas 23 and 24 both have reciprocal connections with the insula. In addition, the insula also has many local connections with itself. Among subcortical regions, the insula also has connections with the basal nuclei, amygdala, hippocampus, entorhinal cortex, and thalamus [Augustine, 1996]. *Post mortem* gross dissection in humans reveals a variety of connections between the insula and the rest of cerebral cortex, as well as numerous subcortical structures [Angevine et al., 1962; Le Gros Clark et al., 1939; Klinger and Gloor, 1960; Yakovlev et al., 1960]. These known connections and those discussed below are summarized in Figure 1.

To date, only two studies have successfully imaged the structural connectivity of the insula in humans *in vivo*. Cerliani et al. [2011] examined the voxel-wise structural connectivity of the insula in 10 adult males using 3-Tesla 15-gradient diffusion-weighted imaging and probabilistic tractography, and found two separate networks. The anterior insula was primarily connected to limbic and paralimbic regions, and the inferior frontal gyrus, while the caudal insula was primarily connected to the parietal and posterior temporal cortices. Cloutman et al. [2012] examined the connectivity of the insula in 24 adult participants using 3-Tesla 61-gradient diffusion-weighted imaging and probabilistic tractography from seven anatomically defined insular ROIs (regions of interest). Similarly, they were able to define two separate networks that the insula participated in: anterior portions of the insula were connected
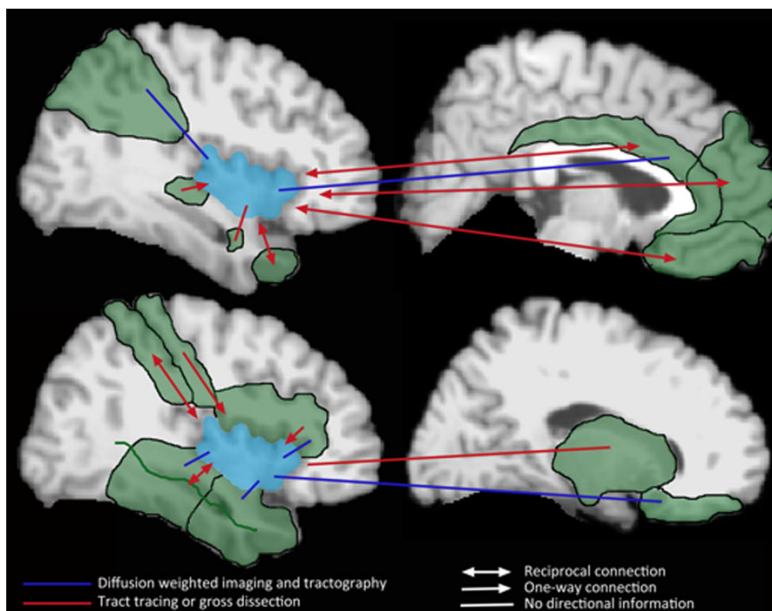
Figure 1.

Connections of the insula discovered by previous researchers. Connections in blue have been identified with diffusion-weighted imaging [Cerliani et al., 2011; Cloutman et al., 2012]. Those in red are known through either tract tracing [Augustine, 1996] or gross dissection [Angevine et al., 1962; Le Gros Clark et al., 1939; Klinger and Gloor, 1960; Yakovlev et al., 1960]. Arrowheads convey directionality of the connection; where there is no arrowhead, no directional information was known.

with orbital frontal, inferior frontal, and temporal regions via a ventral pathway, while posterior portions of the insula were connected with mostly posterior temporal regions via both dorsal and ventral pathways. Both Cerliani et al. [2011] and Cloutman et al. [2012] found a transitional area of the insula, possibly the dysgranular insula, which showed a more heterogeneous, hybrid connectivity pattern. Both of these studies were limited in sample size ($N = 10$ males; $N = 24$ adults), so we set out to look at a larger, cross sectional cohort ($N = 307$) with a high angular resolution diffusion-weighted scan (4-Tesla, 94-gradients) with a greater ability to resolve crossing fibers.

In this study, we characterize how the structural connectivity of the insula changes over adolescence using high angular resolution diffusion imaging (HARDI) in three separate age cohorts—12 year olds, 16 year olds, and 20–30 year olds. We expected to identify many of the same connections observed in prior studies, but expected that we might also find some cortical connections that have not yet been characterized. The insula develops relatively early, earlier than the frontal cortex [Benes, 1994; Chi et al., 1977; Huang et al., 2006], but has a protracted maturational period [Kalani et al., 2009; Hasan et al., 2009; Herting et al., 2012; Muftuler et al., 2011; Paus et al., 1999].

Thus, we hypothesized that we would be able to detect age effects in the age range studied here. During this stage of development, the connections to and from the frontal cortex tend to decrease in fiber density, while those of the temporal cortex tend to increase in fiber density [Dennis et al., 2012]. Given this, we expected to see reductions in the density of the connections between the insula and the frontal cortex, and increases in the density of the connections between the insula and the temporal cortex.

MATERIALS AND METHODS

Participants

Participants were recruited as part of a large-scale imaging genetics project in Australia involving twins. Our analysis included 307 subjects (adult cohort: 150 females/90 males, average age= 23.9, SD = 1.9; 16 year old cohort: 21 females/16 males, average age = 16.2, SD = 0.35; 12-year-old cohort: 14 females/16 males, average age =1 2.4, SD = 0.19). While we refer to them as different age cohorts, this is only because of sparse sampling; age was treated as a continuous variable in our statistical analyses. Our population included 109 monozygotic (MZ) twins, 174 dizygotic

TABLE I. Demographic information listing the number of subjects in each age group, sex breakdown, and zygosity breakdown

	N	M/F	MZ	DZ	SIB
Adults (20–30 yo)	240	90/150	93	123	24
16 yo	37	16/21	9	28	0
12 yo	30	16/14	7	23	0

MZ, monozygotic; DZ, dizygotic; SIB, sibling; yo, year olds. In some cases, singleton twins may be included, leading to an odd number of subjects in the MZ and DZ groups.

(DZ) twins, and 24 nontwin siblings from 204 families. This information is summarized in Table I. The population was homogeneous ethnically; 100% of the sample was Caucasian. In genetic analyses, for which the cohort was originally recruited, a homogeneous population is preferred as common alleles can have different frequencies in different racial/ethnic groups. No subject had a history of significant head injury, neurological or psychiatric illness, substance abuse or dependence, or had a first-degree relative with a psychiatric disorder. Subjects also completed a neurocognitive exam to screen for possible brain pathology [de Zubicaray et al., 2008]. All participants were right-handed, as assessed by 12 items on Annett's Handedness Questionnaire [Annett, 1970].

Scan Acquisition

Whole-brain anatomical and high angular resolution diffusion images (HARDI) were collected with a 4T Bruker Medspec MRI scanner. T1-weighted whole-brain anatomical images were acquired with an inversion recovery rapid gradient echo sequence. Acquisition parameters were: TI/TR/TE = 700/1500/3.35 ms; flip angle = 8 degrees; slice thickness = 0.9 mm, with a 256x256 acquisition matrix. Diffusion-weighted images (DWI) were acquired using single-shot echo planar imaging with a twice-refocused spin echo sequence to reduce eddy-current induced distortions. Imaging parameters were: 23cm FOV, TR/TE 6090/91.7 ms, with a 128x128 acquisition matrix. Each 3D volume consisted of 55 2-mm thick axial slices with no gap and 1.79x.1.79 mm^2 in-plane resolution. 105 images were acquired per subject: 11 with no diffusion sensitization (i.e., T2-weighted b_0 images) and 94 diffusion-weighted (DW) images ($b = 1159$ s/mm^2) with gradient directions evenly distributed on the hemisphere. The younger subjects' HARDI scans were acquired with a 77-gradient protocol (69 DWI; 8 b_0; $b = 1177$ s/mm^2), as the 105-gradient protocol was too long them to sit through. We have previously undertaken several detailed studies [Zhan et al., 2009a, 2012a,b] verifying that we can reliably reconstruct crossing ODFs (orientation distribution functions) with these parameters, and to determine how angular and spatial resolution affect brain connectivity maps; the results

and the stability of connectivity maps at high numbers of diffusion gradients are reported in those papers. The number of gradients affects the accuracy of reconstruction of the diffusion profile, but by the time 50-60 gradients are reached, the primary measures of diffusion, including the principal eigenvector, have converged [Zhan et al., 2008, 2009b,c]. The connectivity matrix depends more on the voxel size than the number of gradients [Zhan et al., 2012a], and the voxel size was kept the same in the adolescents. Scan time for the 105-gradient HARDI scan was 14.2 min. Scan time for the 77-gradient HARDI scan was 10.8 min. Motion artifacts were assessed through detailed visual inspection of all the DWI scans, which occurred in addition to the standard motion correction of the diffusion-weighted image series via registration. The DWI data were pre-processed and visually inspected prior to this study, so the number of subjects discarded for motion artifacts was not mentioned as they were never considered for this analysis.

Cortical Extraction and HARDI Tractography

Connectivity analysis was performed exactly as in Jahanshad et al. [2011]. Briefly, non-brain regions were automatically removed from each T1-weighted MRI scan using ROBEX [Iglesias et al., 2011], and from a T2-weighted image from the DWI set, using the FSL tool "BET" (FMRIB Software Library, http://fsl.fmrib.ox.ac.uk/fsl/). Intracranial volume estimates were obtained from the full brain mask, and included cerebral, cerebellar, and brain stem regions. All T1-weighted images were linearly aligned using FSL (with 9 DOF) to a common space [Holmes et al., 1998] with 1 mm isotropic voxels and a 220×220×220 voxel matrix. Raw diffusion-weighted images were corrected for eddy current distortions using the FSL tool, "eddy_correct". For each subject, the 11 eddy-corrected images with no diffusion sensitization were averaged, linearly aligned and resampled to a downsampled version of their corresponding T1 image (110×110×110, 2×2×2mm). Averaged b_0 maps were elastically registered to the structural scan using a mutual information cost function [Leow et al., 2005] to compensate for EPI-induced susceptibility artifacts. Higher field strength DWI images are susceptible to EPI-induced artifacts. We have been studying this in detail as we recently published a study of a sample of normal subject scanned at both 7-Tesla and 3-Tesla with DTI [Zhan et al., 2012]. In that study, the connectivity pattern was largely similar at higher field.

Thirty-four cortical labels per hemisphere, as listed in the Desikan-Killiany atlas [Desikan et al., 2006], were automatically extracted from all aligned T1-weighted structural MRI scans using FreeSurfer (http://surfer.nmr.mgh.harvard.edu/). As a linear registration is performed by the software, the resulting T1-weighted images and cortical models were aligned to the original T1-weighted input image space and down-sampled using nearest neighbor

interpolation (to avoid intermixing of labels) to the space of the DWIs. To ensure tracts would intersect cortical labeled boundaries, labels were dilated with an isotropic box kernel of width 5 voxels. Since we were interested only in fibers with at least one terminus in the insula for the current study, we thresholded each subject's cortical models to only include left and right insula (kept as separate cortical labels). At this step, the insula masks were visually inspected for quality. Masks were included only if they had complete coverage of the insula (with no areas of the mask with gaps in coverage). Additional reasons for exclusion were failed tractography or very sparse tractography. This resulted in 125 scans (from a total of 432 original subjects) being excluded, all of which were of adults.

The transformation matrix from the linear alignment of the mean b_0 image to the T1-weighted volume was applied to each of the 94 gradient directions to properly reorient the orientation distribution functions (ODFs). At each HARDI voxel, ODFs were computed using the normalized and dimensionless ODF estimator, derived for q-ball imaging (QBI) in [Aganj et al., 2010]. We performed HARDI tractography on the linearly aligned sets of DWI volumes using these ODFs. Tractography was performed using the Hough transform method as described in [Aganj et al., 2011].

Elastic deformations obtained from the EPI distortion correction, mapping the average b_0 image to the T1-weighted image, were then applied to the tracts' 3D coordinates for accurate alignment of the anatomy. Each subject's dataset contained 3,500-5,000 useable fibers (3D curves). At this stage, all 68 cortical labels were used to determine the targets of the tracts originating in the insula. Fibers were filtered to eliminate those that may have arbitrarily been drawn on the brain-boundary due to noise and high FA. All duplicate fibers were removed. Tracts with fewer than 2 points were filtered out, as they were considered to be noise.

After tractography, the left and right outputs were combined to create one 2 × 68 connectivity matrix for each subject. Each element described the proportion of the total number of fibers connecting the left or right insula to each of the 34 labels per hemisphere. These values were calculated as a proportion—they were normalized to the total number of fibers traced for each person in the study—so that results were not skewed by raw fiber count.

Age Regression

Age-related effects on insular structural connectivity were estimated using a general linear mixed model, as some related subjects were included in our analysis:

$$2 \times 68 \text{ matrix elements} \sim A + \beta_{age}\text{Age} + \beta_{sex}\text{Sex}$$
$$+ \beta_{ICV}\text{ICV} + \alpha + \varepsilon \qquad (1)$$

Here, "2x68 matrix elements" is the 2x68 matrix describing the proportional fiber density between the left and right insula and all 68 cortical labels. These matrices were tested on an element-by-element basis. Any statistical effects on the fiber connection matrices were corrected for multiple comparisons using the conventional FDR method [false discovery rate, Benjamini and Hochberg, 1995]. In the regression equation, A is the constant fiber density term, the βs are the covariate regression coefficients, and α is a coefficient that accounts for random effects. Random effects were used to account for familial relatedness. We modeled these variables (age, sex, ICV) as fixed effects. We also tested age^2 to check for any nonlinear age effects, and an interaction term, age*sex, as well. ICV denotes intracranial volume, in mm^3. The analysis was implemented in the R statistical package (version 2.9.2; http://www.r-project.org/) using the 'nlme' library [Pinheiro and Bates, 2000].

Permutation Testing

As we have sparse sampling of certain ages, nonparametric methods may be considered more appropriate that statistical methods described above. Accordingly, we ran 1,000 permutations, permuting age but maintaining the twin structure of our subject pool. This was done by permuting families together—twins were permuted together, family groups of three were permuted together, and individuals were permuted with other individuals. To generate permutation corrected P values, we then used the following formula: $P = (b + 1)/(m + 1)$, where b is the number of test statistics t_{perm} more significant than the observed statistic t_{obs}, and m is the number of permutations performed. With 1,000 permutations, the minimum P value possible is 0.000999, or 0.0010, if none of the t_{perm} is more significant than the t_{obs} [Smyth and Phipson, 2010]. We then used FDR to test which connections survived correction for multiple comparisons.

RESULTS

To assess developmental effects on insula connectivity, we tested connections for which in at least one of the groups (adults or adolescents), 75% of subjects had connections. For example, a connection that existed in 95% of adolescents but only in 50% of adults would be included. This is not 75% averaged across both groups. We chose a threshold of 75% because we wanted to be able to assess both connections that were present in both groups but changed in density, as well as those that were detected more in one group than the other. We thought the results of both of these questions would interest researchers and chose 75% as a threshold that could both assess change, while still being rigorous enough to not include connections existing in only a small subset of subjects. This resulted in 21 of 136 possible connections being tested, with being 14 significant with the original FDR threshold (when modeled by Eq. 1). There were significant age-related decreases in proportional fiber density between the

left insula and the left postcentral gyrus (b=-0.0011, p=4.9x10^{-8}), the left insula and the left precentral gyrus (b=-0.0012, p=3.6x10^{-12}), the left insula and the left temporal pole (b=-0.0020, p=4.2x10^{-6}), the left insula and the left supramarginal gyrus (b=-0.0020, p=1.1x10^{-5}), the right insula and the right supramarginal gyrus (b=-0.0036, p=5.8x10^{-5}), the right insula and the right postcentral gyrus (b=-0.0013, p=0.0047), and the right insula and the right precentral gyrus (b=-0.0018, p=0.00031), the right insula and the right medial orbitofrontal gyrus (b=-0.0011, p=7.0x10^{-12}), the right insula and the right *pars opercularis* (b=-0.0026, p=0.0020), and the right insula and the right *pars triangularis* (b=-0.0035, p=2.0x10^{-6}). There was an age-related increase in proportional fiber density between the left insula and the left superior temporal gyrus (b=0.0041, p=0.0054), the left insula and the left transverse temporal gyrus (b=0.0039, p=1.4x10^{-9}), the right insula and the right superior temporal gyrus (b=0.0041, p=0.0098), and the right insula and the right inferior temporal gyrus (b=0.0019, p=0.00050). These results are summarized in Table II. All results were corrected for multiple comparisons across all connections tested within the model (q<0.05). In other words, because many connections are tested for age effects, we only reported age effects strong enough to overcome the correction for multiple testing that is implicit when analyzing an entire connectivity matrix. After permutation testing, all connections listed above were still significant. Additionally, one connection that was suggestively significant using the parametric model

passed FDR after nonparametric tests – we also saw an age related decrease in fiber density between the left insula and left *pars opercularis* (b=-0.00062, p=0.035). All age-related results are presented in Figure 2. We also examined the raw fiber count matrices to determine if these were in fact increases and decreases in fiber density, or if perhaps a decrease found above was in fact an increase whose rate was slower than the overall changes in the rest of the brain. We found that most of our increases and decreases were in fact true increases or decreases in fiber count. When examining the fiber densities, the age effect on the connection between the left insula and the left superior temporal gyrus now registered as a decrease ($b = -9.8$, $P = 0.020$). A few of our significant connections no longer were significant when examining the raw fiber density matrices.

We found one connection with a significant age-by-sex interaction. The connection between the left insula and the left precentral gyrus existed in 84% of adolescents and 31% of adults and showed a sharper age-related decrease in proportional fiber density in females than in males ($b = -0.0012$, $P = 2.8 \times 10^{-6}$) (Fig. 3). This appeared to be due to a sex difference in adolescents that was no longer detectable in adults.

DISCUSSION

Here, we examined how the structural connectivity of the insula changes between ages 12 and 30, in 307 subjects scanned with HARDI. The insula and its fibers develop relatively early [Benes, 1994; Chi et al., 1977; Huang et al., 2006], but have a protracted maturational period [Kalani et al., 2009; Hasan et al., 2009; Herting et al., 2012; Muftuler et al., 2011; Paus et al., 1999]. Both adults and adolescents show activation in the insula when anxious [Shah et al., 2009; Strawn et al., 2012]. Our prior study examining functional connectivity of the default mode network (DMN) in a different cohort found that the left insula was the only area of overlap between children and adults when self-reported anxiety during the resting-state scan was used as a regressor [Dennis et al., 2011].

Here we were able to determine a number of age-related effects on insular connectivity. These were largely decreases in fiber density for connections to or from the insula,[1] as both the left and right insula showed a decrease in the proportion of fibers passing through them. These were in fact absolute decreases in the number of fibers tracked to or from the insula, as found by examining the raw fiber density matrices. The main exception was connections with the temporal cortex. This is consistent with prior studies finding age-related decreases in the volume

TABLE II. Linear age effects on insular connectivity, when analyses were restricted to connections detectable in at least 75% of subjects in at least one of the two groups (adults and/or children)

	Linear age effects Left Insula		perm. corr.
	b	P	P value
Left postcentral	−0.0011	4.9×10^{-8}	0.0010
Left precentral	−0.0012	3.6×10^{-12}	0.0010
Left *pars opercularis*[a]	−0.00062	0.035	0.035
Left temporal pole	−0.0020	4.2×10^{-6}	0.0010
Left superior temporal	0.0041	0.0054	0.0030
Left supramarginal	−0.0020	1.1×10^{-5}	0.0020
Left transverse temporal	0.0039	1.4×10^{-9}	0.0010
	Right Insula		
Right postcentral	−0.0013	0.0047	0.011
Right precentral	−0.0018	0.00031	0.0020
Right inferior temporal	0.0019	0.00050	0.0010
Right medial orbitofrontal	−0.0011	7.0×10^{-12}	0.0010
Right *pars opercularis*	−0.0026	0.0020	0.0040
Right *pars triangularis*	−0.0035	2.0×10^{-6}	0.0010
Right superior temporal	0.0041	0.0098	0.015
Right supramarginal	−0.0036	5.8×10^{-5}	0.0010

[a]Indicates connection that was suggestively significant with initial parametric model, but passed FDR after nonparametric tests.

[1]Unlike TMS and EEG, diffusion imaging can pick up a fiber connection, but not its direction. Both afferent and efferent connections are identified but not differentiated.

1 Left Sup Temporal
2 Left Precentral
3 Left Temp Pole
4 Left Supramarginal
5 Left Postcentral
6 Left Transverse Temp
7 Right Postcentral
8 Right Precentral
9 Right Supramarginal
10 Right Sup Temporal
11 Right Inf Temporal
12 Right Med Orbitofrontal
13 Right *pars triangularis*
14 Right *pars opercularis*
15 Left *pars opercularis**
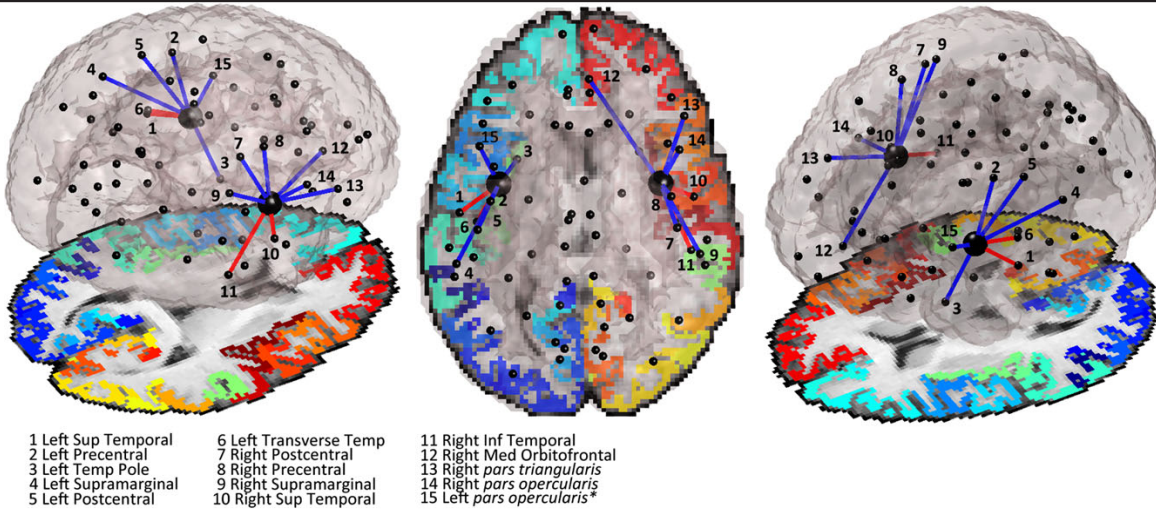
Figure 2.

Summary figure of age-related effects in proportional fiber density between left and right insula and other nodes. Connections shown are those from Table II. Nodes are numbered as indicated in the figure. The two largest nodes are the left and right insula. Paths in blue decreased in density across development, those in red increased in density across development. A legend is included below. *Indicates connection that was suggestively significant with initial parametric model, but passed FDR after nonparametric tests. In the center image, left in the image is left in the brain.

of the insula bilaterally, albeit across a larger age range [20–95 years; Takahashi et al., 2011].

Out of 15 connections showing developmental effects, 11 showed significant decreases in proportional fiber density and 4 showed significant increases (Fig. 2). Decreases in

fiber density with age could reflect synaptic pruning [Huttenlocher, 1979] or continued myelination [Bartzokis et al., 2010]. All age-related increases in fiber density were found in the temporal cortex. One of these, upon examination of the raw fiber density matrices, switched directions. Of the
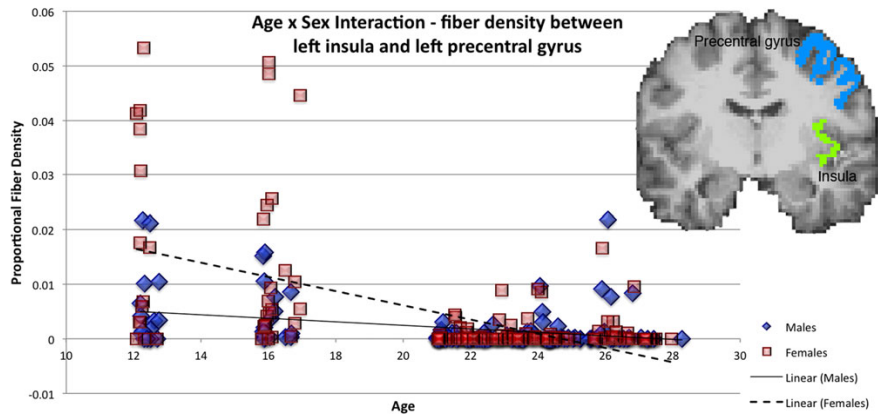
Figure 3.

Scatter plot showing the age by sex (male = 1, female = 2) interaction in the proportional fiber density of the connection between the left insula and the left precentral gyrus, indicating steeper decline with age in girls; includes image with precentral gyrus in blue and insula in green. Values for proportional fiber density are normalized by ICV (intracranial volume). A value of "0" does not necessarily indicate absence of that connection. Most likely, it indicates that we are unable to trace that connection in those subjects, perhaps because other fibers predominate, making it harder to resolve.

54

five significant developmental effects in the temporal cortex, four were increases in fiber density, and one was a decrease in fiber density. Prior work has shown different developmental trajectories across the cortex [Sowell et al., 2003; Gogtay et al., 2004] and these results of more age-related increases in connections of the temporal cortex and decreases in connections of the frontal cortex are consistent with previous results found in a larger, overlapping cohort when the whole connectome was examined [Dennis et al., 2012]. The differences we found could be partly due to differences in the developmental trajectories of the frontal and temporal cortex and their connections. Giedd et al. [1999] found the temporal cortex had a later age of peak when measuring gray matter volume than other cortices. In Sowell et al. [2003], we found the gray matter density (GMD) of the superior frontal sulcus decreased from age 7 on, but the GMD of the superior temporal sulcus increased until age 30. Sowell et al. [2002] also found that the posterior-superior temporal and inferior parietal cortices increased the most in gray matter density between ages 7-30. The insula is one of the first cortical structures to develop [Chi et al., 1977], but it continues to mature throughout childhood, with continued cortical thinning across ages 6-10 [Muftuler et al., 2011]. Similarly, the limbic fibers are among the first to develop [Huang et al., 2006], but the afferent and efferent connections of the insula also continue to develop into adulthood. These include the uncinate fasciculus [Hasan et al., 2009; Kalani et al., 2009], internal capsule fibers, and the arcuate fasciculus [Paus et al., 1999]. Additionally, the white matter of the insula itself changes with age; as Herting et al. [2012], for example, found the FA of the right insula increased with pubertal status.

As the insular connections develop, so too do the roles the insula plays functionally. In trying to find differences in the brains of adolescents that may influence their risk-taking behavior, Van Leijenhorst et al. [2010] found that the anterior insula was more active during anticipation in adolescents than adults. Similarly, Smith et al. [2011] found age-related decreases in insula activation during a sustained attention task. It could be that the maturation of this activity is due in part to the maturation of fibers connecting the insula and the frontal cortex, of which we found five significant age-related trends. As the frontal cortex controls many aspects of higher order cognition such as executive control, sustained attention, and risk analysis [Buchsbaum, 2004], maturation of these connections would likely affect the functional circuits involving both.

We found one connection that showed a significant age × sex interaction effect. The proportional fiber density of the connection between the left insula and the left precentral gyrus showed a steeper decline in females than in males (Fig. 3). Abe et al. [2010] found males had a steeper decline with age than females in the FA of the white matter of the left precentral gyrus, which is contrary to our finding, although we were concerned with the fiber density of this connection rather than its FA. We were examining a different age group, however - Abe et al. [2010] examined a cohort of 245 healthy subjects, aged 21-71. The fact that we could detect this connection in 84% of our young subjects and 31% of our adult subjects could either be due to an actual developmental change in the fiber density of this path, or could be due to it being traced more accurately in one sample than the other. As the scan parameters for both samples were almost identical and data were analyzed in the same way, the first explanation is perhaps more likely. It remains to be seen whether these sex differences have any functional consequences, such as differences in vulnerability to insula-involved neuropsychiatric disorders, such as anxiety. An alternative explanation is non-proportional scaling of brain substructures relative to overall brain size [Brun et al., 2009]. Men generally have larger brains as they are, on average, larger overall. There is an implicit assumption in aligning data to a template, namely that brain structures in each sex occupy the same proportion relative to overall brain size. Even so, it is possible that substructures scale nonlinearly to total brain volume (TBV), rather than proportionally. For example, in a study of 100 young adults, Brun et al. [2009] found that the occipital cortex and the frontal cortex scaled nonlinearly, such that individuals with large TBVs tended to have proportionally larger occipital cortices, while those with small TBVs tended to have proportionally larger frontal cortices.

The insula is involved in a wide variety of functions [Augustine, 1996; Craig, 2008] and has been implicated in a number of neuropsychiatric disorders [Etkin and Wager, 2007; Hamilton et al., 2011; Kubicki et al., 2002; Stein et al., 2007; Uddin and Menon, 2009]. A number of the roles of the insula, such as pain perception and taste, are fairly basic and early to develop, but others, such as emotion and cognitive tasks, are higher order [Kurth et al., 2010; Wager and Barrett, 2004]. Given its many roles, researchers have proposed that the insula is an integrative structure, combining sensory awareness with higher cognition [Craig, 2008; Kurth et al., 2010]. Research on the functional connectivity of the insula suggests that it plays a key role in regulating network dynamics by switching the dominant pattern of brain activity between different intrinsic connectivity networks (ICNs) [Hamilton et al., 2011; Sridharan et al., 2008]. Given its purportedly unique role in integrating disparate functions, investigating the development of insular connectivity is important in understanding how the brain develops. The insular cortex develops quite early *in utero*, before the frontal and temporal cortices [Chi et al., 1977] yet its connections with other cortical targets are still changing throughout adolescence. A number of neuropsychiatric disorders involve the insula [Etkin and Wager, 2007; Hamilton et al., 2011; Kubicki et al., 2002; Stein et al., 2007; Uddin and Menon, 2009], and many of these disorders have a typical age of onset in adolescence or later. A number of neurodevelopmental disorders also involve the insula, including autism [Cheng et al., 2010]

and ADHD [Durston, 2003]. Aberrant development of insular connectivity, still maturing into early adulthood, may be a contributing factor.

This study has several limitations. One of the issues with our study design is the sparse sampling of the ages due to the availability of subjects at specific ages (12 and 16) but not ages in between these. To address this, we followed up our initial analyses with nonparametric permutation testing, which did not affect the conclusions, but did give permutation corrected P-values. While we discuss our subjects in terms of distinct age cohorts, we treated age as a continuous variable in our statistical analyses, and the adults had a wide range of variation. Nonetheless, there were some gaps in subject availability for specific ages (13-14, 17-19). We followed up our initial analyses with nonparametric permutation testing, which did not change the results, but did give permutation corrected P-values. Another limitation is the fact that we did not parcellate the insula into sub-regions, which could have given us finer detail on insular connectivity, especially as prior studies show that it participates in multiple networks. The atlas we used (Desikan-Killiany) did not parcellate the insula further. At this time, there do not seem to be any widely used automated methods to parcellate the insula into smaller subregions, but they could be developed. However, if we included them here, we would be expected to validate them, and it would be difficult to find any independent data that could provide an objective criterion for ground truth to determine if the partition was correct. In the future, the insula might be subdivided effectively based on its connectivity to other regions. Some studies have advocated the use of connection patterns to refine segmentation of nuclei, but doing so is challenging as the large variation in connection patterns across subjects may require the development of complex rules to assign all insular regions to appropriate bundles. Obtaining even higher angular and spatial detail tends to lead to prohibitively long scan times. Ongoing efforts to refine and accelerate hybrid diffusion imaging [Zhan et al., 2011] and diffusion spectrum imaging [van Wedeen et al., 2012], especially at higher field strengths [Zhan et al., 2012c], may allow progressively finer resolution of anatomical connectivity in vivo.

CONCLUSIONS

In this study we detailed developmental changes in the structural connectivity of the insula between ages 12–30. We found that the proportion of fibers that pass through either insula decreases with age. In general, connections to the frontal and parietal cortex decreased with age, while connections to the temporal cortex mostly increased with age. This is likely due to both developmental changes in the insula itself and well-documented changes in the frontal, parietal, and temporal targets. Last, we found an age by sex interaction effect in the connectivity of the insula. It

remains to be seen if this is associated with any differences in vulnerability to insula-involved neuropsychiatric disease or simply nonproportional scaling of brain sub-structures relative to the overall brain size [Brun et al., 2009]. With the insula's heterogeneous collection of roles—some of which are emotion-related—determining the developmental trajectory of the insula and its connections will provide useful normative data and assist efforts to define the mechanisms of various neurodevelopmental and neuropsychiatric diseases.

REFERENCES

Abe O, Yamasue H, Yamada H, Masutani Y, Kabasawa H, Sasaki H, Takei K, Suga M, Kasai K, Aoki S, Ohtomo K (2010): Sex dimorphism in gray/white matter volume and diffusion tensor during normal aging. NMR Biomed 23:446–458.

Aganj I, Lenglet C, Sapiro G, Yacoub E, Ugurbil K, Harel N (2010): Reconstruction of the orientation distribution function in single- and multiple-shell q-ball imaging within constant solid angle. Magn Resonance Med 64:554–566.

Aganj I, Lenglet C, Jahanshad N, Yacoub E, Harel N, Thompson PM, Sapiro G (2011): A Hough transform global probabilistic approach to multiple-subject diffusion MRI tractography. Med Image Analysis 15:414–425.

Angevine JB Jr, Locke S, Yakovlev PI (1962): Limbic nuclei of thalamus and connections of limbic cortex. Arch Neurol 7:518–528.

Annett M (1970): A classification of hand preference by association analysis. Br J Psychol 61:303–321.

Augustine JR (1996): Circuitry and functional aspects of the insular lobe in primates including humans. Brain Res Rev 22:229–244.

Bartzokis G, Lu PH, Tingus K, Mendez MF, Richard A, Peters DG, Oluwadara B, et al. (2010): Lifespan trajectory of myelin integrity and maximum motor speed. Neurobiol Aging 31:1554–1562.

Benes FM (1994): Development of the corticolimbic system. In: Dawson G, Fischer KW, editors. Human Behavior and the Developing Brain. New York: Guilford Press.

Benjamini Y, Hochberg Y (1995): Controlling the false discovery rate: A practical and powerful approach to multiple testing. J Royal Stat Soc Series B 57:289–300.

Brun CC, Lepore N, Luders E, Chou YY, Madsen SK, Toga AW, Thompson PM (2009): Sex differences in brain structure in auditory and cingulate regions. NeuroReport 20:930–935.

Buchsbaum MS (2004): Frontal cortex function. Am J Psychiatry 161:2178.

Buckner RL, Andrews-Hanna JR, Schacter DL (2008): The brain's default network: Anatomy, function, and relevance to disease. Annals NY Acad Sci 1124:1–38.

Cauda F, D'agata F, Sacco K, Duca S, Geminiani G, Vercelli A (2011): Functional connectivity of the insula in the resting brain. NeuroImage 55:8–23.

Cerliani L, Thomas RM, Jbabdi S, Siero JCW, Nanetti L, Crippa A, Gazzola V, D'Arceuil H, Keysers C (2011): Probabilistic tractography recovers a rostrocaudal trajectory of connectivity variability in the human insular cortex. Hum Brain Mapp 33:2005–2034.

Cheng Y, Chou K-H, Chen I-Y, Fan Y-T, Decety J, Lin C-P (2010): Atypical development of white matter microstructure in

adolescents with autism spectrum disorders. NeuroImage 50:873–882.

Chi JG, Dooling EC, Gilles FH (1977): Gyral development of the human brain. Ann Neurol 1:86–93.

Cloutman LL, Binney RJ, Drakesmith M, Parker GJM, Lambon Ralph MA (2012): The variation of function across the human insula mirrors its patterns of structural connectivity: Evidence from in vivo probabilistic tractography. NeuroImage 59:3514–3521.

Craig AD (2008). Interoception and emotion: A neuroanatomical perspective. In: Lewis M, Haviland-Jones JM, Barrett LF, eds. Handbook of Emotions, 3rd ed. New York: Guilford Publications. pp 272–288.

de Zubicaray GI, Chiang M-C, McMahon KL, Shattuck DV, Toga AW, Martin NG, Wright MJ, Thompson PM (2008): Meeting the challenges of neuroimaging genetics. Brain Imaging Behav 2:258–263.

Dennis EL, Gotlib IH, Thompson PM, Thomason ME (2011): Anxiety modulates insula recruitment in resting-state functional magnetic resonance imaging in youth and adults. Brain Connectivity 1:245–254.

Dennis EL, Jahanshad N, Mcmahon KL, de Zubicaray GI, Martin NG, Hickie IB, Toga AW, Wright MJ, Thompson PM: Development of brain structural connectivity between ages 12 and 30: A 4-Tesla diffusion imaging study in 439 adolescents and adults. NeuroImage 64:671–684.

Desikan RS, Ségonne F, Fischl B, Quinn BT, Dickerson BC, Blacker D, Buckner RL, Dale AM, Maguire RP, Hyman BT, Albert MS, Killiany RJ (2006): An automated labeling system for subdividing the human cerebral cortex on MRI scans into gyral based regions of interest. NeuroImage 31:968–980.

Durston S (2003): A review of the biological bases of ADHD: What have we learned from the imaging studies? Ment Retard Dev D R 9:184–195.

Etkin A, Wager TD (2007): Functional neuroimaging of anxiety: A meta-analysis of emotional processing in PTSD, social anxiety disorder, and specific phobia. Am J Psychiatry 164:1476–1488.

Fransson P (2005): Spontaneous low-frequency BOLD signal fluctuations: An fMRI investigation of the resting-state default mode of brain function hypothesis. Hum Brain Mapp 26:15–29.

Giedd JN, Blumenthal J, Jeffries NO, Castellanos FX, Liu H, Zijdenbos A, Paus T, Evans AC, Rapoport JL (1999): Brain development during childhood and adolescence: A longitudinal MRI study. Nat Neurosci 2:861–863.

Gogtay N, Giedd JN, Lusk L, Hayashi KM, Greenstein D, Vaituzis AC, Nugent TF III, Herman DH, Clasen LS, Toga AW, Rapoport JL, Thompson PM (2004): Dynamic mapping of human cortical development during childhood through early adulthood. Proc Natl Acad Sci USA 101:8174–8179.

Gusnard D, Raichle M (2001): Searching for a baseline: Functional imaging and the resting human brain. Nat Rev Neurosci 2:1–10.

Hamilton J, Furman D, Chang C, Thomason ME, Dennis E, Gotlib IH (2011): Default-mode and task-positive network activity in major depressive disorder: Implications for adaptive and maladaptive rumination. Biol Psychiatry 70:327–333.

Hasan KM, Iftikhar A, Kamali A, Kramer LA, Ashtari M, Cirino PT, Papanicolaou AC, Fletcher JM, Ewing-Cobbs L (2009): Development and aging of the healthy human brain uncinate fasciculus across the lifespan using diffusion tensor tractography. Brain Res 1276:67–76.

Herting MM, Maxwell EC, Irvine C, Nagel BJ (2012): The impact of sex, puberty, and hormones on white matter microstructure in adolescents. Cerebral Cortex 22:1979–1992.

Holmes CJ, Hoge R, Collins L, Woods R, Toga AW, Evans AC (1998): Enhancement of MR images using registration for signal averaging. J Computer Assisted Tomography 22:324–333.

Huang H, Zhang J, Wakana S, Zhang W, Ren T, Richards LJ, Yarowsky P, Donohue P, Graham E, van Zijl PCM, Mori S (2006): White and gray matter development in human fetal, newborn, and pediatric brains. NeuroImage 33:27–38.

Huttenlocher P (1979): Synaptic density in the human frontal cortex—Developmental changes and effects of aging. Brain Res 163:195–205.

Iglesias JE, Liu C-Y, Thompson PM, Tu Z (2011): Robust brain extraction across datasets and comparison with publicly available methods. IEEE Transact Medical Imaging 30:1617–1634.

Jahanshad N, Aganj I, Lenglet C, Joshi A, Jin Y, Barysheva M, McMahon KL, de Zubicaray GI, Martin NG, Wright MJ, Toga AW, Sapiro G, Thompson PM (2011): Sex differences in the human connectome: 4-tesla high angular resolution diffusion imaging (HARDI) tractography in 234 young adult twins. In Proc. 8th IEEE ISBI. Chicago, 939–943.

Kalani MYS, Kalani MA, Gwinn R, Keogh B, Tse VCK (2009): Embryological development of the human insula and its implications for the spread and the resection of insular gliomas. J Neurosurg 27:1–6.

Klinger J, Gloor P (1960): The connections of the amygdala and of the anterior temporal cortex in the human brain. J Comp Neurol 115:333–369.

Kubicki M, Shenton ME, Salisbury DF, Hirayasu Y, Kasai K, Kikinis R, Jolesz FA, McCarley RW (2002): Voxel-based morphometric analysis of gray matter in first episode schizophrenia. NeuroImage 17:1711–1719.

Kurth F, Zilles K, Fox PT, Laird AR, Eickhoff SB (2010): A link between the systems: Functional differentiation and integration within the human insula revealed by meta-analysis. Brain Struct Funct 214(5–6):519–534.

Le Gros Clark WE, Russell WR (1939): Observations on the efferent connexions of the centre median nucleus. J Anat 73:255–263.

Leow A, Huang S, Geng A, Becker J, Davis S, Toga A, Thompson P (2005): Inverse consistent mapping in 3D deformable image registration: Its construction and statistical properties. Proc Med Imaging 3565:23–57.

Mega MS, Cummings J, Salloway S, Malloy P (1997): The limbic system: An anatomic, phylogenetic, and clinical perspective. Anatomy Neurochem 9:315–330.

Menon V, Uddin LQ (2010): Saliency, switching, attention and control: A network model of insula function. Brain Struct Funct 214(5–6):655–667.

Mesulam M-M, Mufson EJ (1982): Insula of the Old World Monkey. I. Architectonics in the insulo-orbito-temporal component of the paralimbic brain. J Compar Neurol 212:1–22.

Muftuler LT, Davis EP, Buss C, Head K, Hasso AN, Sandman CA (2011): Cortical and subcortical changes in typically developing preadolescent children. Brain Res 1399:15–24.

Paus TSAA, Zijdenbos A, Worsley K, Collins DL, Blumenthal J, Giedd JN, Rapoport JL, Evans AC (1999): Structural maturation of neural pathways in children and adolescents: In vivo study. Science 283:1908–1911.

Pinheiro JC, Bates DM (2000): Mixed-Effects Models in S and S-PLUS. Springer: New York.

Seeley WW, Menon V, Schatzberg AF, Keller J, Glover GH, Kenna H, Reiss AL, Greicius MD (2007): Dissociable intrinsic connectivity networks for salience processing and executive control. J Neurosci 27:2349–2356.

Shah SG, Klumpp H, Angstadt M, Nathan PJ, Phan KL (2009): Amygdala and insula response to emotional images in patients with generalized social anxiety disorder. J Psychiatry Neurosci 34:296–302.

Smyth GK, Phipson B (2010): Permutation *p*-values should never be zero: Calculating exact *p*-values when permutations are randomly drawn. Stat Appl Gene Mol Biol 9:1–12.

Sowell ER, Peterson BS, Thompson PM, Welcome SE, Henkenius AL, Toga AW (2003): Mapping cortical change across the human life span. Nat Neurosci 6:309–315.

Sowell ER, Thompson PM, Rex D, Kornsand D, Tessner KD, Jernigan TL, Toga AW (2002): Mapping sulcal pattern asymmetry and local cortical surface gray matter distribution *in vivo*: Maturation in perisylvian cortices. Cerebral Cortex 12:17–26.

Sridharan D, Levitin DJ, Menon V (2008): A critical role for the right fronto-insular cortex in switching between central-executive and default-mode networks. Proc Natl Acad Sci USA 105:12569–12574.

Stein MB, Simmons AN, Feinstein JS, Paulus MP (2007): Increased amygdala and insula activation during emotion processing in anxiety-prone subjects. Am J Psychiatry 164:318–327.

Strawn JR, Wehry AM, DelBello MP, Rynn MA, Strakowski S (2012): Establishing the neurobiologic basis of treatment in children and adolescents with generalized anxiety disorder. Depression Anxiety 29:328–339.

Takahashi R, Ishii K, Kakigi T, Yokoyama K (2011): Gender and age difference in normal adult human brain: Voxel-based morphometric study. Hum Brain Mapp 32:1050–1058.

Uddin L, Supekar K, Amin H (2010): Dissociable connectivity within human angular gyrus and intraparietal sulcus: Evidence from functional and structural connectivity. Cerebral Cortex 20:2636–2646.

Van den Heuvel MP, Stam CJ, Kahn RS, Hulshoff Pol HE (2009): Efficiency of functional brain networks and intellectual performance. J Neurosci 29:7619–7624.

Wager T, Barrett L (2004): From affect to control: Functional specialization of the insula in motivation and regulation. Psychextra online 1–23.

Wedeen VJ, Rosene DL, Wang R, Dai G, Mortazavi F, Hagmann P, Kaas JH, Tseng W-YI (2012): The geometric structure of the brain fiber pathways. Science 335:1628–1634.

Yakovlev PI, Locke S, Koskoff DY, Patton RA (1960): Limbic nuclei of the thalamus and connections of the limbic cortex. I. Organization of the projections of the anterior group of nuclei and of the midline nuclei of the thalamus to the anterior cingulate gyrus and hippocampal rudiment in the monkey. Arch Neurol 3:620–641.

Zhan L, Chiang MC, Barysheva M, Toga AW, McMahon KL, de Zubicaray GI, Meredith M, Wright MJ, Thompson PM (2008): How Many Gradients are Sufficient in High-Angular Resolution Diffusion Imaging (HARDI)? Workshop on Diffusion Tensor Imaging, Medical Image Computing and Computer Assisted Intervention (MICCAI). New York, September 10 (2008).

Zhan L, Leow AD, Chiang MC, Barysheva M, Lee AD, Toga AW, McMahon KL, de Zubicaray GI, Wright MJ, Thompson PM (2009a): How does angular resolution affect diffusion imaging measures? NeuroImage 2009.

Zhan L, Leow AD, Barysheva M, Feng A, Toga AW, Sapiro G, Harel N, Lim KO, Lenglet C, McMahon KL, de Zubicaray GI, Wright MJ, Thompson PM (2009b): Investigating the uncertainty in multi-fiber estimation in High Angular Resolution Diffusion Imaging. Workshop on Probabilistic Modeling in Medical Image Analysis (PMMIA), Medical Image Computing and Computer Assisted Intervention (MICCAI), London, September 20 (2009). eds. Kilian Pohl, Sarang Joshi, Sandy Wells.

Zhan L, Leow AD, Zhu S, Chiang MC, Barysheva M, Toga AW, McMahon KL, de Zubicaray GI, Wright MJ, Thompson PM (2009c). Analyzing Multi-Fiber Reconstruction in High Angular Resolution Diffusion Imaging using the Tensor Distribution Function. In Proc. 6th IEEE ISBI. Boston, 1402–1405.

Zhan L, Leow AD, Aganj I, Lenglet C, Sapiro G, Yacoub E, Harel N, Toga AW, Thompson PM (2011): Differential information content in staggered multiple shell HARDI measured by the tensor distribution function. In Proc. 8th IEEE ISBI. Chicago, 305–309.

Zhan L, Franc D, Patel V, Jahanshad N, Yan Jin Mueller BA, Bernstein MA, Borowski BJ, Jack CR Jr, Toga AW, Lim KO, Thompson PM (2012a): How do spatial and angular resolution affect brain connectivity maps from diffusion MRI? In Proc. 9th IEEE ISBI. Barcelona, 1–4.

Zhan L, Jahanshad N, Ennis DB, Bernstein MA, Borowski BJ, Jack CR Jr, Toga AW, Leow AD, Thompson PM (2012b): Angular versus spatial resolution trade-offs for diffusion imaging under time constraints. Hum Brain Mapp. [Epub ahead of print]; DOI: 10.1002/hbm.22094.

Zhan L, Mueller BA, Jahanshad N, Jin Y, Lenglet C, Yacoub E, Sapiro G, Ugurbil K, Harel N, Toga AW, Lim KO, Thompson PM (2012c): MR field strength effects on diffusion measures and brain connectivity networks (in press).

CHAPTER 3

Genetic correlates of structural brain connectivity

3.1 **Altered structural brain connectivity in healthy carriers of the autism risk gene,**

     CNTNAP2

This section is adapted from:

Dennis EL, Jahanshad N, Rudie JD, Brown JA, Johnson K, McMahon KL, de Zubicaray GI, Montgomery G, Martin NG, Wright MJ, Bookheimer SY, Dapretto M, Toga AW, Thompson PM. (2011). Altered Structural Brain Connectivity in Healthy Carriers of the Autism Risk Gene, *CNTNAP2. Brain Connectivity*, 1(6), 447-459.

ORIGINAL ARTICLES

Altered Structural Brain Connectivity in Healthy Carriers of the Autism Risk Gene, *CNTNAP2*

Emily L. Dennis,[1] Neda Jahanshad,[1] Jeffrey D. Rudie,[2] Jesse A. Brown,[3] Kori Johnson,[4,5]
Katie L. McMahon,[4] Greig I. de Zubicaray,[6] Grant Montgomery,[5] Nicholas G. Martin,[5] Margaret J. Wright,[5,6]
Susan Y. Bookheimer,[3] Mirella Dapretto,[2] Arthur W. Toga,[1] and Paul M. Thompson[1]

Abstract

Recently, carriers of a common variant in the autism risk gene, *CNTNAP2*, were found to have altered functional brain connectivity using functional MRI. Here, we scanned 328 young adults with high-field (4-Tesla) diffusion imaging, to test the hypothesis that carriers of this gene variant would have altered structural brain connectivity. All participants (209 women, 119 men, age: 23.4 ± 2.17 SD years) were scanned with 105-gradient high-angular-resolution diffusion imaging (HARDI) at 4 Tesla. After performing a whole-brain fiber tractography using the full angular resolution of the diffusion scans, 70 cortical surface-based regions of interest were created from each individual's co-registered anatomical data to compute graph metrics for all pairs of cortical regions. In graph theory analyses, subjects homozygous for the risk allele (CC) had lower characteristic path length, greater small-worldness and global efficiency in whole-brain analyses, and lower eccentricity (maximum path length) in 60 of the 70 nodes in regional analyses. These results were not reducible to differences in more commonly studied traits such as fiber density or fractional anisotropy. This is the first study that links graph theory metrics of brain structural connectivity to a common genetic variant linked with autism and will help us understand the neurobiology of the circuits implicated in the risk for autism.

Key words: autism; *CNTNAP2*; graph theory; HARDI; structural connectivity; twins

Introduction

MANY NEUROPSYCHIATRIC DISORDERS are thought to involve disrupted brain connectivity, but very little is known about what causes brain connectivity to vary in human populations. Total brain volume (Posthuma et al., 2000), cortical thickness (Schmitt et al., 2008; Thompson et al., 2001), and measures of white matter integrity derived from diffusion tensor imaging (DTI) (Chiang et al., 2009, 2011a; Pfefferbaum et al., 2001) are all under moderately strong genetic control. By analyzing very large cohorts (on the order of 20,000 subjects) with MRI and genome-wide scans (Stein et al., 2012), we recently discovered commonly carried genetic variants that are associated with differences in brain structure. Since these studies searched the genome for effects of up to a million single nucleotide polymor-

phisms (SNPs), very large samples were needed to reduce the risk of false-positive associations. An alternative approach is to study the candidate genes already associated with disease risk. For instance, young adults who carry the Alzheimer's risk allele *CLU-C* have lower white matter integrity in DTI scans of the brain, as measured by fractional anisotropy (FA) (Braskie et al., 2011). In addition, common variants in the growth factor genes, *BDNF* and *NTRK1*, are also associated with altered white matter integrity, making it possible to predict a small proportion of individual differences in brain integrity by genotyping multiple common variants (Kohannim et al., 2011). These early DTI genetics studies have generally mapped brain integrity using maps of FA, either broadly across the brain (Braskie et al., 2011), or in specific brain regions (Chiang et al., 2009; McIntosh et al., 2008; Winterer et al., 2008). Methods that assess brain

[1]Laboratory of Neuro Imaging, UCLA School of Medicine, Los Angeles, California.
[2]Ahmanson Lovelace Brain Mapping Center, UCLA, Los Angeles, California.
[3]Center for Cognitive Neuroscience, UCLA, Los Angeles, California.
[4]Center for Advanced Imaging, University of Queensland, Brisbane, Australia.
[5]Queensland Institute of Medical Research, Brisbane, Australia.
[6]School of Psychology, University of Queensland, Brisbane, Australia.

connectivity may be useful in gauging how these variants affect white matter organization overall. Even so, no studies have yet linked the graph metrics of structural brain connectivity to any specific genetic variants. The power to detect gene effects is limited in small samples, so we scanned a fairly large cohort of twins (118 identical twins, 183 fraternal twins, and 27 nontwin siblings) with high angular resolution diffusion imaging (HARDI), at a relatively high magnetic field (4 Tesla).

The recently discovered autism risk gene, *CNTNAP2*, encodes CASPR2, or contactin-associated protein-like 2, a member of the neurexin superfamily of transmembrane proteins. CASPR2 is involved in clustering voltage-gated potassium channels ($K_v1.1$) at the nodes of Ranvier (Strauss et al., 2006; Vernes et al., 2008). CASPR2 has a suggested developmental role as a cell adhesion molecule responsible for neuroblast migration and laminar organization (Arking et al., 2008; Bakkaloglu et al., 2008; Vernes et al., 2008). In a study of an Amish family, a deletion mutation in *CNTNAP2* was linked with a disorder with many hallmarks of autism, involving seizures, language difficulties, and impaired social abilities (Strauss et al., 2006). Subsequent research in both autistic and language-impaired (but nonautistic) populations has discovered further support that *CNTNAP2* is associated with autism (Alarcón et al., 2008; Arking et al., 2008; Bakkaloglu et al., 2008) and language ability (Alarcón et al., 2008; Vernes et al., 2008). A recent study characterizing *CNTNAP2* knockout mice found behavioral deficits characteristic of autism—namely, seizures—as well as neuronal migration abnormalities, reduced interneuron density, and abnormal neuronal network activity (Peñagarikano et al., 2011). *CNTNAP2* expression is highest in the frontal and temporal lobes (Abrahams et al., 2007; Arking et al., 2008; Bakkaloglu et al., 2008; Vernes et al., 2008), areas responsible for language abilities, particularly in the left hemisphere (Baynes et al., 1998), supporting the link between *CNTNAP2* and language function. Stein et al. (2011) found that a *CNTNAP2* SNP (rs2710102) was associated with increased risk for selective mutism, an anxiety disorder in which a child is unable or unwilling to speak in certain situations, despite having normal language abilities in other situations. This disorder is similar, in some respects, to autism; they both involve characteristic deficits in language and social interactions.

In a recent analysis of *functional* brain connectivity using functional MRI, Scott-Van Zeeland et al. (2010) compared risk and nonrisk allele carriers of *CNTNAP2* (rs2710102) in a cohort consisting of both autistic and typically developing children. Children with the genetic risk allele did not show the same left-lateralized pattern of medial prefrontal cortex connectivity as noncarriers. This association was consistent with previous research linking *CNTNAP2* to language ability. Scott-Van Zeeland et al. also found stronger long-range anterior-posterior connections in the nonrisk subjects and stronger short-range frontal lobe connectivity in the at-risk subjects. Since short-range connections are typically pruned and long-range ones are strengthened over the course of development (Dosenbach et al., 2010; Huttenlocher, 1990), this may be evidence of delayed development in those at risk.

The graph theory can quantify brain connectivity at the network level. This branch of mathematics—for describing and analyzing graphs—examines brain networks as collections of nodes (i.e., specific brain regions) and edges (connections between those regions) (Sporns et al., 2004). The complex web of brain structural or functional connectivity may be quantified using a number of key parameters that summarize network characteristics. Path length, for example, is a measure of the distance (i.e., number of edges) between one brain region and another (Rubinov and Sporns, 2010). A network with a shorter average path length is considered more efficient in terms of information transfer (Bullmore and Sporns, 2009). We recently found these metrics to be heritable in this same sample (Dennis et al., 2011).

Here, we set out to investigate how variations in a *CNTNAP2* SNP (rs2710102) might relate to graph theoretical measures from diffusion-weighted MRI. Further impetus for this work came from a recent report that found an association between a different *CNTNAP2* SNP (rs7794745) and FA (Tan et al., 2010). Tan et al. (2010) found lower FA in individuals homozygous for the risk allele in a number of regions implicated in autism, including the cerebellum, fusiform gyrus, occipital, and frontal cortices. Given this previous success in linking a different *CNTNAP2* SNP with structural connectivity, we decided that this might be a promising method for understanding the results of Scott-Van Zeeland et al., who found an association between our *CNTNAP2* SNP (rs2710102) and alterations in functional connectivity. Functional and structural connectivity are closely related, with functional connectivity existing between areas that are structurally connected; yet functional connections may exist where no structural connections exist (Honey et al., 2009). Results from these different modalities may assess different types of connectivity, but they are complementary and together generate a more complete picture of brain networks. In some cases but not others, differences in functional synchronization may be explained by detectable differences in structural connections. Additionally, findings from different modalities may discover the general principles of neural organization from multiple very different modalities, such as network hubs, small-world properties, as well as metrics of efficiency and resilience to disruption. Previous research associating *CNTNAP2* with cognitive or behavioral traits focused on autistic populations or people with known language difficulties. To test whether this very common genetic variant leads to detectable brain differences outside of populations with language or developmental disorders, we focused on healthy adults with normal variations in language ability. Since Scott-Van Zeeland et al. (2010) were able to find and replicate *CNTNAP2*'s association with brain connectivity in a population of both autistic and typically developing children, we hypothesized that we might be able to detect differences in the structural networks of healthy normal carriers of the *CNTNAP2* risk allele (rs2710102). In this study, we assessed both global and hemisphere-specific brain network properties. We recently reported on genetically influenced left-right asymmetries in white matter tracts (Jahanshad et al., 2010). Given those asymmetries, we expected that the relationship between *CNTNAP2* and network measures might differ by hemisphere, as *CNTNAP2* is linked with language ability (Alarcón et al., 2008; Vernes et al., 2008)—a generally left-lateralized function (Baynes et al., 1998). As such, we tested for the effects on each hemisphere independently.

Materials and Methods

Participants

Participants were recruited as part of a 5-year research project examining healthy young adult Australian twins using structural MRI and DTI with a projected sample size of ~1150 at completion (de Zubicaray et al., 2008). Our analysis included 328 right-handed subjects (209 women/119 men, average age=23.4, SD=2.17). This population included 118 monozygotic (MZ) twins, 183 dizygotic (DZ) twins, and 27 nontwin siblings, from 189 families. The population was racially homogenous: 100% of subjects were Caucasian. In studies of genetic variations, a genetically homogenous population is preferable to avoid incorrectly ascribing effects to alleles that have different frequencies in different racial/ethnic groups. The subjects were screened to exclude those with a history of significant head injury, neurological or psychiatric illness, substance abuse or dependence, or who had a first-degree relative with a psychiatric disorder. All the participants were right handed, as assessed by 12 items on the Annett's Handedness Questionnaire (Annett, 1970). The study participants gave informed consent; the institutional ethics committees at the Queensland Institute of Medical Research, the University of Queensland, the Wesley Hospital, and at UCLA approved the study.

Establishing zygosity and genotyping

Zygosity was established objectively by typing nine independent DNA microsatellite polymorphisms (polymorphism information content > 0.7), using standard polymerase chain reaction methods and genotyping. Results were cross-checked with blood group (ABO, MNS, and Rh), and phenotypic data (hair, skin, and eye color), giving an overall probability of correct zygosity assignment > 99.99%. Genomic DNA samples were analyzed on the Human610-Quad Bead-Chip (Illumina) according to the manufacturer's protocols (Infinium HD Assay; Super Protocol Guide; Rev. A, May 2008). For our SNP of interest, rs2710102, 47 (20.1%) were homozygous for the nonrisk allele (TT), 111 (47.4%) subjects were heterozygous for the risk allele (TC), and 76 (32.5%) subjects were homozygous for the risk allele (CC).

Scan acquisition

Whole-brain anatomical and HARDI were collected with a 4T Bruker Medspec MRI scanner. T1-weighted anatomical images were acquired with an inversion recovery rapid gradient echo sequence. The acquisition parameters were as follows: $TI/TR/TE = 700/1500/3.35$ ms; flip angle=8°; slice thickness=0.9 mm, with an acquisition matrix of 256×256. Diffusion-weighted images (DWIs) were also acquired using single-shot echo planar imaging with a twice-refocused spin echo sequence to reduce eddy-current induced distortions. The acquisition parameters were optimized to provide the best signal-to-noise ratio (SNR) for estimation of diffusion tensors (Jones et al., 1999). The imaging parameters were as follows: 23 cm FOV, TR/TE 6090/91.7 ms, with a 128×128 acquisition matrix. Each three-dimensional (3D) volume consisted of fifty-five 2-mm-thick axial slices with no gap and 1.79×1.79 mm^2 in-plane resolution. One hundred five images were acquired per subject: 11 with no diffusion sensitization (i.e., T2-weighted b_0 images) and 94 DWIs ($b = 1159$ s/mm^2)

with gradient directions evenly distributed on the hemisphere. The scan time for the HARDI scan was 14.2 min.

Cortical extraction and HARDI tractography

Connectivity analysis was performed as in Jahanshad et al. (2011). Briefly, nonbrain regions were automatically removed from each T1-weighted MRI scan, and from a T2-weighted image from the DWI set, using the FSL tool "BET" (FMRIB Software Library, http://fsl.fmrib.ox.ac.uk/fsl/). A trained neuroanatomical expert manually edited the T1-weighted scans to further refine the brain extraction. Total brain volume estimates were obtained from the manually edited full-brain mask, including cerebral, cerebellar, and brainstem regions. All the T1-weighted images were linearly aligned using FSL (with 9 DOF) to a common space (Holmes et al., 1998) with 1 mm isotropic voxels and a $220 \times 220 \times 220$ voxel matrix. Raw DWIs were corrected for eddy current distortions using the FSL tool, "eddy_correct" (http://fsl.fmrib.ox.ac.uk/fsl/). For each subject, the 11 eddy-corrected images with no diffusion sensitization were averaged, linearly aligned, and resampled to a downsampled version of their corresponding T1 image ($110 \times 110 \times 110$, $2 \times 2 \times 2$ mm). Averaged b_0 maps were elastically registered to the structural scan using a mutual information cost function (Leow et al., 2005) to compensate for echo planar imaging (EPI)-induced susceptibility artifacts.

Thirty-five cortical labels per hemisphere, as listed in the Desikan–Killiany atlas (Desikan et al., 2006), were automatically extracted from all aligned T1-weighted structural MRI scans using FreeSurfer (http://surfer.nmr.mgh.harvard.edu/). The Desikan–Killiany atlas lists 34 cortical regions per hemisphere that are based on the main cortical gyri, and FreeSurfer adds the insula to make a total of 35 cortical regions for each hemisphere. A complete list of the regions included is found in Jahanshad et al. (2011). Other parcellations are possible, and some may be more sensitive in principle to picking up gene effects. Previous work by our lab found that connectivity maps based on these 70 regions can be used to detect genetic influences on brain connections (in terms of gross heritability rather than SNP effects); so, we planned our SNP analyses based on this parcellation (Jahanshad et al., 2011; Joshi et al., 2010). The Desikan–Killiany atlas has been widely used for structural connectivity analysis (Hagmann et al., 2010; Honey et al., 2009). Even so, there is ongoing work in the field aiming at optimizing the cortical parcellation for network analyses, and at understanding how different parcellation schemes may influence different kinds of network measures (Bassett et al., 2011; Zalesky et al., 2010). Since a linear registration is performed by the software, the resulting T1-weighted images and cortical models were aligned to the original T1 input image space and down-sampled using nearest-neighbor interpolation (to avoid intermixing of labels) to the space of the DWIs. To ensure the tracts intersect cortical labeled boundaries, the labels were dilated with an isotropic box kernel of five voxels.

The transformation matrix from the linear alignment of the mean b_0 image to the T1-weighted volume was applied to each of the 94 gradient directions to properly re-orient the orientation distribution functions (ODFs). At each HARDI voxel, the ODFs were computed using the normalized and dimensionless ODF estimator, derived for q-ball imaging in (Aganj et al., 2010). We performed HARDI tractography on

the linearly aligned sets of DWI volumes using these ODFs. Tractography was performed using the Hough transform method as described in (Aganj et al., 2011). Briefly, tractography was performed after linearly aligning and scaling the DWI data to anatomical (T1-weighted) image space. Since a linear transform was applied to the diffusion-weighted images, we also reoriented the gradient table so that the tract tracing algorithm could correctly follow the dominant direction of diffusion. The table of gradient vectors was corrected to reflect the nonrigid transformation by applying the same transformation to each directional gradient vector. Running tractography after re-orienting the images, as we did here, might slightly affect the SNR of the diffusion signals, as it would act as a very mild spatial filter on the data.

Elastic deformations obtained from the EPI distortion correction, mapping the average b_0 image to the T1-weighted image, were then applied to the tracts' 3D coordinates for accurate alignment of the anatomy. Each subject's dataset contained 2,000–10,000 useable fibers (3D curves). Fibers were filtered to eliminate those likely to be erroneous. All duplicate fibers were removed; those with a very small number of points (<5) were considered unreliable and were also removed.

For each subject, a full 70×70 connectivity matrix was created. Each element described the proportion of the total number of fibers connecting each of the labels; the diagonal elements of the matrix describe the total number of fibers passing through a certain cortical region of interest. Since these values were calculated as a proportion, they were normalized to the total number of fibers traced for each individual participant, so that the results could not be skewed by raw fiber count.

Graph theory analyses

On the 70×70 matrices just generated, we used the Brain Connectivity Toolbox (Rubinov and Sporns, 2010; https://sites.google.com/a/brain-connectivity-toolbox.net/bct/Home) to compute two standard measures of nodal brain connectivity—regional efficiency (EREG) and eccentricity (ECC). EREG is the global efficiency (EGLOB) computed for each node and is related to the clustering coefficient (Latora and Marchiori, 2001). ECC is the longest characteristic path length (CPL) for any given node (Sporns, 2002). We also computed five standard measures of global brain connectivity—CPL, mean clustering coefficient (MCC), EGLOB, small-worldness (SW), and modularity (MOD) (Rubinov and Sporns, 2010). CPL is a measure of the average path length in a network, with path length being the minimum number of edges that should be traversed to get from one node to another. MCC is a measure of how many neighbors of a given node are also connected to each other, in proportion with the maximum number of connections in the network. EGLOB is inversely related to CPL; networks with a small, average CPL are generally more efficient than those with a large, average CPL. SW represents the balance between network differentiation and network integration, calculated as a ratio of local clustering and CPL of a node relative to the same ratio in a randomized network. We created 10 simulated random networks. The ratio of the clustering coefficient in our network to the clustering coefficient in the simulated random networks was denoted by γ (gamma). The ratio of the CPL in

our network to the CPL in the simulated random network was denoted by λ (lambda). These measures were generated in the same way as the others, integrated across a range, and are listed in the results tables alongside MCC and CPL but were not entered into any association analyses. MOD is the degree to which a system can be subdivided into smaller networks (Bullmore and Bassett, 2011). The equations to calculate each of these measures can be found in Rubinov and Sporns (2010).

One step in graph theory analysis is selecting a threshold for the network, termed the sparsity. Networks with a sparsity of 0.2 retain only 20% of the connections of the "full-sparsity" network. Selecting a single sparsity level may arbitrarily affect the network measures, so we computed measures at multiple sparsities, and integrated across that range to generate more stable scores. We calculated these measures for the whole brain over a range of sparsities (0.2–0.3, in 0.01 increments), and calculated the area under the curve of those 11 data points to generate an integrated score for each measure. Twenty-three participants completed two separate scanning sessions 3 months apart in which DTI data were collected. The measures were calculated for both scans for each of these participants over the whole range of sparsities, and we found that the range 0.2–0.3 gave the most stable network measures. Supplementary Figure S1 (Supplementary Data are available online at www.liebertonline.com/brain) shows the calculations of all five network measures plotted for both groups across the sparsity range 0–0.5. These graphs show that at very low sparsities, the graphs are not stable, while we know that higher sparsities are less biologically plausible (Sporns, 2011). We also calculated the network measures for the left and right hemispheres independently. We hypothesized that we would find evidence of altered structural connectivity between the two groups and, thus, started with global graph theory measures of connectivity. We calculated efficiency at a regional level by considering these measures at each node, to see whether our results were attributable to differences in certain brain regions. For these regional measures, we calculated the measures over the same range of sparsities and integrated them over that range. We calculated ECC at a regional level as well. We not only ran *post hoc* association analyses on the raw fiber density matrices to see whether there were overall differences in connectivity but also ran the analyses on a subset of connections, just those with one terminus in the frontal, parietal, or temporal cortex.

Association controlling for relatedness

We performed a mixed-model regression for each network measure to find the association of the SNP while incorporating a model accounting for family relatedness (Kang et al., 2008). When family members are analyzed, the relatedness among members of the sample should be taken into account, and each individual cannot be treated as independent as some share part (in the case of siblings and DZ twins) or all (MZ twins) of their genome. This analysis was performed using Efficient Mixed-Model Association (EMMA; http://mouse.cs.ucla.edu/emma/) within the R statistical package (version 2.9.2; www.r-project.org). A symmetric $n \times n$ kinship matrix was constructed to describe the relationship of every subject to all others. A kinship matrix coefficient of 1 denoted

the relationship of each subject to himself/herself; the coefficient for MZ twins within the same family was 1; the coefficient for DZ twins and siblings within the same family was 0.5; and the coefficient for subjects not in the same family was 0. Ancestry outliers were removed, so no additional modeling was used in the kinship matrix to adjust for population genetic structure between families. The association of SNP rs2710102 was tested for all network measures just described according to the following formula:

$$y = X\beta + Zu + e$$

Here, y is a vector representing the network property; X is a matrix of fixed effects containing the genetic effect of the SNP for each subject (coded additively or using other models that combine genotype groups; see above) and a constant term; β is a vector representing the fixed-effect regression coefficients; Z is an identity matrix; u is the random effect with $Var(u) = \sigma_g^2 K$, where K is the kinship matrix; and e is a matrix of residual effects with $Var(e) = \sigma_e^2 I$. Age and sex were included as covariates.

False discovery rate correction for multiple comparisons

All results were controlled for multiple comparisons using the standard false discovery rate (FDR) method (Benjamini and Hochberg, 1995). The FDR is the expected proportion of false positives among results that are declared significant. Simply setting the alpha at a value of 0.05 implies that 5% of the results are expected to be false positives. An FDR q value of 0.05, as used in this article, implies that, on average across experiments, 5% of the results declared significant are expected to be false positives.

Results

Carriers of two (CC) but not just one (CT) risk allele have a higher risk of speech development delay and/or impairment (see SNPedia, at www.snpedia.com/index.php/ Rs2710102). Thus, we coded our analyses in a recessive fashion (with regard to the major risk allele), where individuals homozygous for the risk allele formed one group, and those heterozygous for the risk allele or carrying no copies of the risk allele formed the other group. Graph theory measures depend on a choice of threshold on the strength of connectivity, which may be thought of as a sparsity level: pruning away weaker connections leads to a sparser network model. To avoid this dependency, which could lead to arbitrary thresholding effects in the results, connectivity measures were integrated across a range of sparsities (0.2–0.3), as this range was the most stable in an initial analysis (see Methods section for definitions, and Supplementary Fig. S1). This range of sparsities also makes sense biologically, as demonstrated in a number of studies (Sporns, 2011). All the analyses given next were run on integrated scores calculated in this way.

Results—whole brain measures

We tested associations of the rs2710102 *CNTNAP2* SNP with five commonly studied network measures: CPL, MCC, EGLOB, SW, and MOD. The allele dose at the SNP (i.e., the number of risk alleles) was significantly associated with the CPL in the whole-brain structural network ($b = 0.17$,

$p = 0.0069$), as well as SW ($b = -0.6$, $p = 0.00068$) and EGLOB ($b = -0.09$, $p = 0.00099$) in the left hemisphere and the EGLOB in the right hemisphere ($b = -0.077$, $p = 0.0056$). Here, b represents the unnormalized slope of the regression coefficient, where the at-risk group is coded as 0, and the non-at-risk group is coded as 1. These results remained significant after correcting for multiple comparisons using the FDR procedure (Benjamini and Hochberg, 1995) across all 15 tests performed (5 in the left hemisphere, 5 in the right hemisphere, and 5 for whole brain, $q < 0.05$). Individuals homozygous for the risk allele ($N = 99$) had greater EGLOB in both hemispheres and greater SW in the left hemisphere. Individuals carrying one or no copies of the risk allele ($N = 229$) had a greater CPL in the whole-brain structural network. The whole-brain results, with significant results bolded, along with average values for each group, are shown in Table 1. They are visualized in Figures 1 and 2.

Results—EREG

Our association analysis of the rs2710102 *CNTNAP2* SNP with the EREG of each node, integrated across sparsities .2–.3, yielded results in 11 of the 70 nodes that passed $p < 0.05$ but did not pass the more stringent FDR correction. These results, along with average values for each group, are shown in Table 2. To preserve space, only nodes passing $p < 0.05$ are presented in Table 2.

TABLE 1. GLOBAL RESULTS FROM *CNTNAP2* ASSOCIATION ANALYSIS FOR INTEGRATED GRAPH THEORY METRICS FOR WHOLE BRAIN AND LEFT AND RIGHT HEMISPHERES SEPARATELY

	Global measures—recessive model			
Measure	Risk average (CC)	Nonrisk average (CT and TT)	b	p value
Whole brain				
CPL/λ	**17.5**/10.09	**17.67**/10.16	**0.17**	**0.0069**
MCC/γ	8.57/13.74	8.35/14.27	-0.2	0.21
EGLOB	6.16	6.1	-0.049	0.032
SW	13.52	14	0.51	0.021
MOD	5.64	5.53	-0.09	0.12
Left hemisphere				
CPL/λ	19.16/10.67	19.04/10.69	-0.11	0.17
MCC/γ	6.13/17.64	6.16/17.10	0.038	0.54
EGLOB	**5.6**	**5.51**	**-0.09**	**0.00099**
SW	**16.57**	**15.96**	**-0.6**	**0.00068**
MOD	4.54	4.44	-0.098	0.16
Right hemisphere				
CPL/λ	19.02/10.62	18.95/10.66	-0.084	0.3
MCC/γ	6.35/17.37	6.36/17.24	0.02	0.79
EGLOB	**5.64**	**5.56**	**-0.077**	**0.0056**
SW	16.33	16.14	-0.17	0.31
MOD	4.39	4.28	-0.11	0.079

Significant results are bolded. Results pass FDR correction for multiple comparisons across all 15 p values.

Whole-brain results showing *CNTNAP2* SNP associations with graph theory measures of structural connectivity. Results are separated by hemisphere and are shown for the recessive model's SNP effect.

CPL, characteristic path length; MCC, mean clustering coefficient; EGLOB, global efficiency; SW, small-worldness, MOD, modularity; FDR, false discovery rate; SNP, single nucleotide polymorphism.

Results–ECC

To more fully examine the distribution of path lengths in the network, we tested the effect of *CNTNAP2* on ECC, a nodal measure of the maximal shortest path length for each node, meaning the length computed between that node and the farthest node it is connected to. Given the significant results in CPL, EGLOB, and SW, all of which are related to path length, we decided to look further into other measures related to path length. Of course, these are not entirely independent analyses, and should be considered *post hoc* and exploratory. Our analyses of the associations between the rs2710102 *CNTNAP2* SNP and the ECC of each node, integrated across sparsities .2–.3, yielded significant results for 60 of the 70 nodes, 30 in the left hemisphere and 30 in the right hemisphere, as seen in Figure 3 ($q < 0.05$). These results are displayed in Figure 3 along with averages and resultant b and p values in Table 3. To preserve space, only nodes passing $q < 0.05$ are presented in Table 3.

Post hoc analysis—additive and dominant models

Based on evidence that only carriers of two risk alleles (CC) are affected (see SNPedia, at www.snpedia.com/index.php/Rs2710102), we started with a recessive model, with carriers of the CC genotype forming one group and those with CT or TT forming the other. However, we also ran *post hoc* analyses with the other two possible models: additive, in which each genotype forms one group, and dominant, in which the CC and CT genotypes form one group and participants with the TT genotype form the other group. In the additive model, we detected significant associations between allele dose and CPL in the whole-brain network ($b = 0.10$, $p = 0.0096$), and EGLOB ($b = -0.062$, $p = 0.00041$) and SW ($b = -0.34$, $p = 0.0030$) in the left hemisphere. The global *post hoc* results that survive multiple comparisons correction are presented in Table 4 ($q < 0.05$). For the whole-brain measures in the dominant model, none of the measures were significantly associated with the allele dose at the SNP. For the EREG analyses, the additive model yielded results in 14 nodes ($p < 0.05$), as shown in Supplementary Table S1. The dominant model yielded results in five nodes as well ($p < 0.05$). Neither of these passed FDR correction. These results can be seen in Supplementary Table S2. For the analysis of nodal eccentricities, in the additive model, there were results in 64 of the 70 nodes that passed FDR correction. Six nodes were found to be significant here that had not been originally found in the recessive model, and two were not found in the additive model
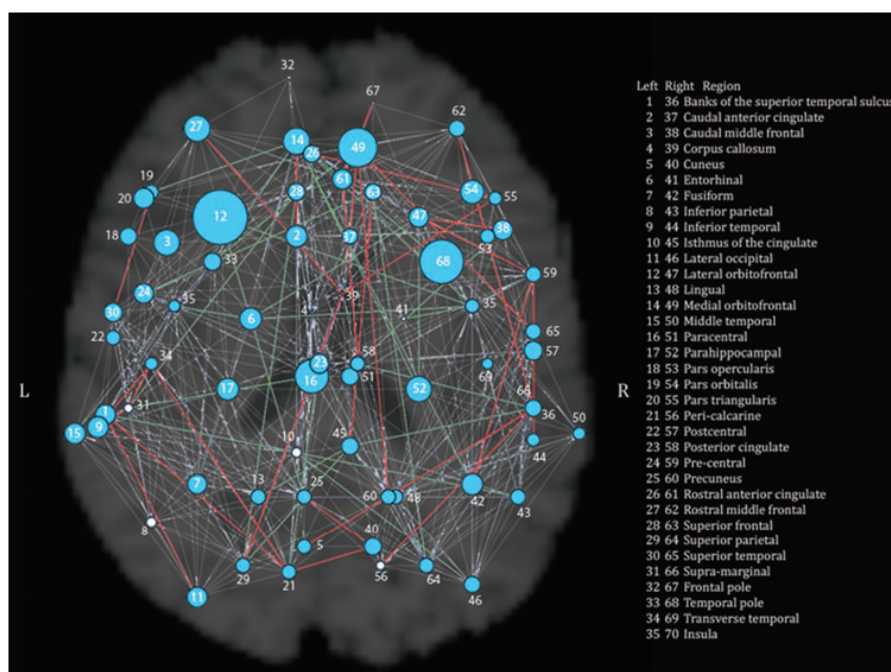
FIG. 1. Global results of *CNTNAP2* association with graph theory metrics for the whole brain. The radius of each node is proportional to the inverse of the p value for the comparison between risk (CC) and nonrisk (CT, TT) subjects in the measure of eccentricity. Thus, larger radii indicate nodes showing significant differences between the two groups. Significant nodes are in blue, and nonsignificant nodes are in white. Nodes are labeled with numbers: the legend on the figure lists numbers as they correspond to regions in each hemisphere. Additionally, differences in paths are shown in this figure. Paths that both risk and nonrisk groups have are in gray, those only present in the risk group are in red, and those only present in the nonrisk group are in green. Nodes are labeled with numbers; the legend in the figure lists numbers in each hemisphere as they correspond to regions. Figures 1 and 2 were generated at sparsity = 0.25, using the UCLA Multimodal Connectivity Package (https://github .com/jbrown81/umcp).
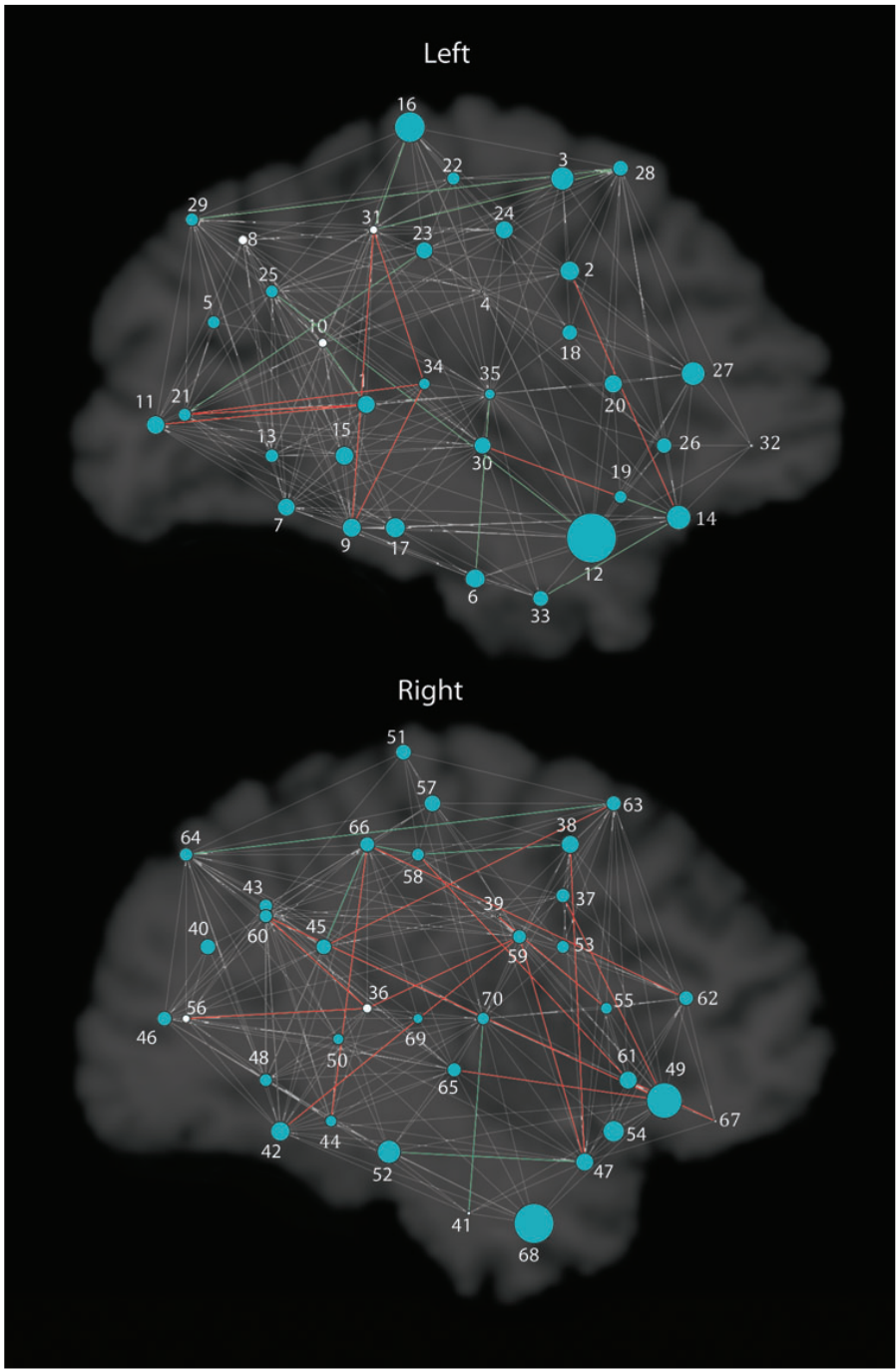
FIG. 2. Global results of *CNTNAP2* association with graph theory metrics for each hemisphere separately. As in Figure 1, larger radii indicate nodes showing significant differences between the two groups in the measure of eccentricity. Significant nodes are in blue, and nonsignificant nodes are in white. Gray paths are present in both groups, red in risk only, and green in nonrisk only. Nodes are labeled with numbers; the legend in the figure lists numbers in each hemisphere as they correspond to regions.

that had been found with the recessive. The two nodes that were significant in the recessive model but not in the additive model were the left fusiform and right insula. The six nodes that were significant in the additive model but not in the recessive model were the left inferior parietal lobule, left isthmus of the cingulate, left supramarginal gyrus, right bank of the superior temporal sulcus, right cuneus, and right pericalcarine cortex. In the dominant model, there were no significant associations with group membership.

Post hoc analysis—fiber density in frontal, parietal, and temporal lobes and FA

We had initially analyzed whether our two groups differed in their whole fiber density matrices, that is, the number of

TABLE 2. RESULTS FROM INTEGRATED REGIONAL
EFFICIENCY ANALYSIS IN RECESSIVE MODEL

Regional efficiency–recessive model

Node	Risk average (CC)	Nonrisk average (CT and TT)	b	p value
L caudal anterior cingulate	9.20	8.77	−0.44	0.0061
L caudal middle frontal	8.24	7.78	−0.45	0.0062
L *pars triangularis*	5.63	5.56	−0.060	0.048
L superior frontal	6.63	6.72	0.094	0.0034
L superior parietal	6.32	6.40	0.080	0.0046
L frontal pole	5.36	5.04	−0.27	0.016
R inferior frontal	6.11	6.02	−0.078	0.013
R *pars triangularis*	5.75	5.66	−0.097	0.017
R rostral anterior cingulate	6.00	5.90	−0.11	0.0074
R superior temporal	6.02	5.97	−0.056	0.036
R frontal pole	5.33	4.93	−0.34	0.012

Nonrisk (CT and TT) coded as "1" and risk (CC) coded as "0" such that positive *b* value indicates greater average in nonrisk participants. Only results passing $p < 0.05$ are presented.

Regional efficiency results showing *CNTNAP2* SNP associations with graph theory measures according to recessive model.

L, left; R, right.

FIG. 3. Image of nodes showing association between eccentricity and the *CNTNAP2* allele dose in the recessive model. Results pass false discovery rate correction for multiple comparisons across all 70 nodes. Colors differentiate each node, with the same color representing one node bilaterally. See Table 3 for color code. From top to bottom, left to right, slices are as follows: Z=46, Z=60, Y=41, Y=52, Y=70, X=36, and X=72.

fibers per unit volume connecting each node, and found no significant differences. Given the promising findings suggesting associations with global and nodal network measures, we ran *post hoc* tests on the fiber density in the frontal and temporal lobes, where *CNTNAP2* gene expression is enriched (Abrahams et al., 2007; Arking et al., 2008; Strauss et al., 2006; Vernes et al., 2008). In addition, Scott-Van Zeeland et al. had found associations between this gene and measures of functional connectivity in the frontal and parietal lobes; so, we included parietal nodes in this analysis as well. The nodes counted in this subset are listed in Supplementary Table S3. There was a trend for greater fiber density in the nonrisk subjects in all three lobes, but these results did not pass FDR correction. We also checked whether our two groups differed in FA or apparent diffusion coefficient (ADC) along the tracts connecting each node and found no association for any of the connections. One reason we focused our genetic analysis on FA was that we had completed a series of earlier papers that aimed at finding out which DTI-derived measures were most highly heritable. In a twin sample scanned with DTI, it is possible to estimate the proportion of variance in a measure that is attributable to genetic variation, by examining covariances between different types of twins (MZ and DZ). In these early analyses, FA was found to be highly heritable (Lepore et al., 2008) and so were the three diffusion eigenvalues when treated as a multivariate vector (Lee et al., 2009a). The full tensor was also highly heritable, so long as the meaning of heritability was appropriately redefined using a Lie group metric to measure tensor differences (Lee et al., 2009b, 2010). Since FA was more highly heritable than mean diffusivity, we preferred to use it as the target for our subsequent genetic association analyses (Braskie et al., 2011, Jahanshad et al., 2012). In addition, we weighted our fiber density matrices to emphasize those tracts that are expected to be more heavily myelinated by multiplying our fiber density and FA matrices element wise; even so, we

found no associations between the *CNTNAP2* dose and those values. Thus, the global and nodal network differences in carriers of the risk gene were not readily reducible to the effects on more common network properties, such as fiber density.

Post hoc analysis—interhemispheric connections

Given evidence that individuals with autism may have abnormalities in interhemispheric connectivity (Just et al., 2007), we generated 35×35 matrices of interhemispheric connections for all participants. We analyzed these for differences in fiber density for these interhemispheric connections between the two groups, and found no significant differences that passed FDR correction. We also analyzed whether the number of interhemispheric connections present differed between the groups, meaning the number of elements in the 35×35 matrix where >95% of the subjects had nonzero entries, again finding no significant differences.

Discussion

In this study, we found that carriers of a common variant in the autism risk gene, *CNTNAP2,* had differences in structural brain connectivity computed from high-field DTI. Graph theory measures differed in individuals homozygous for the risk allele. This higher-risk group had shorter CPL in the whole-brain network, greater SW and greater EGLOB in the left

	Eccentricity			
Node	Risk average (CC)	Nonrisk average (CT and TT)	b	p value
L banks of the superior temporal sulcus (lime green)	12.81	15.33	2.4	0.013
L caudal anterior cingulate (purple)	14.21	16.28	2.1	0.011
L caudal middle frontal (dark blue)	16.66	18.79	2.1	0.0078
L cuneus (magenta)	20.96	22.40	1.5	0.026
L entorhinal (green)	21.17	22.38	1.3	0.011
L fusiform (dark magenta)	21.30	22.34	1.0	0.014
L inferior temporal (magenta)	21.66	22.89	1.3	0.012
L lateral occipital (light blue)	21.66	22.95	1.3	0.013
L lateral orbitofrontal (dark blue)	21.16	22.37	1.3	0.0017
L lingual (magenta)	21.63	22.69	1.1	0.023
L medial orbitofrontal (gold)	21.09	22.05	1.0	0.0072
L middle temporal (red)	21.72	23.06	1.3	0.012
L parahippocampal (pale yellow)	21.53	22.79	1.3	0.011
L paracentral (gold)	21.25	22.30	1.1	0.0046
L pars opercularis (dark blue)	21.93	23.18	1.3	0.017
L pars orbitalis (orange)	22.00	23.41	1.4	0.026
L pars triangularis (red)	21.78	23.15	1.4	0.013
L peri-calcarine (pink)	21.67	22.77	1.1	0.025
L postcentral (gold)	21.70	22.83	1.1	0.025
L posterior cingulate (blue)	21.23	22.20	0.93	0.014
L pre-central (blue)	21.41	22.45	1.0	0.013
L precuneus (yellow-green)	21.38	22.28	0.9	0.026
L rostral anterior cingulate (dark purple)	21.36	22.38	1.0	0.018
L rostral middle frontal (orange)	21.50	22.73	1.2	0.0075
L superior frontal (red)	21.29	22.23	0.93	0.017
L superior parietal (green)	21.50	22.48	1.0	0.024
L superior temporal (forest green)	21.71	22.91	1.2	0.015
L temporal pole (dark blue)	21.85	23.17	1.3	0.017
L transverse temporal (dark blue)	21.98	23.53	1.4	0.032
L insula (lime green)	21.53	22.45	0.9	0.038
R caudal anterior cingulate (purple)	21.46	22.58	1.0	0.021
R caudal middle frontal (dark blue)	21.37	22.42	1.0	0.013
R cuneus (magenta)	21.77	23.10	1.3	0.017
R fusiform (dark magenta)	21.19	22.22	1.0	0.011
R inferior parietal (yellow)	21.44	22.46	1.0	0.023
R inferior temporal (magenta)	21.55	22.72	1.1	0.031
R isthmus of the cingulate (lime green)	21.28	22.39	1.0	0.017
R lateral occipital (light blue)	21.45	22.47	1.0	0.02
R lateral orbitofrontal (dark blue)	21.17	22.25	1.0	0.013
R lingual (magenta)	21.42	22.47	1.0	0.025
R medial orbitofrontal (gold)	21.02	22.03	1.1	0.0034
R middle temporal (red)	21.80	23.01	1.2	0.034
R parahippocampal (pale yellow)	21.41	22.70	1.3	0.0078
R paracentral (gold)	21.35	22.36	1.0	0.017
R pars opercularis (dark blue)	21.83	23.21	1.3	0.025
R pars orbitalis (orange)	21.80	23.44	1.8	0.0093
R pars triangularis (red)	21.83	23.09	1.3	0.03
R postcentral (gold)	21.46	22.59	1.1	0.015
R posterior cingulate (blue)	21.36	22.26	0.87	0.026
R pre-central (blue)	21.34	22.29	0.92	0.022
R precuneus (yellow-green)	21.33	22.29	0.91	0.024
R rostral anterior cingulate (dark purple)	21.41	22.54	1.1	0.013
R rostral middle frontal (orange)	21.46	22.55	1.1	0.019
R superior frontal (red)	21.29	22.25	0.93	0.019
R superior parietal (green)	21.39	22.35	0.92	0.024
R superior temporal (forest green)	21.79	23.04	1.3	0.021
R supra-marginal (green)	21.61	22.74	1.1	0.019
R temporal pole (dark blue)	21.45	23.19	1.8	0.0027
R transverse temporal (dark blue)	22.24	23.57	1.3	0.042
R insula (lime green)	21.45	22.40	0.93	0.027

Nonrisk coded as "1" and risk coded as "0"; b value represents gain in eccentricity for nonrisk group (CT and TT) compared with risk group (CC). All passing FDR corrected across all 70 nodes tested ($q < 0.05$). Only significant results are presented. Colors refer to Figure 3.

Regional results showing *CNTNAP2* SNP associations with node eccentricity.

L, left; R, right.

Table 4. Results from *Post hoc* Analyses of Additive Models for Integrated Global Measures That Pass False Discovery Rate

Global measures–additive model				
Measure	CC	CT	TT	b	p *value*
Whole Brain					
CPL	17.47	17.68	17.7	0.10	0.0096
Left Hemisphere					
EGLOB	5.56	5.52	5.53	−0.062	0.00041
SW	16.32	16.04	16.14	−0.34	0.003

Post hoc analyses of the additive model passing FDR.

hemisphere, and greater EGLOB in the right hemisphere. These results may seem counter-intuitive given findings of higher efficiency, but higher efficiency in structural networks may reflect more random connections in the risk-group's brain networks, as random networks have high levels of EGLOB (Bullmore and Sporns, 2009). Further analysis at the nodal level revealed that the homozygous at-risk participants had lower ECC across 60 of the 70 network nodes in the non-risk participants, and borderline significant results (passed $p < 0.05$ but not FDR correction) in EREG in 11 of the 70 nodes. A final analysis attempted to further simplify the results by assessing FA and fiber density differences, but did not detect associations with these more common fiber measures. In other words, several global and nodal properties of the structural network were different in carriers of the risk gene, but they were not attributable to more common characteristics of fibers, such as fiber density or FA. A larger sample size might detect differences in FA in carriers of the risk gene, but our findings suggest that differences are more prominent at the network level.

In their recent study, Scott-Van Zeeland et al. (2010) found that a *CNTNAP2* SNP was associated with differences in the functional connectivity of frontal and parietal cortical networks, including effects on the strength of short- and long-range connections to the frontal and parietal cortex. In this case, the range reflected the physical distance between two regions, while in graph theory, distance instead reflects the number of paths between one node and another. While path distance and physical distance are not the same, they both indicate distance between one brain region and another. Since this is the property measured by CPL and EGLOB using graph theoretical methods, we hypothesized that we could assess corresponding measures from structural networks using DTI, and that these measures might be altered in carriers of the *CNTNAP2* risk allele. We found that carriers have altered structural connectivity—as measured by a number of graph theory metrics—which may partly underlie the alterations in functional connectivity.

SW is a well-developed concept from graph theory (Watts and Strogatz, 1998) that has more recently been applied to brain networks (Sporns et al., 2004). A network with high SW has high local clustering and a short CPL. Subjects homozygous for the risk allele had greater SW and greater EGLOB in their left hemispheres, which are both driven in part or wholly by shorter CPLs. Risk subjects also had higher EGLOB in the right hemisphere as well as shorter CPL at a whole-brain level. Since there were no significant differences in clustering,

differences in path length may drive the observed differences in SW. Greater efficiency in those at risk is unexpected, as Hagmann et al. (2010) found greater efficiency as development progressed, and Pollonini et al. (2010) found decreased EGLOB in autistic subjects. However, Hagmann et al. based their calculations on 1/ADC, while we based ours on fiber density, and Pollonini et al. was a magnetoencephalography (MEG) study with Granger causality, so the comparison is not direct. A random network has high efficiency (Bullmore and Sporns, 2009), but it may not be functionally advantageous if the proper connections are not made. Neural network complexity is typically achieved by a balance of randomness and regularity—at either extreme, you have a system less able to learn, because it is either never stable enough to remember or never flexible enough to adapt (Sporns, 2011). A more random network, while having a shorter average path length, will be less complex, and arguably further from ideal in terms of brain function. A more random network, while having a shorter average path length, will be less complex, and may not reflect the organization found in real functional brain networks. Individuals differ widely in brain structure and function, but complete "randomness" of connections is not typical of functional circuitry in the brain. A random network, with no stability in time or logical set up, does not tend to make the most efficient use of the brain's resources (Chialvo, 2010). While additional studies are required, higher EGLOB may reflect more random connections in the structural networks of the at-risk participants, as random networks have low path lengths.

Based on our global results, we decided to look further into various nodal measures of connectivity. In these *post hoc* tests, we found a significant association between *CNTNAP2* allele dose and the ECC at 60 of the 70 nodes, with nonrisk carriers having greater ECC across all nodes. ECC is the distance, in paths traversed, between a given node and the node farthest from it (Sporns, 2002). Nonrisk participants had greater ECC across most of the brain. Studies of ECC in brain networks are few (Pollonini et al., 2010) and have not generated any significant results so far; so, we have little context for these results. However, given that they are across a majority of nodes in the brain, they could underlie the global trends we found as well. We found 11 nodes with borderline significant differences (passed $p < 0.05$ but not FDR correction) in EREG, 8 of which were in the frontal lobe, 2 in the temporal lobe, and 1 in the parietal lobe. These are the areas where *CNTNAP2* expression is especially enriched (Abrahams et al., 2007; Arking et al., 2008; Strauss et al., 2006; Vernes et al., 2008) and where Scott-Van Zeeland found differences in functional connectivity.

In attempting to discover a simpler underlying cause of these results, we looked into possible differences in the fiber density matrices of the two groups. We had initially ruled out differences in overall connectivity by running our analysis of *CNTNAP2* on the whole fiber density matrices. However, in trying to understand our results of greater EGLOB and shorter CPL in the risk allele carriers, we decided to look only at those connections with at least one terminus in the frontal, parietal, or temporal lobes. While we found a trend for greater fiber density in the nonrisk subjects in a large number of frontal, parietal, and temporal connections, these results did not pass FDR correction. Tan et al. (2010) conducted a study of a different *CNTNAP2* SNP, rs7794745, in a large cohort of healthy subjects as well. Regional gray and white matter volumes were lower in those homozygous for the risk allele. We will continue

to search for an explanation for our unexpected findings, but currently they do not appear to be reducible to more simple measures of structural connectivity.

Our findings relating a common risk variant in *CNTNAP2* with structural connectivity suggests that the protein it codes for, CASPR2, may be involved in white matter tract structure. This seems likely, as CASPR2 has a role in neuroblast migration (Strauss et al., 2006) and in stabilizing K$^+$ channels in the juxtaparanodal region (Poliak et al., 1999, 2003). *CNTNAP2* risk allele carriers may have aberrant neuroblast migration or K$^+$ channel clustering early in development; this may even underlie the differences we see in structural connectivity. Abnormal neuronal migration early in development could lead to altered development of white matter, leading to the changes we see. Abnormal K$^+$ channel clustering could affect axonal physiology for developing tracts, perhaps even affecting overall tract structure. The recent study characterizing the *CNTNAP2* knockout found, along with various behavioral hallmarks of autism, neuronal migration abnormalities, including abnormal clustering of neurons in the deep layers of the cortex (Peñagarikano et al., 2011). *CNTNAP2* is a risk gene for autism, but it also has effects in nonautistic populations with language disorders. It may be more appropriate to consider it as a risk gene for language difficulties—a key component of autism. A disorder as complex and varied as autism most likely results from a constellation of genetic variations interacting with environmental influences (Szatmari et al., 2007). The SNP rs2710102 in *CNTNAP2* may be one of these polymorphisms that, when combined with others, could increase te risk for autism by increasing the susceptibility to language difficulties. In this article, our focus was the effects of *CNTNAP2* on brain structural connectivity. Understanding why a gene increases risk for a disorder is as crucial as determining that it increases risk in the first place, as a more mechanistic understanding is necessary for ultimately developing interventions. Here, we discovered a mechanistic clue that might explain the association between *CNTNAP2* and autism and language disorders. This altered connectivity may represent an intermediate phenotype for one source of language difficulties. Our participants were a large cohort of twins screened for psychiatric disorders and developmental conditions; thus, they fall within the normal range of language ability.

Of the three different models, the recessive model yielded the strongest results. We chose this model based on information that individuals with the CC genotype have an increased risk of language impairment (www.snpedia.com/index.php/Rs2710102). However, Scott-Van Zeeland's study supports a dominant effect of the *CNTNAP2* SNP. Vernes et al. (2008) found that a haplotype of nine SNPs, including this *CNTNAP2* SNP, had a dominant effect, but no other studies have produced evidence on the dominance of *CNTNAP2* rs2710102 by itself. Our analyses were based on healthy subjects, while previous studies have been conducted on autistic or language-impaired participants, so we followed our analyses with *post hoc* tests to check the other two models in case the effect differed from that in our healthy population.

Conclusions

In this study, the first to link graph theory measures of brain structural connectivity with a specific genetic variant associated with autism, we searched for structural differences that might contribute to the reported effects of *CNTNAP2* on functional networks. In our large cohort of healthy adults, the same *CNTNAP2* SNP was also associated with detectable differences in structural connectivity. In comparing findings from different imaging modalities, these efforts lead to a better understanding of genetic liability for autism and related disorders. Our results not only add to previous work on the effects of *CNTNAP2* on brain structure but also raise new questions regarding the underlying difference. A new approach to neuroimaging genetics is combining multiple polymorphisms–in the same or different genes—when testing for associations with phenotypes, leading to increased predictive accuracy (Chiang et al., 2011b; Hibar et al., 2011). Studies using this method have already been conducted on another autism risk gene (Kohannim et al., in review) that was a top hit in a genome-wide scan for risk alleles (Anney et al., 2010). *CNTNAP2* is classified as an autism risk gene, but we have shown that it has effects in a healthy population as well. These results will further our understanding of how vulnerabilities for various genetically influenced disorders are displayed in the brain.

Author Contributions

K.L.M., G.I.d.Z., G.M., N.G.M., and M.J.W. collected the data. E.L.D., N.J., J.D.R., J.A.B., and P.M.T. analyzed the data. E.L.D., N.J., and P.M.T. wrote the initial manuscript draft. All authors contributed to revisions and commented on drafts.

Author Disclosure Statement

The authors have no competing financial interests.

References

Abrahams BS, Tentler D, Perederiy JV, Oldham MC, Coppola G, Geschwind DH. 2007. Genome-wide analyses of human perisylvian cerebral cortical patterning. Proc Natl Acad Sci U S A 104:17849–17854.

Aganj I, Lenglet C, Jahanshad N, Yacoub E, Harel N, Thompson PM, Sapiro G. 2011. A Hough transform global probabilistic approach to multiple-subject diffusion MRI tractography. Med Image Analysis 15:414–425.

Aganj I, Lenglet C, Sapiro G, Yacoub E, Ugurbil K, Harel N. 2010. Reconstruction of the orientation distribution function in single- and multiple-shell q-ball imaging within constant solid angle. Magn Reson Med 64:554–566.

Alarcón M, Abrahams BS, Stone JL, Duvall JA, Perederiy JV, Bomar JM, Sebat J, Wigler M, Martin CL, Ledbetter DH, Nelson SF, Cantor RM, Geschwind DH. 2008. Linkage, association, and gene-expression analyses identify CNTNAP2 as an autism-susceptibility gene. Am J Hum Genet 82:150–159.

Annett M. 1970. A classification of hand preference by association analysis. Br J Psychol 61:303–321.

Anney R, Klei L, Pinto D, et al. 2010. A genome-wide scan for common alleles affecting risk for autism. Hum Mol Genet 19:4072–4082.

Arking D, Cutler D, Brune CW, Teslovich TM, West K, Ikeda M, Rea A, Guy M, Lin S, Cook Jr., EH, Chakravarti A. 2008. A common genetic variant in the neurexin superfamily member CNTNAP2 increases familial risk of autism. Am J Hum Genet 82:160–164.

Bakkaloglu B, O'Roak B, Louvi A, Gupta AR, Abelson JF, Morgan TM, Chawarska K, Klin A, Ercan-Sencicek AG, Stillman AA, Tanriover G, Abrahams BS, Duvall JA, Robbins EM, Geschwind DH, Biederer T, Gunel M, Lifton RP, State MW. 2008. Molecular cytogenetic analysis and resequencing of contactin associated protein-like 2 in autism spectrum disorders. Am J Hum Genet 82:165–173.

Bassett DS, Brown JA, Deshpande V, Carlson JM, Grafton ST. 2011. Conserved and variable architecture of human white matter connectivity. NeuroImage 54:1262–1279.

Baynes K, Eliassen J, Lutsep HL, Gazzaniga MS. 1998. Modular organization of cognitive systems masked by interhemispheric integration. Science 280:902–905.

Benjamini Y, Hochberg Y. 1995. Controlling the false discovery rate: a practical and powerful approach to multiple testing. J R Stat Soc B 57:289–300.

Braskie M, Jahanshad N, Stein J, Barysheva M, McMahon K, de Zubicaray GI, Martin NG, Wright MJ, Ringman JM, Toga AW, Thompson PM. 2011. Common Alzheimer's disease risk variant within the CLU gene affects white matter microstructure in young adults. J Neurosci 31:6764–6770.

Bullmore E, Bassett D. 2011. Brain graphs: graphical models of the human brain connectome. Annu Rev Clin Psychol 7:113–140.

Bullmore E, Sporns O. 2009. Complex brain networks: graph theoretical analysis of structural and functional systems. Nat Rev Neurosci 10:186–198.

Chialvo DR. 2010. Emergent complex neural dynamics. Nat Phys 6:744–750.

Chiang M-C, Avedissian C, Barysheva M, Toga A, McMahon K, de Zubicaray GI, Wright MJ, Thompson PM. 2009. Extending genetic linkage analysis to diffusion tensor images to map single gene effects on brain fiber architecture. Med Image Comput Comput Assist Interv MICCAI 12:506–513.

Chiang M-C, McMahon KL, de Zubicaray GI, Martin NG, Hickie I, Toga A, Wright MJ, Thompson PM. 2011a. Genetics of white matter development: a DTI study of 705 twins and their siblings aged 12 to 29. NeuroImage 54:2308–2317.

Chiang MC, McMahon KL, de Zubicaray GI, Martin NG, Toga AW, Wright MJ, Thompson PM. Hierarchical Clustering of the Genetic Connectivity Matrix Reveals the Network Topology of Gene Action on Brain Microstructure. In Proceedings of the 8th IEEE ISBI, Chicago, Illinois, USA, 2011b, pp. 832–835.

de Zubicaray GI, Chiang M-C, McMahon KL, Shattuck DV, Toga AW, Martin NG, Wright MJ, Thompson PM. 2008. Meeting the challenges of neuroimaging genetics. Brain Imaging Behav 2:258–263.

Dennis EL, Jahanshad N, Toga A, Brown J, Rudie J, Bookheimer S, Dapretto M, Johnson K, McMahon K, de Zubicaray G, Martin N, Wright M, Thompson P. Heritability of Structural Brain Connectivity Network Measures in 188 Twins. In Proceedings of the 41st Annual Meeting of the Society for Neuroscience, Washington, D.C., USA, 12 to 16 November 2011.

Desikan RS, Ségonne F, Fischl B, Quinn BT, Dickerson BC, Blacker D, et al. 2006. An automated labeling system for subdividing the human cerebral cortex on MRI scans into gyral based regions of interest. NeuroImage 31:968–980.

Dosenbach NUF, Nardos B, Cohen AL, Fair DA, Power JD, Church JA, Nelson SM, Wig GS, Vogel AC, Lessov-Schlaggar CN, Barnes KA, Dubis JW, Feczko E, Coalson RS, Pruett JR, Barch DM, Petersen SE, Schlaggar BL. 2010. Prediction of individual brain maturity using fMRI. Science 329:1358–1361.

Hagmann P, Sporns O, Madan N, Cammoun L, Pienaar R, Wedeen VJ, Meuli R, Thiran JP, Grant PE. 2010. White matter maturation reshapes structural connectivity in the late developing human brain. Proc Natl Acad Sci U S A 107:19067–19072.

Hibar D, Kohannim O, Stein JL, Chiang MC, Thompson PM. 2011. Multilocus Genetic Analysis of Brain Images. Front Genet 2:73 .

Holmes CJ, Hoge R, Collins L, Woods R, Toga AW, Evans AC. 1998. Enhancement of MR images using registration for signal averaging. J Comput Assist Tomogr 22:324–333.

Honey CJ, Sporns O, Cammoun L, Gigandet X, Thiran JP, Meuli R, Hagmann P. 2009. Predicting human resting-state functional connectivity from structural connectivity. Proc Natl Acad Sci U S A 106:2035–2040.

Huttenlocher PR. 1990. Morphometric study of human cerebral cortex development. Neuropsychologia 28:517–527.

Jahanshad N, Aganj I, Lenglet C, Jin Y, Joshi A, Barysheva M, McMahon KL, de Zubicaray GI, Martin NG, Wright MJ, Toga AW, Sapiro G, Thompson PM, High Angular Resolution Diffusion Imaging (HARDI) Tractography in 234 Young Adults Reveals Greater Frontal Lobe Connectivity in Women. In Proceedings of the 8th IEEE ISBI, Chicago, Illinois, USA, 2011, pp. 939–943.

Jahanshad N, Kohannim O, Hiber DP, Stein JL, McMahon KL, de Zubicaray GI, Medland SE, Montgomery GW, Whitfield JB, Martin NG, Wright MJ, Toga AW, Thompson PM. 2012. Brain structure in healthy adults is related to serum transferrin and the H63D polymorphism in the *HFE* gene. Proc Natl Acad Sci U S A [Epub ahead of print].

Jahanshad N, Lee A, Barysheva M, McMahon KL, de Zubicaray GI, Martin NG, Wright MJ, Toga AW, Thompson PM. 2010. Genetic influences on brain asymmetry: a DTI study of 374 twins and siblings. NeuroImage 52:455–469.

Jones DK, Horsfield MA, Simmons A. 1999. Optimal strategies for measuring diffusion in anisotropic systems by magnetic resonance imaging. Magn Reson Med 42:515–525.

Joshi AA, Lepore N, Joshi S, Lee AD, Barysheva M, de Zubicaray GI, Wright MJ, McMahon KL, Toga AW, Thompson PM. A Genetic Analysis of Cortical Thickness in 372 Twins. In Proceedings of the 7th IEEE ISBI, Rotterdam, The Netherlands, 2010, pp. 101–104.

Just MA, Cherkassky VL, Keller TA, Kana RK, Minshew NJ. 2007. Functional and anatomical cortical underconnectivity in autism: evidence from an fMRI study of an executive function task and corpus callosum morphometry. Cereb Cortex 17:951–961.

Kang HM, Zaitlen NA, Wade CM, Kirby A, Heckerman D, Daly MJ, Eskin E. 2008. Efficient control of population structure in model organism association mapping. Genetics 178:1709–1723.

Kohannim O, Jahanshad N, Braskie MN, Stein JL, Chiang M-C, Reese AH, Hibar DP, Toga AW, McMahon KL, de Zubicaray GI, Medland SE, Wright MJ, Thompson PM. 2011. Predicting white matter integrity from multiple common genetic variants. Neuropsycopharmacology (accepted).

Latora V, Marchiori M. 2001. Efficient behavior of small-world networks. Phys Rev Lett 87:198701.

Lee AD, Lepore N, Brun CC, Barysheva M, Chou YY, Chiang MC, Madsen SK, McMahon KL, de Zubicaray GI, Wright MJ,

Toga AW, Thompson PM. The Multivariate A/C/E Model and the Genetics of Fiber Architecture. In Proceedings of the 6th IEEE ISBI, Boston, Massachusetts, 2009a, pp. 125–128.

Lee AD, Lepore N, Brun CC, Chou YY, Barysheva M, Chiang MC, Madsen SK, de Zubicaray GI, McMahon KL, Wright MJ, Toga AW, Thompson PM. Tensor-Based Analysis of Genetic Influences on Brain Integrity using DTI in 100 Twins, Medical Image Computing and Computer Assisted Intervention. In Proceedings of the 12th MICCAI, London, United Kingdom, 2009b, pp. 967–974.

Lee AD, Lepore N, de Leeuw J, Brun CC, Barysheva M, McMahon KL, de Zubicaray GI, Martin NG, Wright MJ, Thompson PM. Multivariate Variance-Components Analysis in DTI. In Proceedings of the 7th IEEE ISBI, Rotterdam, The Netherlands, 2010, pp. 1157–1160.

Leow A, Huang S-C, Geng A, Becker J, Davis S, Toga A, Thompson P. 2005. Inverse consistent mapping in 3D deformable image registration: its construction and statistical properties. Inf Process Med Imaging 19:493–503.

Lepore N, Brun CC, Chou YY, Lee AD, Barysheva M, de Zubicaray GI, Meredith M, McMahon K, Wright MJ, Toga AW, Thompson PM. Multi-Atlas Tensor-Based Morphometry and its Application to a Genetic Study of 92 Twins. Workshop on Mathematical Foundations of Computational Anatomy, International Conference on Medical Image Computing and Computer Assisted Intervention (MICCAI), New York, New York, September 6 (2008).

McIntosh AM, Moorhead TWJ, Job D, Lymer GKS, Muñoz Maniega S, McKirdy J, Sussman JED, Baig BJ, Bastin ME, Porteous D, Evans KL, Johnstone EC, Lawrie SM, Hall J. 2008. The effects of a neuregulin 1 variant on white matter density and integrity. Mol. Psychiatry 13:1054–1059.

Peñagarikano O, Abrahams BS, Herman EI, Winden KD, Gdalyahu A, Dong H, Sonnenblick LI, Gruver R, Almajano J, Bragin A, Golshani P, Trachtenberg JT, Peles E, Geschwind DH. 2011. Absence of CNTNAP2 leads to epilepsy, neuronal migration abnormalities, and core autism-related deficits. Cell 147:235–246.

Pfefferbaum A, Sullivan EV, Carmelli D. 2001. Genetic regulation of regional microstructure of the corpus callosum in late life. NeuroReport 12:1677–1681.

Poliak S, Gollan L, Martinez R, Custer A, Einheber S, Salzer JL, Trimmer JS, Shrager P, Peles E. 1999. Caspr2, a new member of the Neurexin superfamily, is localized at the juxtaparanodes of myelinated axons and associated with K+ channels. Neuron 24:1037–1047.

Poliak S, Salomon D, Elhanany H, Sabanay H, Kiernan B, Pevny L, Stewart CL, Xu X, Chiu S-Y, Shrager P, Furley AJW, Peles E. 2003. Juxtaparanodal clustering of Shaker-like K+ channels in myelinated axons depends on Caspr2 and TAG-1. J Cell Biology 162:1149–1160.

Pollonini L, Patidar U, Situ N, Rezaie R, Papanicolaou AC, Zouridakis G. Functional Connectivity Networks in the Autistic and Healthy Brain Assessed Using Granger Causality. In Proceedings of the 32nd IEEE EMBS, Buenos Aires, Argentina, 2010, pp. 1730–1733.

Posthuma D, De Geus EJC, Neale MC, Hulshoff Pol HE, Baaré WEC, Kahn RS, Boomsma D. 2000. Multivariate genetic analysis of brain structure in an extended twin design. Behav Genet 30:311–319.

Rubinov M, Sporns O. 2010. Complex network measures of brain connectivity: uses and interpretations. NeuroImage 52:1059–1069.

Schmitt JE, Lenroot RK, Wallace GL, Ordaz S, Taylor KN, Kabani N, Greenstein D, Lerch JP, Kendler KS, Neale MC, Giedd JN. 2008. Identification of genetically mediated cortical networks: a multivariate study of pediatric twins and siblings. Cereb Cortex 18:1737–1747.

Scott-Van Zeeland A, Abrahams B, Alvarez-Retuerto A, Sonnenblick L, Rudie J, Ghahremani D, Mumford JA, Poldrack RA, Dapretto M, Geschwind DH, Bookheimer SY. 2010. Altered functional connectivity in frontal lobe circuits is associated with variation in the autism risk gene CNTNAP2. Sci Transl Med 2:1–6.

Sporns O. 2002. Graph theory methods for the analysis of neural connectivity patterns, In: Kötter R (ed.) *Neuroscience Databases. A Practical Guide.* Boston, MA: Klüwer; pp. 171–186.

Sporns O. 2011. *Networks of the Brain.* Cambridge, MA: The MIT Press.

Sporns O, Chialvo DR, Kaiser M, Hilgetag CC. 2004. Organization, development and function of complex brain networks. Trends Cogn Sci 8:418–425.

Stein JL, Medland SE, Vasquez AA, et al. 2012. Common genetic polymorphisms contribute to the variation in human hippocampal and intracranial volume. Nat Genet (in press).

Stein MB, Yang B-Z, Chavira DA, Hitchcock CA, Sung SC, Shipon-Blum E, Gelernter J. 2011. A common genetic variant in the Neurexin superfamily member CNTNAP2 is associated with increased risk for selective mutism and social anxiety-related traits. Biol Psychiatry 69:825–831.

Strauss K, Puffenberger E, Huentelman M, Gottlieb S, Dobrin S, Parod J, et al. 2006. Recessive symptomatic focal epilepsy and mutant contactin-associated protein-like 2. N Engl J Med 354:1370–1377.

Szatmari P, Paterson A, Zwaigenbaum L, et al. 2007. Mapping autism risk loci using genetic linkage and chromosomal rearrangements. Nat Genet 39:319–328.

Tan G, Doke T, Ashburner J, Wood N, Frackowiak R. 2010. Normal variation in fronto-occipital circuitry and cerebellar structure with an autism-associated polymorphism of CNTNAP2. NeuroImage 53:1030–1042.

Thompson PM, Cannon TD, Narr KL, van Erp T, Poutanen VP, Huttunen M, Lonnqvist J, Standertskjold-Nordenstam CG, Kaprio J, Khaledy M, Dail R, Zoumalan CI, Toga AW. 2001. Genetic influences on brain structure. Nat Neurosci 4:1253–1258.

Vernes SC, Newbury DF, Abrahams BS, Winchester L, Nicod J, Gorszner M, Alarcón M, Oliver PL, Davies KE, Geschwind DH, Monaco AP, Fisher SE. 2008. A functional genetic link between distinct developmental language disorders. N Engl J Med 359:2337–2345.

Watts DJ, Strogatz SH. 1998. Collective dynamics of "small-world" networks. Nature 393:440–442.

Winterer G, Konrad A, Vucurevic G, Musso F, Stoeter P, Dahmen N. 2008. Association of the 5′ end neuregulin-1 (NRG1) gene variation with subcortical medial frontal microstructure in humans. NeuroImage 40:712–718.

Zalesky A, Fornito A, Harding IH, Cocchi L, Yücel M, Pantelis C, Bullmore ET. 2010. Whole-brain anatomical networks: does the choice of nodes matter? NeuroImage 50:970–983.

Address correspondence to:
Paul M. Thompson
Department of Neurology
Laboratory of Neuro Imaging
UCLA School of Medicine
635 Charles Young Drive South
Suite 225
Los Angeles, CA 90095-7334
E-mail: thompson@loni.ucla.edu

3.2 **Obesity gene *NEGR1* affects white matter integrity differently in young and old adults**

This section is adapted from:

Dennis EL, Jahanshad N, Braskie MN, Warstadt NM, Hibar DP, Kohannim O, Nir T, McMahon KL, de Zubicaray GI, Montgomery G, Martin NG, Toga AW, Wright MJ, Thompson PM. (2013). Obesity Gene *NEGR1* Affects White Matter Integrity Differently in Young and Old Adults. *NeuroImage,* **Submitted Oct 21**.

Obesity Gene *NEGR1* Affects White Matter Integrity Differently in Young and Old Adults

Emily L. Dennis[1,2], Neda Jahanshad[1,2], Meredith N. Braskie[2], Nicholus M. Warstadt[2], Derrek P. Hibar[2], Omid Kohannim[1], Talia M. Nir[2], Katie L. McMahon[3], Greig I. de Zubicaray[4], Grant W. Montgomery[5], Nicholas G. Martin[5], Clifford R. Jack Jr[6], Matt A. Bernstein[6], Michael W. Weiner[7,8], Arthur W. Toga[2], Margaret J. Wright[4,5], the Alzheimer's Disease Neuroimaging Initiative (ADNI)*, Paul M. Thompson[2,9†]

[1]University of California, Los Angeles, CA, USA
[2]Imaging Genetics Center, Institute for Neuroimaging and Informatics, USC, Los Angeles, CA, USA
[3]Center for Advanced Imaging, University of Queensland, Brisbane, Australia
[4]School of Psychology, University of Queensland, Brisbane, Australia
[5]Queensland Institute of Medical Research, Brisbane, Australia
[6]Department of Radiology, Mayo Clinic and Foundation, Rochester, Minnesota, USA.
[7]Departments of Radiology, Medicine, and Psychiatry, University of California, San Francisco, California, USA.
[8]Veteran Affairs Medical Center, San Francisco, California, USA.
[9]Department of Psychiatry & Biobehavioral Sciences, Semel Institute for Neuroscience & Human Behavior, UCLA School of Medicine, Los Angeles, CA, USA

Please address correspondence to:
[†]Paul Thompson PhD
Professor of Neurology & Psychiatry
Laboratory of Neuro Imaging, UCLA School of Medicine
635 Charles Young Drive South, Suite 225
Los Angeles, CA 90095-7334
310-206-2101
thompson@loni.ucla.edu

Abstract (241 words; 250 max.)

Obesity is a crucial public health issue in developed countries, with implications for cardiovascular and brain health as we age. A number of commonly-carried genetic variants are associated with obesity. Elderly carriers of one of these variants, in the *FTO* gene, show different patterns of brain structure, on average. Here we aim to see whether variants in other obesity-associated genes - *NEGR1*, *FTO*, *MTCH2*, and 11 others - are associated with white matter integrity, measured through HARDI (high angular resolution diffusion imaging) in young healthy adults between 20-30 years old from the Queensland Twin Imaging study (QTIM). We began with a multi-locus approach testing how a number of SNPs (single nucleotide polymorphisms) that have been associated with obesity may jointly influence voxel-wise FA (fractional anisotropy). Risk allele dosage of rs2815752 in *NEGR1* was associated with lower white matter integrity across a substantial portion of the brain in young adults. Across the area of significance, each risk allele was associated with a 2.2% decrease in average FA. In a subsequent study of elderly people from the Alzheimer's Disease Neuroimaging Initiative (ADNI), *NEGR1* variants were associated with FA in the same areas but in the opposite direction. Effects of the *NEGR1* risk allele appear to be age-dependent. These results are consistent with prior findings that obesity in midlife is cognitively detrimental, while late-life obesity may be cognitively protective. The effects of obesity to cognition across the lifespan may be in part genetically influenced.

1. Introduction

Obesity is a major public health issue facing developed countries. In the United States over a third of adults are classified as obese, and another third are considered to be overweight (Ogden et al., 2012). Obesity has well-established links to serious health issues such as diabetes, heart disease, and premature death (Must et al., 1999). High body mass index (BMI)[1] in midlife is linked to poorer cognitive functioning in old age (Fitzpatrick et al., 2009; Walther et al., 2009). Greater BMI is associated with lower brain volume (Walther et al., 2009; Ward et al., 2005; Taki et al., 2008), brain atrophy (Gustafson et al., 2004), and lower gray matter density (Pannacciulli et al., 2006), and neuronal and myelin abnormalities (Gazdzinski et al., 2010). Obese people have abnormalities in white matter volume (Haltia et al., 2007; Raji et al., 2009), diffusivity (Alkan et al., 2008) and integrity across many brain regions (Stanek et al., 2009; Verstynen et al., 2012; Xu et al., 2013). These brain differences in obese people may be attributable to a less healthy diet and lifestyle, which negatively affect brain health (Molteni et al., 2002; Northstone et al., 2012; Ars, 2012). They may be partly due to genetic variants with joint effects on the brain and obesity risk. A gene may directly affect the brain, and its effects on appetite and physical activity could affect obesity. Alternatively, a gene could affect vascular health, reducing cerebral blood flow, and therefore delivery of oxygen and nutrients to the brain, with concomitant effects on brain function.

Diet and lifestyle are the most readily identifiable causes of obesity, yet it is highly heritable (Wardle et al., 2008), and genetic vulnerabilities interact with lifestyle factors. A number of genes have been repeatedly associated with obesity in cohorts worldwide (Frayling et

---

[1] Body mass index is a ratio of weight to height, intended as an approximate but readily computed assessment of fat mass. The equation to calculate BMI (in SI units) is BMI=mass (kg)/(height (m))^2.

al., 2007; Loos et al., 2008; Ng et al., 2012; Okada et al., 2012; Wen et al., 2012). We previously found that elderly carriers of the *FTO* risk allele had lower frontal and occipital lobe volumes (Ho et al., 2010). Recent genome-wide association studies (GWAS) identified a number of loci associated with BMI (Speliotes et al., 2010; Thorleifsson et al., 2008; Willer et al., 2008).

Here we investigated whether 16 common variants in obesity-related genes relate to the brain's white matter integrity. Using a multi-locus approach to assess their combined effect, we tested whether obesity-related variants might predict differences in white matter integrity assessed using high angular resolution diffusion imaging (HARDI) (Kohannim et al., 2012). As a *post hoc* test, we evaluated the most promising SNP (single nucleotide polymorphism) driving the effects in the multi-locus model. Initial analyses were completed in 499 young adults (aged 20-30), to test if there was any evidence of a link between obesity-related genetic variants and brain integrity. We followed up with an exploratory sample of 78 elderly subjects aged 55-90 years to examine effects of the obesity-related SNPs in an older cohort. We did not expect the older sample (ADNI) to replicate results from the younger cohort; rather, we were interested in examining whether these effects might differ in a much older population.

2. Materials and Methods

2.1 Participants

We examined two different cohorts – young Australian twins (the Queensland Twin Imaging study; QTIM) and elderly people in the United States (the Alzheimer's Disease Neuroimaging Initiative; ADNI). These cohorts were selected because of the large amount of high quality neuroimaging and genome-wide genetic data.

2.2 QTIM Cohort

For the QTIM cohort, participants were recruited as part of a 5-year project research

project examining healthy Australian twins with structural MRI and diffusion-weighted imaging

(de Zubicaray et al., 2008). Our analysis included 499 right-handed subjects (326 females/173

males, mean age=23.8, SD=2.5 years, range=20-30 years). This sample included 163

monozygotic (MZ) twins, 274 dizygotic (DZ) twins, and 62 non-twin siblings, from 309

families. This information is summarized in **Table 2**, along with BMI information for each

group. A histogram of BMI for the QTIM cohort is shown in **Figure 1**. All QTIM subjects were

Caucasian, and ancestry outliers, defined as individuals more than 6 SD from the PC1/PC2

centroid after principal components analyses of the GWAS data (Medland et al., 2009), were

excluded. Gene allele frequencies can differ between ethnicities, as can the risks associated with

various alleles, so ethnically homogenous groups are generally preferred in genetic studies.

Additionally, the three published studies (Speliotes et al., 2010; Thorleifsson et al., 2008; Willer

et al., 2008) – which we used to select our SNPs of interest – were analyses of sampled

populations that were 99.7% Caucasian (one of the studies [Thorleifsson et al., 2008] included a

very small number of African American subjects as well).

2.2.1 Scan Acquisition

Whole-brain anatomical and high angular resolution diffusion images (HARDI) were

collected with a 4T Bruker Medspec MRI scanner. T1-weighted anatomical images were

acquired with an inversion recovery rapid gradient echo sequence. Acquisition parameters were:

TI/TR/TE = 700/1500/3.35ms; flip angle = 8 degrees; slice thickness = 0.9mm, with a 256x256

acquisition matrix. HARDI was also acquired using single-shot echo planar imaging with a

twice-refocused spin echo sequence to reduce eddy-current induced distortions. Imaging

parameters were: 23cm FOV, TR/TE 6090/91.7ms, with a 128x128 acquisition matrix. Each 3D

volume consisted of 55 2-mm thick axial slices with no gap, and 1.79 x 1.79 mm^2 in-plane resolution. 105 images were acquired per subject: 11 with no diffusion sensitization (i.e., T2-weighted b_0 images) and 94 diffusion-weighted (DW) images ($b = 1159$ s/mm^2) with gradient directions evenly distributed on a hemisphere in the q-space. Scan time for the 105-gradient HARDI scan was 14.2 min.

2.2.2 Establishing Zygosity and Genotyping

Zygosity was objectively established by typing nine independent DNA microsatellite polymorphisms (polymorphism information content > 0.7), using standard PCR methods and genotyping. Results were crosschecked with blood group (ABO, MNS, and Rh), and phenotypic data (hair, skin, and eye color), giving an overall probability of correct zygosity assignment > 99.99%, and these were subsequently confirmed by GWAS. Genomic DNA samples were analyzed on the Human610-Quad BeadChip (Illumina) according to the manufacturers protocols (Infinium HD Assay; Super Protocol Guide; Rev. A, May 2008).

2.3 Follow-up sample - Participants

We found one SNP that individually appeared to show a significant association with FA (rs2815752). We also evaluated how this SNP related to DTI measures of white matter integrity in an independent sample from the second phase of the Alzheimer's Disease Neuroimaging Initiative (ADNI). The ADNI2 sample included 78 individuals (29 female/49 male; average age=74.3, SD=7.28 years, range=55-90) scanned from 14 sites across North America. This information is also included in **Table 2**, along with the BMI data for each group. We only included the subgroup of ADNI subjects who were Caucasian, as our initial subject group was 100% Caucasian and gene allele frequencies and the risks they confer can differ by ethnicity. A histogram of BMI of subjects can be seen in **Figure 1**. For this sample we used MDS

80

(multidimensional scaling) parameters as covariates to control for any remaining genetic variability. The ADNI sample is more ethnically heterogenous than the QTIM sample, and while we limited our analyses to individuals who self-identified as "Caucasian", we wanted to control for any remaining genetic variability. Ancestry outliers had already been removed from the QTIM sample in previous analyses, so this was not a concern in the QTIM sample.

2.3.1 Follow-up sample – Scan Acquisition

All ADNI2 subjects underwent whole-brain MRI scans on 3 tesla GE Medical Systems scanners at 14 acquisition sites across North America. Anatomical T1-weighted SPGR (spoiled gradient echo) sequences were collected (256x256 display matrix; acquired voxel size = 1.2x1.0x1.0 mm^3; TI=400 ms; TR = 6.98 ms; TE = 2.85 ms; flip angle=11°), as were diffusion-weighted images (DWI; 256x256 matrix; voxel size: 2.7x2.7x2.7 mm^3; TR=9000ms; scan time = 9 min; more imaging details may be found at http://adni.loni.ucla.edu/wp-content/uploads/2010/05/ADNI2_GE_3T_22.0_T2.pdf). 46 separate images were acquired for each DTI scan: 5 T2-weighted images with no diffusion sensitization (b_0 images) and 41 diffusion-weighted images (b=1000 s/mm²). This protocol was chosen after we conducted a detailed comparison of several different DTI protocols, to optimize the signal-to-noise ratio in a fixed scan time (Zhan et al., 2012). All T1-weighted MR and DWI images were checked visually for quality assurance to exclude scans with excessive motion and/or artifacts; none was excluded for quality reasons.

2.3.2 Follow-up sample – Genotyping

DNA samples were genotyped using the Illumina (San Diego, CA, USA) OmniExpress genotyping array; note that this chip was used for the from 434 ADNI-GO/ADNI-2 participants, and differs from the Illumina Human 610-Quad BeadChip used for the QTIM cohort and for the

81

818 participants in the first phase of ADNI, ADNI-1. Because these genotyping chips do not contain *APOE* biomarkers, ADNI researchers collected separate blood samples for DNA analysis, and *APOE* genotyping was done via PCR amplification and HhaI restriction enzyme digestion (Potkin et al., 2009).

2.4 Diffusion Tensor Image (DTI) Processing

For both cohorts, non-brain regions were automatically removed from each T1-weighted MRI scan using ROBEX (Iglesias et al., 2011) a robust brain extraction program trained on manually "skull-stripped" MRI data and FreeSurfer (Fischl et al., 2004), and from a T2-weighted image from the DWI set, using the FSL tool "BET" (Smith, 2002; FMRIB Software Library, http://fsl.fmrib.ox.ac.uk/fsl/).. Intracranial volume estimates were obtained from the full brain mask, and included cerebral, cerebellar, and brain stem regions. All T1-weighted images were linearly aligned using FSL *flirt* (with 9 DOF) (Jenkinson et al., 2002) to a common space (Holmes et al., 1998) with 1mm isotropic voxels and a $220\times220\times220$ voxel matrix. Raw diffusion-weighted images were corrected for eddy current distortions using the FSL tool, "eddy_correct". For each subject, the eddy-corrected images with no diffusion sensitization were averaged (QTIM: 11 images, ADNI: 5 images), linearly aligned and resampled to a downsampled version of their corresponding T1-weighted image ($110\times110\times110$ matrix, $2\times2\times2mm^3$ voxel size). Averaged b_0 maps were elastically registered to the structural scan using a mutual information cost function (Leow et al., 2005) to compensate for EPI-induced susceptibility artifacts. The resulting 3D deformation fields were then applied to the remaining 94 DWI volumes (QTIM) or 41 DWI volumes (ADNI).

We compared fractional anisotropy (FA) values at each voxel across *NEGR1* genotypes. Diffusion tensors were computed at each voxel using FSL software (http://fsl.fmrib.ox.ac.uk/fsl/).

From the tensor eigenvalues (λ_1, λ_2, λ_3), FA was calculated according to the following formula:

$$FA = \sqrt{\frac{3}{2}} \frac{\sqrt{(\lambda_1 - \bar{\lambda})^2 + (\lambda_2 - \bar{\lambda})^2 + (\lambda_3 - \bar{\lambda})^2}}{\sqrt{\lambda_1^2 + \lambda_2^2 + \lambda_3^2}}$$

Eq. 1

$$\bar{\lambda} = \frac{\lambda_1 + \lambda_2 + \lambda_3}{3}$$

We also analyzed radial diffusivity (D_{rad} = the average of λ_2 and λ_3), mean diffusivity ($D_{mean} = \bar{\lambda}$) and axial diffusivity (λ_1) to clarify the extent to which each might be contributing to the changes in FA.

We used nonlinear fluid registration to create a minimal deformation target (MDT) from the FA images (calculated after b_0 susceptibility correction) (Jahanshad et al., 2010a) for both the QTIM and ADNI cohorts. Further details on the MDT can be found in the Supplementary Methods. Using a customized template from subjects in the study (rather than a standard atlas or a single optimally chosen subject) can reduce bias in the registrations. Thresholded FA maps were then re-registered to the thresholded MDT and smoothed with a Gaussian kernel (7 mm full width at half-maximum). In this way, the outlines of the major white matter structures are stable and have been normalized to a very fine degree of matching across subjects, greatly reducing the neuroanatomical variations in these structures across subjects.

2.5 QTIM MDT

The MDT (minimal deformation template) is the template that deviates least from the anatomy of the subjects, and, in some circumstances, it can improve statistical power (Leporé et al., 2007). Included in the MDT were 32 randomly selected unrelated subjects (16 female/16 male). The N 3D vector fields that fluidly registered a specific individual to all other N subjects were averaged and applied to that subject, preserving the image intensities and anatomical

features of the template subject. Susceptibility-corrected FA maps were registered to the final

population-averaged FA-based MDT using a 3D elastic warping technique with a mutual

information cost function (Leow et al., 2005). To better align white matter regions of interest, the

MDT and all whole- brain registered FA maps were thresholded at 0.25 (excluding contributions

from non-white matter).

2.6 ADNI MDT

A study-specific MDT was created using 29 cognitively healthy elderly control (CTL)

subjects' baseline spatially-aligned corrected anatomical volumes. The MDT was generated by

creating an initial affine mean template from all 29 subjects, then registering all the aligned

individual scans to that mean using a fluid registration (Leow et al., 2007) while regularizing the

Jacobians (Hua et al., 2008). A new mean was created from the registered scans; this process was

iterated several times.

2.7 MultiSNP Analysis

Linear mixed-effects models were used to study the joint associations of SNPs with

imaging measures, while taking into account any relatedness among the subjects. For *N* subjects

and *p* independent predictors (SNPs or other covariates), regression coefficients (*β*) were

obtained, using the efficient mixed-model association (EMMA; http://mouse.cs.ucla.edu/emma/)

software with restricted maximum likelihood estimation (Kang et al., 2008), according to the

formula:

Eq. 2 $$y = X\beta + Zb + \varepsilon$$

Here, *y* represents an n-component vector of voxelwise FA measures, *X* is a matrix of

SNP genotypes (coded additively as 0, 1, or 2 for the number of minor alleles) and/ or covariates

(sex and age), *Z* is the identity matrix, *b* is a vector of random effects with a variance of $\sigma^2_g K$,

where K is the $N \times N$ kinship matrix for the twins and siblings, and ε is a matrix of residual effects with a variance of $\sigma^2_e I$, where I is identity matrix. A kinship matrix coefficient of 1 denoted the relationship of each subject to him/herself; the coefficient for MZ twins within the same family was 1; the coefficient for DZ twins and siblings within the same family was 0.5; and the coefficient for subjects not in the same family was 0, corresponding to the expected proportion of their shared genetic polymorphisms, respectively. Ancestry outliers were removed, so no additional modeling was used in the kinship matrix to adjust for population genetic structure between families. ε is a matrix of residual effects with a variance of $\sigma^2_e I$, and I is an identity matrix. P-values for the significance of individual and joint SNP associations with FA were assessed using a partial F-test, according to the formula:

Eq. 3
$$F = \frac{(RSS_{covariates} - RSS_{full}) \big/ (p_{full} - p_{covariates})}{RSS_{full} \big/ (n - p_{full})}$$

Where RSS represents the residual sum-of-squares, a reduced model includes only covariates, and a full model contains both SNPs and covariates. Further details can be seen in (Kohannim et al., 2012). For all statistical analyses, the LONI pipeline (http://pipeline.loni.ucla.edu/) was used for voxelwise parallelization on a multi-CPU grid computer. The searchlight false discovery rate method (Langers et al., 2007) was used for multiple comparisons correction across all voxels. As described in further detail in Kohannim et al., 2012, we do correct for the number of SNPs input into the model, and for each statistical test performed. However as is the case with all voxelwise neuroimaging studies, the number of tests is far greater than the number of subjects, so multiple comparisons correction across all voxels is necessary and often involves controlling the false

discovery rate at a stringent threshold (Hibar et al., 2011; Jahanshad et al., 2013). We also ran the multiSNP analysis covarying for BMI, which resulted in somewhat reduced areas of significance.

2.8 Candidate gene follow-up

Of the SNPs in our multiSNP model, one appeared to be driving the association (rs2815752), so we ran a follow-up analysis again examining voxel-wise measures of microstructural integrity, but focusing on just the rs2815752 (*NEGR1*) SNP. The statistical model is that listed in **Eq. 2**, again co-varying for age and sex, and correcting for multiple comparisons using searchlight FDR (Langers et al., 2007). We additionally ran the same analysis also co-varying for BMI, to assess whether BMI was responsible for out results. BMI was not significantly associated with rs2815752 risk allele dosage (*p*=0.30), and in our cohort, BMI was not associated with FA.

2.9 Follow-up sample – Statistical Analysis

Using the statistical model shown in **Eq. 2**, we tested the voxelwise association between measures of microstructural integrity (FA, D_{rad}, D_{mean}, D_{ax}) and rs2815752 risk allele dosage in our ADNI sample, using age and sex as covariates. We also ran this analysis with BMI as a covariate, which decreased the extent of the significant areas slightly. We ran this analysis both co-varying for disease status (AD, MCI, HC) and not co-varying for disease status, and also examined this association in just the healthy controls. We did this by adding a dummy variable for AD or MCI. Again we corrected for multiple comparisons using searchlight FDR (Langers et al., 2007). We also only ran statistics on voxels of the thresholded MDT present in all subject scans, as some scans had a slightly cropped FOV (field of view). As such we did not consider the inferior parts of the cerebellum and brain stem.

2.10 Additional NEGR1 Analyses

To examine the effects *NEGR1* has on white matter integrity in more depth, we next ran a gene-based test, PCReg (principal components regression) (Hibar et al., 2011). In PCReg, the entire list of genotyped SNPs within a gene can be assessed for joint association with a brain measure (here, voxelwise FA). It is similar to the multiSNP method (Kohannim et al., 2012), but can be run on SNPs that are in LD, and thus can be used as a gene-based test. PCReg works by first running a principal components analysis on the SNPs, to reduce the dimensions of the analysis, and avoid the complications of collinearity. Components with the highest eigenvalues (higher proportions of explained variance) were included until 80% of the SNP variance was explained, and the rest were discarded. This was followed by a multiple partial-*F* test, similar to **Eq. 3**. As this is a gene-based test encompassing the effects of possibly hundreds of SNPs, it does not suggest a directionality for the association; it tests whether a model containing SNPs that explain at least 80% of the variance in *NEGR1* are a better predictor of voxelwise FA than a reduced model containing only age and sex. We generated a list of SNPs within 100kb of *NEGR1* and filtered out those with an MAF<0.2236 leaving us with 275 *NEGR1* SNPs input into PCReg. In this method, the number of degrees of freedom of the F statistic accounts for the number of predictors, and corrects for the number of SNPs input into the model. Further details of this method may be found in Hibar et al., 2011.

3. Results

Axonal integrity is vital for efficient brain function; well-myelinated tracts propagate signals quickly, but poor or impaired myelination can decrease the speed or reliability of neuronal transmission (Purves et al., 2001). FA is a widely accepted measure of white matter integrity, and evaluates the degree to which water diffuses along the primary direction of the axon rather than across it. Lower FA has been found in many diseases, such as Alzheimer's

disease, multiple sclerosis, epilepsy, and many neuropsychiatric diseases (Ciccarelli et al., 2008). Genetic variants have also been discovered that may affect white matter integrity as measured by FA. Associations have been reported between FA and number of genetic variants, including polymorphisms in *CLU*, *HFE*, *NTRK1*, and many other genes (Braskie et al., 2011; Jahanshad et al., 2012; Braskie et al., 2012). These are genes that are already closely tied to cognitive function or neuropsychiatric disorders.

For our initial analyses in the young adult sample (QTIM – Queensland Twin Imaging study), we selected our SNPs of interest based on the following 3 reports: Speliotes et al. conducted a genome-wide association study (GWAS) across nearly 250,000 individuals to find loci associated with BMI. Willer et al. ran a meta-analysis of 15 genome-wide association studies searching for loci reliably associated with BMI, giving them a total N>32,000, with a follow-up analysis in another dataset of around 59,000 individuals. Thorleifsson et al. also conducted a GWAS of nearly 35,000 individuals to find loci associated with weight and BMI. We imputed to Hapmap3. Information on the imputation protocols and quality control steps may be found at http://enigma.loni.ucla.edu/wp-content/uploads/2010/09/ImputationProtocolsv1.2.pdf. Some of the SNPs in the 3 GWAS papers (Speliotes et al., 2010; Thorleifsson et al., 2008; Willer et al., 2008) were not in Hapmap3 so we could not include them on our list. We further narrowed the list down to those with a minor allele frequency (MAF) >0.2236 (to make sure that at least 5% of our subject pool of 499 were homozygous carriers of the minor allele). We additionally excluded 3 SNPs that were in high linkage disequilibrium (LD) with another SNP we were evaluating (LD>0.4) to reduce data redundancy and remove multicollinearity for the multiSNP analysis. This left us with 16 SNPs, listed in **Table 1**. All genetic analyses – multiSNP and individual SNP – used an additive genetic model that assessed the effect of each additional risk allele. No SNPs

deviated significantly from Hardy-Weinberg equilibrium, as shown in **Supplementary Table 1**.

3.1 MultiSNP Analysis – FA

Using FA images from 499 healthy young adults (mean age = 23.8 years, SD = 2.5, **Table 2**), we jointly assessed the effect of 16 SNPs (**Table 1**) that have been recently associated with BMI. We started with the multiSNP analysis, as none of these SNPs had yet been associated with brain imaging measures so there was no reason to prioritize any one specifically. This analysis yielded associations between our SNPs and FA in the bilateral *corona radiata*, corpus callosum, fornix, arcuate, and an area corresponding to both the uncinate and IFOF (inferior fronto-occipital fasciculus), as shown in **Figure 1**. The multiSNP analysis yields an R^2 coefficient, which is the predictability of our model; in **Figure 1**, R^2 is shown only in areas where the association was declared significant after multiple comparisons correction across all voxels in the image considering all the SNPs tested (see Methods). The maximum R2 value (predictability) in these regions was 0.115. The voxelwise multiSNP method allowed us to determine where in the brain joint information on all 16 SNPs was significantly better able to predict FA than just age and sex alone by establishing significance maps from the partial F-test. We additionally explored submodels to determine if any single one of the 16 SNPs was better at predicting FA when added to the model than sex, age and the remaining 15 SNPs all together; this implies that the SNP is able to predict FA even when covarying for sex, age and all other SNPs. We found several SNPs showed borderline significant associations on their own even when covarying for the other 15 SNPs. While it is not necessary to correct across the number of SNPs tested in the multiSNP model, it is necessary to correct for this when examining the effect of these individual SNPs, if a *post hoc* inference is made about whether any one of them is explaining variance in the model. While their joint effect, did survive voxelwise multiple

comparisons corrections across the whole brain, when covarying for all additional 15 SNPs included, none of the individual SNPs passed a multiple comparisons corrections threshold controlling the false positive rate at $q<0.003125$ (0.05/16). This underscores the utility of the multiSNP method. Rs2815752 (*NEGR1*) had by far the largest cluster of borderline significant voxels ($p<0.05$), and so likely was the main driving factor behind the multiSNP results. While for this analysis, we covaried for age and sex, we also ran a model also covarying for BMI, which reduced the area of significance somewhat, but showed similar results. The searchlight FDR critical p-values and minimum p-values for each SNP tested within the model, and the whole model, are shown in **Table 3**.

3.1 Candidate Gene Analysis – NEGR1

As the multiSNP results were strongly driven by *NEGR1* (rs2815752), we examined the effect of this SNP alone across the whole brain in the young adult sample. 188 subjects were homozygous risk (AA), 233 were heterozygous (AG), and 78 were homozygous non-risk (GG). The minor allele (G) frequency for rs2815752 is 0.301. *NEGR1* risk allele dosage was not significantly associated with BMI in our sample ($p=0.30$). We examined voxel-wise FA, D_{rad}, D_{mean}, and D_{ax}. *NEGR1* risk allele dosage (A) was widely negatively associated with FA, as shown in **Figure 2**. The posterior body of the corpus callosum and nearby *corona radiata* showed strongest associations with *NEGR1* risk allele dosage (in terms of lowest p-value), but the area of association covered the entire corpus callosum, large areas of the corona radiata, arcuate fasciculus, fornix, internal capsule, and areas that could be the inferior fronto-occipital fasciculus, inferior longitudinal fasciculus, and/or uncinate fasciculus. Across a mask of the areas of significance, each risk allele was associated with a 2.2% decrease in average FA. These last tracts overlap in these areas so we cannot say with confidence that one specific fasciculus is

selectively affected. D_{rad}, D_{mean}, and D_{ax} were also widely positively associated with *NEGR1* risk allele dosage, across the same area, as shown in **Figure 3**. Again, we covaried for age and sex.

3.2 Additional NEGR1 Analyses

Our gene-based test, PCReg, yielded significant associations between *NEGR1* and voxel-wise FA in the young adults (QTIM) in the corpus callosum, anterior commissure, *corona radiata*, inferior frontal gyrus, arcuate fasciculus, superior temporal gyrus, and regions corresponding to the inferior fronto-occipital fasciculus or uncinate (**Figure 6**). Like the multiSNP analysis, PCReg does not yield information on the direction of the association, just the *p*-value. Additionally, like the multiSNP analysis, there is an implicit correction for the effective number of genetic predictors included in the model, but we avoid the need to correct for the number of SNPs included, as PCA performs data reduction and compaction (see Methods section and Hibar et al., 2011).

3.3 Follow-up Analysis (ADNI)

We next examined our ADNI cohort (Alzheimer's Disease Neuroimaging Initiative) to see if the association between *NEGR1* and alterations in white matter integrity were also significant there. *NEGR1* was indeed associated with FA, in overlapping brain regions, but in the opposite direction to that of the young adult sample. Of our subjects 20 were healthy controls, 47 had mild cognitive impairment, and 10 had Alzheimer's disease. 33 subjects were homozygous risk (AA), 36 were heterozygous (AG), and 9 were homozygous non-risk (GG) (**Table 2**). *NEGR1* risk allele dosage was associated with *increased* FA and decreased D_{rad}, D_{mean}, and D_{ax} in the ADNI follow-up cohort across the *corona radiata*, arcuate fasciculus, middle frontal gyral WM, and superior longitudinal fasciculus (**Figure 4** and **5)**. For this analysis we covaried for age and sex. When covarying for BMI, the area of association was reduced, but still significant.

Directionality was not influenced when we additionally covaried for APOE4 status (apolipoprotein E (*APOE*) allele 4, is the genetic variant that confers the highest known odds ratio for late-onset Alzheimer's disease, Corder et al., 1993).

4. Discussion

Many genes have been linked to obesity, yet thus far only one study has examined the effect these obesity genes may have on the brain (Ho et al., 2010). Here, we revealed a joint effect of a set of obesity-associated SNPs on the brain in young adults, using a multiSNP approach we recently developed for screening brain images (Kohannim et al., 2012). The predictive power of these SNPs overlapped in the bilateral posterior *corona radiata*, arcuate, corpus callosum, fornix, and uncinate or IFOF (**Figure 1**). A *post hoc* analysis of the SNP contributing most to this effect yielded widespread negative associations between FA and *NEGR1* risk allele dosage in our young adult sample. In contrast, we detected associations between FA and *NEGR1* risk allele dosage in the same areas in an older, independent sample (ADNI), but in the opposite direction. To our knowledge this is the first paper to report an association between an obesity-related gene and a brain effect in humans in two populations. While our results overlapped in our second sample, they were in the opposite direction, which suggests an age-dependent effect of the *NEGR1* gene.

We began with the multiSNP analysis because it is a way to search for joint effects of a set of genetic variants on brain measures (Kohannim et al., 2012). *FTO* is the only obesity-related gene previously associated with brain differences, so we did not have prior evidence to supported prioritizing a particular gene initially (besides *FTO*). Of our 16 SNPs associated with obesity, a number of them converged in effect in the posterior *corona radiata*. Again, this analysis results in a summed R^2 value across the SNPs input into the model, without *beta* values,

and because only one statistical test is performed, there is no further correction for the number of SNPs included in the model, apart from the implicit correction made for the number of covariates in the null distribution of the statistic. Effects were driven primarily by one SNP, rs2815752 (*NEGR1*). The rs2815752 SNP is just upstream of the *NEGR1* gene, and the A risk allele tags a 45kb deletion (Jarick et al., 2011). *NEGR1* codes for the protein NEGR1 or neurotractin - a member of the neural IgLON subgroup of the immunoglobin superfamily. Neurotractin is a cell adhesion molecule that plays a key role in neural development (Marg et al., 1999). In mice, *NEGR1* is widely expressed in the brain. Mutations causing *NEGR1* loss of function led to decreased body mass in mice *in vivo*, and decreases in cell adhesion and neurite growth *in vitro* (Lee et al., 2012). The *NEGR1* risk allele (A) is associated with higher BMI (per allele change 0.10-0.13 kg/m^2; Speliotes et al., 2010; Willer et al., 2008).

No prior studies have linked *NEGR1* risk allele dosage to brain differences in humans. However, its role in mouse brain neural development makes it a plausible candidate. Adults carrying the risk allele had decreased FA across a wide swath of central white matter (**Figure 2**). Combined with the results of increased D_{rad}, D_{mean}, and D_{ax} in risk allele carriers, our results point to lower white matter integrity with *NEGR1* risk allele dosage. Across the area of significance, the decrease in mean FA per risk allele was 2.2%. Alzheimer's disease has been associated with decreases up to 33% in FA (Nir et al., 2013), so this is a modest but perhaps eventually significant difference among young, healthy individuals. Future studies will hopefully be able to test this association in independent samples. For example, we recently created a worldwide consortium dedicated to replicating genetic effects on the brain (Stein et al., 2012; Hibar et al., 2013; Thompson et al., 2013), and a multi-site GWAS of diffusion images is underway (Jahanshad et al., 2013). Obese individuals have significantly decreased volume in the

corona radiata, where we detected significant associations (Alkan et al., 2008). Although there are exceptions, lower FA and higher MD are usually signs of decreased myelination or fiber coherence (Thomason & Thompson et al., 2011; Dennis & Thompson et al., 2013). Middle-aged obese patients show widespread increases in ADC (apparent diffusion coefficient, equivalent to mean diffusivity – D_{mean}) in middle-aged obese patients (Alkan et al., 2008). As *NEGR1* plays a role in neural development, we could be detecting effects of lower myelination in *NEGR1* risk allele carriers. We did not find any significant associations between BMI and FA in the QTIM cohort, and those subjects were aged 20-30, so it is less likely that these results are chronic effects of obesity and lifestyle factors. We did have some overweight and obese subjects in our population, as noted in **Figure 7**, but did not find any significant differences in overweight or obese groups. We believe this is a strength of our paper, as it demonstrates that our results are more gene-related, rather than a consequence of obesity. A more likely scenario is that these decreases in white matter integrity point to a *precursor effect* of the obesity gene, and that lower white matter integrity in these areas is somehow related to the risk of becoming obese. Investigating this is beyond the scope of the current paper, but future studies may reveal whether these effects are linked.

We also conducted a second *NEGR1* analysis, running a gene-based test (called 'PCReg') on 275 SNPs in *NEGR1* (Hibar et al., 2011). We found a large cluster of significant association in the bilateral posterior *corona radiata*, where we found associations in our multiSNP analysis and in our analysis of rs2815752. PCReg does not output a *beta* value summed across SNPs used in the model, it shows areas where the effects on a brain measure within a gene aggregate. In other smaller clusters, voxel-wise FA was significantly associated with *NEGR1*. The fact that we found a large association in the same area as the rs2815752 analysis suggests that there are other

variations within *NEGR1* that are associated with FA in the posterior *corona radiata*. PCReg shows the associations of the SNPs in aggregate; many may have effects too small to detect individually, and rs2815752 may not be the main effect SNP within *NEGR1*. PCReg allows us to see small effects summed, and gives us greater confidence in our rs2815752 results.

Our initial *NEGR1* results in 499 young adult subjects largely overlapped in our second sample of 78 elderly subjects from the ADNI cohort. These associations overlapped with the QTIM sample in the *corona radiata* and arcuate fasciculus (**Figures 2 and 4**), with additional associations in the right middle frontal gyral WM, and superior longitudinal fasciculus. These associations were in the opposite direction in the ADNI sample. Another study of the QTIM sample found a genotype*age interaction, examining skin cancer genetics in the cohort participants and their parents (Duffy et al., 2010). The *NEGR1* risk allele may have changing effects with age - detrimental effects of the rs2815752 A allele in younger life may not be detrimental in older age. The *NEGR1* risk allele may be protective against degeneration later in life, as older individuals carrying the A allele had increased FA and decreased D_{rad}, D_{mean}, and D_{ax} (**Figure 4** and **Figure 6**). With a small sample of elderly subjects and a cross-sectional design, we cannot answer these questions, but they deserve further investigation, and offer future hypotheses for testing by worldwide imaging genetics consortia.

One consideration is where our results are localized. Our results are largely in tracts with a high density of parallel-organized fiber bundles, which some suggest may tend to favor overlapping results as we are more likely to find associations in these regions anyway. To investigate this, we examined the overlap between the average FA from our MDT with areas of significant association with *NEGR1* allele dosage (**Supplementary Figure 1**). As is evident, there are many regions of high FA (meaning high density of parallel-organized fibers) where we

95

did not find associations with *NEGR1* risk allele dosage, such as the highest FA region, the main aspect of the splenium. This supports that our overlapping results are not simply because of an increased ability of pick up genetic effects in these areas, and are true genetic associations.

Obesity (BMI > 30 kg/m^2) in midlife is associated with an increased risk of dementia later in life (Fitzpatrick et al., 2009). However, this association is reversed for late-life BMI and dementia risk, as being underweight (BMI < 20) is associated with an increased dementia risk, while obesity is associated with decreased dementia risk, compared to people with a normal BMI (20-25) (Fitzpatrick et al., 2009). The boundary between obesity being a risk factor and a potential protective factor for dementia is not well defined in the literature. Our two cohorts had an average age of 23.8 and 74.3, a gap too large to help in defining this boundary. Many factors can promote an association that changes with age, and the *NEGR1* gene may be part of this mechanism. Our young adults did not show any associations between BMI and FA, and *NEGR1* risk allele dosage was not associated with BMI. Our young adults may not have had a chance for *NEGR1* to have an effect, and we only had 499 subjects, which is very large for a brain imaging study, but small for a genetics study. The original studies finding an effect of *NEGR1* on obesity did so in sample sizes >30,000 with an average age around 50. We are examining a younger cohort, so brain changes may pre-date any clinical effects on BMI. The three GWAS studies (Speliotes et al., 2010; Thorleifsson et al., 2008; Willer et al., 2008) all included cohorts with average ages largely between 30-80, and were heavily weighted towards middle-aged subjects (~50 years old). In our elderly cohort, we found a trend indicating greater BMI in risk allele (A) carriers, but it was not significant. Obese subjects may have lower white matter integrity in the corpus callosum (Mueller et al., 2011; Xu et al., 2013; Marks et al., 2011) and fornix (Marks et al., 2011). We did not find any areas of significant association between FA and BMI, but these

areas are generally those where we found our *NEGR1* associations. *NEGR1* genotype may be one of many factors contributing to the association between BMI and white matter integrity of the corpus callosum and fornix. Further, we propose that the *NEGR1* gene effect on FA is age-dependent, and much like the association between BMI and dementia risk, factors that confer risk in young adulthood may even be protective in old age.

5. Conclusions

In this study we used an innovative multi-locus approach to examine the joint effect of obesity-associated SNPs on white matter integrity in young healthy adults. We found the effects were largely driven by a variant in one gene, *NEGR1*, which was associated with a decrease in FA of 2.2% per allele across the area of significance. We then examined elderly members of the ADNI (Alzheimer's Disease Neuroimaging Initiative) cohort, and found associations in the same regions, however in the opposite direction. Obesity has an age-dependent effect on cognitive function, which we propose has a partially genetic basis.

Author Disclosure Statement: The authors have no competing financial interests.

References

Alkan, A., Sahin, I., Keskin, L., Cikim, A. S., Karakas, H. M., Sigirci, A., & Erdem, G. (2008). Diffusion-weighted imaging features of brain in obesity. Magnetic Resonance Imaging, 26(4), 446–450.

Ars, C. (2012). The Effects of Prenatal and Early Postnatal Fat and Sugar Intake on Hippocampal Volume and Memory Performance in Healthy Dutch Children aged 6-8 (Doctoral dissertation). Retrieved from http://arno.unimaas.nl/show.cgi?fid=26241

Braskie, M. N., Jahanshad, N., Stein, J. L., Barysheva, M., Johnson, K., McMahon, K. L., et al. (2012). Relationship of a variant in the NTRK1 gene to white matter microstructure in young adults. J Neuroscience, 32(17), 5964-5972.

Braskie, M. N., Jahanshad, N., Stein, J. L., Barysheva, M., McMahon, K. L., de Zubicaray, G. I., et al. (2011). Common Alzheimer's disease risk variant within the CLU gene affects white matter microstructure in young adults. J Neuroscience, 31(18), 6764-6770.

Ciccarelli, O., Catani, M., Johansen-Berg, H., Clark, C., & Thompson, A. (2008). Diffusion-based tractography in neurological disorders: concepts, applications and future developments. The Lancet Neurology, 7(8), 715-727.

Corder, E. H., Saunders, A. M., Strittmatter, W. J., Schmechel, D. E., Gaskell, P. C., Small, G. W., et al. (1993). Gene dose of apolipoprotein E type 4 allele and the risk for Alzheimer's disease in late onset families. Science, 261(5123), 921-923.

Dennis, E. L. & Thompson, P. M. (2013). Mapping connectivity in the developing brain. International Journal of Developmental Neuroscience, 31(7), 525-542.

de Zubicaray, G. I., Chiang, M.-C., McMahon K. L., Shattuck, D. V., Toga, A. W., Martin, N.

    G., Wright, M. J., & Thompson, P.M. (2008). Meeting the challenges of neuroimaging

    genetics. Brain Imaging and Behavior, 2, 258-263.

Duffy, D. L., Iles, M. M., Glass, D., Zhu, G., Barrett, J. H., Höiom, V., et al. (2010). *IRF4*

    Variants have age-specific effects on nevus count and predispose to melanoma. Am J Hum

    Genetics, 87, 6-16.

Fischl, B., van der Kouwe, A., Destrieux, C., Halgren, E., Ségonne, F., Salat, D. H., et al. (2004).

    Automatically parcellating the human cerebral cortex. Cerebral Cortex, 14(1), 11-22.

Fitzpatrick, A. L., Kuller, L. H., Lopez, O. L., Diehr, P., O'Meara, E. S., Longstreth, W. T., &

    Luchsinger, J. A. (2009). Midlife and late-life obesity and the risk of dementia:

    cardiovascular health study. Archives of Neurology, 66(3), 336–342.

Frayling, T. M., Timpson, N. J., Weedon, M. N., Zeggini, E., Freathy, R. M., Lindgren, C. M., et

    al. (2007). A common variant in the FTO gene is associated with body mass index and

    predisposes to childhood and adult obesity. Science, 316, 889–894.

Gazdzinski, S., Millin, R., Kaiser, L. G., Durazzo, T. C., Mueller, S. G., Weiner, M. W., &

    Meyerhoff, D. J. (2010). BMI and neuronal integrity in healthy, cognitively normal elderly:

    A proton magnetic resonance spectroscopy study. Obesity, 18(4), 743-748.

Gustafson, D., Lissner, L., Bengtsson, C., Björkelund, C., & Skoog, I. (2004). A 24-year follow-

    up of body mass index and cerebral atrophy. Neurology, 63(10), 1876-1881.

Haltia, L. T., Viljanen, A., Parkkola, R., Kemppainen, N., Rinne, J. O., Nuutila, P., & Kaasinen,

    V. (2007). Brain white matter expansion in human obesity and the recovering effect of

    dieting. Journal of Clinical Endocrinology & Metabolism, 92(8), 3278–3284.

Hibar, D. P., Stein, J. L., Kohannim, O., Jahanshad, N., Saykin, A. J., Shen, L. et al. (2011). Voxelwise gene-wide association study (vGeneWAS): Multivariate gene-based association testing in 731 elderly subjects. NeuroImage, 56(4), 1875-1891.

Hibar, D. P., + 200 authors for the ENIGMA Consortium (2013). ENIGMA2: Genome-wide scans of subcortical brain volumes in 16,125 subjects from 28 cohorts worldwide. OHBM, Seattle, WA, June 2013.

Ho, A. J., Stein, J. L., Hua, X., Lee, S., Hibar, D. P., Leow, A. D., et al. (2010). A commonly carried allele of the obesity-related FTO gene is associated with reduced brain volume in the healthy elderly. Proceedings of the National Academy of Sciences, 107(18), 8404–8409.

Holmes, C. J., Hoge, R., Collins, L., Woods, R., Toga, A. W., & Evans, A. C. (1998). Enhancement of MR Images Using Registration for Signal Averaging. Journal of Computer Assisted Tomography, 22(2), 324-333.

Hua, X., Leow, A. D., Lee, S., Klunder, A. D., Toga, A. W., Lepore, N., et al. (2008). 3D characterization of brain atrophy in Alzheimer's disease and mild cognitive impairment using tensor-based morphometry. NeuroImage, 41(1), 19-34.

Iglesias, J. E., Liu, C.-Y., Thompson, P. M., & Tu, Z. (2011). Robust extraction across datasets and comparison with publicly available methods. IEEE Trans Med Imaging, 30, 1617-1634.

Jahanshad, N., Kochunov, P. V., Sprooten, E., Mandl, R. C., Nichols, T. E., Almasy, L., et al. (2013) Multi-site genetic analysis of diffusion images and voxelwise heritability analysis: A pilot project of the ENIGMA-DTI working group. Neuroimage, 81, 455-469.

Jahanshad, N., Kohannim, O., Hibar, D. P., Stein, J. L., McMahon, K. L., de Zubicaray, G. I., et al. (2012). Brain structure in healthy adults is related to serum transferrin and the H63D polymorphism in the *HFE* gene. PNAS, 109(14), E851-E859.

Jahanshad, N., Lee, A., Barysheva, M., McMahon, K., de Zubicaray, G. I., Martin, N. G., Wright, M. J., Toga, A. W., & Thompson, P. M. (2010a). Genetic influences on brain asymmetry: A DTI study of 374 twins and siblings. NeuroImage, 52, 455-469.

Jahanshad, N., Rajagopalan, P., Hua, X., Hibar, D. P., Nir, T. M., Toga, A. W., et al. (2013). Genome-wide scan of healthy human connectome discovers *SPON1* variant influencing dementia severity. PNAS, In Press.

Jarick, I., Vogel, C. I. G., Scherag, S., Schäfer, H., Hebebrand, J., Hinney, A., & Scherag, A. (2011). Novel common copy number variation for early onset extreme obesity on chromosome 11q11 identified by a genome-wide analysis. Human Molecular Genetics, 20(4), 840-852.

Jenkinson, M., Bannister, P., Brady, M., & Smith, S. (2002). Improved optimization for the robust and accurate linear registration and motion correction of brain images. NeuroImage, 17, 825-841.

Kang, H. M., Zaitlen, N. A., Wade, C. M., Kirby, A., Heckerman, D., Daly, M. J., Eskin, E. (2008). Efficient control of population structure in model organism association mapping. Genetics, 178(3), 1709-1723.

Kohannim, O., Jahanshad, N., Braskie, M. N., Stein, J. L., Chiang, M.-C., Reese, A. H., et al. (2012). Predicting White Matter Integrity from Multiple Common Genetic Variants. Neuropsychopharmacology, 37(9), 2012–2019.

Langers, D. R., Jansen, J. F. & Backes, W. H. (2007). Enhanced signal detection in neuroimaging by means of regional control of the global false discovery rate. NeuroImage, 38, 43-56.

Lee, A. W. S., Hengstler, H., Schwald, K., Berriel-Diaz, M., Loreth, D., Kirsch, M., et al. (2012). Functional inactivation of the genome-wide association study obesity gene neuronal growth regulator 1 in mice causes a body mass phenotype. PLoS ONE, 7(7), e41537.

Leow, A., Huang, S.-C., Geng, A., Becker, J., Davis, S., Toga, A., & Thompson, P. (2005). Inverse consistent mapping in 3D deformable image registration: its construction and statistical properties. Processing in Medical Imaging, 3565, 23-57.

Leow, A. D., Yanovsky, I., Chang, M.-C., Lee, A. D., Klunder, A. D., Lu, A. et al. (2007). Statistical properties of Jacobian maps and the realization of unbiased large-deformation nonlinear image registration. IEEE Trans Med Imaging 26, 822–832.

Leporé, N., Brun, C., Pennec, X., Chou, Y.-Y., Lopez, O., L., Aizenstein, H. J., et al. (2007). Mean template for tensor-based morphometry using deformation tensors. In Proc. 10th MICCAI, Brisbane, Australia, 826-833.

Loos, R. J. F., Lindgren, C. M., Li, S., Wheeler, E., Zhao, J. H., Prokopenko, I., et al. (2008). Common variants near MC4R are associated with fat mass, weight and risk of obesity. Nature Genetics, 40, 768-775.

Marg, A., Sirim, P., Spaltmann, F., Plagge, A., Kauselmann, G., Buck, F., Rathjen, F. G., & Brümmendorf, T. (1999). Neurotractin, a novel neurite outgrowth-promoting Ig-like protein that interacts with CEPU-1 and LAMP. The Journal of Cell Biology, 145(4), 865–876.

Marks, B. L., Katz, L. M., Styner, M., & Smith, J. K. (2011). Aerobic fitness and obesity: relationship to cerebral white matter integrity in the brain of active and sedentary older adults. Br J Sports Med, 45, 1208-1215.

Medland, S. E., Nyholt, D. R., Painter, J. N., McEvoy, B. P., McRae, A. F., Zhu, G., et al. (2009). Common variants in the trichohyalin gene are associated with straight hair in europeans. Am J Hum Gen, 85(5), 750-755.

Molteni, R., Barnard, R. J., Ying, Z., Roberts, C. K., & Gomez-Pinilla, F. (2002). A high-fat, refined sugar diet reduces hippocampal brain-derived neurotrophic factor, neuronal plasticity, and learning. Neuroscience, 112(4), 803–814.

Mueller, K., Anwander, A., Möller, H. E., Horstmann, A., Lepsien, J., Busse, F., et al. (2011). Sex-dependent influences of obesity on cerebral white matter investigated by diffusion-tensor imaging. PLoS ONE, 6(4), e18544.

Must, A., Spadano, J., Coakley, E. H., Field, A. E., Colditz, G., & Dietz, W. H. (1999). The disease burden associated with overweight and obesity. JAMA, 282(16), 1523-1529.

Ng, M. C. Y., Hester, J. M., Wing, M. R., Li, J., Xu, J., Hicks, P. J. et al. (2012). Genome-wide association of BMI in African Americans. Obesity, 20(3), 622-627.

Nir, T. M., Jahanshad, N., Villalon-Reina, J. E., Toga, A. W., Jack, C. R., Weiner, M. W., et al. (2013). Effectiveness of regional DTI measures in distinguishing Alzheimer's disease, MCI and, normal aging. NeuroImage: Clinical, In Press.

Northstone, K., Joinson, C., Emmett, P., Ness, A., & Paus, T. (2012). Are dietary patterns in childhood associated with IQ at 8 years of age? A population-based cohort study. Journal of Epidemiology & Community Health, 66, 624–628.

Ogden, C. L., Carroll, M. D., Kit, B. K., & Flegal, K. M. (2012). Prevalence of obesity in the United States, 2009-2010. NCHS Data Brief, 82.

Okada, Y., Kubo, M., Ohmiya, H., Takahashi, A., Kumasaka, N., Hosono, N. et al. (2012). Common variants at *CDKAL1* and *KLF9* are associated with body mass index in east Asian populations. Nature Genetics, 44, 302-306.

Pannacciulli, N., Del Parigi, A., Chen, K., Le, D. S. N. T., Reiman, E. M., & Tataranni, P. A. (2006). Brain abnormalities in human obesity: A voxel-based morphometric study. NeuroImage, 31, 1419–1425.

Potkin, S. G., Guffanti, G., Lakatos, A., Turner, J. A., Kruggel, F., Fallon, J. H., et al. (2009). Hippocampal atrophy as a quantitative trait in a genome-wide association study identifying novel susceptibility genes for Alzheimer's disease. PLoS ONE, 4(8), e6501.

Purves, D., Augustine, G. J., Fitzpatrick, D., et al., editors. (2001). Increased Conduction Velocity as a Result of Myelination. Neuroscience. 2nd edition. Sunderland (MA): Sinauer Associates. Available from: http://www.ncbi.nlm.nih.gov/books/NBK10921/

Raji, C. A., Ho, A. J., Parikshak, N. N., Becker, J. T., Lopez, O. L., Kuller, L. H., Hua, X., Leow, A. D., Toga, A. W., & Thompson, P. M. (2009). Brain structure and obesity. Human Brain Mapping, 31, 353-364.

Smith, S. M. (2002). Fast robust automated brain extraction. Human Brain Mapping, 17(3), 143-155.41.

Speliotes, E. K., Willer, C. J., Berndt, S. I., Monda, K. L., Thorleifsson, G., Jackson, A. U., et al. (2010). Association analyses of 249,796 individuals reveal 18 new loci associated with body mass index. Nature Genetics, 42(11), 937–948.

Stanek, K. M., Grieve, S. M., Brickman, A. M., Korgaonkar, M. S., Paul, R. H., Cohen, R. A., & Gunstad, J. J. (2009). Obesity is associated with reduced white matter integrity in otherwise healthy adults. Obesity, 19, 500-504.

Stein, J. L., Medland, S. E., Vasquez, A. A., Hibar, D. P., Senstad, R. E., Winkler, A. M., et al. (2012). Identification of common variants associated with human hippocampal and intracranial volumes. Nature Genetics, 44(5), 552-562.

Taki, Y., Kinomura, S., Sato, K., Inoue, K., Goto, R., Okada, K., Uchida, S., Kawashima, R., & Fukuda, H. (2008). Relationship between body mass index and gray matter volume in 1,428 healthy individuals. Obesity, 16, 119–124.

Thomason, M. E., & Thompson, P. M. (2011). Diffusion imaging, white matter, and psychopathology. Annual Review of Clinical Psychology, 7, 63–85.

Thompson, P. M., Stein, J. L., Medland, S. E., Vasquez, A. A., Hibar, D. P., Renteria, M., et al. for the ENIGMA Consortium# (2013). The ENIGMA Consortium: Large-scale Collaborative Analyses of Neuroimaging and Genetic Data. Brain Imaging & Behavior, Special Issue on Imaging Genetics (ed. John D. van Horn), in press.

Thorleifsson, G., Walters, G. B., Gudbjartsson, D. F., Steinthorsdottir, V., Sulem, P., Helgadottir, A., et al. (2008). Genome-wide association yields new sequence variants at seven loci that associate with measures of obesity. Nature Genetics, 41(1), 18–24.

Verstynen, T. D., Weinstein, A. M., Schneider, W. W., Jakicic, J. M., Rofey, D. L., & Erickson, K. I. (2012). Increased body mass index is associated with a global and distributed decrease in white matter microstructural integrity. Psychosom Med, 74(7), 682-690.

Walther, K., Birdsill, A. C., Glisky, E. L., & Ryan, L. (2009). Structural brain differences and cognitive functioning related to body mass index in older females. Human Brain Mapping, 31, 1052–1064.

Ward, M. A., Carlsson, C. M., Trivedi, M. A., Sager, M. A., & Johnson, S. C. (2005). The effect
of body mass index on global brain volume in middle-aged adults: a cross sectional study.
BMC Neurology, 5(23), 10.1186/1471-2377-23.

Wardle, J., Carnell, S., Haworth, C. M. A., & Plomin, R. (2008). Evidence for a strong genetic
influence on childhood adiposity despite the force of the obesogenic environment. Am J Clin
Nutr, 87(2), 398-404.

Wen, W., Cho, ,Y.-S., Zheng, W., Dorajoo, R., Kato, N., Qi, L. et al. (2012). Meta-analysis
identified common variants associated with body mass index in east Asians. Nature
Genetics, 44, 307-311.

Willer, C. J., Speliotes, E. K., Loos, R. J. F., Li, S., Lindgren, C. M., Heid, I. M., et al. (2008).
Six new loci associated with body mass index highlight a neuronal influence on body weight
regulation. Nature Genetics, 41(1), 25–34.

Xu, J., Li, Y., Lin, H., Sinha, R., & Potenza, M. N. (2013). Body mass index correlates
negatively with white matter integrity in the fornix and corpus callosum: A diffusion tensor
imaging study. Hum Brain Mapp, 34, 1044-1052.

Zhan, L., Jahanshad, N., Ennis, D. B., Jin, Y., Bernstein, M. A., Borowski, B. J., Jack, Jr., C. R.,
Toga, A. W., Leow, A. W., & Thompson, P. M. (2012). Angular versus spatial resolution
trade-offs for diffusion imaging under time constraints. Hum Brain Mapp, April 25. [Epub
ahead of print].

Table 1. SNPs included in the multiSNP model.

SNP	Nearest Gene	MAF	Risk Allele	GWAS Study
rs10913469	SEC16B	0.234	C	Thorleifsson et al., 2009
rs7647305	ETV5	0.2248	C	Thorleifsson et al., 2009
rs925946	BDNF-AS	0.2285	T	Thorleifsson et al., 2009
rs10501087	BDNF-AS	0.2436	T	Thorleifsson et al., 2009
rs8049439	ATXN2L	0.359	C	Thorleifsson et al., 2009
rs6499640	FTO	0.4835	A	Thorleifsson et al., 2009
rs3751812	FTO	0.2413	T	Thorleifsson et al., 2009
rs9931989	ATP2A1	0.2514	G	Willer et al., 2008
rs2815752	NEGR1	0.3008	A	Willer et al., 2008
rs10838738	MTCH2	0.2834	G	Willer et al., 2008
rs571312	MC4R	0.2372	A	Speliotes et al., 2010
rs29941	KCTD15	0.3965	C	Speliotes et al., 2010, Thorleifsson et al., 2009
rs7138803	FAIM2	0.292	A	Speliotes et al., 2010, Thorleifsson et al., 2009
rs2241423	MAP2K5	0.4006	G	Speliotes et al., 2010
rs1514175	TNN13K	0.3864	A	Speliotes et al., 2010
rs10968576	LRRN6C	0.2422	G	Speliotes et al., 2010

Table 2. Subject demographics for the QTIM and ADNI cohorts.

Genetic group	QTIM Cohort			ADNI follow-up cohort					
	N	F/M	BMI	N	F/M	BMI	HC	MCI	AD
AA	188	125/63	23.1	33	10/23	27.5	11	21	1
AG	233	154/79	23.4	36	13/23	27.0	8	22	6
GG	78	47/31	23.6	9	6/3	24.5	1	5	3

Figure 1. MultiSNP results: Associations between FA and SNPs linked with BMI.
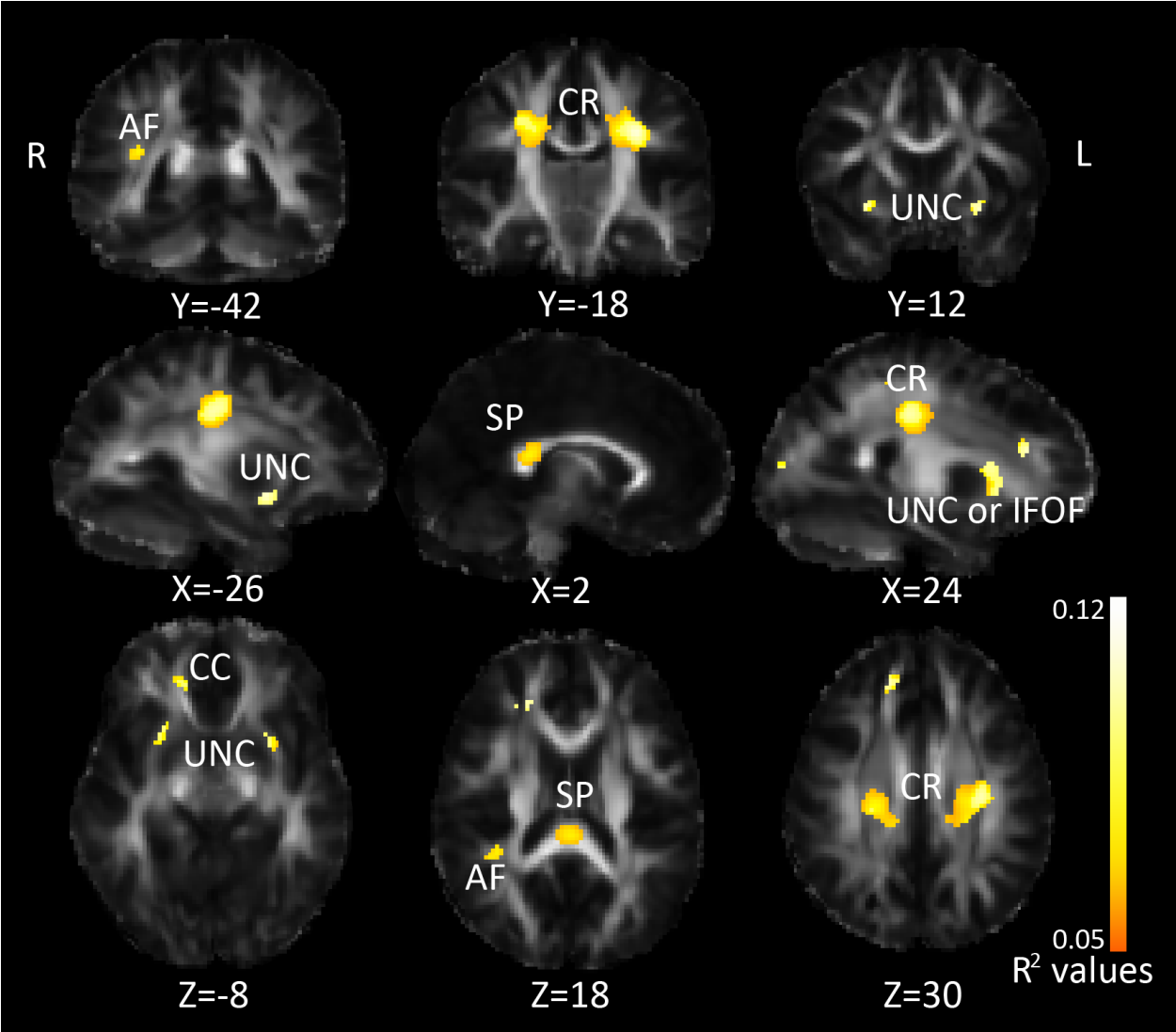
Table 3. Individual results of SNPs included in multiSNP model, as well as the results of the multiSNP model as a whole.

| SNP	Nearest Gene	FDR critical *p*-value	Voxels surviving *p*<0.05	Minimum *p*-value
MultiSNP model		**6.80E-05**	**8027**	**1.60E-06**
rs10913469	SEC16B	NA	3358	0.0005
rs7647305	ETV5	NA	536	0.0012
rs925946	BDNF-AS	NA	6419	0.00019
rs10501087	BDNF-AS	NA	1130	0.00079
rs8049439	ATXN2L	NA	315	0.004
rs6499640	FTO	NA	497	0.0025
rs3751812	FTO	NA	1757	0.00029
rs9931989	ATP2A1	NA	369	0.0044
rs2815752	NEGR1	NA	13433	0.00012
rs10838738	MTCH2	NA	1295	0.00081
rs571312	MC4R	NA	8118	3.50E-05
rs29941	KCTD15	NA	569	0.00072
rs7138803	FAIM2	NA	485	0.00048
rs2241423	MAP2K5	NA	7574	3.20E-05
rs1514175	TNN13K	NA	2247	0.001
rs10968576	LRRN6C	NA	2528	1.90E-05

Figure 2. Association between FA and *NEGR1* risk allele dosage in the QTIM sample.
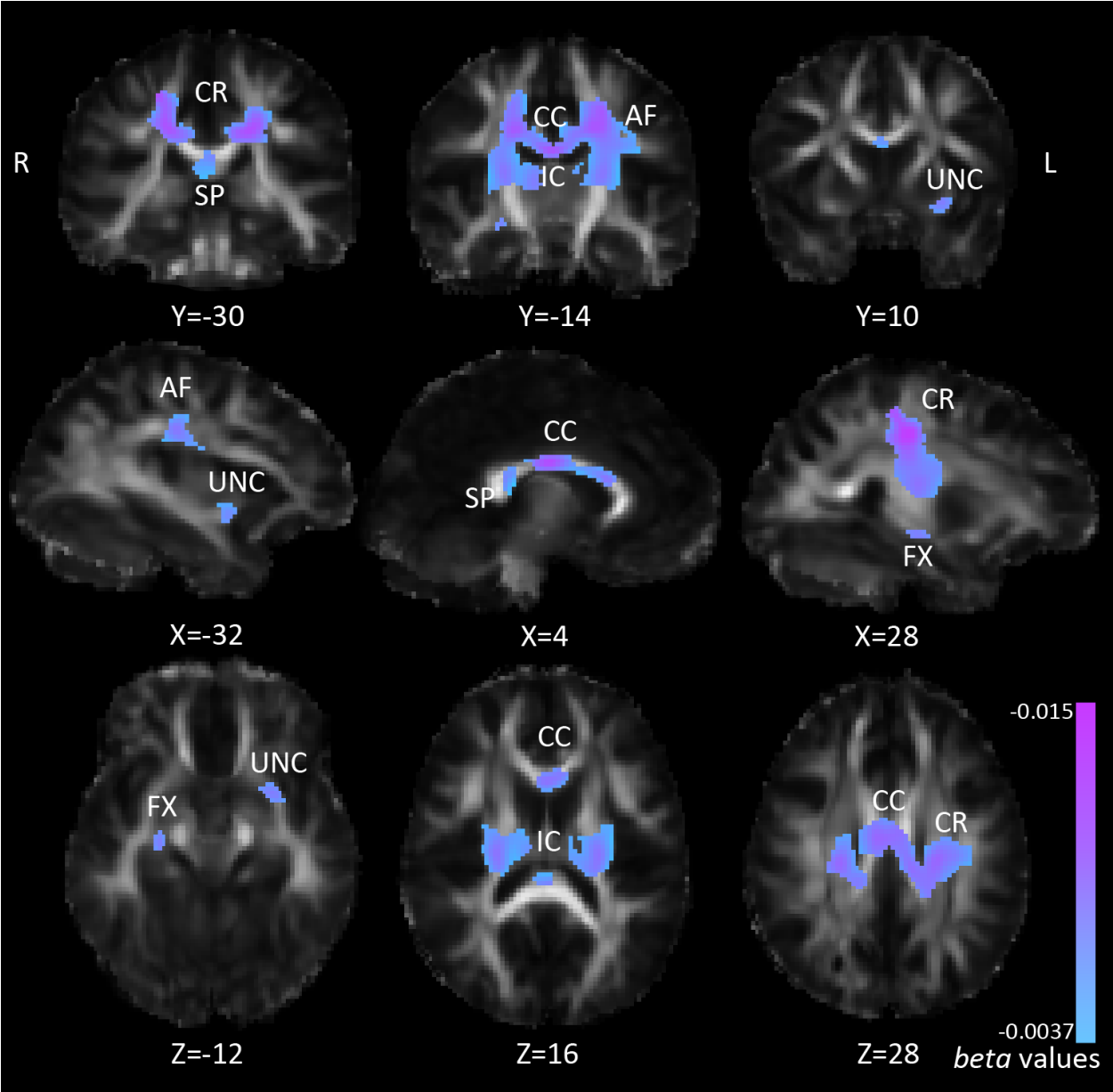
Figure 3. Voxelwise associations between *NEGR1* risk allele dosage and D_{ax}, D_{rad}, and D_{mean} in the QTIM cohort.
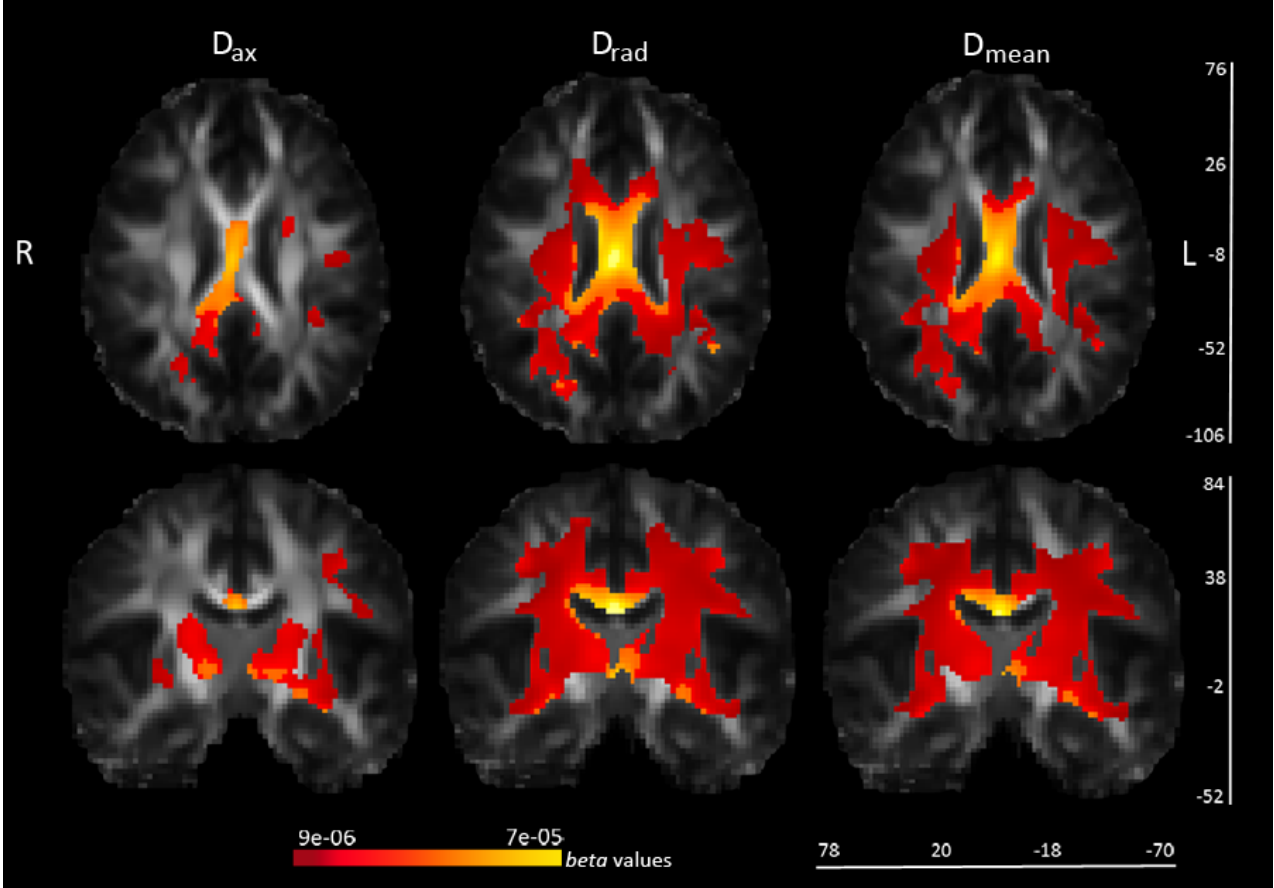
**Figure 4**. Association between FA and *NEGR1* risk allele dosage in the ADNI follow-up sample.
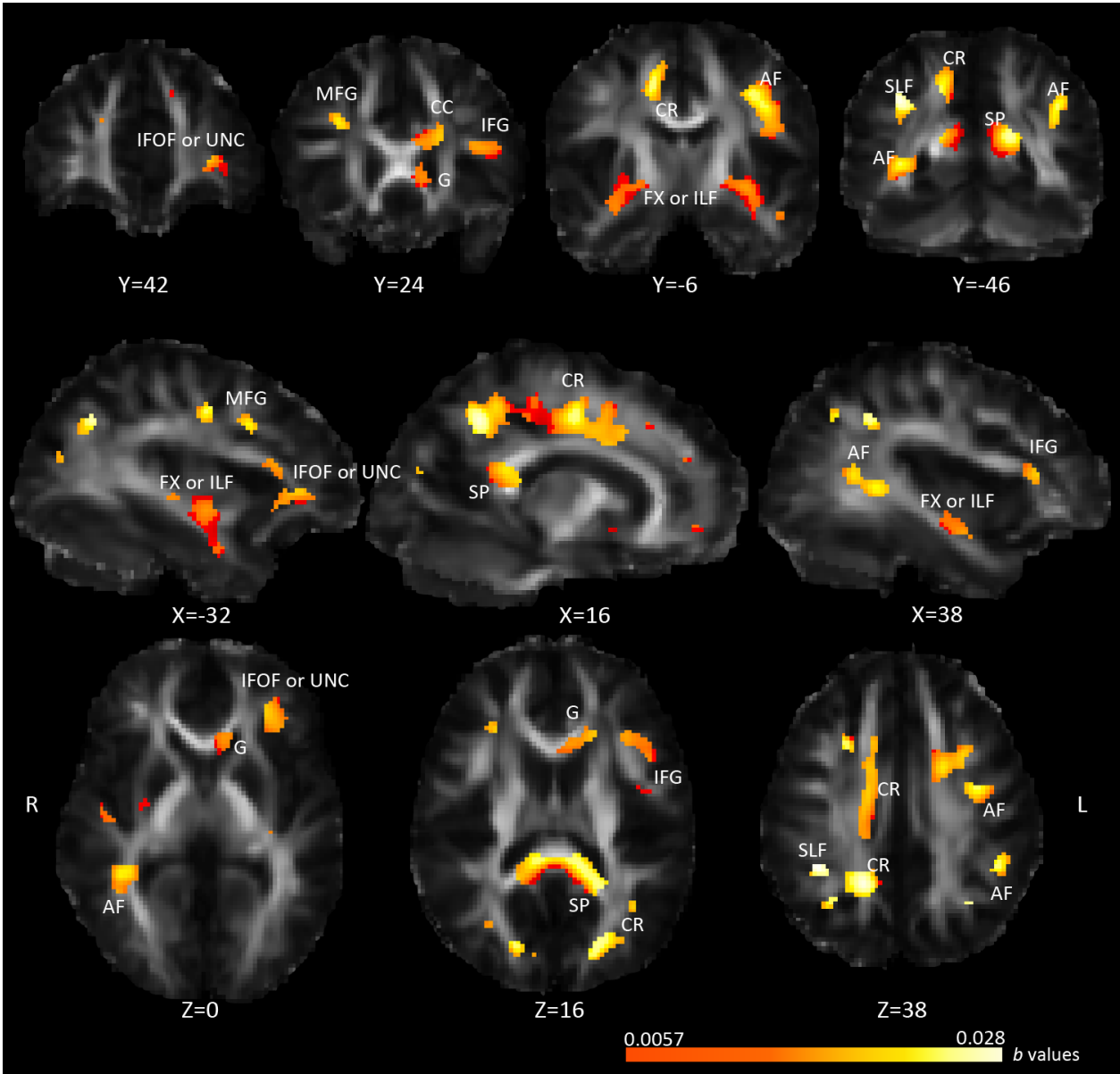
Figure 5. Voxelwise associations between *NEGR1* risk allele dosage and D_{ax}, D_{rad}, and D_{mean} in the ADNI cohort.
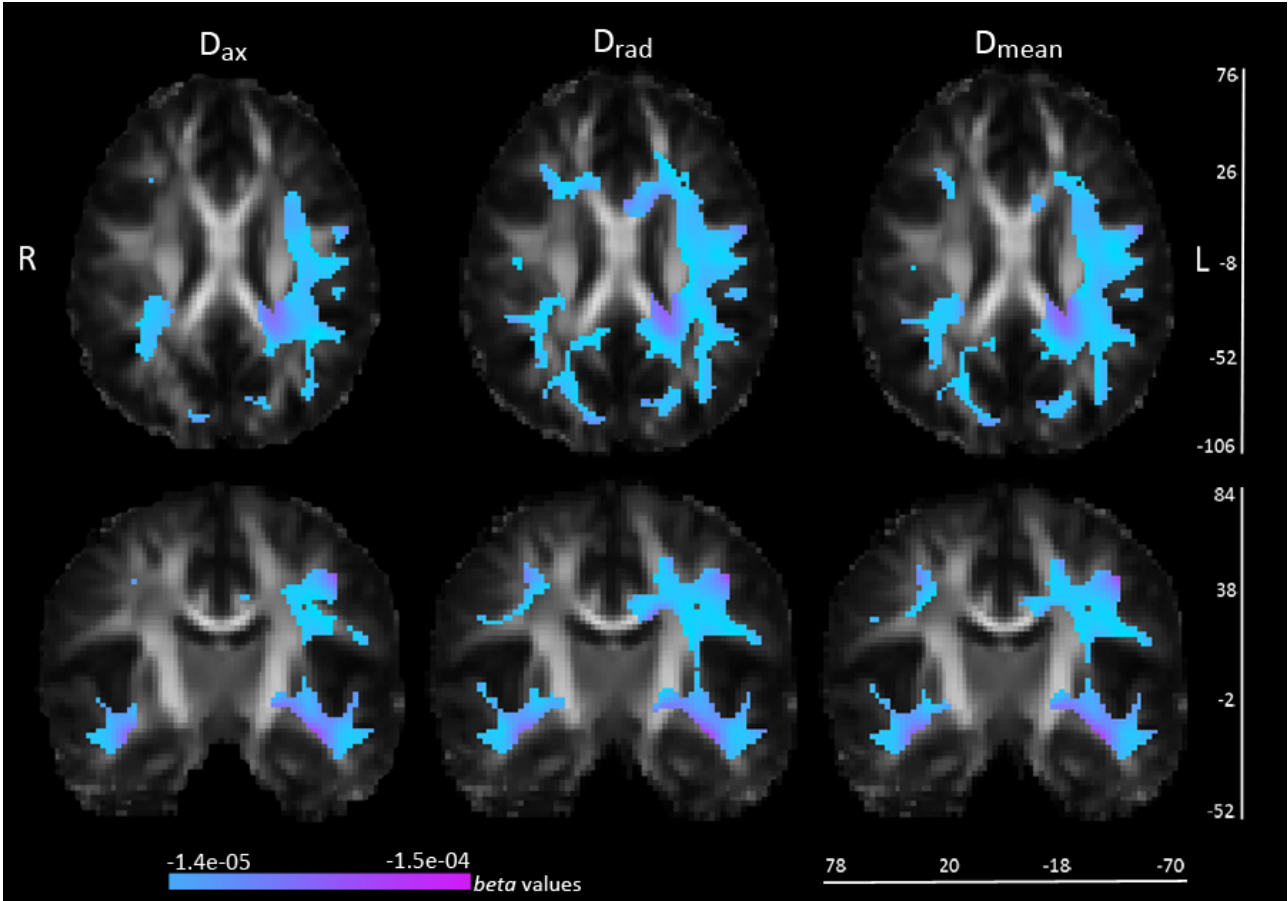
**Figure 6**. Voxelwise associations from *NEGR1* whole gene principal components regression in the QTIM cohort.
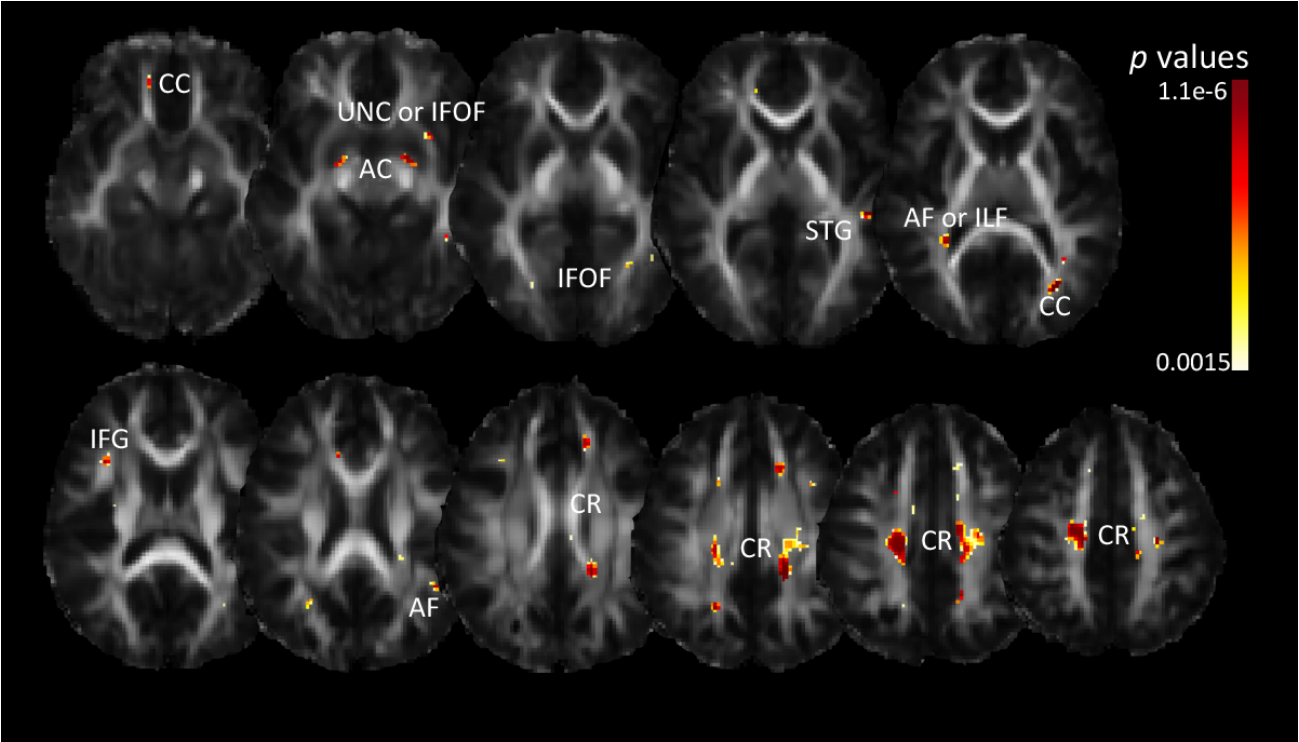
Figure 7. Histogram of BMIs in the QTIM and ADNI cohorts.
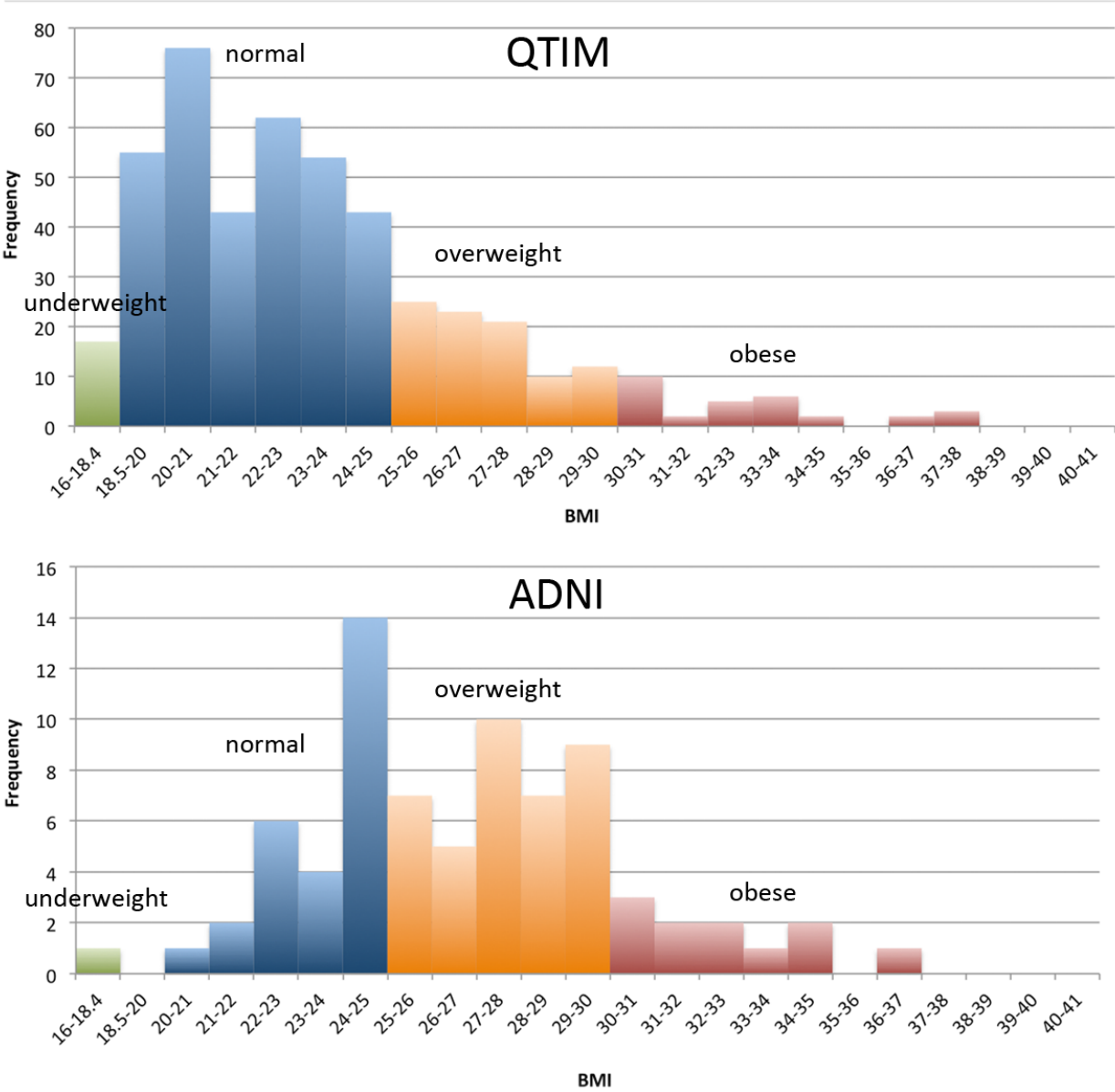
Figure and Table Legends

Table 1. SNPs included in the multiSNP model. The gene (nearest when SNP is intergenic), minor allele frequency (as listed in dbSNP), risk allele associated with obesity for each SNP, and the GWAS study each SNP was taken from.

Table 2. Subject demographics for the QTIM and ADNI cohorts. Number of subjects, female/male, mean BMI (body mass index), genetic group, and in the case of ADNI, how many subjects had Alzheimer's disease (AD), mild cognitive impairment (MCI), or were healthy controls (HC).

Figure 1. MultiSNP results: Associations between FA and SNPs linked with BMI. R^2 values are combined predictive value of our SNPs, white areas are areas with higher R^2 values, as shown by the color bar. CR=corona radiata, IFOF=inferior fronto-occipital fasciculus, CC=corpus callosum, AF=arcuate fasciculus, UNC=uncinate, SP=splenium. Left in the image is right in the brain, coordinates are in MNI space.

Table 3. Individual results of SNPs included in multiSNP model, as well as the results of the multiSNP model as a whole. The FDR critical *p*-value (when applicable), minimum *p*-value, and number of voxels below *p*<0.05 are shown for each SNP. These values are for each SNP controlling for the effect of all the other SNPs, thus, the output is a different that if the SNPs were each run individually, with no other SNPs in the model. **Bold** entries are those that survived FDR.

Figure 2. Association between FA and *NEGR1* risk allele dosage in the QTIM sample. Pink corresponds to stronger *b*-values (more negative); only areas surviving FDR across the brain are shown. CR=corona radiata, CC=corpus callosum, IC=internal capsule, AF=arcuate fasciculus, SP=splenium, FX=fornix, UNC=uncinate. Left in the image is right in the brain, coordinates are in MNI space.

Figure 3. Voxelwise associations between *NEGR1* risk allele dosage and D_{ax}, D_{rad}, and D_{mean} in the QTIM cohort. Yellow corresponds to stronger *b*-values (more positive); only areas surviving FDR across the brain are shown. Left in the image is right in the brain, coordinates are in MNI space.

Figure 4. Association between FA and *NEGR1* risk allele dosage in the ADNI follow-up sample. Yellow corresponds to stronger *b*-values (more positive); only areas surviving FDR across the brain are shown. CR=corona radiata, CC=corpus callosum, G=genu, SP=splenium, AF=arcuate fasciculus, FX=fornix (or ILF), SLF=superior longitudinal fasciculus, MFG=middle frontal gyrus, IFG=inferior frontal gyrus, IFOF=inferior fronto-occipital fasciculus, UNC=uncinate. Left in the image is right in the brain, coordinates are in MNI space.

Figure 5. Voxelwise associations between *NEGR1* risk allele dosage and D_{ax}, D_{rad}, and D_{mean} in the ADNI cohort. Pink corresponds to stronger *b*-values (more negative); only areas surviving FDR across the brain are shown. Left in the image is right in the brain, coordinates are in MNI space.

Figure 6. Voxelwise associations from *NEGR1* whole gene principal components regression in the QTIM cohort. Dark red corresponds to more significant *p*-values; only areas surviving FDR across the brain are shown. CR=corona radiata, AF=arcuate fasciculus, CC=corpus callosum, IFG=inferior frontal gyrus, ILF=inferior longitudinal fasciculus, STG=superior temporal gyrus, IFOF=inferior fronto-occipital fasciculus, UNC=uncinate, AC=anterior commissure. Left in the image is right in the brain, coordinates are in MNI space.

Figure 7. Histogram of BMIs in the QTIM and ADNI cohorts. Green=underweight, blue=normal weight, orange=overweight, red=obese.

118

Supplementary Table 1. Results of χ^2 test of deviation from Hardy-Weinburg.

SNP	χ^2	*p*-value
rs10913469	2.52	0.11
rs7647305	0.13	0.72
rs925946	4.08	0.0433
rs10501087	3.38	0.066
rs8049439	1.19	0.28
rs6499640	0.17	0.68
rs3751812	4.13	0.042
rs9931989	0.05	0.82
rs2815752	0.57	0.45
rs10838738	0.27	0.6
rs571312	0.34	0.56
rs29941	0.2	0.65
rs7138803	0.18	0.67
rs2241423	0.6	0.44
rs1514175	2.41	0.12
rs10968576	0.09	0.76

Supplementary Figure 1. Overlap of QTIM *NEGR1* results and FA.
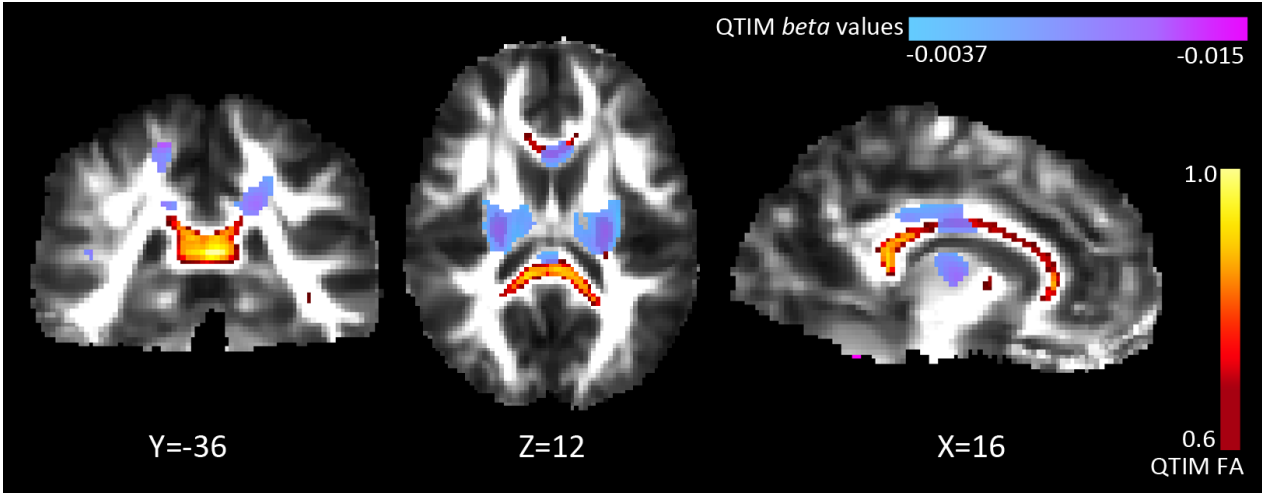
Supplementary Figure and Table Legends

Supplementary Table 1. Results of χ^2 test of deviation from Hardy-Weinburg. The SNPs included in the multiSNP model are listed, along with the χ^2 values from the goodness of fit test and the corresponding *p*-values. No SNPs deviate from the distribution expected by Hardy-Weinburg.

Supplementary Figure 1. Overlap of QTIM *NEGR1* results and FA. The FA from the QTIM MDT (creation detailed in the methods) is mapped, with a skeleton of only high FA areas (FA>0.6) shown in red-yellow, and the *beta*-values from the QTIM *NEGR1* analysis shown in blue-purple. As is evident, there are many high FA areas where we did not find effects, including the highest FA region, the main aspect of the splenium. This supports that our overlapping results are not simply because of an increased ability of pick up genetic effects in these areas.

CHAPTER 4

Cognitive correlates of structural brain connectivity

4.1 Differences in rich club organization based on IQ measures

The rich club was first applied to brain networks by Van den Heuvel & Sporns (2011). The rich club is the high degree, densely interconnected core of the brain. An attack on a rich club node has a highly detrimental effect on the efficiency of the network. The rich club coefficient [see **Chapter 1.4**] describes the density of connections among the rich club nodes. The normalized rich club coefficient is calculated by comparing the rich club coefficient in our network to that averaged across a series of randomly generated networks of the same size and degree distribution. This step is necessary for determining at what point rich club organization exists, as a network is only said to have rich club organization when the normalized coefficient is greater than 1.

Since the initial paper by Van den Heuvel & Sporns, we have charted the developmental trajectory of rich club organization [See **Chapter 2.2**], and shown that it is altered in Alzheimer's disease [Daianu et al., 2013 submitted]. We do not know, however, how the rich club supports cognition. As a new measure of brain connectivity, there are many unknowns about the rich club, and one of the most important of these is how it impacts cognitive function. The rich club is a fairly costly arrangement, from a network perspective, so we would not expect the brain to keep such a costly organization if it did not confer some benefit, perhaps cognitive benefits. We have shown that rich club organization is stable among healthy adults [See **Chapter 2.2**]. In this study we sought to examine what differences there may be in rich club organization between high and low IQ individuals. For this we examined FIQ (full scale), PIQ (performance) and VIQ (verbal) in individuals scoring more than one standard deviation away from the mean for each of those measures. Given the central role the rich club is suggested to play in brain

efficiency, and the regions it includes, we might expect individual differences in rich club organization to be related to individual differences in cognition.

The Parieto-Frontal Integration Theory (P-FIT) of intelligence postulates that cognitive abilities are supported by a distributed set of brain regions primarily in the parietal and frontal cortex [Jung & Haier, 2007]. This theory was generated based on findings from 37 neuroimaging studies across various functional and structural paradigms. There are a number of subsequent studies validating this model [Colom et al., 2009; Gläscher et al., 2010; Langer et al., 2012]. Given this, we expected to find differences in which frontal and parietal nodes make up the rich club.

Materials and Methods

Participants were recruited as part of a 5-year research project scanning healthy young adult Australian twins with structural brain MRI and DTI [de Zubicaray et al., 2008]. We analyzed scans from 201 right-handed subjects (119 female/82 male, average age=23.9 years, SD=2.5). This population included 66 monozygotic (MZ) twins, 118 dizygotic (DZ) twins, and 17 non-twin siblings, from 179 families. For the sake of valid comparison, two members from the same family were not included in a comparison (high vs. low). If two siblings satisfied criteria for inclusion in the high or low IQ groups, one was randomly chosen to be included. Between comparisons, however (high PIQ vs. high VIQ), siblings may be included. Whole-brain anatomical and high angular resolution diffusion images (HARDI) were collected with a 4T Bruker Medspec MRI scanner. T1-weighted anatomical images were acquired with an inversion recovery rapid gradient echo sequence, with parameters: TI/TR/TE = 700/1500/3.35ms; flip angle = 8 degrees; slice thickness = 0.9mm, and a 256x256 acquisition matrix. HARDI was also acquired using single-shot echo planar imaging with a twice-refocused spin echo sequence to

reduce eddy-current induced distortions. Imaging parameters were: 23cm FOV, TR/TE 6090/91.7ms, with a 128x128 acquisition matrix. Each 3D volume consisted of 55 2-mm thick axial slices with no gap and 1.79x1.79 mm^2 in-plane resolution. 105 images were acquired per subject: 11 with no diffusion sensitization (i.e., T2-weighted b_0 images) and 94 diffusion-weighted (DW) images ($b = 1159$ s/mm^2) with gradient directions evenly distributed on a hemisphere in the q-space. Scan time was 14.2 min for the 105-gradient HARDI scan. Subjects completed the Multidimensional Aptitude Battery II (MAB-II) IQ test [Jackson, 1998]. 84% of subjects completed the MAB-II at age 16, 10% completed it between age 17-22, and the remainder completed it at their scan session (between age 21-30).

Cortical Extraction and HARDI Tractography

Connectivity analysis was performed as in [Jahanshad et al., 2011]. Briefly, non-brain regions were automatically removed from each T1-weighted MRI scan, and from a T2-weighted image from the DWI set, using the FSL tool "BET" (FMRIB Software Library, http://fsl.fmrib.ox.ac.uk/fsl). A neuroanatomical expert manually edited the T1-weighted scans to refine the brain extraction. All T1-weighted images were linearly aligned using FSL (with 9 DOF) to a common space with 1*mm* isotropic voxels and a 220×220×220 voxel matrix. For each subject, the 11 eddy-corrected images (using FSL tool "eddy_correct") with no diffusion sensitization were averaged, linearly aligned and resampled to a downsampled version of their corresponding T1 image (110×110×110, 2×2×2mm). Averaged b_0 maps were elastically registered to the structural scan using a mutual information cost function to compensate for EPI-induced susceptibility artifacts. 34 cortical labels per hemisphere, as listed in the Desikan-Killiany atlas [Desikan et al., 2006], were automatically extracted from all aligned T1-weighted structural MRI scans using FreeSurfer (http://surfer.nmr.mgh.harvard.edu/). T1-weighted images

and cortical models were aligned to the original T1 input image space and down-sampled to the space of the DWIs, using nearest neighbor interpolation (to avoid intermixing of labels). To ensure tracts would intersect cortical labeled boundaries, labels were dilated with an isotropic box kernel of size 5×5×5 voxels.

The matrix transforming the mean b_0 image to the T1-weighted volume was applied to each of the 94 gradient directions to properly re-orient the orientation distribution functions (ODFs). At each HARDI voxel, ODFs were computed using the normalized and dimensionless ODF estimator derived for q-ball imaging (QBI) [Aganj et al., 2010]. We performed HARDI tractography on the linearly aligned sets of DWI volumes using these ODFs, using the Hough transform method [Aganj et al., 2011]. Elastic deformations obtained from the EPI distortion correction, mapping the average b_0 image to the T1-weighted image, were then applied to the tracts' 3D coordinates to accurately align the anatomy. Each subject's dataset contained 5000-10000 useable fibers (3D curves). For each subject, a full 68×68 connectivity matrix was created. Each element described the proportion of the total number of fibers connecting each of the labels; diagonal elements describe the total number of fibers passing through a certain cortical region of interest. Values were calculated as a proportion - normalized to the total number of fibers traced for each individual participant, to avoid skewing results by the raw fiber count.

Rich Club Analyses

On the 68x68 matrices generated above, we used the Brain Connectivity Toolbox (Rubinov & Sporns, 2010, https://sites.google.com/site/bctnet/) to compute the rich club coefficient (Φ) across the whole range of nodal degree levels (k), 0-68. The fiber count matrices were first binarized for each subject. We normalized our rich club coefficient based on coefficients calculated from 50 random networks to generate a normalized rich club coefficient

(Φ_{norm}). Below we use the same symbols as the original paper on this topic [Van den Heuvel &

Sporns, 2011]. We tested the high vs. low groups for differences in Φ and Φ_{norm} using the

following

Eq. 1 $\quad\quad\quad\quad\quad\quad \Phi \text{ or } \Phi_{norm} \sim A + \beta_{age}Age + \beta_{sex}Sex + \beta_{IQ}IQ + \beta_{ICV}ICV + \alpha + \varepsilon$

A is the constant graph theory metric term, the βs are the covariate regression coefficients, and α

is a coefficient that accounts for random effects. IQ can represent any of the three IQ tests – FIQ,

PIQ, or VIQ. Random effects were used to account for familial relatedness. We modeled these

variables (age, sex, IQ) as fixed effects. ICV is intracranial volume, in mm^3. ε is a matrix of

residual effects with a variance of $\sigma^2_e I$, and I is an identity matrix. Results were corrected for

multiple comparisons using the false discovery rate method across all 68 levels of k tested [FDR;

Benjamini & Hochberg, 1995].

Group Analyses

For FIQ, PIQ and VIQ analyses, we created groups of high and low IQ by determining

which subjects were more than 1 SD above or below the average IQ of the sample. Among those

groups formed, we made sure only one member of a family was represented both within a group

(e.g. high PIQ) and between groups (e.g. high PIQ vs. low PIQ) to ensure no additional similarity

between subjects would obscure or artificially amplify results. Between comparisons, however

(e.g. high PIQ vs. high FIQ vs high VIQ) there were some siblings included. For the FIQ

comparison, there were 62 individuals in the high group, and 63 in the low group. For the PIQ

comparison, there were 64 individuals in the high group, and 61 in the low group. For the VIQ

group, there were 57 individuals in the high group, and 53 in the low group.

Within these groups, we created averaged connectivity matrices. These were thresholded

to only include connections present in at least 75% of subjects. We then calculated the degree of

these networks, and used the criteria set forth by Van den Heuvel & Sporns, 2011, to determine which nodes were included in the rich club in each group.

We followed up on these analyses by examining the 105-direction HARDI data that these matrices were computed from. We examined these for voxel-wise differences between the high and low groups across FIQ, PIQ and VIQ. We used a linear mixed effects model to study the voxel-wise association of each IQ test with fractional anisotropy (FA), while taking into account any relatedness among the subjects. We used the same basic model as above:

Eq. 2 $$\text{Voxelwise FA} \sim A + \beta_{age}\text{Age} + \beta_{IQ}\text{IQ} + \beta_{ICV}\text{ICV} + \alpha + \varepsilon$$

Random effects were again used to account for familial relatedness. For all statistical analyses, the LONI pipeline (http://pipeline.loni.usc.edu/) was used for voxel-wise parallelization on a multi-CPU grid computer. These results were FDR corrected for multiple comparisons across all voxels tested, and across the two subtests ($q<0.025$) (as PIQ and VIQ are sub-measures of FIQ, and therefore not independent) [searchlight FDR, Langers et al., 2007].

Results

When comparing high and low groups, we found no differences in Φ or Φ_{norm}, across all 68 levels of k. When examining rich club organization, however, we found a number of differences in which nodes were included in the rich club. In both the FIQ and PIQ groups, the average degree was higher in the high IQ groups (this was flipped in VIQ). This was not a significant difference, however it did affect what the degree cutoff was for rich club membership. The low FIQ group did have a slightly lower average degree (25.7 vs. 25.0), leading to a lower degree cutoff, but these groups were the most similar of our three comparisons. In the high vs. low VIQ comparison, we saw an opposite trend. The low VIQ group had a slightly higher average degree (25.3 vs. 25.7), leading to a higher degree cutoff, and yet a larger rich club in the

low VIQ group. In comparable networks, we would expect a lower degree cutoff to lead to a larger rich club, unless there was a difference in degree overall. There were two nodes unique to the low VIQ rich club, while the high VIQ rich club only had one unique node. In the high PIQ vs. low PIQ comparison, we found the most differences. The low PIQ group had a lower average degree (26.0 vs. 25.2), leading to a lower degree cutoff, and yet a smaller rich club. The high PIQ rich club had an additional four nodes, 3 parietal nodes and 1 frontal node.

When comparing unrelated subjects more than 1 SD above or below the average FIQ, the RC threshold for the high group was 26, while the RC threshold for the low group was 25. This resulted in 14 nodes in the high FIQ RC, and 15 nodes in the low FIQ RC. The only difference was in the one additional node in the low FIQ RC, which was the right supra-marginal gyrus. We additionally examined group differences in connections between RC nodes. This was a binary analysis – simply done on a basis of whether one group possessed a connection and the other did not. These results can be seen in **Figure 4.1.1.**

When comparing unrelated subjects more than 1 SD above or below the average PIQ, the RC threshold was 26 for both groups. This resulted in 14 nodes in the high PIQ RC, and 10 nodes in the low PIQ RC. The differences were in the additional 4 nodes seen in the high PIQ RC, which were the right posterior cingulate, right precuneus, left paracentral, and left precentral gyri. These results can also be seen in **Figure 4.1.1.**

When comparing unrelated subjects more than 1 SD above or below the average VIQ, the RC threshold was 26 for both groups again. This resulted in 12 nodes in the high VIQ RC, and 13 nodes in the low VIQ RC. There was one additional node in the high VIQ RC – the right posterior cingulate – and 2 additional nodes in the low VIQ RC – the right supra-marginal and left paracentral gyri.
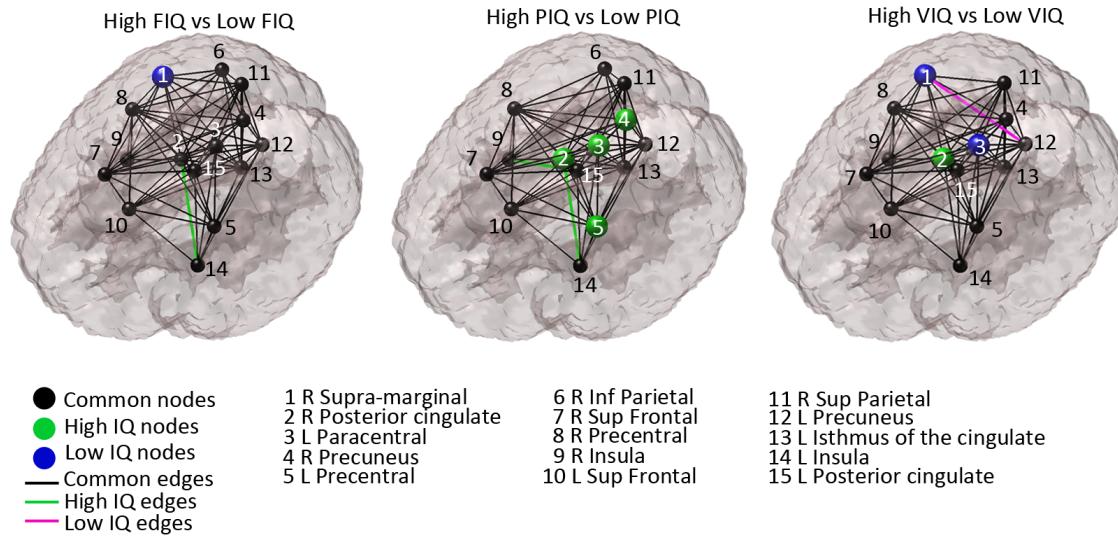
Figure 4.1.1. Differences in rich club organization between high and low IQ individuals, **across FIQ (full scale IQ), PIQ (performance IQ), and VIQ (verbal IQ).** Left in the image is left in the brain.

When analyzing differences in the voxel-wise FA between groups, we found consistent significant differences across all comparisons. Consistency across comparisons is expected, as many subjects who have high PIQ also have high FIQ and thus were included in both comparisons. We found that individuals with higher IQs had greater FA in the left inferior longitudinal fasciculus (ILF), and a region corresponding to both the ILF and the uncinate (UNC), suggesting greater white matter integrity in these tracts. These results are shown in **Figure 4.1.2**.

Discussion

In this study, we examined how rich club organization was associated with IQ performance. We found that the nodes included in the rich club differed when we compared the highest performing (>1 SD above average) and lowest performing (>1 SD below average) subjects as measured by FIQ, and its two subtests, PIQ and VIQ. We found the most differences

when examining the high vs. low PIQ contrast. This is the first study examining cognitive correlates of rich club connectivity.

In the high FIQ vs. low FIQ comparison, we found very similar rich clubs, only differing by the addition of one node in the low FIQ rich club, the right supramarginal gyrus. In the high VIQ vs. low VIQ comparison, we found a mix. The high VIQ group had one additional node (posterior cingulate), while the low VIQ group had two additional nodes (supramarginal and paracentral gyri). In the high PIQ vs. low PIQ comparison, we found the most differences. The high PIQ rich club had an additional 4 nodes – 3 parietal nodes (posterior cingulate, paracentral, precuneus) and 1 frontal node (precentral gyrus).

Our findings provide further support for the Parieto-Frontal Integration Theory (P-FIT). The parieto-frontal integration theory lists a number of regions, mainly in the frontal and parietal cortex, that it suggests support cognition and may be responsible for individual differences in intelligence [Jung & Haier, 2007]. Some of the regions it includes are the precentral gyrus,
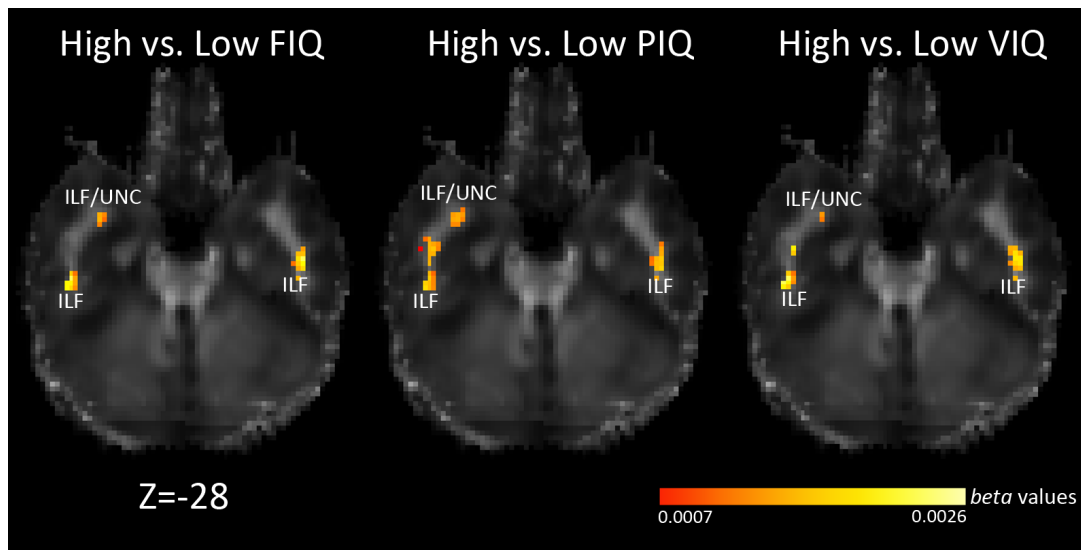

Figure 4.1.2. Voxel-wise differences in FA between individuals scoring >1 SD above or below the average FIQ, PIQ and VIQ. Yellow indicates to greater *b*-values. ILF=inferior longitudinal fasciculus, UNC=uncinate. Left in the image is right in the brain, coordinates are in MNI space.

inferior and superior parietal lobule, prefrontal cortex, inferior frontal gyrus, and anterior cingulate. All subjects had a rich club made up of a distributed set of regions across the parietal, frontal, and temporal cortices. Perhaps the rich club serves as the hub of integration between these disparate regions supporting cognition, as they are nodes that are highly connected and highly important for global information transfer. In the PIQ comparison, we found four nodes in the high PIQ group in the frontal and parietal cortices that have been shown in previous papers to be hubs in the structural network [Hagmann et al., 2008]. One of these, the precentral gyrus is implicated as well by the P-FIT. This suggests that individuals with higher PIQ, due to their higher degree overall, may be better able to integrate more of these key areas together. By better integrating these regions, subjects may be able to have more efficient global information transfer.

In addition to the differences we found in the rich club, we also found differences in fractional anisotropy between the highest and lowest IQ individuals. Across all three comparisons (high vs. low FIQ, PIQ and VIQ) we found greater fractional anisotropy in the high IQ individuals in the bilateral inferior longitudinal fasciculus (ILF) and the ILF/UNC (uncinate). These two tracts join at the anterior aspect of the ILF [Catani et al., 2003]. The ILF connects the temporal and occipital cortices, and is suggested to support visual tasks such as object recognition [Ortibus et al., 2012]. Additionally, decreased integrity of the ILF has been associated with schizophrenia, especially in patients with a history of visual hallucinations [Ashtari et al., 2007]. We might expect that the integrity of circuitry responsible for recognizing and categorizing objects would be associated with both performance and verbal IQ. These fundamental tasks are involved in vocabulary, spatial awareness, and other abilities assessed by IQ tests.

As the first study to examine cognitive correlates of the rich club, there is little context for interpreting our results. While we may intuitively expect that more rich club nodes is "better", we do not truly know if this is the case, or what an optimum rich club organization may be. From a network perspective the rich club is fairly costly, so it would not make sense for the brain to maintain this costly arrangement without some benefit to the brain. In this study we were attempting to determine whether this benefit comes in the form of increased cognitive abilities, but further research is needed in this field to establish norms and the implications of individual differences in rich club organization.

IQ is admittedly not an ideal measure of cognitive function, as its generalizability across cultures has been challenged [Fish, 2013]. Our sample was ethnically homogeneous, however, making this not a factor in our analysis. In the future we will investigate other measures of cognitive function that assess specific functional domains, such as working memory. Additionally, we used binarized matrices for these analyses, which do not use the full information available. Future analyses in the full weighted matrices will hopefully shed more light on these questions. Obviously, the specific parcellation scheme chosen will affect graph theory metrics. Zalesky et al. (2010) found that graph theory metrics were sensitive to parcellation resolution (i.e., the number of nodes), so it may be that other parcellation schemes are more or less sensitive to differences in IQ. The Desikan-Killiany atlas has been shown by our laboratory to yield connectivity measures that are genetically influenced [Jahanshad et al., 2011; Jahanshad et al., 2012] and change over development [Dennis et al., 2013b].

4.2 High school completion is associated with differences in fiber density and graph theoretical measures of structural connectivity

Many environmental factors throughout life influence brain structure and function. Education is an especially influential factor, playing a key role in individual differences in both brain structure and the cognitive functions it supports. The concept of reserve suggests that some aspect of brain structure or function enables people with more reserve to be able compensate for greater levels of pathology or atrophy [Stern, 2002], and it has been suggested that education increases one's " cognitive reserve" [Piras et al., 2010]. Level of education has been associated with intracranial volume [Mortimer et al., 2003] and differences in diffusivity [Piras et al., 2010]. Other studies have found that even when elderly individuals with higher education levels have more severe metabolic deficits in key brain regions, they are able to perform at the same level of cognitive ability as less educated subjects with less severe pathology [Alexander et al., 1997], suggesting education confers some neuroprotection. Educational attainment is a measure of time, not a measure of intelligence, although we expect it to add cognitive benefit. This must be kept in mind when interpreting results.

Noble et al. (2013) found that educational attainment was significantly associated with fractional anisotropy (FA), a commonly used measure of white matter integrity, in a sample of 47 young adults. Surprisingly, they found more education was associated with decreased FA in a number of tracts critical for cognitive control – the superior longitudinal fasciculus (SLF) and cingulum bundle (CB). They offered no explanation for this, except that others have also found decreased FA with increased cognitive abilities [Tuch et al., 2005]. Tuch et al. (2005) suggest that this could be due to crossing fibers or individual differences in axonal diameter. Piras et al.

(2010), found decreased MD (mean diffusivity, it would be expected to decrease when FA increases, generally) with increasing education, but this was in an elderly population, specifically examining subcortical structures, so it is minimally comparable to Noble et al. (2013). Beyond these, there is not a thorough investigation of how education affects the brain.

In this study, we examined how educational attainment, measured by months of high school completed, in a population of 287 young adults (20-30 years old) was associated with fiber density and nodal graph theoretical measures of connectivity calculated on our fiber density matrices. Despite the conflicting results from previous studies, we expected to find increased fiber density with increasing educational attainment, as well as increased clustering coefficient, degree, and regional efficiency.

Materials and Methods

Participants were recruited as part of a 5-year research project scanning healthy young adult Australian twins with structural brain MRI and DTI [de Zubicaray et al., 2008]. We analyzed scans from 287 right-handed subjects (187 female/100 male, average age=23.9 years, SD=2.3). This population included all monozygotic (MZ) twins from 194 families. The average months of school for the sample was 32.4 (6.8 SD) with a range of 18-48. This is not total months of school, but months of high school completed. As the minimum age of our subject pool was 20, all had completed high school. Education beyond high school was not measured. Whole-brain anatomical and high angular resolution diffusion images (HARDI) were collected with a 4T Bruker Medspec MRI scanner. T1-weighted anatomical images were acquired with an inversion recovery rapid gradient echo sequence, with parameters: TI/TR/TE = 700/1500/3.35ms; flip angle = 8 degrees; slice thickness = 0.9mm, and a 256x256 acquisition matrix. HARDI was also acquired using single-shot echo planar imaging with a twice-refocused

spin echo sequence to reduce eddy-current induced distortions. Imaging parameters were: 23cm FOV, TR/TE 6090/91.7ms, with a 128x128 acquisition matrix. Each 3D volume consisted of 55 2-mm thick axial slices with no gap and 1.79x1.79 mm^2 in-plane resolution. 105 images were acquired per subject: 11 with no diffusion sensitization (i.e., T2-weighted b_0 images) and 94 diffusion-weighted (DW) images (b = 1159 s/mm^2) with gradient directions evenly distributed on a hemisphere in the q-space. Scan time was 14.2 min for the 105-gradient HARDI scan.

Cortical Extraction and HARDI Tractography

Connectivity analysis was performed as in [Jahanshad et al., 2011]. Briefly, non-brain regions were automatically removed from each T1-weighted MRI scan, and from a T2-weighted image from the DWI set, using the FSL tool "BET" (FMRIB Software Library, http://fsl.fmrib.ox.ac.uk/fsl). A neuroanatomical expert manually edited the T1-weighted scans to refine the brain extraction. All T1-weighted images were linearly aligned using FSL (with 9 DOF) to a common space with 1*mm* isotropic voxels and a 220×220×220 voxel matrix. For each subject, the 11 eddy-corrected images (using FSL tool "eddy_correct") with no diffusion sensitization were averaged, linearly aligned and resampled to a downsampled version of their corresponding T1 image (110×110×110, 2×2×2mm). Averaged b_0 maps were elastically registered to the structural scan using a mutual information cost function to compensate for EPI-induced susceptibility artifacts. 34 cortical labels per hemisphere, as listed in the Desikan-Killiany atlas [Desikan et al., 2006], were automatically extracted from all aligned T1-weighted structural MRI scans using FreeSurfer (http://surfer.nmr.mgh.harvard.edu/). T1-weighted images and cortical models were aligned to the original T1 input image space and down-sampled to the space of the DWIs, using nearest neighbor interpolation (to avoid intermixing of labels). To

ensure tracts would intersect cortical labeled boundaries, labels were dilated with an isotropic box kernel of size 5×5×5 voxels.

The matrix transforming the mean b_0 image to the T1-weighted volume was applied to each of the 94 gradient directions to properly re-orient the orientation distribution functions (ODFs). At each HARDI voxel, ODFs were computed using the normalized and dimensionless ODF estimator derived for q-ball imaging (QBI) [Aganj et al., 2010]. We performed HARDI tractography on the linearly aligned sets of DWI volumes using these ODFs, using the Hough transform method [Aganj et al., 2011]. Elastic deformations obtained from the EPI distortion correction, mapping the average b_0 image to the T1-weighted image, were then applied to the tracts' 3D coordinates to accurately align the anatomy. Each subject's dataset contained 5000-10000 useable fibers (3D curves). For each subject, a full 68×68 connectivity matrix was created. Each element described the proportion of the total number of fibers connecting each of the labels; diagonal elements describe the total number of fibers passing through a certain cortical region of interest. Values were calculated as a proportion - normalized to the total number of fibers traced for each individual participant, to avoid skewing results by the raw fiber count.

Months of School Regression

We used a linear mixed effects model to study the element-wise association of months of school (MOS) with fiber density, while taking into account any relatedness among the subjects. For *N* subjects and *p* independent predictors (MOS and other covariates), regression coefficients (*β*) were obtained according to the formula:

Eq. 1 $\qquad$ NxN $\sim A + \beta_{age}$Age $+ \beta_{sex}$Sex $+ \beta_{ICV}$ICV $+ \beta_{MOS}$MOS $+ \alpha + \varepsilon$

Here, NxN is each of the entries in the 68x68 fiber density matrices. *A* is the constant fiber density term, the βs are the covariate regression coefficients, and α is a coefficient that

accounts for random effects. Random effects were used to account for familial relatedness. We modeled these variables (age, sex, ICV, MOS) as fixed effects. ICV denotes intracranial volume, in mm^3. ε is a matrix of residual effects with a variance of $\sigma^2_e I$, and I is an identity matrix. We also tested a model including FIQ as a covariate, to be sure we were not measuring the effects of cognitive ability instead. For all statistical analyses, the LONI pipeline (http://pipeline.loni.usc.edu/) was used for element-wise parallelization on a multi-CPU grid computer. The false discovery rate method [Benjamini & Hochberg, 1995] was used for multiple comparisons correction across all voxels.

We used the same model (Eq. 1) to test our graph theoretical measures of structural connectivity. We examined three measures of nodal connectivity – clustering coefficient, regional efficiency, and degree. Clustering coefficient, on a nodal scale, is a measure of how "cliquish" a node's neighbors are. Regional efficiency is the inverse of the average shortest path connecting all neighbors of a given node. Degree is simply how many connections each node has. We corrected for multiple comparisons across all 68 nodes and all 3 measures tested ($q<0.05$) [Benjamini & Hochberg, 1995].

Lastly, in an attempt to find some overlap with our previous study under the cognitive aim, we also examined voxel-wise FA for any associations with months of school. This analysis was completed with age, sex, and intracranial volume as covariates. We again used a linear mixed effects model to study the voxel-wise association of MOS with fractional anisotropy (FA), while taking into account any relatedness among the subjects. We used the same basic model as above:

Eq. 2 $\qquad$ Voxelwise FA $\sim A + \beta_{age}$Age $+ \beta_{mos}$MOS $+ \beta_{ICV}$ICV $+ \alpha + \varepsilon$

Random effects were again used to account for familial relatedness. For all statistical analyses, the LONI pipeline (http://pipeline.loni.usc.edu/) was used for voxel-wise parallelization on a multi-CPU grid computer. These results were FDR corrected for multiple comparisons across all voxels tested ($q<0.05$) [searchlight FDR, Langers et al., 2007].

Results

NxN Analyses

When we analyzed the 68x68 fiber density matrices, we found 2 connections whose fiber density was significantly associated with months of school. The fiber density of the connections between the left insula and left lingual gyrus, and between the right postcentral gyrus and right caudal middle frontal gyrus was greater in individuals who had attended more school. This analysis was done co-varying for age, as we know age could significantly influence fiber density [Dennis et al., 2013b]. We additionally co-varied for sex and intracranial volume, and one model was run co-varying for FIQ. Co-varying for FIQ did not affect the results. A *p*-map for this analysis can be seen in **Figure 4.2.1.** In this figure, the color represents the *p*-value of the association, as shown in the legend. We restricted our analyses to only connections present in >95% of subjects, to ensure we were finding differences in reliably tracked pathways. This resulted in 418 connections being examined, out of a possible 2,346 (68x68, symmetrical, including diagonal), and of these, 2 survived multiple comparisons correction. The location of these results can be seen in **Figure 4.2.2.**

Nodal Graph Theoretical Measures of Structural Connectivity

Given that we found significant differences in the 68x68 fiber density matrices, we decided to examine more nodal measures of connectivity – those generated from graph theoretical analyses. We found significant differences in all three nodal measures we examined –
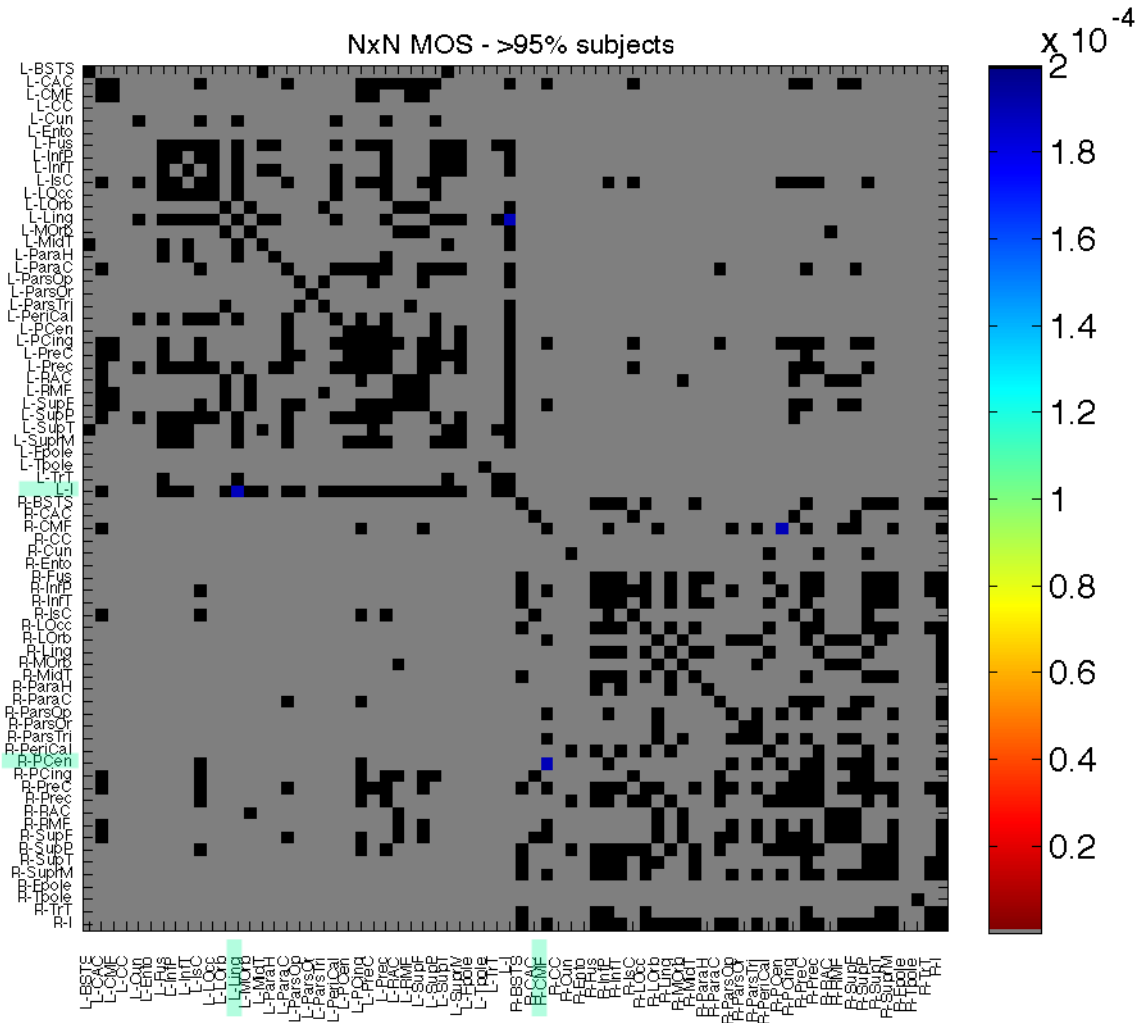
Figure 4.2.1. *P*-values for the NxN fiber density analysis. Two connections showed *p*-values surviving FDR correction − both the connection between the left insula and left lingual gyrus, and between the right caudal middle frontal gyrus and right postcentral gyrus had greater fiber density in individuals who had completed more school, correcting for age (and sex and intracranial volume). Gray boxes were not tested, black boxes were tested but not significant.

clustering coefficient (CC), regional efficiency (EREG), and degree (DG). The left *pars orbitalis* had a negative association between MOS and CC, EREG, and DG. The left insula had a negative association between MOS and CC, while the right lateral occipital gyrus had a positive association between MOS and CC. Lastly, the left inferior temporal gyrus had a negative
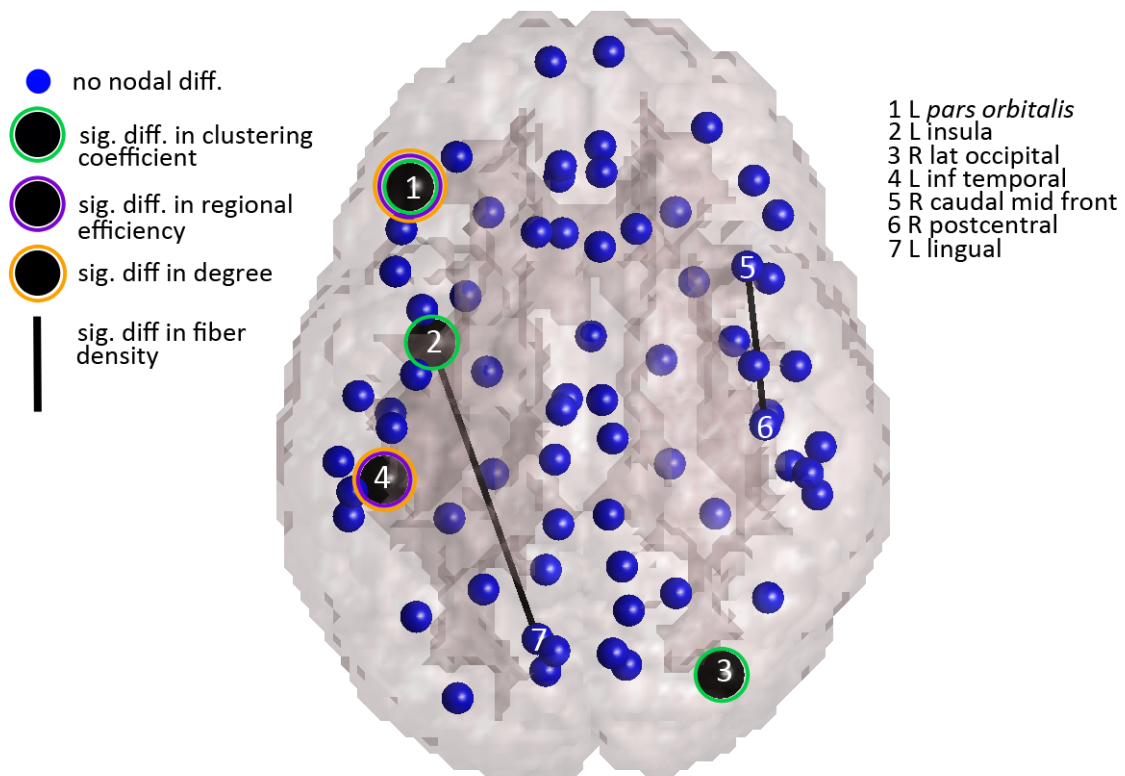
Figure 4.2.2. Differences in fiber density and nodal measures of connectivity associated with months of school. All nodes tested (68) are shown, nodes in blue showed no significant associations. Large nodes in black showed significant associations between nodal graph theoretical measures of structural connectivity and months of school, as indicated in the legend. We tested clustering coefficient, regional efficiency, and degree, and results were FDR corrected across all nodes tested and all three nodal measures tested ($q<0.05$). These were largely negative associations. Black bars also indicate where significant associations with fiber density were found, both positive associations. Left in the image is left in the brain.

association between MOS and EREG and DG. These can all be seen in **Figure 4.2.2**, along with the differences in fiber density.

Voxel-wise FA

Our examination of associations between MOS and voxel-wise FA yielded significant positive correlations. MOS was positively associated with FA in the isthmus of the corpus callosum (CC – Is) and the posterior genu (CC – G). These can be seen in **Figure 4.2.3**. We
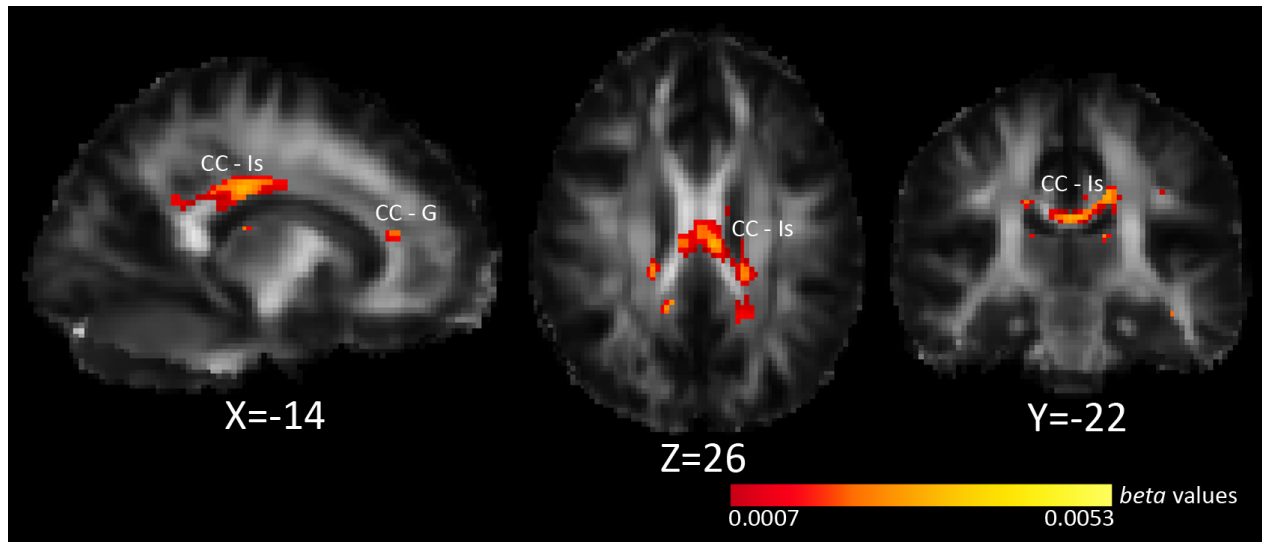
Figure 4.2.3. Voxel-wise associations between months of school and FA. Yellow indicates to greater *b*-values. CC – Is = isthmus of the corpus callosum, CC – G = genu of the corpus callosum. Left in the image is right in the brain, coordinates are in MNI space.

additionally found a small area of significant positive association in the right ILF/UNC (inferior longitudinal fasciculus/uncinate – at the anterior end of the ILF these two tracks merge; Catani et al., 2003; this is not pictured in the figure). When we co-varied for FIQ, these results were unchanged, including the small area of association in the ILF/UNC.

Discussion

In this study we examined associations between months of high school completed and differences in structural brain connectivity. We found a number of significant differences in fiber density and nodal graph theoretical measures of connectivity. We found a significant positive association between months of school and fiber density between the left insula and left lingual gyrus, and between the right postcentral gyrus and right caudal middle frontal gyrus. We additionally found negative associations between months of school and degree, clustering, and regional efficiency in the left *pars orbitalis*, left inferior temporal gyrus, and left insula, and a positive association with clustering in the right lateral occipital gyrus.

142

As we expected, we found greater fiber density with greater educational attainment. The connections affected cover a wide range of brain regions – frontal, parietal, temporal, and occipital. This suggests that education could lead to increased connectivity across distributed brain regions. We found mostly lower nodal measures of connectivity with increased educational attainment. Besides a positive association between MOS and the clustering coefficient of the right lateral occipital gyrus, all other associations with clustering coefficient, regional efficiency, and degree were negative. As highly mathematical measures, we need to consider how these measures are actually calculated and what other factors could influence their calculation when we try to interpret them. Clustering coefficient is calculated by examining all of the connections of a given node and determining what proportion of those connections are also connected to each other. It is considered a measure of local efficiency, but it is also a measure of segregation [Rubinov & Sporns, 2010]. Thus, our results could mean that individuals who have greater educational attainment could have decreased integrity of their nodal neighborhoods for an unknown reason, or they could be less "cliquish" and better integrated into the whole network. Degree is simply the number of connections of a given node, so lower degree with greater educational attainment means these individuals have fewer connections originating from these nodes. Regional efficiency is the inverse of the shortest path going through all of the node's neighbors. Perhaps because there are fewer connections for these nodes (as shown in lower degree), the path length increases. This could occur if the nodes now missing from the neighborhood were local hub nodes, highly connected within the neighborhood and key to local efficiency. Over development, we have previously found both increases and decreases in clustering coefficient, degree, and regional efficiency distributed across the brain. Given this, we cannot categorically say that increases in degree or efficiency are "good", for example. As there

143

are no other studies investigating graph theoretical correlates of educational attainment, and very few examining cognitive function, it is difficult to put these results in context. We are exploring which metrics are best for detecting individual differences. These results point out the need to investigate the correlations between graph theoretical measures of connectivity and cognition, in order to better interpret these data.

In an attempt to find some common ground with our previous cognitive study, relating IQ to rich club organization and voxel-wise FA, we examined voxel-wise FA for associations with months of school. We found that completion of more months of high school was associated with greater FA in the isthmus of the corpus callosum, the posterior genu of the corpus callosum, and the right ILF/UNC. These associations remained the same when we co-varied for FIQ. These results suggest that individuals with greater educational attainment have greater white matter integrity in a known language pathway, which connects the temporal and parietal language areas across hemispheres. These results contrast the previous study by Noble et al. (2013) finding decreased FA with further education. The age range of their subjects (17-23 years old) overlaps with ours (20-30 years old), and they were similarly using a sample collected in Australia, so the sociological factors impacting education should be similar between our samples. While we used months of high school completed, Noble et al. (2013) used total years of school, which could account for some differences as their sample included a larger range of educational attainment. Additionally, while Noble et al. (2013) had data from 47 subjects, we included 287 subjects in our study.

Our results of greater fiber density and greater FA with greater educational attainment suggest that the cognitive enrichment of higher education has positive effects on brain structure. However, our findings of mostly decreases in nodal clustering, efficiency, and degree are

difficult to interpret in this context, as there are no other studies linking these factors. The measures of fiber density and fractional anisotropy are closer to biological measures of connectivity, while the graph theoretical measures are a little farther removed from the true biological substrates we are attempting to assess. This does not mean these measures cannot be used to analyze the brain – graph theory can give us a bird's eye view of network topology that we cannot see with other methods. But the results of the current study need further review to determine how graph theoretical methods can accurately be used and interpreted in the case of cognitive function.

Another factor to consider is that our variable of interest, months of school, is a measure of time spent in school, and while we expect it to be correlated with cognitive abilities (although in specific domains), it is not a measure of intelligence. Intelligence quotient (IQ) is expected to be fairly stable across the lifespan, as it is not a measure of knowledge of discrete facts, and there is research to support this [Deary et al., 2000]. Thus, we cannot extend our results to general cognitive function; rather, they are a measure of how a specific and broadly applicable environmental source of cognitive enrichment is associated with differences in brain structure. With the age of our sample and cross-sectional design, we cannot say for certain whether these differences are because of education, or if they were pre-existing differences perhaps related to a subject's likelihood to continue education. We ran all analyses additionally co-varying for FIQ (which was not correlated with MOS), and found no changes, adding support to the interpretation that these associations are in fact pointing to changes that occurs with advanced education, rather than basic differences in cognitive ability. To conclusively determine this, we would need to examine subjects before and after their course of education. As this is the first study linking graph theoretical measures of connectivity with education, further research, preferably in a

younger group, is necessary to validate and gain a deeper understanding of these associations and how to interpret them.

CHAPTER 5

Summary

The common thread between all of these studies is an examination of structural brain connectivity and the various factors that influence measures of brain connectivity. Across development, we see a transition towards increased structural integration and segregation, demonstrated in our findings of decreased characteristic path length, clustering, and increased modularity [Dennis et al., 2013b] and increased density among rich club nodes [Dennis et al., 2013c]. This occurs as useful connections are potentiated, and less used connections are not. As many studies have shown, the timeline of this process varies across brain regions [Gogtay et al., 2004]. We found distinctly different trajectories in the frontal and temporal cortices, with connections among the frontal cortex generally showing decreases in fiber density and degree (number of connections), and the temporal cortex generally showing increases in fiber density and degree between ages 12 and 30 [Dennis et al., 2013b; Dennis et al., 2013d]. This does fit with earlier studies showing an earlier age of peak in frontal vs. temporal gray matter volume [Giedd et al., 1999; Tanaka et al., 2012], and gray matter density (GMD) [Sowell et al., 2003]. Sowell et al., 2003, found a continuous decline in the GMD of the superior frontal sulcus between age 10 and 90, leveling off towards the end, while the GMD of the superior temporal sulcus increased until age 30, at which point it decreased. These together support a more protracted development in the temporal cortex than the frontal cortex.

These studies have focused on typical development, but these trajectories are significantly different in children with developmental disorders such as autism. Investigations

147

into how *functional* graph theoretical measures of connectivity are altered in children with autism have found decreased path length, possibly a sign of increased randomness [Rudie et al., 2013]. We similarly found decreased path length, but in the structural networks of healthy *risk-allele carriers* of an autism-associated gene, *CNTNAP2* [Dennis et al., 2011a]. This demonstrates the utility of examining healthy carriers of risk genes, as often the disorder itself causes changes in the brain, making it difficult to tease apart the causes and effects. Similarly, we examined associations between an obesity risk gene, *NEGR1*, and white matter integrity in our QTIM sample, whose BMI (body mass index – an approximate assessment of fat mass) covers the range seen in the population. This was not an exclusively obese sample, but we believe that is a strength of the study as obesity is associated with a wide range of brain changes that are not well understood [Stanek et al., 2011]. We found that risk allele dosage was associated with widespread decreases in white matter integrity. When we examined this variant in our follow-up sample from ADNI (Alzheimer's Disease Neuroimaging Initiative), we found similar areas of association, but in the opposite direction. Obesity has an age-dependent effect on cognition [Fitzpatrick et al., 2009], and our results suggest that this may be genetically influenced. Both of these studies will aid our understanding of the mechanisms by which these genes confer vulnerability. *CNTNAP2* is associated with more random network organization, but how does this occur? A recently characterized *CNTNAP2* knockout mouse model found neuronal migration abnormalities [Peñagarikano et al., 2011]. Abnormal development and migration could theoretically lead to the effects we found. With *NEGR1*, our subjects were fairly young (20-30 years old) so it is possible that they may become obese later in life. How decreased white matter integrity is linked with obesity risk, when it is clearly not caused by already-present obesity, is unclear. Further investigation of this topic will hopefully reveal the mechanisms by which

NEGR1 increases risk of obesity, as well as how obesity and cognitive function are linked throughout the lifespan.

As brain structure matures towards a more organized pattern of connectivity, cognition develops as well. These two factors influence the development of the other in a dynamic interplay. Our two investigations into cognitive correlates of structural connectivity are quite different, as one uses a putative measure of cognitive ability (IQ) [Dennis et al., 2013f], and the other uses a measure of cognitive enrichment (months of school) [Dennis et al., 2013g]. In one study, we examined rich club organization and white matter integrity [Dennis et al., 2013f], while in the other, we examined fiber density between cortical regions and nodal graph theoretical measures of structural connectivity [Dennis et al., 2013g]. In searching for some overlap in effects, we examined associations with white matter integrity (as measured by FA – fractional anisotropy) with months of school as well, with and without co-varying for FIQ. Here, we found some common ground, as both IQ scores and months of school were associated with increased integrity in the right ILF/UNC (inferior longitudinal fasciculus/uncinate, at the anterior end of the ILF these tracks merge). As might be expected, we generally found evidence of increased neural resources or integrity with greater cognitive ability and greater cognitive enrichment, as measured by white matter integrity, fiber density between cortical regions, or nodes included in the "rich club". With more neural resources (fiber density, rich club nodes) and better integrity (white matter integrity), we would expect there to be more efficient information transfer in the brain, which would support cognitive function. Our findings of decreased nodal clustering, efficiency, and degree with further educational attainment are difficult to fit into this framework, as we are only beginning to examine what they mean for brain health and what are normal measures. As very few studies have examined these measures in

149

relation to cognitive abilities, and they are more mathematical measures of connectivity, further research is necessary to determine their utility and how to accurately interpret these results. Graph theory has a lot to offer the field of neuroscience, but at this earlier stage we need to tread carefully when assigning value to specific measures.

CHAPTER 6

Future work

From the work presented here, there is a clear trend toward examining brain structural connectivity across development and the factors that may influence it. From here, two natural extensions are to examine functional connectivity, and to examine connectivity in atypical development. This is exactly what I intend to do, investigating functional connectivity in the QTIM dataset, and joining a project in progress at UCLA examining moderate-to-severe traumatic brain injury in children and adolescent patients.

6.1 Functional connectivity

Functional connectivity is complimentary to the information gained from structural connectivity. While an analysis of functional connectivity data was originally planned as part of my dissertation, unforeseen factors barred me from analyzing the data. We now have access and the data are currently being processed.

Functional connectivity assesses the integration of brain activity across distant brain regions, regardless of their structural connectivity. Various methods may be used to measure this type of functional synchronization or coherence, and different kinds of information can be collected, depending on whether subjects are performing a specific task, or no task in particular. Functional MRI methods can assess connectivity by measuring correlations in the BOLD (blood oxygenation level dependent) time-series of activations in different brain regions; other types of analysis focus on the mutual information between two different profiles of activation.

Synchronized low-frequency fluctuations (~0.01-0.1 Hz) in the BOLD signal across distant brain regions were first discovered by Biswal et al. (1995). This sparked the discovery of a number of temporally coherent networks that are remarkably consistent across individuals [Damoiseaux et al., 2006; Fox et al., 2005; Beckmann et al., 2005].

Many possible roles have been attributed to these ICNs (intrinsic connectivity networks): memory functions, organization and coordination of neuronal activity, and priming the brain for coordinated activity [Fox and Raichle, 2007; Seeley et al., 2007]. The cognitive correlates of the networks are not fully known, but we do know that these networks are present in the descent to sleep [Larson-Prior et al., 2009] and they are even detectable in developing fetuses [Thomason et al., 2013]. ICN connectivity is disrupted in a wide range of psychiatric and developmental disorders [Greicius, 2008], motivating the quest to understand how they contribute to cognitive function, and how they decline as we age.

The ICN that has received the most attention is the *default mode network* (DMN): this is a collection of brain regions whose activity *increases* in the absence of a task. As such, the DMN is also called the "task negative" network, anti-correlated to the "task positive" network [Fox et al., 2005]. The DMN is generally thought to include the posterior cingulate cortex/precuneus, medial prefrontal cortex, inferior parietal lobules, lateral temporal cortices, and hippocampus [Buckner et al., 2008; Raichle et al., 2001]. There has been a great deal of interest in the DMN: many theorize that the activity of this network during rest is necessary for memory consolidation [Fox and Raichle, 2007], making it especially interesting in the field of Alzheimer's research [Dennis & Thompson, 2013h]. The *executive control network* (ECN) seems to include regions inversely correlated with the default mode network (DMN), and is thus dubbed part of the "task-positive" network of the brain.

The regions of the ECN include some of those that are last to mature; yet a comprehensive examination of the developmental trajectory of the ECN and how it relates to cognitive development has not been done. Based on the regions the ECN encompasses, it is assumed to underlie executive function, but even that assumption has yet to be researched. I hope that by investigating measures of executive function, I will be able to test new theories of the cognitive correlates of resting connectivity and how it supports and influences function. It is vital to relate executive connectivity and executive function - making decisions, abstract thought, and planning ahead, as they are all central to our human experience, and highly vulnerable to psychopathology. Research on the DMN has found altered connectivity in disease. There are fewer studies of how psychopathology affects the ECN. Systematic investigation of the ECN will reveal how it contributes to behavioral executive ability and how it relates to known aspects of brain maturation. Normative data on executive network development is vital for us to understand the basis of disorders with abnormal and characteristic fMRI responses.

With the QTIM dataset that I have used for the vast majority of my dissertation studies, I will examine the developmental trajectory of various aspects of functional connectivity, focusing on the ECN. For this I will use seed-based, ICA, and graph theoretical approaches, depending on which is most appropriate for the specific question. We will additionally investigate how these trajectories differ between males and females. Another aim of this future work is to determine the genetic influences on functional connectivity. For this, we will use both a candidate SNP (single nucleotide polymorphism) approach, examining SNPs that we have found to be associated with changes in structural connectivity, and more complicated multi-locus and genome-wide approaches. Lastly, we will investigate the association between functional connectivity and measures of cognitive function, and how the developmental trajectory of these

measures track together. We expect this work will both further our understanding of the role functional connectivity serves in the healthy brain, as well as creating a foundation for investigations into atypical development.

6.2 Pediatric traumatic brain injury

My dissertation has focused on healthy development, which serves as an ideal foundation for investigating factors that cause deviations from the typical trajectory. TBI is a major public health issue in children and adolescents, affecting an estimated 180 children and 660 adolescents per 100,000 per year in the US. It is responsible for half of traumatic injury fatalities [Kraus et al., 1995; Langlois et al., 2003]. TBI at any point in life can have long-term negative consequences, but in children and adolescents these effects are exaggerated as the brain is rapidly developing. Children who sustain TBI show poorer performance in school [Taylor et al., 2002; Ewing-Cobbs et al., 1998] and are at an increased risk for psychiatric disorders [Max et al., 1997; Max et al., 1998]. While there is clear damage to the grey matter, there are also significant deficits in white matter (WM) connectivity, caused by Wallerian degeneration that damages myelin and disrupts axonal ultrastructure [Wilde et al., 2008; Yuan et al., 2007]. Axonal injury is the main pathological lesion in TBI. These differences can be seen acutely [Chu et al., 2009; Wilde et al., 2008], years post injury [Yuan et al., 2007; Wozniak et al., 2007; Ewing-Cobbs et al., 2008], and can be sensitive indicators of disease. Children vary in how well they can recover from TBI, as with most injuries. If we can tell who can recover more quickly, and what factors predict better outcomes, we can develop more effective interventions. Early interventions do have an impact on recovery from TBI [Ponsford et al., 2001].

Hemorrhagic and nonhemorrhagic shearing lesions associated with diffuse axonal injury (DAI) are found in up to 40% pediatric TBI patients, especially more severe cases, and are responsible for a wide range of impairments [Ashwal et al., 2006a]. DAI is characterized by widespread damage to the corpus callosum, brain stem, gray-white matter junctions, and the parasagittal white matter (dorso-medial white matter, in the frontal cortex generally) [Ashwal et al., 2006a]. A definitive diagnosis of DAI can only be made *post mortem*, but sophisticated imaging methods can provide compelling evidence of DAI. Traditional CT (computed tomography) and MRI (magnetic resonance imaging) methods have not proven sensitive enough to DAI [Tong et al., 2003]. Newer methods such as diffusion weighted imaging (DWI) – a strength of our lab – and magnetic resonance spectroscopy (MRS) have recently been applied in TBI research, and show great promise in detecting DAI and its related effects.

DWI methods such as high angular resolution diffusion imaging (HARDI) combined with tractography allow us to visualize axonal pathways *in vivo* and approximate their integrity. Fractional anisotropy (FA), the degree to which water diffuses in one direction (along axons), is the most common measure of white matter integrity. Generally, higher FA means better myelinated, more highly developed tracts [Thomason & Thompson, 2011]. In addition to voxel-wise measures of white matter integrity, we can also use these data to construct matrices describing the structural connectivity between all points in the brain (e.g., fiber density between each region of interest - ROI). Using the framework of graph theory, we can investigate the complex topology of the structural "connectome". Graph theory represents the brain as a set of nodes (brain regions) and edges (connections between them, e.g., fiber density). By representing the data in this way, a number of standard parameters exist to investigate network metrics such as efficiency and modularity [Rubinov & Sporns, 2010]. The benefit of graph theoretical

methods is that they can reveal changes in global topology as well as local connectivity. MRS is another technique to assess damage following TBI. The most widely used type of MRS is ^{1}H-MRS, which detects the signals from protons in neurochemicals other than water (as opposed to MRI, which detects protons in water). ^{1}H-MRS can measure key brain metabolites such as *N*-acetylaspartate (NAA, a neuronal and axonal marker that decreases in neuronal loss), total creatine (Cr, marker for intact brain energy metabolism), total choline (Cho, marker for membrane repair, inflammation, or demyelination), and lactate (Lac, may be a response to release of glutamate in TBI) [Ashwal et al., 2006b]. Metabolite ratios such as NAA/Cr or Cho/Cr are sensitive markers of DAI and predict long-term outcomes [Holshouser et al., 2005; Sinson et al., 2001]. Even brain regions that do not appear injured have altered metabolite ratios that are correlated with injury [Ashwal et al., 2006b].

I will work with my mentor, our research team, and collaborators, to use multiple types of data – MRS (magnetic resonance spectroscopy) data, HARDI (high angular resolution diffusion imaging) data, and clinical data – that have been collected longitudinally, to examine how TBI impacts the developmental trajectory of white matter connectivity in the brain. Data collection for this project is on-going, but we already have a large cohort. With our range of intake ages, we hope to discover how age of injury affects recovery. With our longitudinal design, we hope to discover what imaging measures best predict clinical outcome. Determining the neuroimaging differences in children with TBI, and how they change longitudinally will shed light on the mechanisms of recovery, providing foundational knowledge for researchers developing more effective interventions. Even in mild TBI, effects persist well after the injury, such as difficulty in school, but they are often blamed on laziness on the part of the child, even if they are truly a consequence of the injury. By receiving blame and punishment, when they are truly in need of

understanding and additional help, the child's progress may be set back [Ponsford et al., 2001]. A comprehensive understanding of what happens to the developing brain's white matter as it recovers from injury is necessary to know how to respond.

The specific questions of this study concern the best markers of injury in pediatric TBI and the rate of recovery. We will look cross-sectionally to determine how various measures of diffusivity are affected following TBI and which of these correlate best with cognitive function. We will examine the rates of recovery of white matter and cognitive function to better understand this process. Additionally we will examine the longitudinal data for age effects, to determine how age of injury impacts the recovery process. Lastly, we will attempt to find a model combining our various brain and cognitive measures from the Time 1 scans to determine what combination is most predictive of rate of recovery between Time 1 and Time 2.

We hope that our study will aid future researchers in developing more effective treatments for pediatric TBI. Once we have an accurate assessment of the extent of the damage, clinicians may have a better idea of what sort of neurorehabilitation will be most effective, in the case of moderate-to-severe TBI. In the case of mild TBI, most existing treatments center on giving the parents information about what to expect and coping strategies, which have proven effective [Ponsford et al., 2001]. By developing better predictors of outcome, and assessing what methods give us the clearest picture of the damage, we can give patients and their families the most information possible. We also hope that this will lead to a better informed public. As is the case with combat veterans who have sustained head injuries, patients and families may think that they are healed once the physical scars have disappeared. But the effects of TBI can last long after this, and without being aware of that patients are not given the best recovery support. Increased awareness of the effects of TBI will also hopefully lead to increased reporting of injury

and more patients seeking treatment. Underreport is a major problem in TBI, for a wide range of factors, but better information about the consequences of TBI in children should help this issue [Meehan et al., 2011]. This project will have a broad impact in our communities. Traumatic brain injury in children and adolescents is far too common, but we are only beginning to understand how this damage may impact their continuing development. The information from this study will inform development of effective treatments, and will hopefully increase public awareness about the subtle, long-term effects of traumatic brain injury.

REFERENCES

Aganj, I., et al.. (2010). Reconstruction of the orientation distribution function in single- and multiple-shell q-ball imaging within constant solid angle. Mag Res Med, 64, 554-566.

Aganj, I., et al. (2011). A Hough transform global probabilistic approach to multiple-subject diffusion MRI tractography. Med Image Analysis, 15, 414-425.

Alexander, G., et al. (1997). Association of premorbid intellectual function with cerebral metabolism in Alzheimer's disease: Implications for the cognitive reserve hypothesis. Am J Psychiatry, 154, 165-172.

Ashtari, M., et al. (2007). Disruption of white matter integrity in the inferior longitudinal fasciculus in adolescents with schizophrenia as revealed by fiber tractography. Arch Gen Psychiatry, 64(11), 1270-1280.

Ashwal, S., et al. (2006). Susceptibility-weighted imaging and proton magnetic resonance spectroscopy in assessment of outcome after pediatric traumatic brain injury. Arch Phys Med Rehabil, 87(S2), S50-S58.

Ashwal, S., et al. (2006). Use of advanced neuroimaging techniques in the evaluation of pediatric traumatic brain injury. Dev Neurosci-Basel, 28, 309-326.

Beckmann, C. F., et al. (2005). Investigations into resting-state connectivity using independent component analysis. Philos T R Soc B, 360, 1001–1013.

Benjamini, Y. & Hochberg, Y. (1995). Controlling the false discovery rate: a practical and powerful approach to multiple testing. Journal of the Royal Statistical Society Series B, 57(1), 289-300.

Biswal, B., et al. (1995). Functional connectivity in the motor cortex of resting human brain using echo-planar MRI. Magn Res Med, 34, 537–541.

Braskie, M., et al. (2011). Common Alzheimer's disease risk variant within the *CLU* gene affects white matter microstructure in young adults. J Neurosci, 31, 6764-6770.

Brown, J. A. et al. (2011). Brain network local interconnectivity loss in aging *APOE*-4 allele carriers. PNAS, 108(51), 20760-20765.

Buckner, R. L., et al. (2008). The brain's default network: Anatomy, function, and relevance to disease. Ann NY Acad Sci, 1124, 1–38.

Bunge, S. A., et al. (2002). Immature frontal lobe contributions to cognitive control in children: Evidence from fMRI. Neuron, 33, 301-311.

Burchinal, M. R., et al. (1996). Quality of center child care and infant cognitive and language development. Child Dev, 67(2), 606-620.

Catani, M., et al. (2003). Occipito-temporal connections in the human brain. Brain, 126(9), 2093-2107.

Chiang, M.-C., et al. (2009). Extending genetic linkage analysis to diffusion tensor images to map single gene effects on brain fiber architecture. Med. Image Comput. Comput. Assist. Interv. MICCAI, 12, 506–513.

Chiang, M.-C., et al. (2011). Genetics of white matter development: A DTI study of 705 twins and their siblings aged 12 to 29. NeuroImage, 54, 2308-2317.

Chu, Z., et al. (2009). Voxel-based analysis of diffusion tensor imaging in mild traumatic brain injury in adolescents. Am J Neuroradiol, 31, 340-346.

Colizza, V., et al. (2006). Detecting rich-club ordering in complex networks. Nat Phys, 2, 110-115.

Colom, R. et al. (2009). Gray matter correlates of fluid, crystallized, and spatial intelligence: Testing the P-Fit model. Intelligence, 37, 124-135.

Daianu, M. et al. (2013). Alzheimer's disease disrupts rich club organization in brain connectivity networks. **Submitted** to 11th IEEE ISBI.

Damoiseaux, J. S., et al. (2006). Consistent resting-state networks across healthy subjects. PNAS, 103, 13848–13853.

Deary, I. J., et al. (2000). The stability of individual differences in mental ability from childhood to old age: Follow-up from the 1932 Scottish Mental Survey. Intelligence, 28(1), 49-55.

Dennis, E. L., et al. (2011). Heritability of structural brain connectivity network measures in 188 twins. *Society for Neuroscience*: Washington, DC.

Desikan, R. S. et al. (2006). An automated labeling system for subdividing the human cerebral cortex on MRI scans into gyral based regions of interest. NeuroImage, 31, 968-980.

Deutsch, G. K., et al. (2005). Children's reading performance is correlated with white matter structure measures by diffusion tensor imaging. Cortex, 41(3), 354-363.

de Zubicaray, G. I., et al., (2008). Meeting the challenges of neuroimaging genetics. Brain Imaging and Behavior, 2, 258-263.

Durston, S., et al. (2002). A neural basis for development of inhibitory control. Dev Sci, 5, 9-16.

Ewing-Cobbs, L., et al. (1998). Academic achievement and academic placement following traumatic brain injury in children and adolescents: a two-year longitudinal study. J Clin Exp Neuropsyc, 20(6), 769-781.

Ewing-Cobbs, L., et al. (2008). Arrested development and disrupted callosal microstructure following pediatric traumatic brain injury: relation to neurobehavioral outcomes. NeuroImage, 42, 1305-1315.

Fish, J. M. (Ed.). (2013). *Race and intelligence: Separating science from myth*. Routledge.

Fitzpatrick, A. L., et al. (2009). Midlife and late-life obesity and the risk of dementia: cardiovascular health study. Arch Neurol-Chicago, 66(3), 336–342.

Fox, M. D., et al. (2005). The human brain is intrinsically organized into dynamic, anticorrelated functional networks. PNAS, 102, 9673–9678.

Fox, M. D., & Raichle, M. E. (2007). Spontaneous fluctuations in brain activity observed with functional magnetic resonance imaging. Nat Rev Neurosci, 8, 700–711.

Giedd, J. N., et al. (1999). Brain development during childhood and adolescence: a longitudinal MRI study. Nature Neurosci, 2(10), 861-863.

Gläscher, J., et al. (2010). Distributed neural system for general intelligence revealed by lesion mapping. PNAS, 107(10), 4705-4709.

Gogtay, N., et al. (2004). Dynamic mapping of human cortical development during childhood through early adulthood. PNAS, 101(21), 8174–8179.

Greicius, M. (2008). Resting-state functional connectivity in neuropsychiatric disorders. Curr Opin Neurol, 21, 424–430.

Hagmann, P., et al. (2008). Mapping the structural core of the human cerebral cortex. PLoS Biology, 6(7), e159.

Holshouser, B. A., et al. (2005). Proton MR spectroscopic imaging depicts diffuse axonal injury in children with traumatic brain injury. Am J Neuroradiol, 26, 1276-1285.

Jackson, D. N. (1998). Multidimensional Aptitude Battery II. Sigma Assessment Systems, Port Huron, MI.

Jahanshad, N. et al. (2010). Genetic influences on brain asymmetry: A DTI study of 374 twins and siblings. NeuroImage, 52(2), 455–469.

Jahanshad, N., et al. (2011). High angular resolution diffusion imaging (HARDI) tractography in

234 young adults reveals greater frontal lobe connectivity in women. In Proc 8th IEEE ISBI, Chicago, 939-943.

Jahanshad, N. et al. (2012). Brain structure in healthy adults is related to serum transferrin and the H63D polymorphism in the *HFE* gene. PNAS, 109, E851-E859.

Jung, R. E. & Haier, R. J. (2007). The parieto-frontal integration theory (P-FIT) of intelligence: Converging neuroimaging evidence. Behavioral and Brain Sciences, 30, 135-187.

Kraus, J. F. (1995). Epidemiological features of brain injury in children: occurrence, children at risk, causes and manner of injury, severity, and outcomes. In: Broman SH, Michel ME, eds. Traumatic Head Injury in Children. New York, NY: Oxford University Press.

Langer, N., et al. (2012). Functional brain network efficiency predicts intelligence. Hum Brain Mapp, 33(6), 1393-1406.

Langers, D. R., et al. (2007). Enhanced signal detection in neuroimaging by means of regional control of the global false discovery rate. NeuroImage, 38, 43-56.

Langlois J. A, et al. (2003). Traumatic brain injury-related hospital discharges: results from a 14-state surveillance system, 1997. MMWR Surveill Summ, 52, 1–20.

Larson-Prior, L., et al. (2009). Cortical network functional connectivity in the descent to sleep. PNAS, 106, 4489–4494.

Li, Y., et al. (2009). Brain anatomical network and intelligence. PLoS Comput Biol, 5(5), e1000395.

Max, J. E., et al. (1997). Traumatic brain injury in children and adolescents: Psychiatric disorders at two years. J Am Acad Child Psy, 36(9), 1278-1285.

Max, J. E., et al. (1998). Psychiatric disorders in children and adolescents after severe traumatic brain injury: A controlled study. J Am Acad Child Psy, 37(8), 832-840.

Meehan III M. P., et al. (2011). The pediatric athlete: Younger athletes with sports-related concussion. Clin Sports Med, 30(1), 133.

Monk, C. S., et al. (2003). Adolescent immaturity in attention-related brain engagement to emotional facial expressions. NeuroImage, 20, 420-428.

Mortimer, J. A., et al. (2003). Head circumference, education and risk of dementia: findings from the nun study. J Clin Exp Neuropsychol, 25, 671–679.

Noble, K. G., et al. (2013). Higher education is an age-independent predictor of white matter integrity and cognitive control in late adolescence. Developmental Science, 16(5), 653-664.

Ortibus, E., et al. (2012). Integrity of the inferior longitudinal fasciculus and impaired object recognition in children: a diffusion tensor imaging study. Dev Med Child Neurol, 54(1), 38-43.

Pfefferbaum, A., et al. (2001). Genetic regulation of regional microstructure of the corpus callosum in late life. NeuroReport, 12, 1677–1681.

Piras, F., et al. (2010). Education mediates microstructural changes in bilateral hippocampus. Hum Brain Mapp, 32, 282-289.

Ponsford, J., et al. (2001). Impact of early intervention on outcome after mild traumatic brain injury in children. Pediatrics, 108(6), 1297-1303.

Posthuma, D., et al. (2000). Multivariate genetic analysis of brain structure in an extended twin design. Behav Genet, 30, 311-319.

Raichle, M. E., et al. (2001). A default mode of brain function. PNAS, 98, 676–682.

Rijlaarsdam, J., et al. (2013). Home environments of infants: relations with child development through age 3. J Epidemiol Commun H, 67, 14-20.

Rubinov M. & Sporns O. (2010). Complex network measures of brain connectivity: uses and interpretations. NeuroImage, 52(3), 1059-1069.

Rudie, J. D., et al. (2013). Altered functional and structural brain network organization in autism. NeuroImage: Clinical, 2, 79-94.

Schmithorst, V. J., et al. (2005). Cognitive functions correlate with white matter architecture in a normal pediatric population: A diffusion tensor MRI study. Hum Brain Mapp, 26(2), 139-147.

Schmitt, J. E., et al. (2008). Identification of genetically mediated cortical networks: a multivariate study of pediatric twins and siblings. Cereb. Cortex, 18, 1737–1747.

Seeley, W. W., et al. (2007). Dissociable intrinsic connectivity networks for salience processing and executive control. J Neurosci, 27, 2349–2356.

Sinson, G., et al. (2001). Magnetization transfer imaging and proton MR spectroscopy in the evaluation of axonal injury: Correlation with clinical outcome after traumatic brain injury. Am J Neuroradiol, 22, 143-151.

Sowell, E. R., et al. (2003). Mapping cortical change across the human life span. Nat Neurosci, 6(3), 309-315.

Sporns, O., et al. (2004). Organization, development and function of complex brain networks. Trends Cogn Sci, 8(9), 418–25.

Stanek, K. M., et al. (2011). Obesity is associated with reduced white matter integrity in otherwise healthy adults. Obesity, 19, 500-504.

Stern, Y. (2002): What is cognitive reserve? Theory and research appli- cation of the reserve concept. Int Neuropsychol Soc, 88, 448–460.

Tanaka, C. et al. (2012). Developmental trajectories of the fronto-temporal lobes from infancy to adulthood in healthy individuals. Dev Neurosci, 34(6), 477-487.

Takeuchi, H. et al. (2010). Training of working memory impacts structural connectivity. J Neurosci, 30(9), 3297-3303.

Taylor, H. G., et al. (2002). A prospective study of short- and long-term outcomes after traumatic brain injury in children: behavior and achievement. Neuropsychology, 16(1), 15-27.

Thomason, M. E., et al. (2013). Cross-hemispheric functional connectivity in the human fetal brain. Science Translational Medicine, 5, 173ra24.

Thomason, M. E. & Thompson, P. M. (2011). Diffusion imaging, white matter and psychopathology, Annu Rev Clin Psycho, 7, 63-85.

Thompson, P. M., et al. (2001). Genetic influences on brain structure. Nat. Neurosci, 4, 1253–1258.

Thompson, P. M., et al. (2010). Imaging genomics. Curr Opin Neurol, 23, 368-373.

Tong, K. A., et al. (2003). Hemorrhagic shearing lesions in children and adolescents with posttraumatic diffuse axonal injury: improved detection and initial results. Radiology, 227, 332-339.

Tuch, D. S., et al. (2005). Choice reaction time performance correlates with diffusion anisotropy in white matter pathways supporting visuospatial attention. PNAS, 102(34), 11212-11217.

Van den Heuvel, M. P. & Sporns, O. (2011). Rich-club organization of the human connectome. J Neurosci, 31(44), 15775–86.

Wilde, E. A., et al. (2008). Diffusion tensor imaging of acute mild traumatic brain injury in adolescents. Neurology, 70, 948-955.

Wozniak, J. R., et al. (2007). Neurocognitive and neuroimaging correlates of pediatric traumatic brain injury: A diffusion tensor imaging (DTI) study. Arch Clin Neuropsych, 22, 555-568.

Yuan, W., et al. (2007). Diffusion tensor MR imaging reveals persistent white matter alteration after traumatic brain injury experienced during early childhood. Am J Neuroradiol, 28, 1919-1925.

Zalesky, A., et al. (2010). Whole-brain anatomical networks: Does the choice of nodes matter? NeuroImage 50: 970–983.